NUREG/CR-0761
UCRL-52707
R4

Extended Analysis of Data from the 1/5-Scale Mark I Boiling Water Reactor Pressure Suppression Experiment

Manuscript Completed: September 1979
Date Published: July 1980

Prepared by
E.W. McCauley, G.S. Holman, E.W. Carr, W. Lai, and J.E. Mellor

Lawrence Livermore Laboratory
7000 East Avenue
Livermore, CA 94550

Prepared for
Division of Reactor Safety Research
Office of Nuclear Regulatory Research
U.S. Nuclear Regulatory Commission
Washington, D.C. 20555
NRC FIN No. A0118-9

8009110500

CONTENTS

APPENDICES:

LIST OF ILLUSTRATIONS

LIST OF TABLES

ABSTRACT

An extensive analysis of data from the 1/5-scale Mark I BWR Pressure Suppression Experiment (PSE) air transient tests has been completed. Primary focus was placed on computing a best estimate of the hydrodynamic vertical load function (HVLF) and determining the associated peak forces and their standard error. These results were then applied to develop the sensitivity of the HVLF to various major parameters (for example, drywell pressurization rate), to evaluate the impulse of the HVLF, and to analytically model the response vertical load function (RVLF). In addition, a complete evaluation of the enthalpy flux distribution in the vent system was provided for each test. Finally, pool swell dynamics were quantified for a subset of the test series and correlated to the observed ringheader strut loads.

BACKGROUND

In light-water reactor pressure suppression containment design, the success of the system is based on the capability of the water heat sink to provide rapid and stable condensation of the released primary coolant during a hypothetical loss-of-coolant accident (LOCA). The General Electric Mark I pressure suppression system encompasses a drywell which surrounds the reactor and channels the steam released during a LOCA into a toroidal suppression pool. There are several BWR Mark I designs. The reference plant used here is the 1065 MW(e) Peach Bottom 2.

Performance of the Mark I pressure suppression system under hypothetical loss-of-coolant accident (LOCA) conditions has been the subject of continuing investigations by many agencies. The Lawrence Livermore Laboratory Mark I BWR Pressure Suppression Experiment (PSE)[1] provided a large-scale (1/5) model to extend these investigations into three dimensions. The experimental program consisted of a comprehensive series of 24 tests which modeled the initial air transient. The need for these tests exists, not only for the assessment of existing Mark I system designs, but also to provide insight into the basic hydrodynamic phenomena associated with wetwell behavior. In addition, the test results provide an extensive data base for computer code development and validation.

In order to obtain experimental data leading to a verifiable analysis of the dynamic loading on the Mark I pressure suppression system, a three-part program was initiated consisting of: (1) the design and construction of a 1/5-scale BWR Mark I facility, (2) benchtop experimental studies to establish scaling laws and phenomena, and (3) a comprehensive series of air transient pressure suppression tests. Each part of the program is described below.

(1) 1/5-Scale BWR Mark I Facility[2]

A 1/5-scale BWR Mark I experimental facility (Figs. 1, 2, and 3) was designed and built for simulating the three-dimensional transient conditions that are encountered in all phases of a wetwell pressure suppression system during a hypothetical loss-of-coolant accident. While the three-dimensional wetwell (90° sector) was the primary focus of the tests, a fully instrumented, two-dimensional wetwell

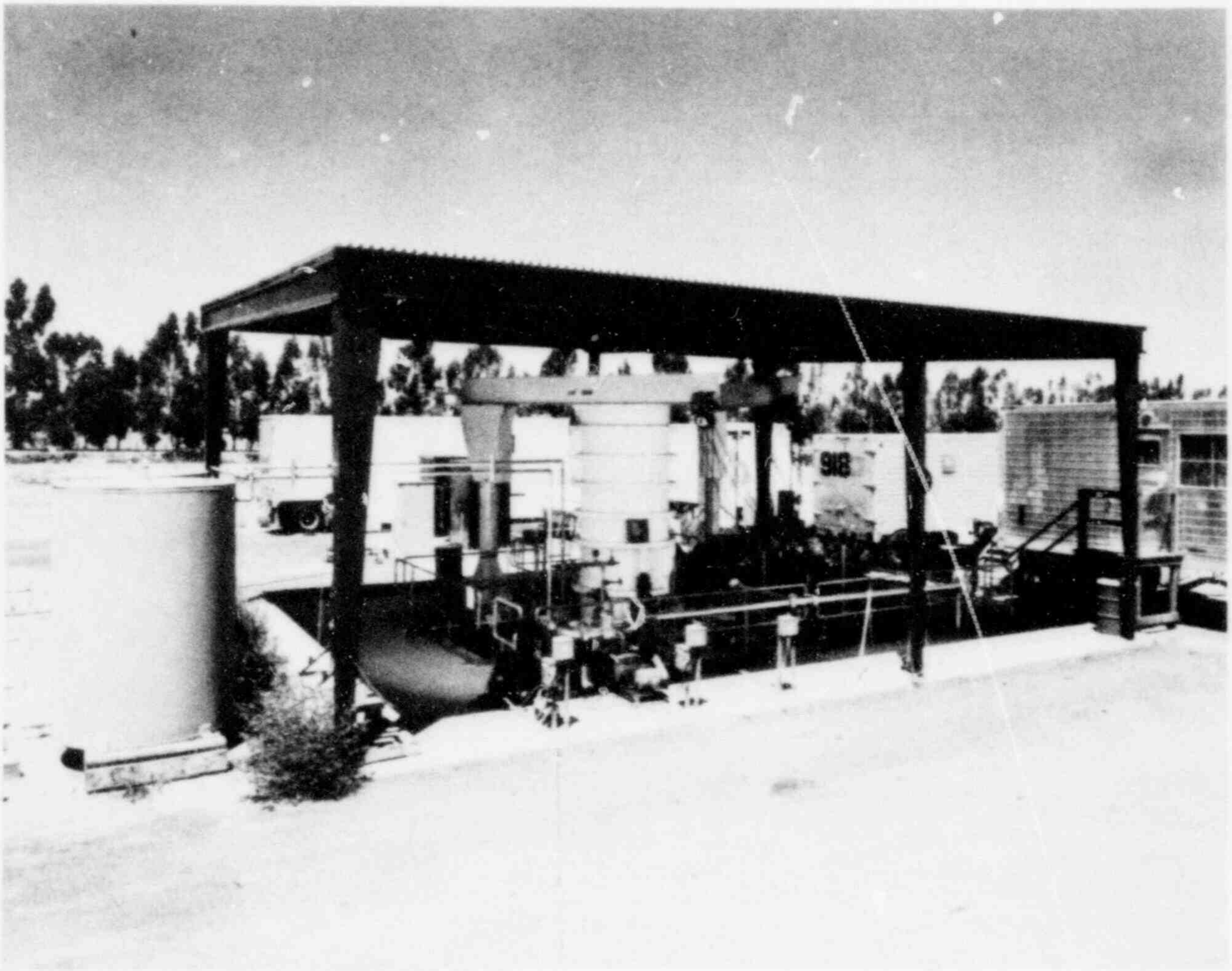

FIG. 1. One-fifth scale model of Mark I BWR pressure suppression facility.

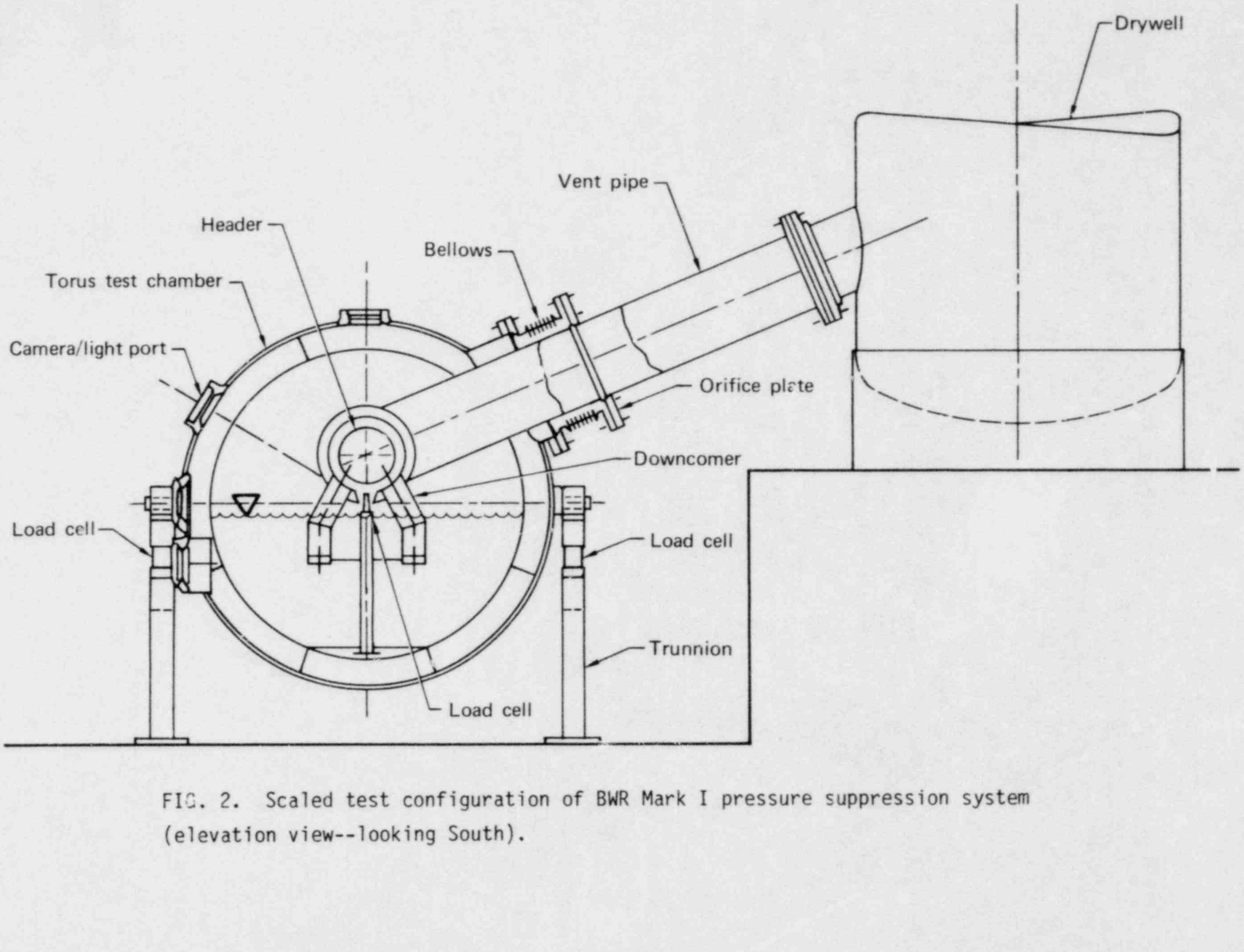

FIG. 2. Scaled test configuration of BWR Mark I pressure suppression system (elevation view--looking South).

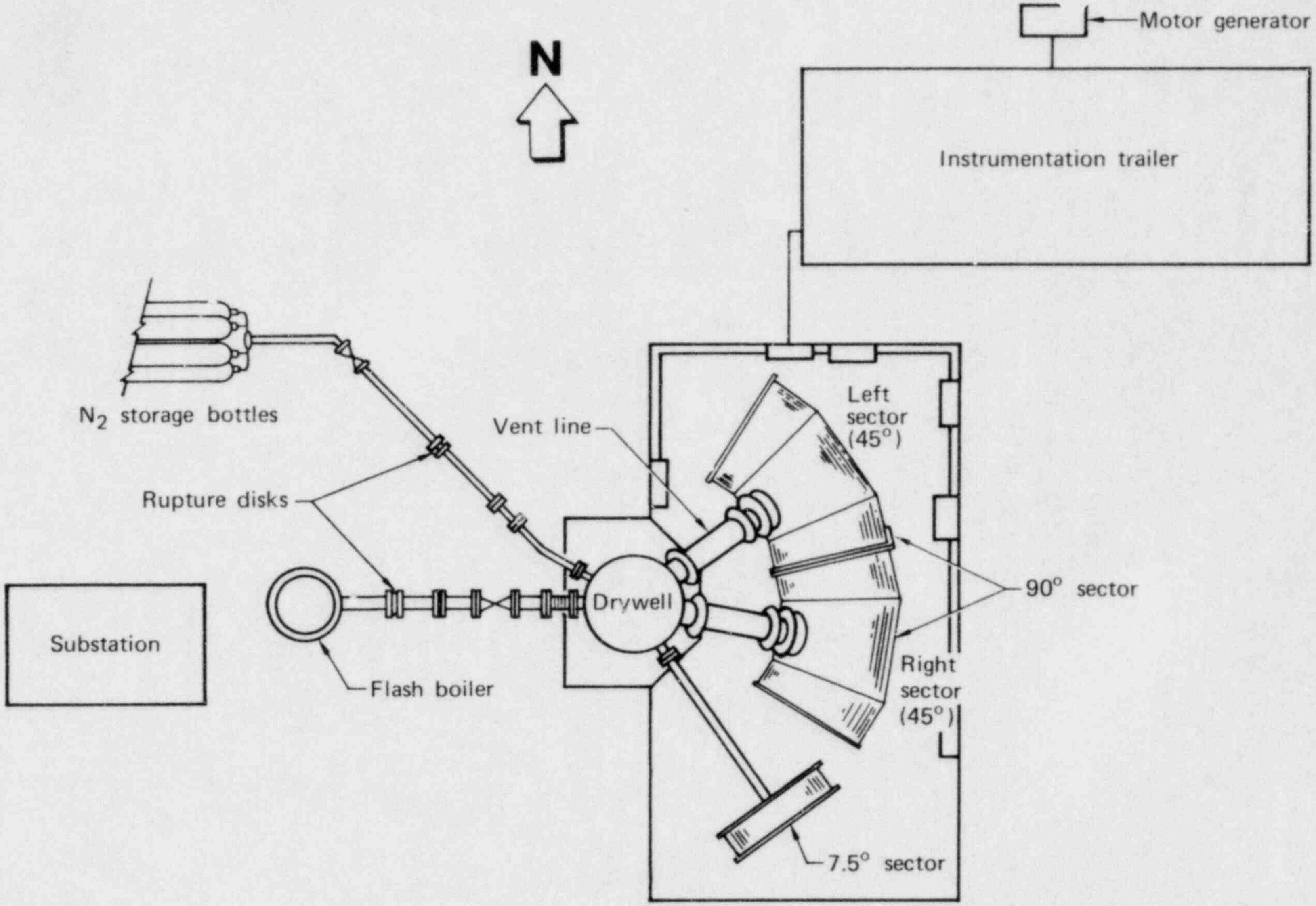

FIG. 3. Schematic diagram of 1/5-scale pressure suppression experiment facility.

(7.5° sector) was also incorporated to provide a comparative data base. In general, the wetwells are faithfully-scaled geometric representations of the Peach Bottom 2 plant; the Peach Bottom 2 plant downcomer configuration is representative of several, but not all, Mark I pressure suppression systems (Fig. 4).

(2) Scaling Relationship Studies[3]

Experimental data necessary to validate the selection of a 90° sector for the 1/5-scale facility was developed from a complete 1/64-scale model of the BWR Mark I drywell/wetwell system (Fig. 5). The experiments determined the appropriate angular relationships and the similarity in response to full-scale systems. Extensive scaling law and phenomenology experiments were also conducted through a series of simple benchmark tests utilizing flasks to simulate portions of the toroidal wetwell.

(3) Pressure Suppression Tests[1,4,5,6]

An experimental program conducted using the 1/5-scale BWR Mark I test facility obtained the air-transient induced dynamic vertical load function and determined the response of the torus structure. These air tests used high-pressure nitrogen gas (N_2) to purge drywell air gas and thereby expel water from the downcomers. These tests were based on a full-scale initial drywell pressurization rate of 61 psi/s as predicted by the CONTEMPT-LT licensing code. This criterion was specified by the United States Nuclear Regulatory Commission (NRC). In comparison, the Peach Bottom Final Safety Analysis Report (FSAR) specified an initial drywell pressurization rate of 41.6 psi/s. This phase of the test program focused on the vertical load function that resulted from the clearing of downcomer water, and each test simulated 3 to 4 seconds of equivalent plant time.

PURPOSE OF THE PRESENT STUDY

Because of time constraints, the PSE final air test results report[1] presented complete test results without critical analysis of the data. In particular, the hydrodynamic vertical load function (HVLF) was computed by a simplified method without determination of error bound.

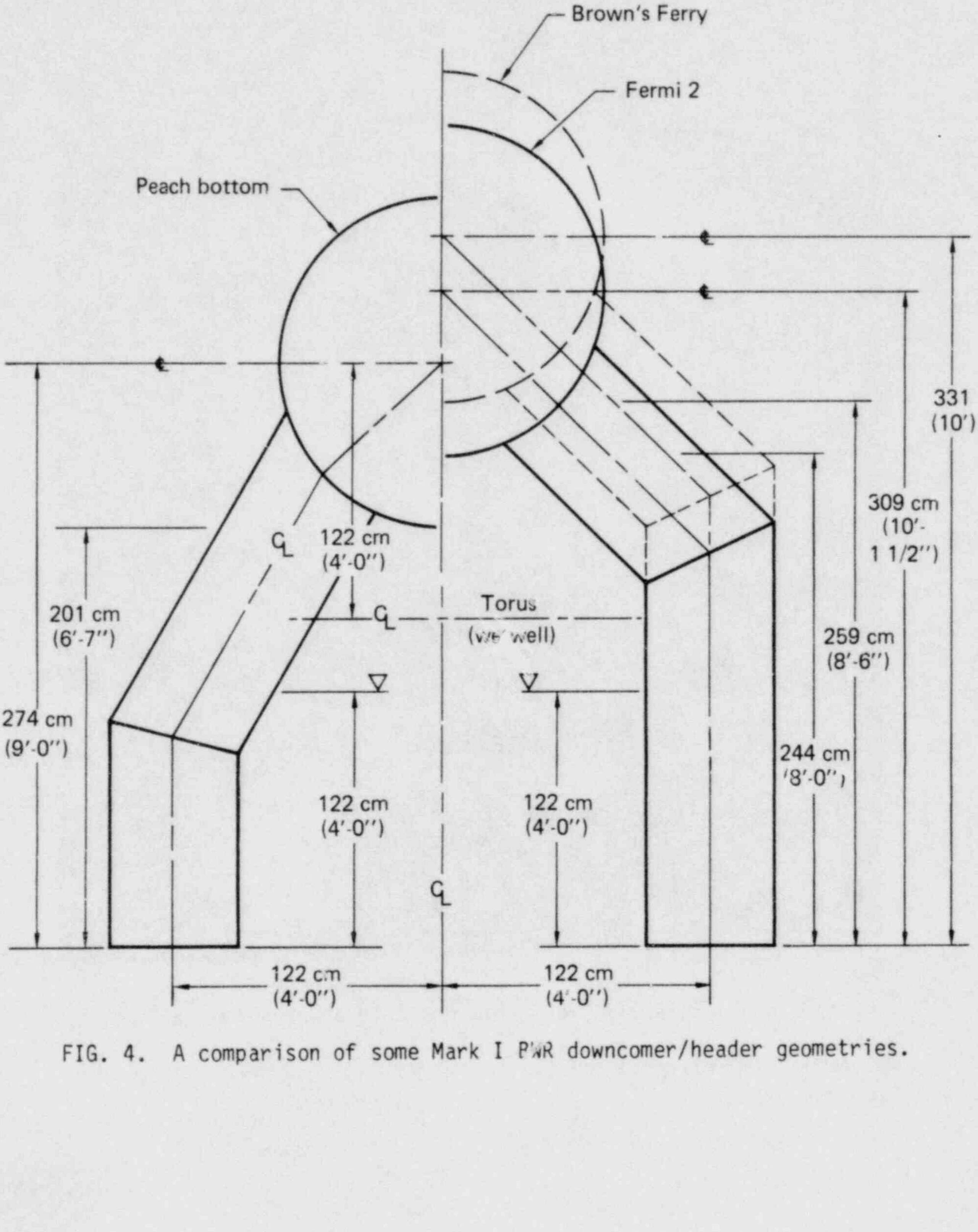

FIG. 4. A comparison of some Mark I PWR downcomer/header geometries.

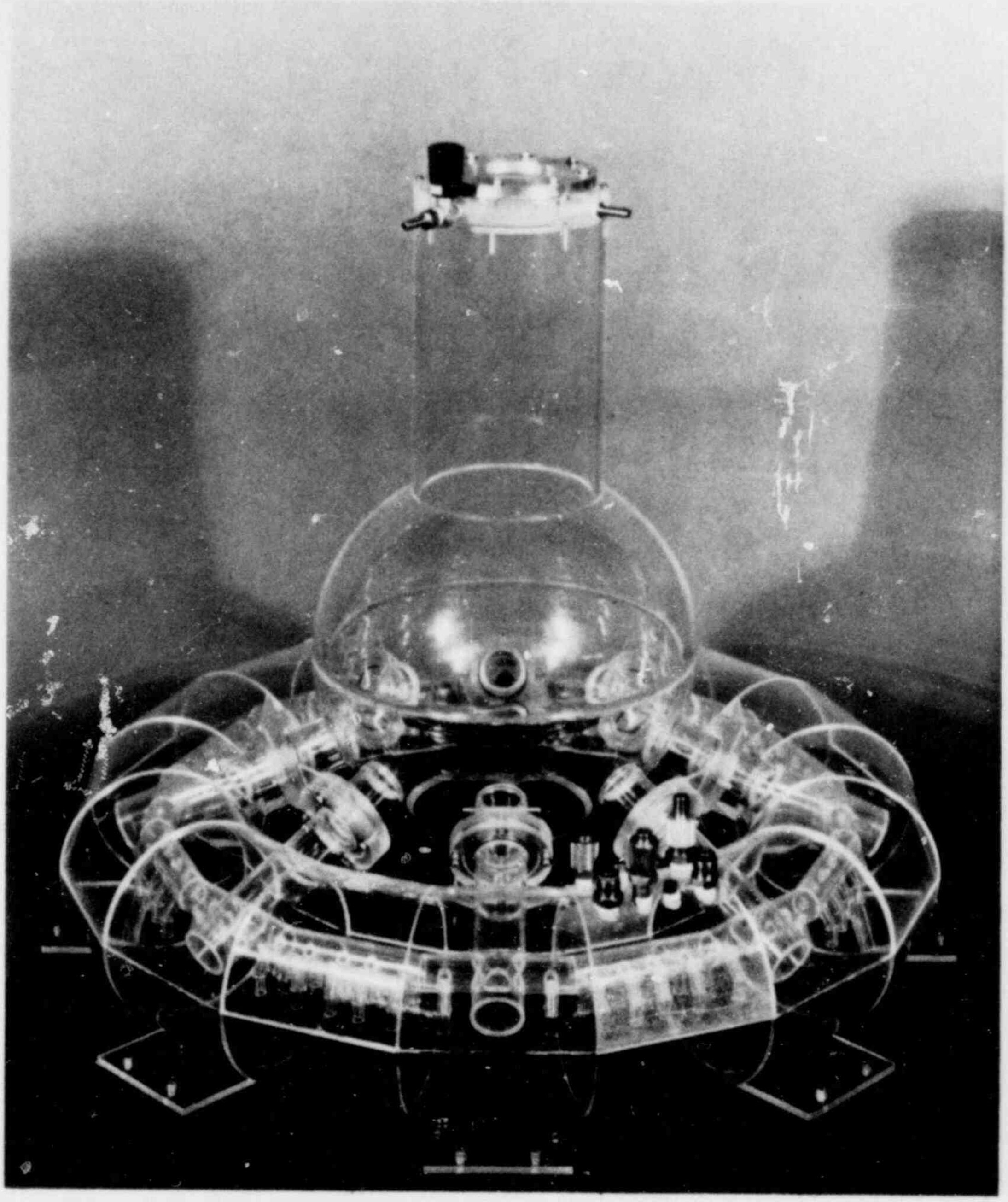

FIG. 5. 1/64-scale BWR Mark I Pressure Suppression System.

The purpose of the current study, therefore, is twofold. The first section of this report details the development of a best estimate calculation of the HVLF for the 90° (3-D) sector and for the 7.5° (2-D) sector, as well as the 3-D to 2-D ratios of maximum upload and maximum download, all with associated error bounds, for each air transient test. The second section provides the results of an in-depth analysis program which addreses several topics, including the following:

- parametric sensitivity of peak upload and peak download
- total impulse of the HVLF
- structural analysis of the 90° torus sector, including modeling of the response vertical load function
- enthalpy flux and flow distribution in the overall vent system
- pool swell effects.

In total, then, these extended analyses provide an important companion document to the final air test results report and allow both qualitative and quantitive understanding of the effects to be expected from a hypothetical loss-of-coolant accident (LOCA) in a Mark I BWR pressure suppression system.

PART I. BEST ESTIMATE ANALYSIS OF THE HYDRODYNAMIC VERTICAL LOAD FUNCTION (HVLF)

1.1 HYDRODYNAMIC VERTICAL LOAD FUNCTION

1.1.1 DESCRIPTION OF THE HYDRODYNAMIC VERTICAL LOAD FUNCTION

The hydrodynamic vertical load (HVL) is defined as the integral of the torus net vertical dynamic pressure over the area defined by the cross-section circumference projected on the horizontal axis and the torus axial length. The HVL may be expressed

$$\mathrm{HVL} = \int_A p\,dA \cdot \bar{j} \quad , \tag{1-1}$$

where $\bar{j}$ is a unit vector in the vertical direction. The HVLF is then the sum of the resulting sequence of HVLs, evaluted at each discrete time point for a given experiment.

The net dynamic pressure acting on a differential area element is simply the difference between the upward component of the pressure, as marked above the projected torus centerline (i.e., ullage pressure), and the downward component of the pressure, corrected for the static waterhead, as measured below the pool surface. The net dynamic force is expressed as the difference in the ullage and pool forces

$$\begin{aligned}\mathrm{HVL} &= \int_A (p_{ullage} - p_{pool})d\bar{A} \cdot \bar{j} \\ &= \int_A p_{ullage}\, d\bar{A} \cdot \bar{j} - \int_A p_{pool}\, d\bar{A} \cdot \bar{j} \quad .\end{aligned} \tag{1-2}$$

By breaking down the area of integration, the equation for the HVL in each sector can be written:

$$\mathrm{HVL} = \int_0^L \left[\int_0^w p_{ullage}\, dx\right] dz - \int_0^L \left[\int_0^w p_{pool}\, dx\right] dz \quad , \tag{1-3}$$

where L is the axial length and w is the width of the torus measured at the pool surface.

1.1.2 INTEGRATION GEOMETRY

The limits of integration are defined by the horizontal projection of the water surface. For the 7.5° torus integration, the axial length (L) is taken to be 17.66 inches so that an integer multiplier, 6, may be used to compare the 2-D HVLF to the HVLF computed in the 45° (3-D) torus sector. The subareas of integration across the pool (x direction) and axially (z direction) are defined by the positions of the transducers and the instrumented planes (Figs. 1-1 and 1-2). These figures show that instrumented plane 4 is parallel to the miter joint and that plane 9 jogs to avoid the miter joint. The x distances used for all planes are measured in the planes; therefore, the total pool (and ullage) widths for planes 4 and 9 (as well as symmetry planes 3 and 8) are greater than those of planes perpendicular to the axis. Appendix A provides facility and test related geometry evaluations. Appendix B lists the accummulated x distances and the associated Δz between planes. Since the dimensions vary with pool level, a separate set of data are supplied in Appendix B for each of the four pool levels used in the tests. The angular position (θ) of the torus wall pressure transducers is indicated in Figs. 1-1 and 1-2 and clarified in Fig. 1-3.

In a given instrumentation plane, there are 11 pool transducer positions defining 12 sectors (1P to 12P) and 4 ullage transducer positions defining 5 sectors (1U to 5U).

All pool and ullage transducers used in both the 2-D and the 3-D test sections are Senso-Metrics, Inc., Model No. 601087. A complete discussion of PSE instrumentation is provided in Ref. (4).

1.1.3 ACTUAL AND VIRTUAL TRANSDUCERS

For any given test, measured pressure data are not available for every instrumentation location. In the pool, this is compensated for by interpolation between points where pressure data were measured by "actual," or available, transducers. In the ullage, "virtual" transducers are used to fill in locations for which actual measured data are unavailable; virtual transducer locations are those at which the pressure history of an actual transducer is assigned on symmetry arguments. Measured pressure histories are

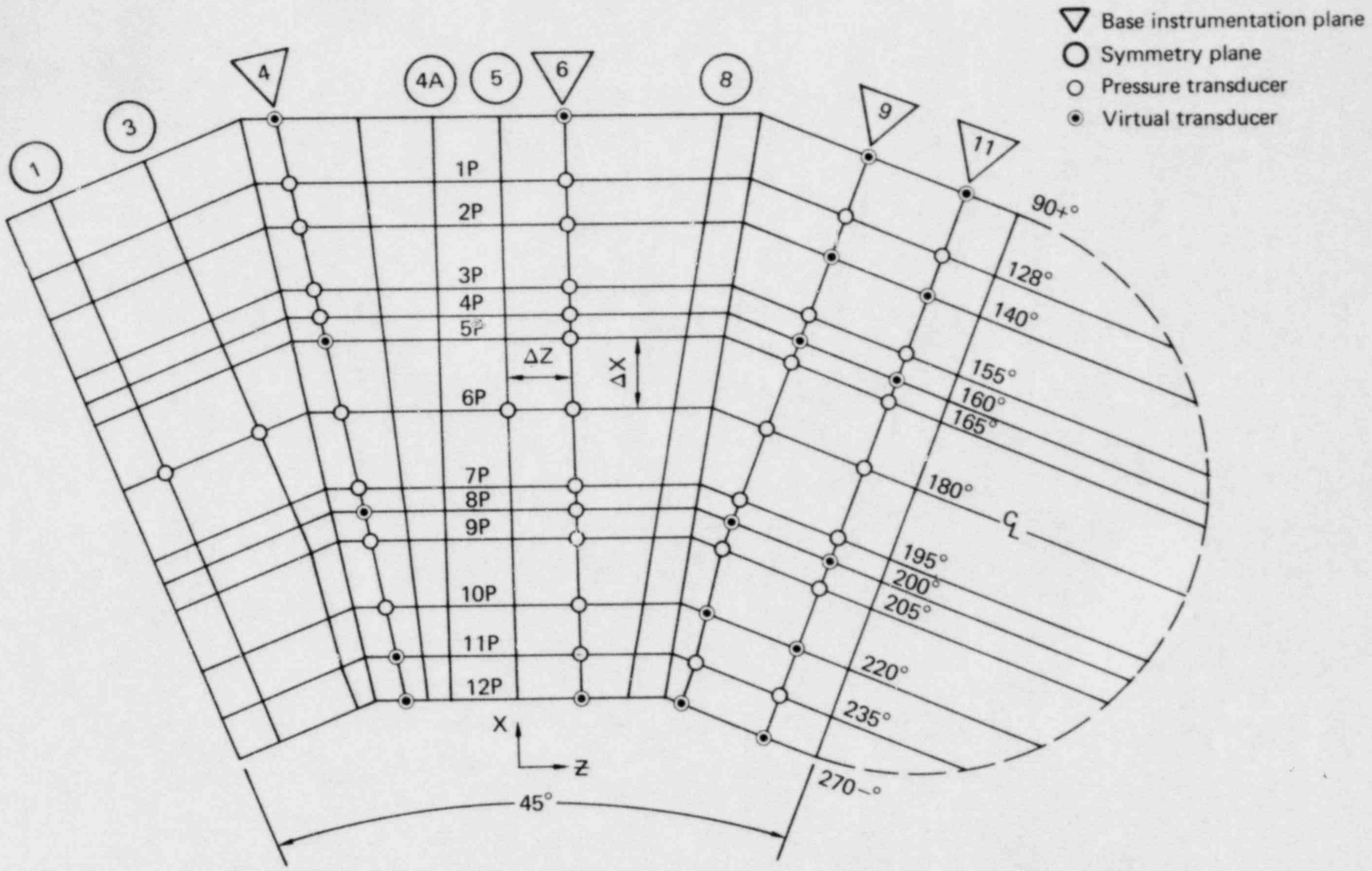

FIG. 1-1. 45° torus sector viewed from top, pool.

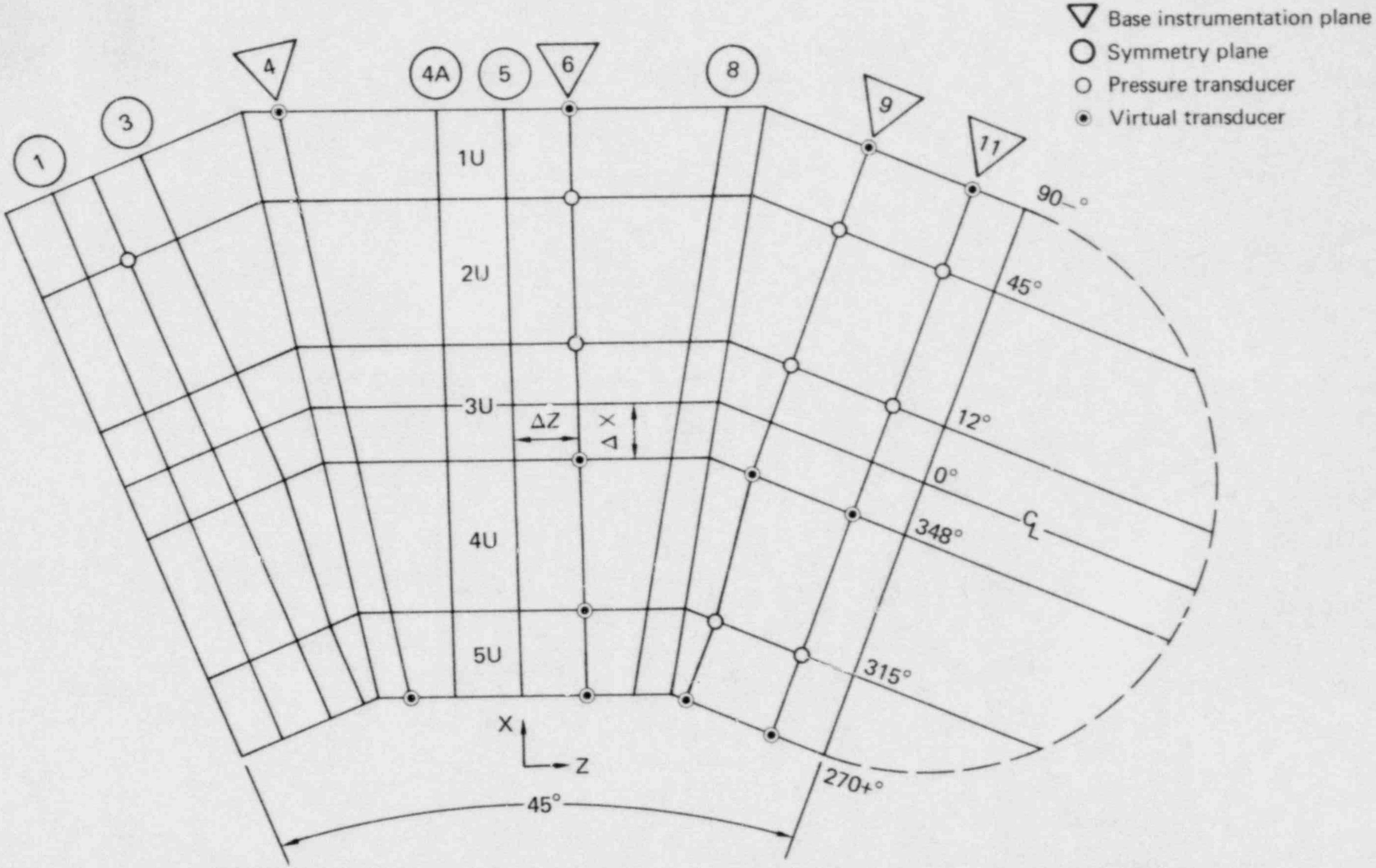

FIG. 1-2. 45^0 torus sector viewed from top, ullage.

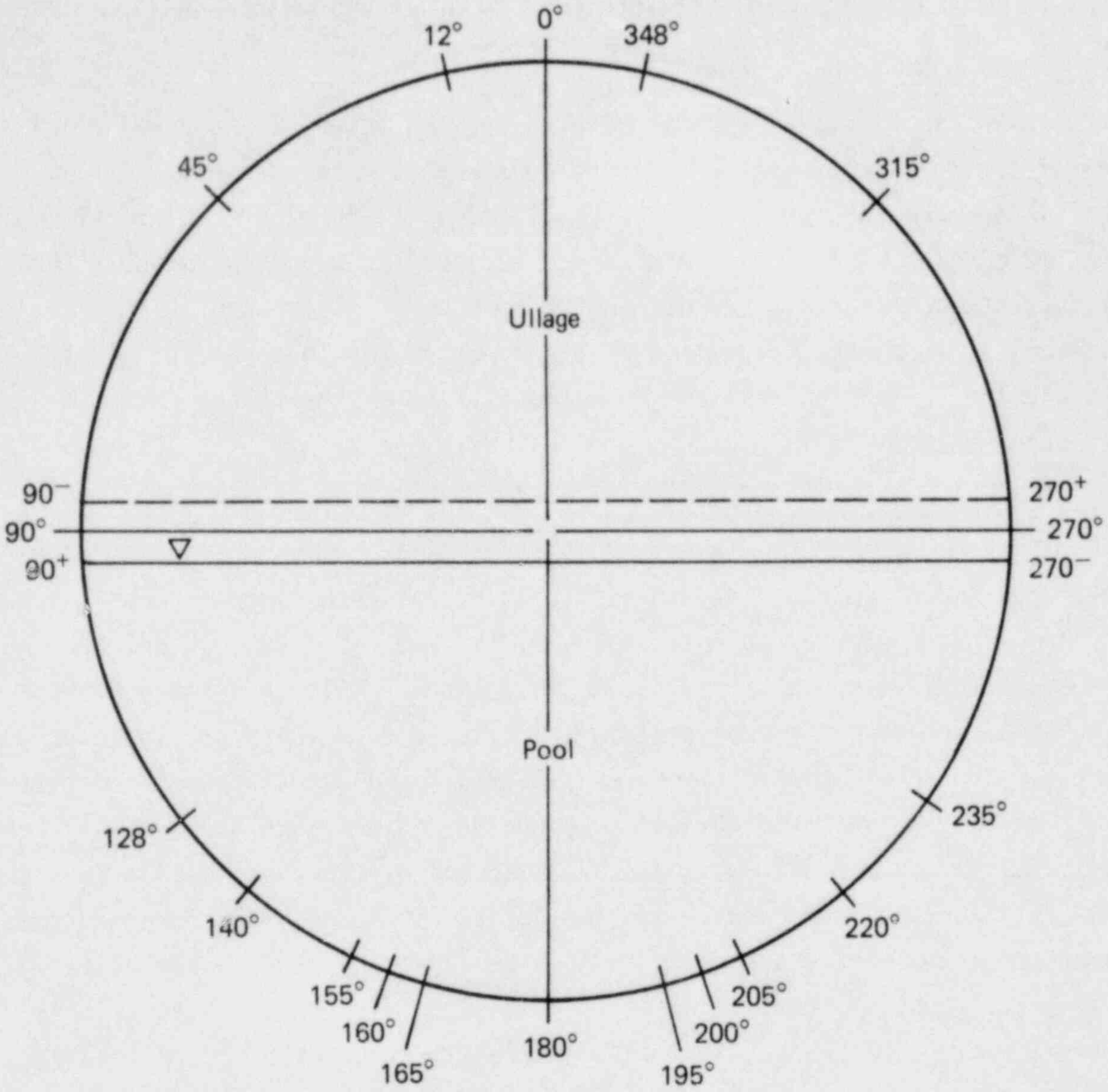

FIG. 1-3. Angular location of torus wall pressure transducers.

used at virtual locations only in the ullage, and never displace actual measured data. Virtual positions, defined in the pool by Fig. 1-1, are filled only by data interpolation (sectors 2P through 11P) or extrapolation (sectors 1P and 12P).

In example, in Fig. 1-4, virtual transducers and actual transducers are identified by circles with or without center dots, respectively. Pool positions where interpolated or extrapolated data are used are indicated by crossed circles. Similarly, the ullage and pool pressure curves have the type of data at each location represented by appropriate tick marks. Note that the "virtual" transducers identified at the edges of the pool surface are the extrapolated histories obtained from the fitting of the ullage data. This is discussed below.

1.1.4 INTEGRATION METHOD

In the procedure for the in-plane integration, at each time step and for each of the 5 instrumentation planes (4, 6, 9, 11, and 2-D), the $\int_0^w pdx$ is accomplished in two steps. First, an analytical fit is made through the available corrected pressure data in the ullage. End point pressures at the virtual pool level intersections (90^- and 270^+) are extrapolated from this fit (see Fig. 1-3). These ullage end point pressures are then assigned as virtual pressures to the pool at 90^+ and 270^-, respectively, and are included in the pool data array. Subsequently, an analytical fit is provided for this pool data. An example of the results of this procedure is shown graphically by Fig. 1-4. In this particular case there are two virtual pressure histories used in the ullage (at 12^o and 348^o) and four interpolated pool pressure histories developed (at 140^o, 160^o, 200^o, and 220^o).

Rather than directly integrate the resulting equations over w to provide a total pool and ullage force in each instrumented plane, separate integrations covering each of the 5 ullage sectors and the 12 pool sectors are carried out, so that, for a given plane

$$\int_0^w pdx = \sum_{i=1U}^{5U} \int_i pdx \quad ; \text{ ullage} \tag{1-4a}$$

$$\int_0^w pdx = \sum_{i=1P}^{12P} \int_i pdx \ . \quad ; \text{ pool} \ . \tag{1-4b}$$

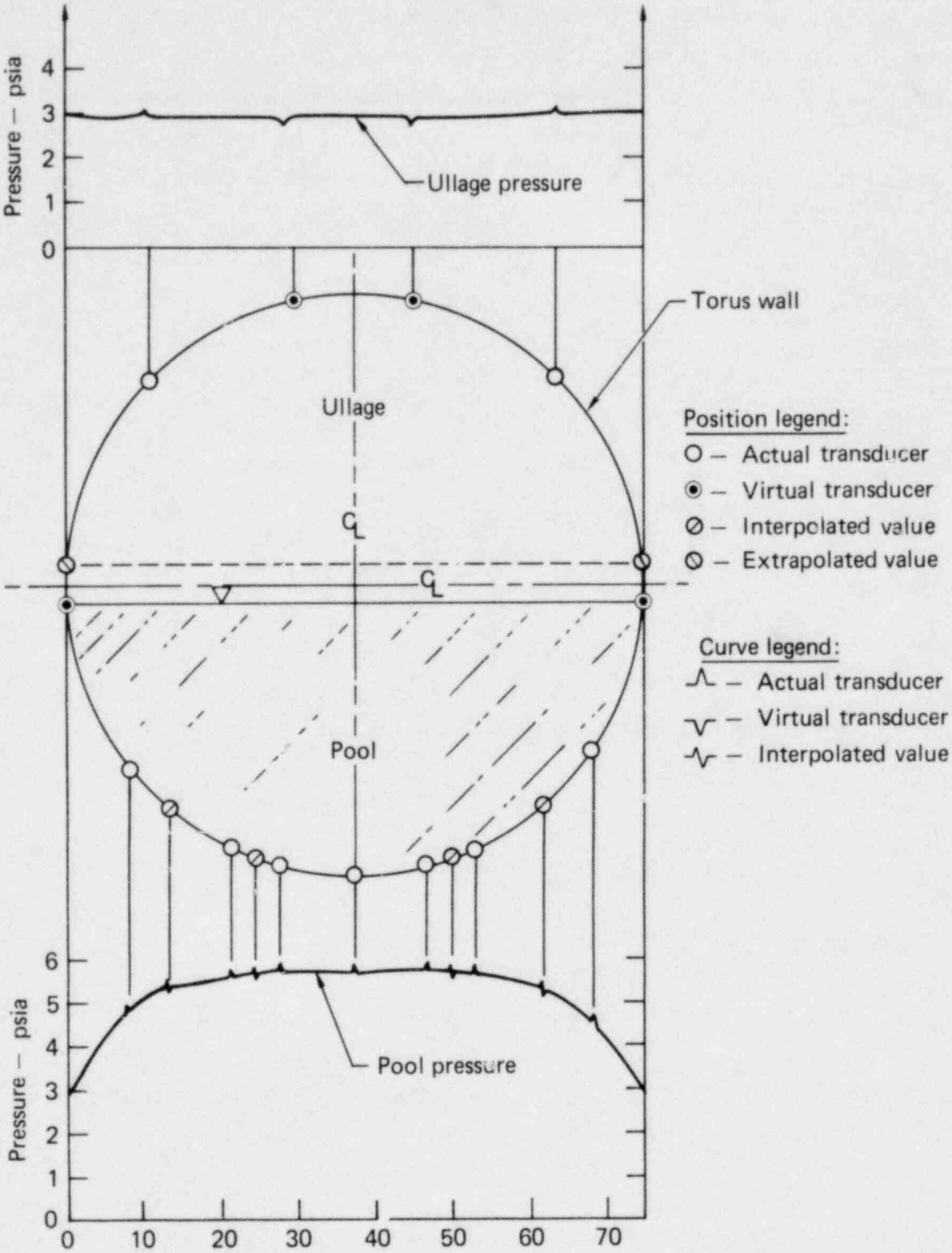

FIG. 1-4. Typical analytical pressure profiles in pool and ullage (Test 1.3.1 at time of peak download).

In this way we define a force per unit length (FUL) for each sector of the plane. A typical example from the 45° torus sector* is shown in Fig. 1-5 for the time of peak download. This procedure is repeated for all four instrumented planes in the 3-D facility and for the single plane of the 2-D facility. At this point, maximum utilization is made of symmetry planes in context with the additional pressure transducers located at pool bottom (180°) in planes 1, 3, and 5. The pool FULs of plane 11 are transferred to plane 1 after multiplying them by the ratio of the pool bottom pressures,† $P1(t)_{180^{\circ}}/P11(t)_{180^{\circ}}$, that is:

$$\text{FUL(plane 1)} = \text{FUL(plane 11)} \times \left(\frac{P1}{P11}\right)_{180^{\circ}} \qquad \text{(1-5a)}$$

similarly, for plane 3,

$$\text{FUL(plane 3)} = \text{FUL(plane 9)} \times \left(\frac{P3}{P9}\right)_{180^{\circ}} \qquad \text{(1-5b)}$$

and for plane 5,

$$\text{FUL(plane 5)} = \text{FUL(plane 6)} \times \left(\frac{P5}{P6}\right)_{180^{\circ}} \qquad \text{(1-5c)}$$

Additionally, to enlarge the axial fit data base in the pool, we take, for plane 4A,

$$\text{FUL(plane 4A)} = \text{FUL(plane 6)} \qquad \text{(1-5d)}$$

and for plane 8,

$$\text{FUL(plane 8)} = \text{FUL(plane 4)} \quad . \qquad \text{(1-5e)}$$

In a similar manner, the FULs for all 9 planes in the ullage are defined. Ullage transducers are, however, more sparsely located; therefore,

$$\text{FUL(plane 1)} = \text{FUL(plane 11)} \times \left(\frac{P2}{P11}\right)_{45^{\circ}} \qquad \text{(1-6a)}$$

---

*Using 4P(160°), 5P(165°), and 6P(180°) for angular sectors.

†For these tests where the plane 1-180° transducer was not available, the plane 1-195° transducer was used.

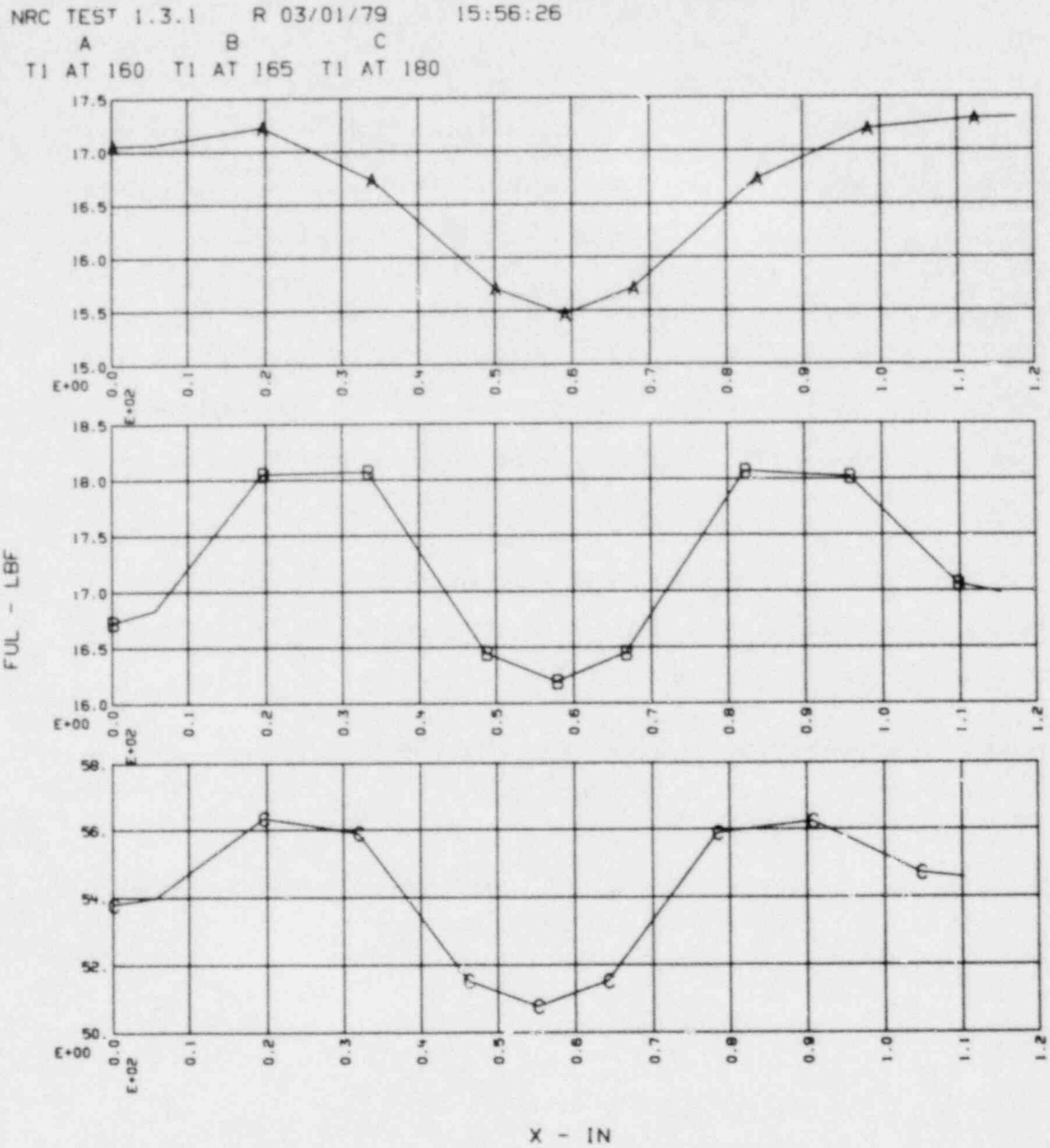

FIG. 1-5. Plot of vertical force per unit length (FUL) values along the 45° torus (sectors 4P, 5P, and 6P) at time of peak down force.

$$FUL(plane\ 3) = FUL(plane\ 9) \times \left(\frac{P2}{PI1}\right)_{45^o} \quad (1\text{-}6b)$$

$$FUL(plane\ 8) = FUL(plane\ 4) \quad (1\text{-}6c)$$

$$FUL(plane\ 4A) = FUL(plane\ 5) = FUL(plane\ 6)\ , \quad (1\text{-}6d)$$

where P2 refers to a transducer located in the ullage space, between planes 1 and 3, at an angle of $\theta = 45^o$.

Along the torus axis, a force per unit length (FUL) has now been defined at the 9 planes for each of the 12 pool sectors and each of the 5 ullage sectors. Each FUL is concentrated in-plane at the midpoint of the projection of each sector. The nine FUL values along each sector are then used to establish a corresponding analytical description of the vertical force distributed along the torus axis. Again, symmetry is invoked so the slope of the vertical force at both ends of the 45^o torus sector is constrained to be zero. Figures 1-6 and 1-7 provide a three-dimensional plot of the fitted FULs in sectors 6P and 3U of the 45^o torus sector, respectively, for a time period which includes both peak download and peak upload.

By proceeding in this manner, additional detailed information is generated regarding the three-dimensional nature of the dynamic loading in the theta (θ) direction as well as the axial (z) dimension. This information is useful in understanding the dynamic rotational loading of the torus structure during a hypothetical LOCA.

Finally, the HVL becomes

$$HVL_{net} = HVL_{ullage} - HVL_{pool}, \quad (1\text{-}7a)$$

where

$$HVL_{ullage} = \sum_{i=1}^{5} \int_0^{L_i} F_i(z)dz \quad (1\text{-}7b)$$

and

$$HVL_{pool} = \sum_{i=1}^{12} \int_0^{L_i} F_i(z)dz\ , \quad (1\text{-}7c)$$

where L_i equals the effective torus length for sector i. An example of the results of this procedure at the time of peak download is depicted in Fig. 1-8.

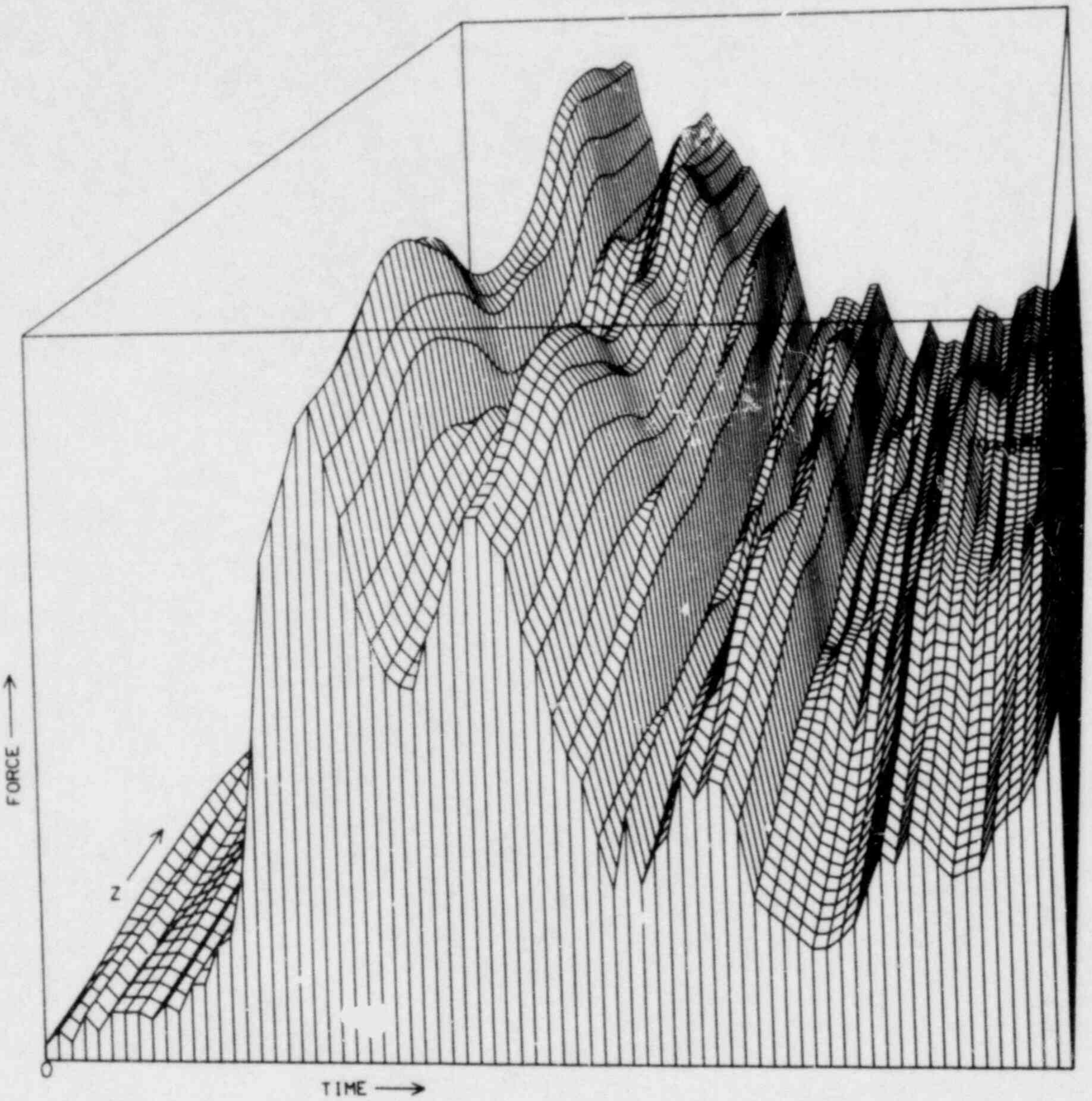

FIG. 1-6. Vertical force distribution in pool--sector 6P (165°-180°).

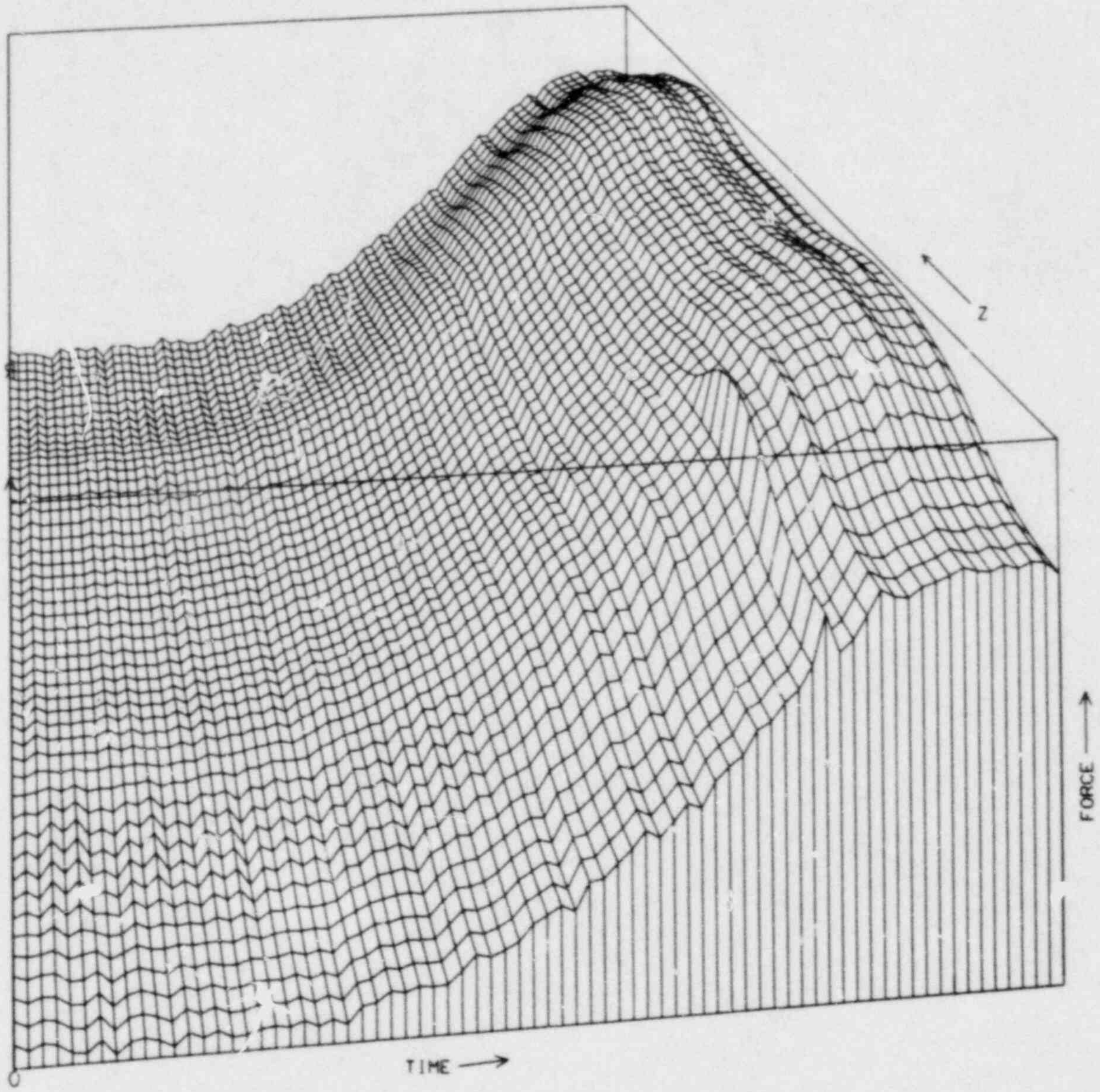

FIG. 1-7. Vertical force distribution in ullage--sector 3U (12°-348°).

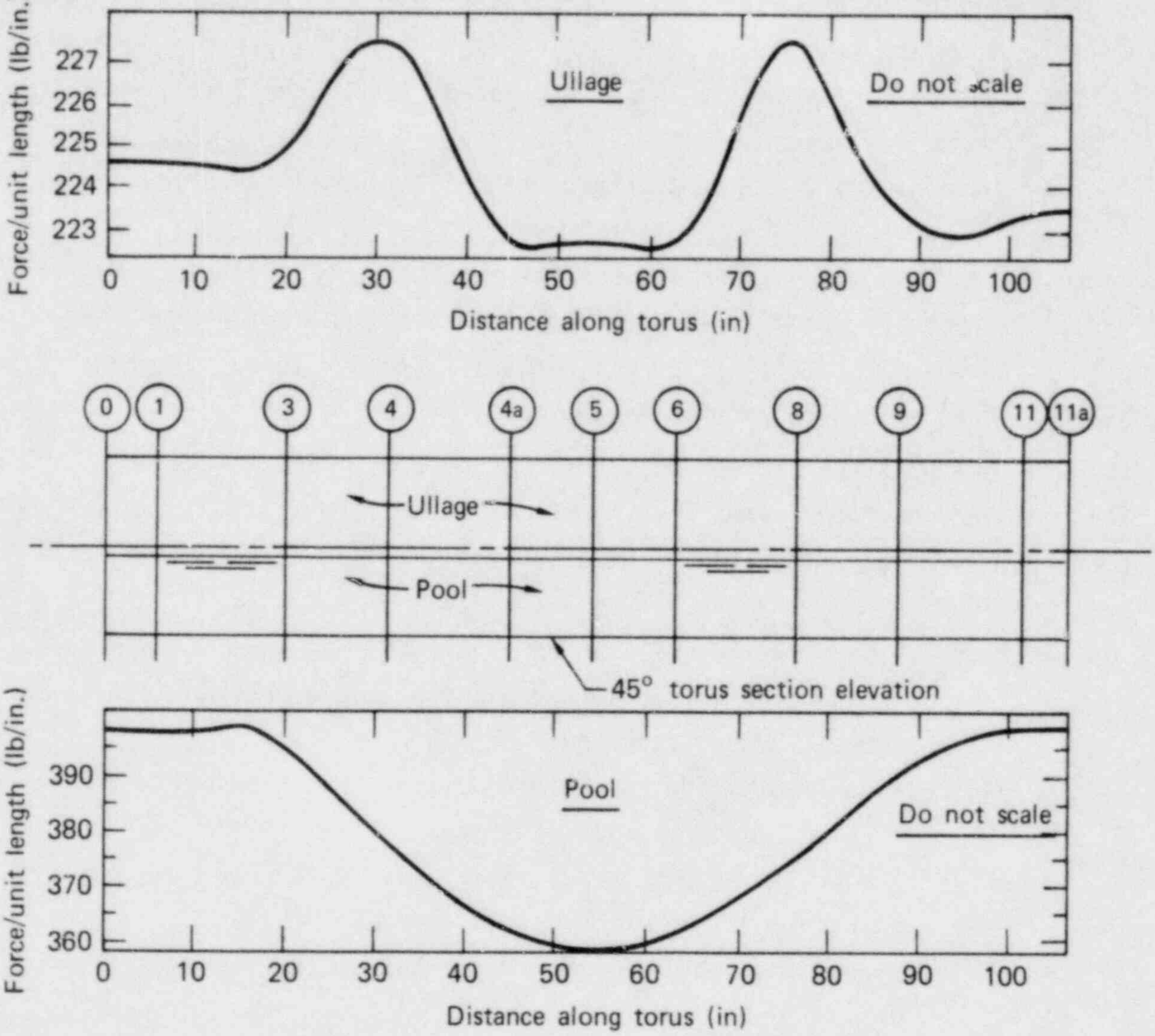

FIG. 1-8. Typical ullage and pool vertical force distributions along the torus axis at time of peak download.

1.1.5 CALCULATIONAL PROCEDURES

Four basic steps are required to proceed from raw pressure data to the final 3-D and 2-D hydrodynamic vertical load function. These steps are as follows:

- management of data records and retrieval of PSE pressure transducer data from archival storage,
- correction of the pressure data to account for systematic transducer error and static head,
- calculation of the HVLF and associated standard deviation using the corrected pressure data,
- postprocessing of computational results to obtain required output.

Because the HVLF calculation requires the systematic manipulation of up to 66 individual pressure data files for each of 24 tests, computer-aided methods of processing the PSE data on a production basis were developed to automate the calculational procedure as much as possible.

The pressure data are processed by four independent computer routines (controllees) developed specifically for the HVLF calculation. These routines, which are discussed in greater detail in Appendix C, are as follows:

- PSEPREP--performs general record management for the PSE data base, including extraction of all applicable pressure data files from archival storage.
- PRESLOC--calculates pool geometry and static head based on the elevation of the pool surface.
- INTERPP--corrects the PSE pressure data for systematic and random error and, where applicable, for static head.
- TORIS--calculates the HVLF and error based on the corrected pressure data.

A controller named PSEHVLF executes the PSEPREP, PRESLOC, and INTERPP routines to produce the input files required by the stand-alone TORIS code. Postprocessing of the HVLF results is executed using SOCKITTOME,[7] a general graphics postprocessor currently available and in use by Lawrence Livermore Laboratory's L-Division (computational physics).

1.1.5.1 Transducer Location Matrix

A separate version of the controller PSEHVLF is developed for each test. Each version specifies the pool levels of a particular test and the pressure transducers to be used in the subsequent HVLF calculation. To determine the final pressure transducer matrix for a given test correctly, an initial pass is made using PSEPREP to determine the particular transducers that are available.* This output, called MATRIX for AVAILABLE HVLF TRANSDUCERS, is then modified to delete transducers not required in the HVLF calculations and to specify virtual transducers in the ullage. The final matrix used in the PSEHVLF controller is called the MATRIX for ACTUAL + VIRTUAL HVLF TRANSDUCERS. Examples of these matrices for test 2.7 are included here as Table 1-1 and Table 1-2, respectively. The following steps are taken in the transition from available matrix to final matrix.

a) Reference to transducers in planes 7, 16, and 20 (P-14, P-56, and P-57) are eliminated.
b) Plane 1 transducers, not required (P-2, P-3, and P-5), are eliminated.
c) Virtual transducer assignments are specified for the ullage ($\Theta = 45^o$ through $\Theta = 315^o$). The assignments made for $\Theta = 90^-$ and $\Theta = 270^+$ are actually dummy assignments for ease in software development; these values are later determined from extrapolation of the fitted pressure data.
d) Virtual transducer assignments are specified at the pool end points ($\Theta = 90^+$ and $\Theta = 270^-$); however these data are replaced by the extrapolated ullage end points following analytical fitting of the ullage data.

1.1.5.2 Error Analysis--Pressure Corrections

The experimental pressure transducer outputs maintained in archival storage are unfiltered, calibrated data in engineering units (psia). As such, they have not been corrected for systematic error or for pool head (for those transducers located in the torus pool). In addition, no direct assignment of random error has been made.

---

*Based on the contents of the archival data record.

TABLE 1-1. Matrix of available transducers for test 2.7.

LOCATION MATRIX FOR AVAILABLE HVLF TRANSDUCERS

PSE TEST NUMBER: 2.7 DATE: Z 02/14/79

THETA	1	2	3	4	5	6	7	9	11	16	20	20
90												
45		P-110				P-30		P-43	P-45			P-75
12						P-29		P-42	P-7	P-56	P-57	
348												
315								P-55				P-86
270												
90												
128				P-17		P-31		P-44	P-8			P-76
140				P-18		P-32						
155	P-2			P-19		P-33		P-46	P-47			P-77
160				P-20		P-34						P-78
165	P-3			P-21		P-35		P-48	P-9			P-79
180	P-4		P-111	P-22	P-13	P-36	P-14	P-49	P-10			P-80
195	P-5			P-23		P-37		P-50	P-11			P-81
200						P-38						P-82
205				P-25		P-39		P-52	P-51			P-83
220				P-26		P-40						P-84
235				P-27		P-41		P-54	P-53			P-85
270												

TABLE 1-2. Final transducer matrix for test 2.7.

LOCATION MATRIX FOR ACTUAL+VIRTUAL HVLF TRANSDUCERS

PSE TEST NUMBER: 2.7 DATE: Z 02/14/79

THETA	1	2	3	4	5	6	7	9	11	16	20	2D
90-				P-30		P-30		P-43	P-45			P-75
45	P-110	P-110	P-110	P-30		P-30		P-43	P-45			P-75
12				P-29		P-29		P-42	P-7			P-75
348				P-29		P-29		P-42	P-7			P-85
315				P-30		P-30		P-55	P-45			P-86
270-				P-30		P-30		P-55	P-45			P-86
90+				P-30		P-30		P-43	P-45			P-75
128				P-17		P-31		P-44	P-8			P-76
140				P-18		P-32						
155				P-19		P-33		P-46	P-47			P-77
160				P-20		P-34						P-78
165				P-21		P-35		P-48	P-9			P-79
180	P-4		P-111	P-22	P-13	P-36		P-49	P-10			P-80
195				P-23		P-37		P-50	P-11			P-81
200						P-38						P-82
205				P-25		P-39		P-52	P-51			P-83
220				P-26		P-40						P-84
235				P-27		P-41		P-54	P-53			P-85
270-				P-30		P-30		P-55	P-45			P-86

During the air test series, separate experiments were conducted to establish the end-to-end (ETE) error and the random error of the installed pressure transducers.[4] Using dry torus sectors, the wetwells were pressurized in a stable manner from 1/5 atm to 1 atm using steps of 1/5 atm. Data were collected for 30 s. The data were processed at each pressure step in the normal manner and yielded calibrated data in engineering units. The actual pressure at each step was determined by a National Bureau of Standards (NBS) traceable gage that communicated to the wetwells. The calibrated data were then subjected to a least-squares analysis to determine the indicated mean pressure and its standard deviation. From this information a data base was developed specifying the systematic error (difference between apparent pressure and actual pressure) and the associated pressure dependent random error (standard deviation) for each of the transducers. The INTERPP routine (see Appendix C) was developed to expedite interpolation of the ETE data and the random error data associated with each calibrated data point from a particular pressure transducer. Each data point of each experimental pressure transducer history for the time interval of interest that was used to develop a HVLF is corrected as

$$p_C(t) = p_{obs}(t) - h + ETE \; ; \; t = t_{start} , t_{end} , \tag{1-8}$$

where p_C is the corrected pressure at time t, p_{obs} is the observed pressure at time t, h is the static head correction (pool transducers only), and ETE is the end-to-end or systematic error. Note that ETE may be positive or negative. Typical values for these corrections and the static head for the 11 pool transducers of nominal test 2.7 are indicated in Table 1-3. Table 1-4 lists the ETE and standard deviation data base of pool transducer P-40, which is located in plane 6 at 220° in the 3-D torus sector. The results of this operation for all transducers are written into a single ASCII disk file called INTORI. INTORI and the spatial definition file, DXDZ (see Appendix B), provide the required input for the TORIS code.

1.1.5.3 Error Analysis--Error Propagation

The corrected pressure sets provided by INTORI are used in the TORIS code to provide mean value estimates of the HVLF. In order to observe the effect of the random error associated with the pressure data, an additional pass through

TABLE 1-3. Typical static head corrections (test 2.7).

```
PSE TEST NUMBER:   2.7
90 DEG POOL ELEVATION (INCHES BELOW CENTERLINE):    2.40E+00
7.5 DEG POOL ELEVATION (INCHES BELOW CENTERLINE):    2.10E+00

CORRECTION FACTORS FOR STATIC HEAD (PSIA)

    THETA          HC90              HC7.5
    -----      ------------      ------------
     128        7.4037E-01        7.5121E-01
     140        9.4239E-01        9.5322E-01
     155        1.1308E+00        1.1416E+00
     160        1.1757E+00        1.1865E+00
     165        1.2109E+00        1.2217E+00
     180        1.2567E+00        1.2675E+00
     195        1.2109E+00        1.2217E+00
     200        1.1757E+00        1.1865E+00
     205        1.1308E+00        1.1416E+00
     220        9.4239E-01        9.5322E-01
     235        6.8384E-01        6.9467E-01
```

TABLE 1-4. Typical end-to-end corrections (pressure transducer P-40, plane 6-220^{o}).

Pressure, psia			
Actual	Apparent	ETE, psi	σ_p, psi
2.98	2.9819	-0.0019	0.0143
5.98	5.9500	+0.0300	0.0194
8.94	8.9825	-0.0424	0.0155
11.89	11.9320	-0.0420	0.0125
14.37	14.3960	-0.0260	0.0148

TORIS is taken to adjust the pressure data by one standard deviation, i.e., $p_C(t) = p_C(t) + \sigma_p$. This procedure is a drastic measure in the statistical sense, since it gives no weight to randomness. However, it provides an acceptable upper bound on the effect of random error on the computation of all values. This approach is acceptable due to the extremely small random errors associated with the pressure data. The approach is also effective in reducing the time required to complete the overall analysis, as the methodology for propagation of error would have necessitated extensive algebraic manipulation without producing any better understanding of the computed results.

Assuming a normal distribution of error, we estimate propagated error for pool force, ullage force, and net vertical force at each of the four peak load times.* The standard deviation associated with the 3-D to 2-D force ratio at these times is also computed. In these calculations we use the following equations:

$$\sigma_p = |F_p^{mean} - F_p(+\sigma_p)| \tag{1-9a}$$

$$\sigma_u = |F_u^{mean} - F_u(+\sigma_p)| \tag{1-9b}$$

$$F_N = F_p + F_u \tag{1-9c}$$

so that

$$\sigma_N^2 = \left(\frac{\partial F_N}{\partial F_p}\right)^2 \sigma_p^2 + \left(\frac{\partial F_N}{\partial F_u}\right)^2 \sigma_u^2 \tag{1-9d}$$

$$= \sigma_p^2 + \sigma_u^2 \ ,$$

where

F_p^{mean} = mean pool force

$F_p(+\sigma_p)$ = pool force at $p_c = p_c + \sigma_p$

F_u^{mean} = mean ullage force

---

*The four times chosen to characterize peak forces in the HVLF are associated with a) first peak down force, b) first force reversal, c) second peak down force, and d) peak up force.

$F_u(+\sigma_p)$ = ullage force at $p_c = p_c + \sigma_p$

F_N = mean net force

σ_u = standard deviation of mean ullage force

σ_p = standard deviation of mean pool force

σ_N = standard deviation of mean net force.

These quantities are computed for both the 45° torus sector and the 7.5° torus sector at the four times of interest. The force ratio at a given time of interest is

$$R = \frac{F_N^{45^\circ}}{6 \times F_N^{7.5^\circ}} \tag{1-10}$$

so that

$$\sigma_R^2 = \left(\frac{\partial R}{\partial F_N^{45^\circ}} \right)^2 (\sigma_N^{45^\circ})^2 + \left(\frac{\partial R}{\partial F_N^{7.5^\circ}} \right)^2 (\sigma_N^{7.5^\circ})^2 \tag{1-11a}$$

$$= (6F_N^{7.5^\circ})^2 (\sigma_N^{45^\circ}) + \left(\frac{R}{F_N^{7.5^\circ}} \right)^2 (\sigma_N^{7.5^\circ})^2 . \tag{1-11b}$$

These estimates of error are included in the force summary table for each test, as discussed in the following section.

1.1.5.4 TORIS Code--Theory, Operation, and Output

The primary purpose in developing the TORIS code was to compute the HVLF and its associated error in a best estimate manner. Due to the complexities introduced by the many input pressure histories (each with 525 data points)*

---

*Corresponds to 1.5 seconds of a test and chosen to encompass the peak vertical loads of primary interest.

and the three-dimensional nature of the calculations, a complete hand calculation was done before code writing began. This was completed, both in-plane and along the axis for test 1.3.1, using trapezoidal fitting for the times of peak download and peak upload. The resulting quantification of all interpolated pressures in the instrumented planes as well as the FULs and the integral pool and ullage forces in each of the 17 pool and ullage sectors provided a set of detailed guides and checks during the subsequent code writing.

The hydrodynamic vertical load function is calculated twice for each experiment: first, using a trapezoidal integration scheme; then, using a sliding parabolic integration scheme. The trapezoidal method is computationally faster and amenable to hand calculation, but the sliding parabolic method represents the physical constraints of the experiments far better, and therefore, the results can be accepted with greater confidence.

Every numerical integration method has an implied interpolation method associated with it. To provide processing checks and report graphics, this implied interpolation is made explicit by preceding the integration with the calculation of interpolation function coefficients. The integration is then performed using these coefficients explicitly.

Two sets of interpolation coefficients are developed for each time point of the experimental data. One set for the pressures* in each plane along X, and one for the force per unit length distribution along Z (FUL) in each angular sector.

The interpolation differs mathematically between these two sets only in the constraints imposed upon the end zones, i.e., for each plane, at X = 0 and at the relevent pool or ullage width (PW or UW), and for each angular sector, at $Z = 0$ and at $Z = Z_{max}$ along the torus.

---

*This includes actual, virtual and interpolated pressures. (See Fig. 1-4.)

The ranges of the independent variable X and Z are divided into segments either by the position of the experimentally determined pressure (along X) or the position of FULs (in each angular sector). The pressure positions are governed by transducer location, while the FUL positions are governed by the instrumented planes. The in-plane pressures are designated by p_i where the correspondence between i and angular position* is shown in the following tabulation:

Pool		Ullage	
i	θ	i	θ
0	90^+	0	90^-
1	128°	1	45°
2	140°	2	12°
3	155°	3	348°
4	160°	4	315°
5	165°	5	270^+
6	180°		
7	195°		
8	200°		
9	205°		
10	220°		
11	235°		
12	270^-		

The pool index, i = 0, corresponds to the pool edge nearest the torus edge of greatest major radius (X = 0), whereas i = 12 corresponds to the pool edge nearest the torus edge of least major radius (X = PW). There is a similar correspondence for the ullage indices, i = 0 (X = 0) and i = 5 (X = UW). Pressure interpolation using the trapezoidal interpolation function for each interval (X_i, X_{i+1}) is given by

$$A_i + B_i X \qquad (1\text{-}12a)$$

---

*See Figs. 1-1, 1-2, and 1-3.

where A_i and B_i are such that

$$A_i + B_i X_i = p_i \tag{1-12b}$$

$$A_i + B_i X_{i+1} = p_{i+1} \quad . \tag{1-12c}$$

For sliding parabolic pressure interpolation, two sets of coefficients are developed for each interval (X_i, X_{i+1}), as follows:

$$A_j + B_j X + C_j X^2 \tag{1-13a}$$

$$A_{j+1} + B_{j+1} X + C_{j+1} X^2 \quad , \tag{1-13b}$$

where

$$A_j + B_j X_{i-1} + C_j X_{i-1}^2 = p_{i-1} \tag{1-13c}$$

$$A_j + B_j X_i + C_j X_i^2 = p_i = A_{j+1} + B_{j+1} X_i = C_{j+1} X_i^2 \tag{1-13d}$$

$$A_j + B_j X_{i+1} + C_j X_{i+1} = p_{i+1} = A_{j+1} + B_{j+1} X_{i+1} + C_{j+1} X_{i+1}^2 \tag{1-13e}$$

$$p_{i+2} = A_{j+1} + B_{j+1} X_{i+2} + C_{j+1} X_{i+2}^2 \quad . \tag{1-13f}$$

Over each such interval an angle, α, is associated with x by

$$\alpha = \frac{\pi(X-X_i)}{2(X_{i+1}-X_i)} \quad . \tag{1-14}$$

The interpolation function is then given by

$$p = \left[A_j + B_j X + C_j X^2\right] \mathrm{Cos}^2\alpha + \left[A_{j+1} + B_{j+1} X + C_{j+1} X^2\right] \mathrm{Sin}^2\alpha \quad . \tag{1-15}$$

For trapezoidal interpolation, the conditions imposed upon the ullage pressure at X = 0 and X = UW are given by $p_0^u = p_1^u$ and $p_5^u = p_4^u$, respectively, so that the pressure is treated as constant over these end segments.

For sliding parabolic interpolation, each of the two ullage segments $\langle X_1, X_2 \rangle$ and $\langle X_3, X_4 \rangle$ are represented by a single set of parabolic coefficients. The pressure P_0^u is the value arrived at by evaluating the interpolation function for $\langle X_1, X_2 \rangle$ at X = 0; p_5^u is similarly determined by evaluating the function for $\langle X_3, X_4 \rangle$ at X = UW. The p_0^u

and p_5^u values are simple extrapolations from adjacent segments; therefore, segment $\langle X_0, X_2 \rangle$ is represented by a single set of parabolic coefficients, as in $\langle X_3, X_5 \rangle$. In theory, a minimum set of ullage pressure values, either $[p_1, p_2, p_4]^u$ or $[p_1, p_3, p_4]^u$, must be assigned to the ullage before interpolation proceeds. If only a minimum set is assigned, then the sliding parabolic interpolation scheme amounts to evaluating a single set of parabolic coefficients. In practice, assignments were made for p_1 through p_5 for all tests (see Section 1.1.4).

Before either interpolation is used on the pool pressure data in a particular plane, the pool pressure, p_0^p, is assigned the ullage value, p_0^u, and the pool pressure p_{12}^p, is assigned the ullage value p_5^u. These assignments establish the end segment conditions for both interpolation schemes. A set of coefficients is determined for the trapezoidal interpolation and a single set of parabolic coefficients is determined for sliding parabolic interpolation for segments $\langle X_0, X_1 \rangle$, and $\langle X_{11}, X_{12} \rangle$.

As has already been described, the interpolation function is integrated separately over each segment to arrive at the FUL for each angular sector at each plane calculated. Mapping of the forces calculated from instrumented planes into symmetrical positions occurs according to the conventions described in Section 1.1.4. The FUL interpolation along the axis proceeds in the manner described for ullage pressure; therefore, for trapezoidal interpolation, $FUL_0 = FUL_{\text{plane 1}}$ and $FUL_{Z\text{max}} = FUL_{\text{plane 11}}$.

The values of FUL_0 and $FUL_{Z_{max}}$ for the sliding parabolic interpolation are governed by a different constraint, namely, that the first derivative of the interpolation shall be zero at $Z = 0$ and $Z = Z_{max}$. These latter conditions retain the continuity of the first derivative across the symmetry planes of the experimental torus at its ends.

In the final calculation, the vertical force contribution for each angular sector is evaluated, the forces for both the pool and ullage angular sectors are summed and, finally, the pool force is subtracted from the ullage force giving the final net hydrodynamic vertical force.

The primary thrust of the results we report here are based on the use of the parabolic fitting procedures, which do not lend themselves to ease in checking using hand calculations. For this reason, companion HVLF results using trapezoidal fitting were developed for each test.

The set of output information that characterizes the hydrodynamic vertical load function and associated error for each of the air transient tests consists of the following:

a) a force summary table including 3-D and 2-D force ratios, with associated errors, for each of four characteristic times,[*]
b) plots of the HVLF for the 45° torus section and the 7.5° torus sector, and a co-plot of the 45° HVLF and the 7.5° HVLF (multiplied by six),
c) plots of the analytically fitted along-axis total force distribution at the four characteristic times for both the pool and the ullage, and for the net force,[†]
d) plots of the analytically fitted in-plane pressure profiles at the four characteristic times for both pool and ullage for planes 4, 6, 9, 11, and a plot of the 2-D pressure profile,
e) discrete, along-axis, FUL plots for the 12 pool and 5 ullage sectors at the four characteristic times.

Examples of this information, taken from test 1.3.1, are shown in Figs. 1-9 through 1-13. A full set of this output data for test 1.3.1 characterizing the best estimate analysis for both the parabolic and trapezoidal fitting procedures, is included in Appendix D. In our general reporting of results, primary focus is placed on the output resulting from use of the preferred parabolic fitting method. This output information for all tests is contained in the fiche of Appendix E. Additional information on the results obtained using the trapezoidal fitting, also provided in Appendix E, is limited to the force summary tables. In general, when the results are compared, the parabolic fitting procedure results in somewhat higher force values than the trapezoidal. The force ratios are, however, little changed.

---

[*] See footnote, page 1-20.

[†] The 2-D and 3-D mean forces with associated standard errors are also included on the net force plot. See Fig. 1-11c.

```
NRC AIR TEST NO. 1.3.1                                          SECOND ORDER

                    FORCE SUMMARY  (MEAN    STANDARD DEVIATION)

45 DEGREE SECTOR - 3D
                    T1               T2               T3               T4

TIME,SECONDS   3.1126E+00       3.1269E+00       3.1470E+00       3.2472E+00

POOL        -40773.  111.4   -35048.  109.6   -39261.  103.0   -32387.   19.3

ULLAGE       23892.   69.7    24401.   81.9    25808.  106.9    40617.  401.8

NET         -16882.  131.5   -10647.  136.8   -13454.  148.4     8230.  402.2


7.5 DEGREE SECTOR - 2D
                    T1               T2               T3               T4

TIME,SECONDS   3.1069E+00       3.1212E+00       3.1327E+00       3.2358E+00

POOL          -6663.   15.0    -5592.   14.8    -6329.   15.0    -5397.   14.5

ULLAGE         3935.   11.4     4041.   11.5     4121.   11.6     6562.   12.7

NET           -2728.   18.8    -1551.   18.8    -2208.   19.0     1164.   19.3


NET FORCE RATIOS

3D/2D          1.031  0.011     1.144  0.020     1.016  0.014     1.178  0.061
```

FIG. 1-9. Parabolic fit force summary table, test 1.3.1.

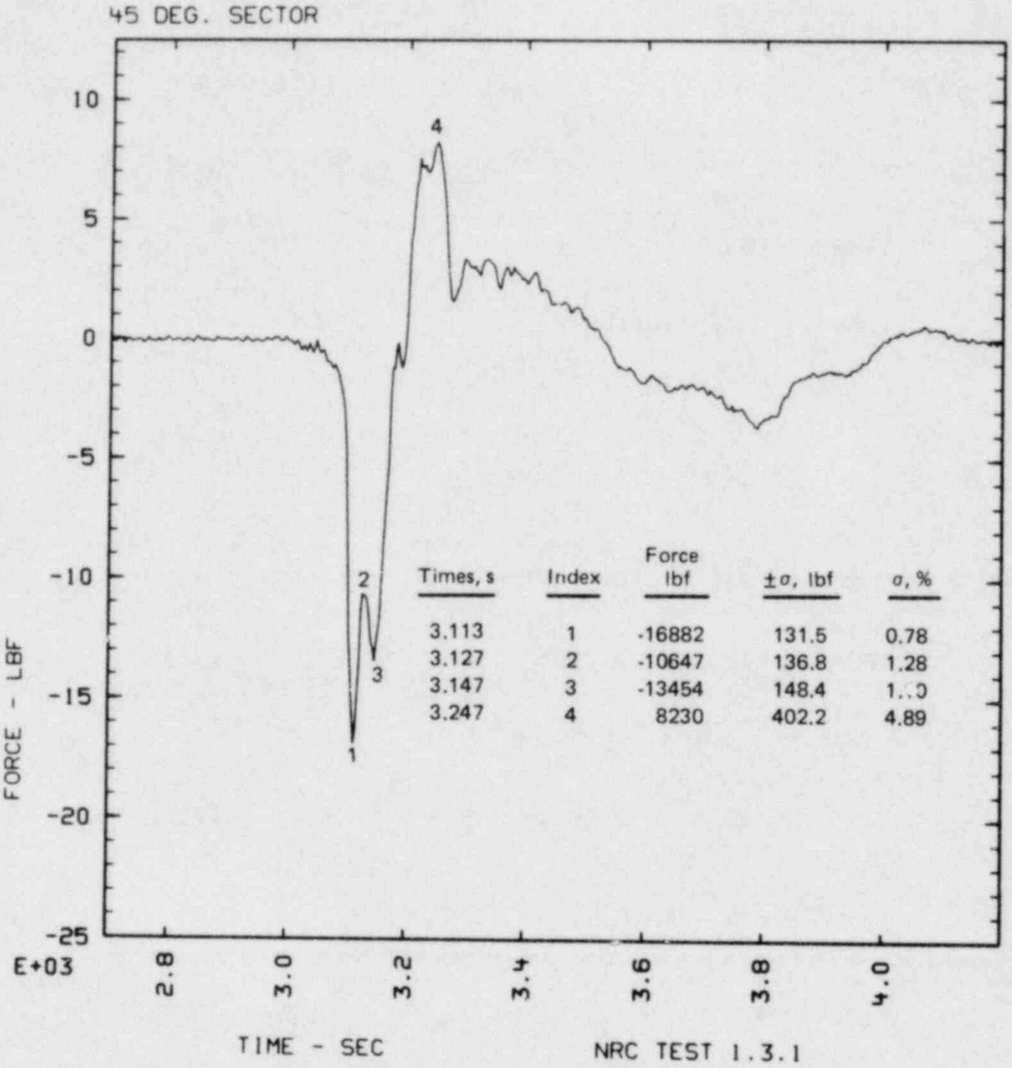

Times, s	Index	Force lbf	±σ, lbf	σ, %
3.113	1	-16882	131.5	0.78
3.127	2	-10647	136.8	1.28
3.147	3	-13454	148.4	1.10
3.247	4	8230	402.2	4.89

FIG. 1-10a. 3-D HVLF, test 1.3.1.

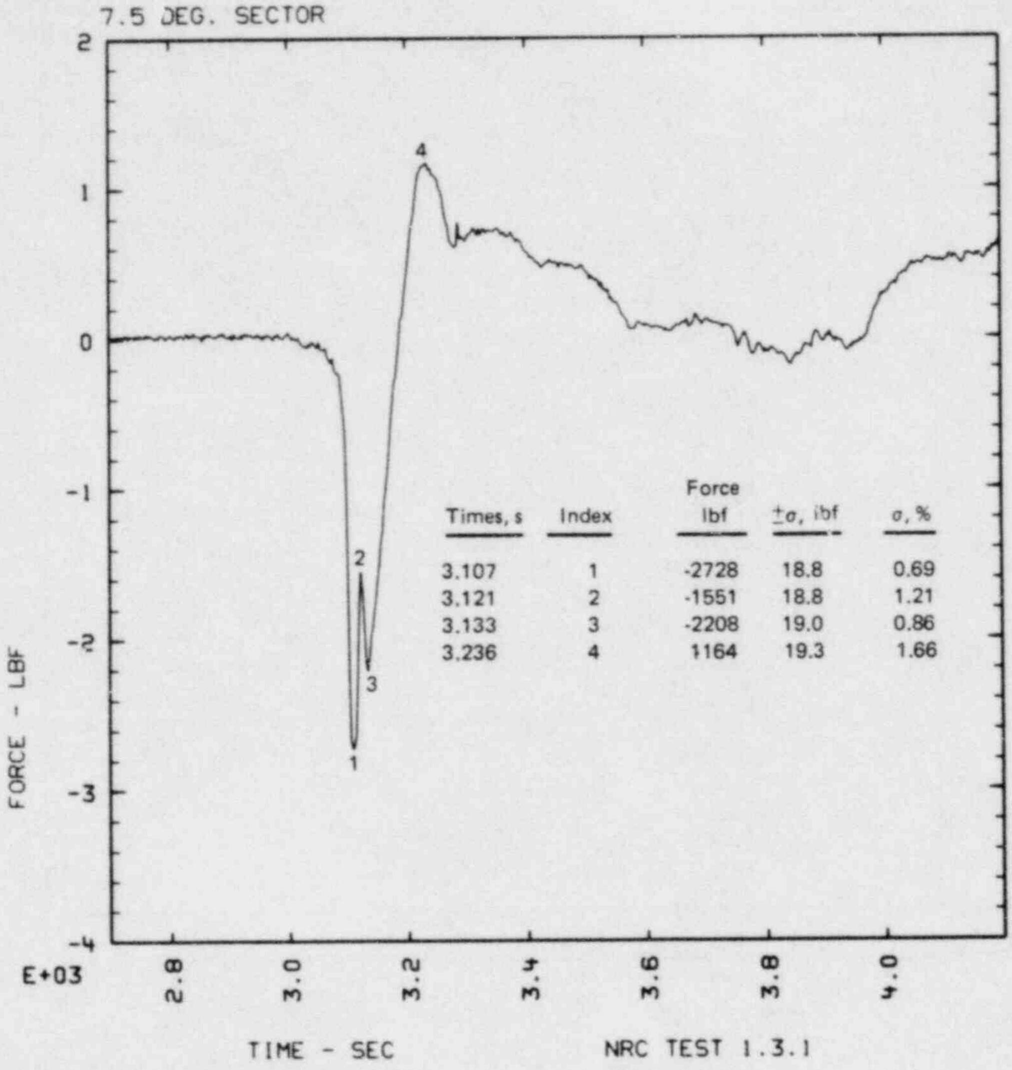

Times, s	Index	Force lbf	±σ, lbf	σ, %
3.107	1	-2728	18.8	0.69
3.121	2	-1551	18.8	1.21
3.133	3	-2208	19.0	0.86
3.236	4	1164	19.3	1.66

FIG. 1-10b. 2-D HVLF, test 1.3.1.

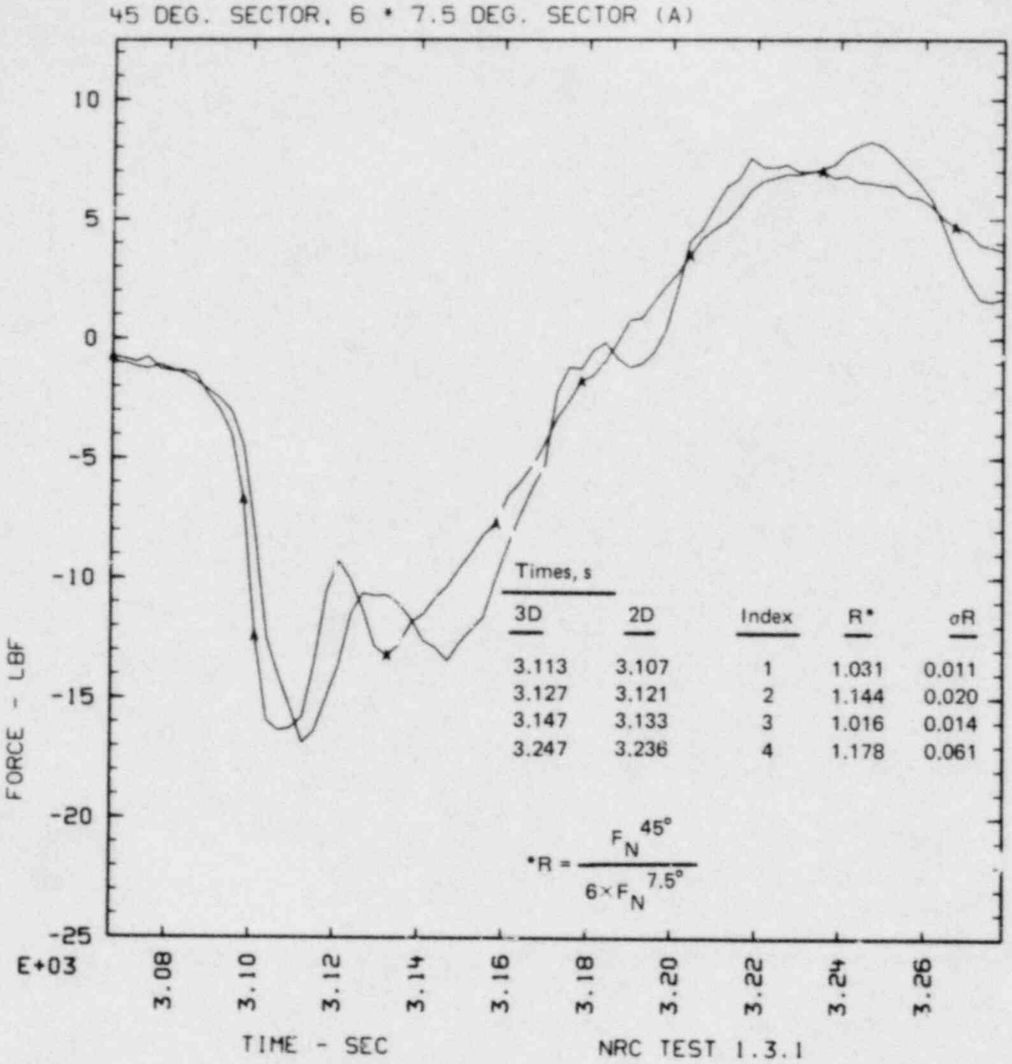

Times, s				
3D	2D	Index	R*	σR
3.113	3.107	1	1.031	0.011
3.127	3.121	2	1.144	0.020
3.147	3.133	3	1.016	0.014
3.247	3.236	4	1.178	0.061

$$^*R = \frac{F_N^{45°}}{6 \times F_N^{7.5°}}$$

FIG. 1-10c. 2-D HVLF multiplied by six and overlaid on 3-D HVLF, test 1.3.1 (3.066 s to 3.276 s).

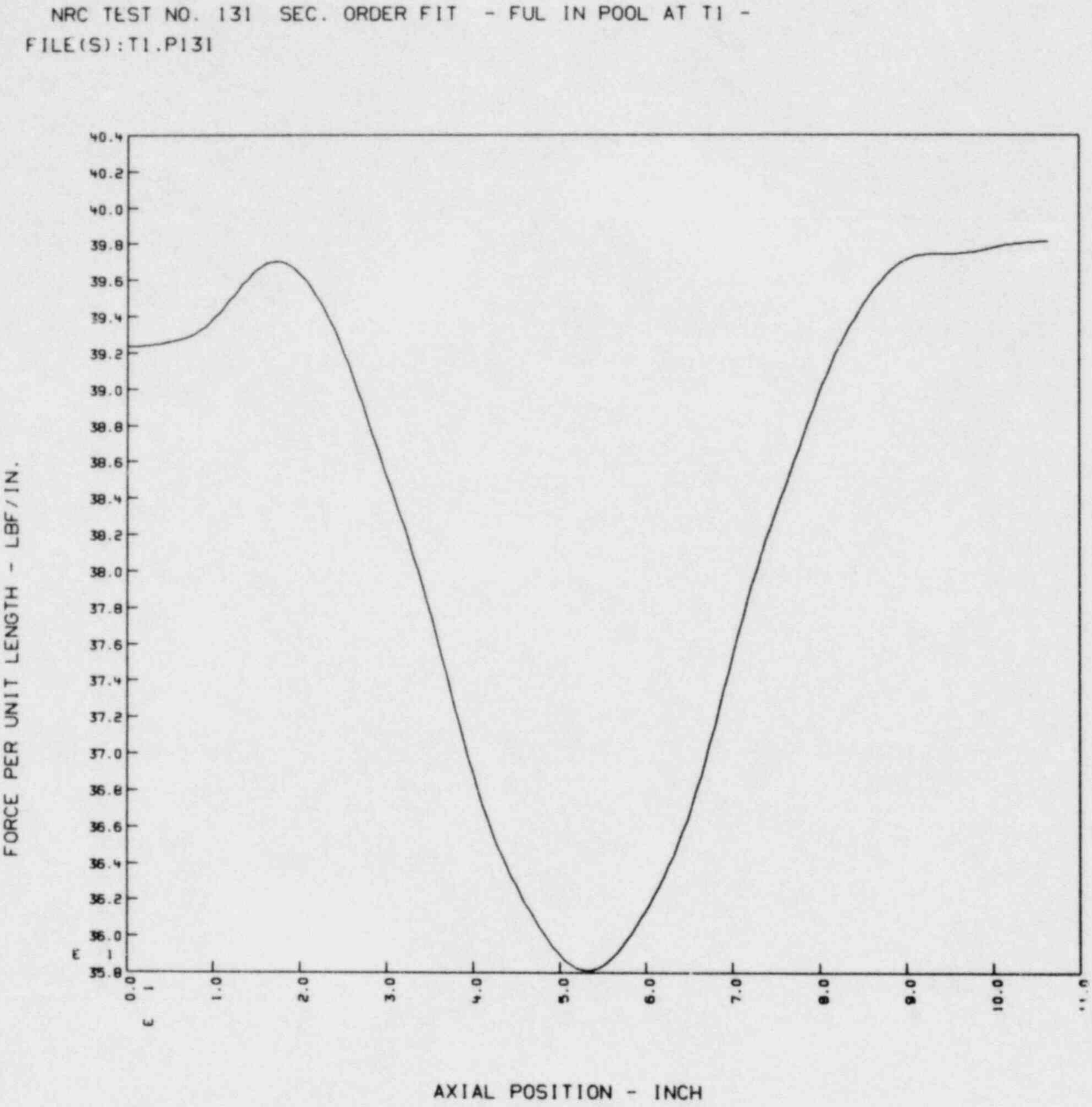

FIG. 1-11a. Force per unit length (FUL) versus axial position in 3-D pool at time T_1, test 1.3.1.

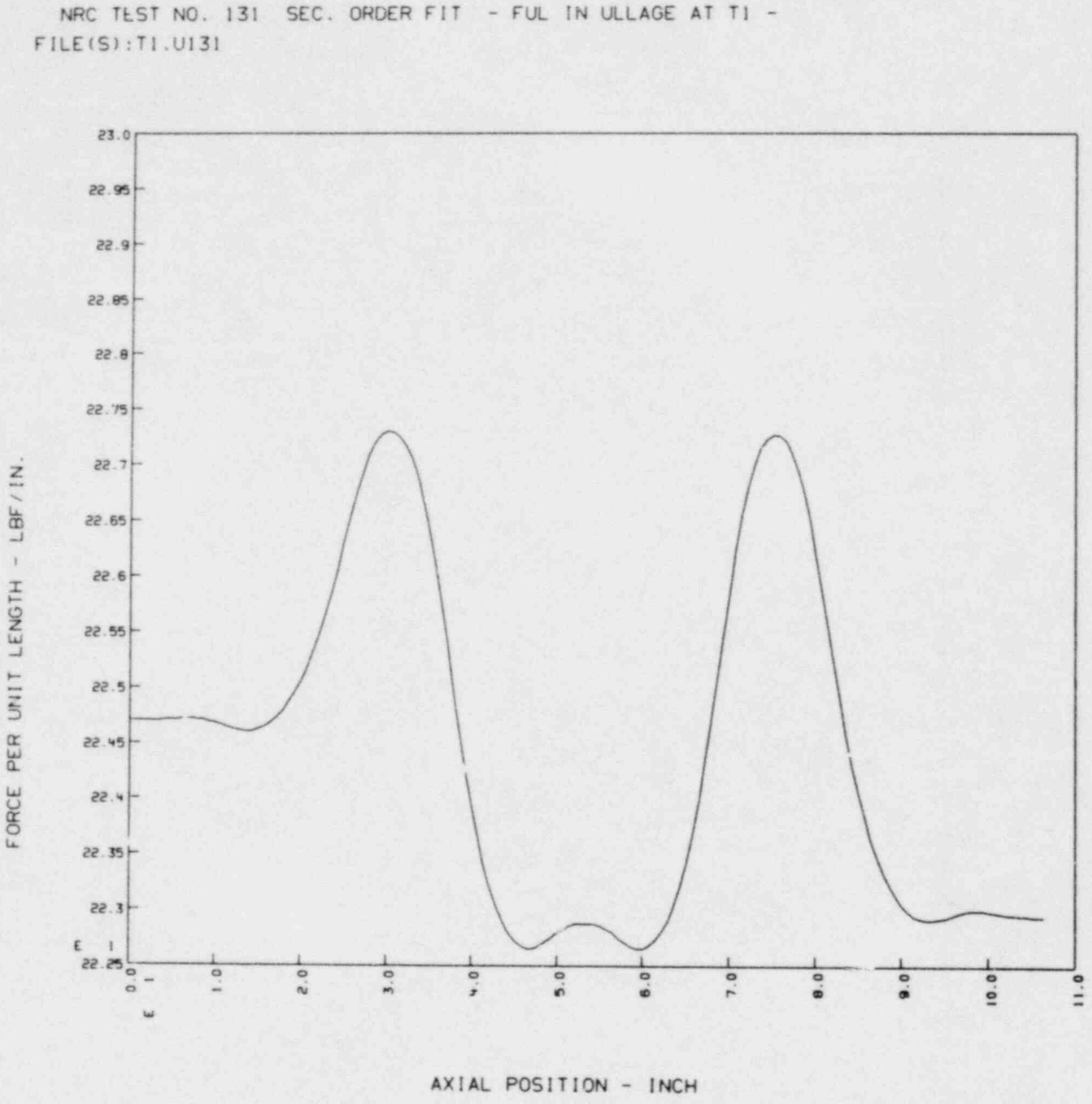

FIG. 1-11b. Force per unit length (FUL) versus axial position in 3-D ullage at time T_1, test 1.3.1.

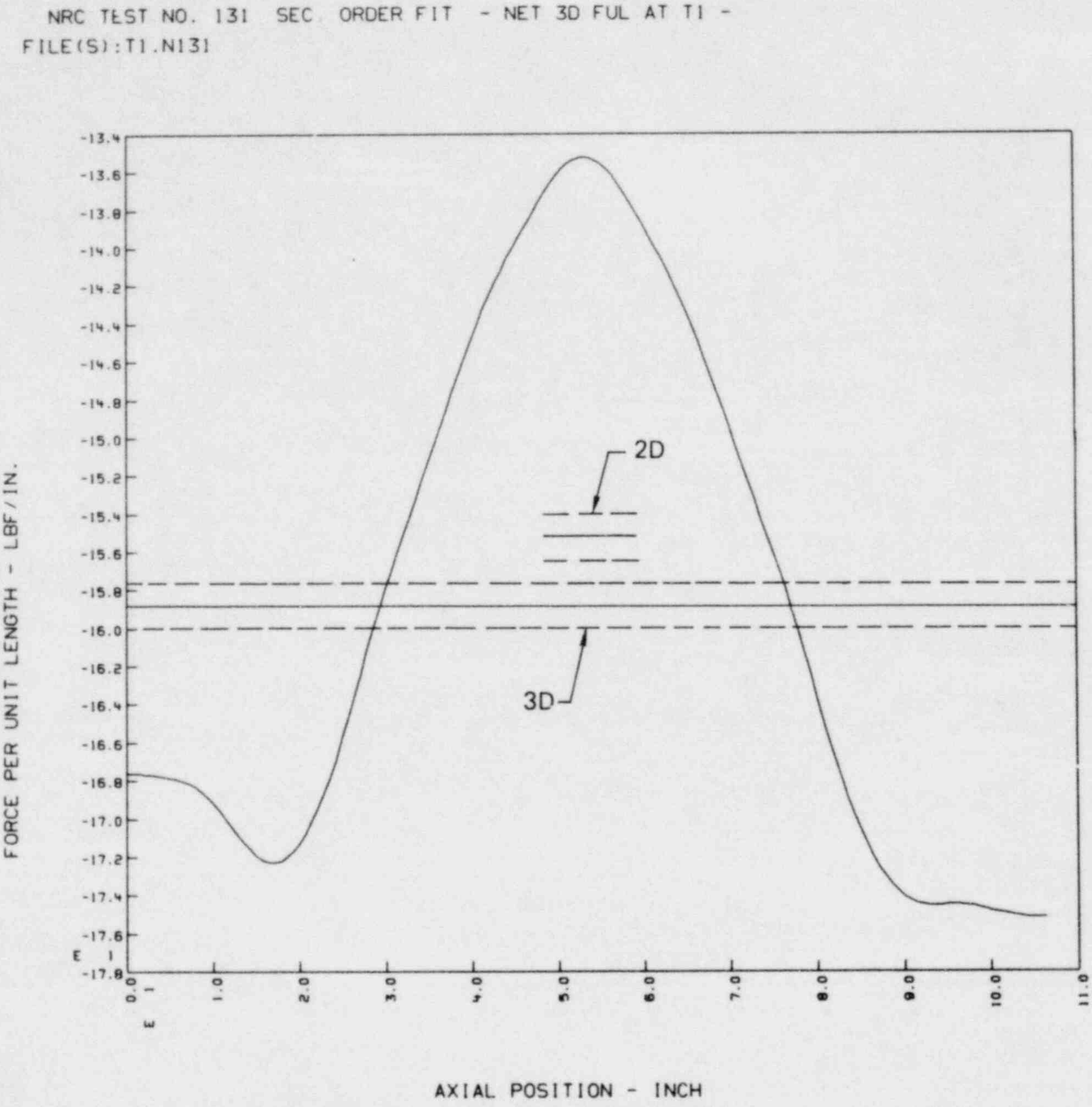

FIG. 1-11c. Net FUL versus axial position in the 45^0 sector at time T_1, test 1.3.1, with 3-D and 2-D mean force included.

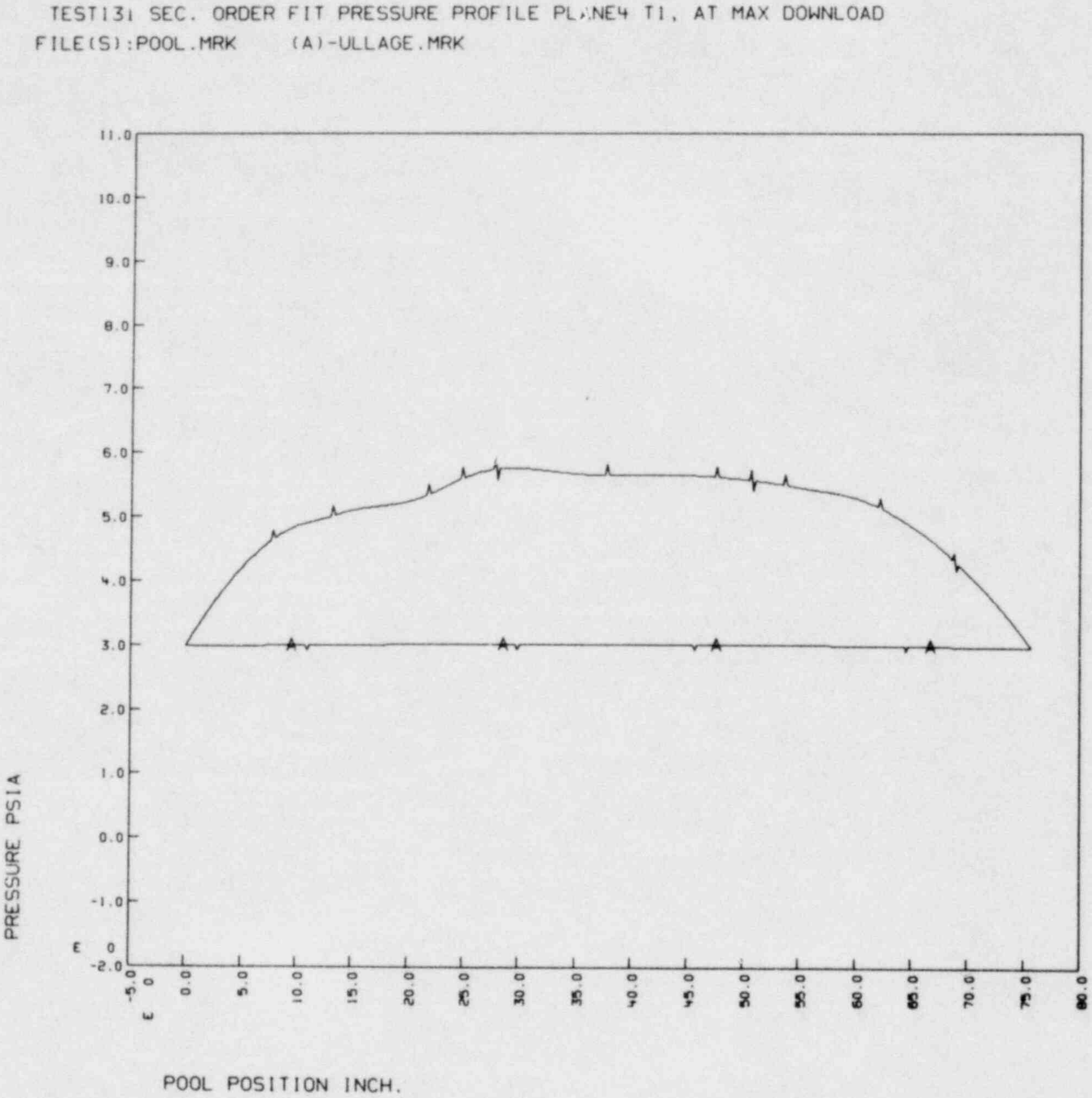

FIG. 1-12. Pool and ullage pressure profiles in plane 4 at time T_1, test 1.3.1.

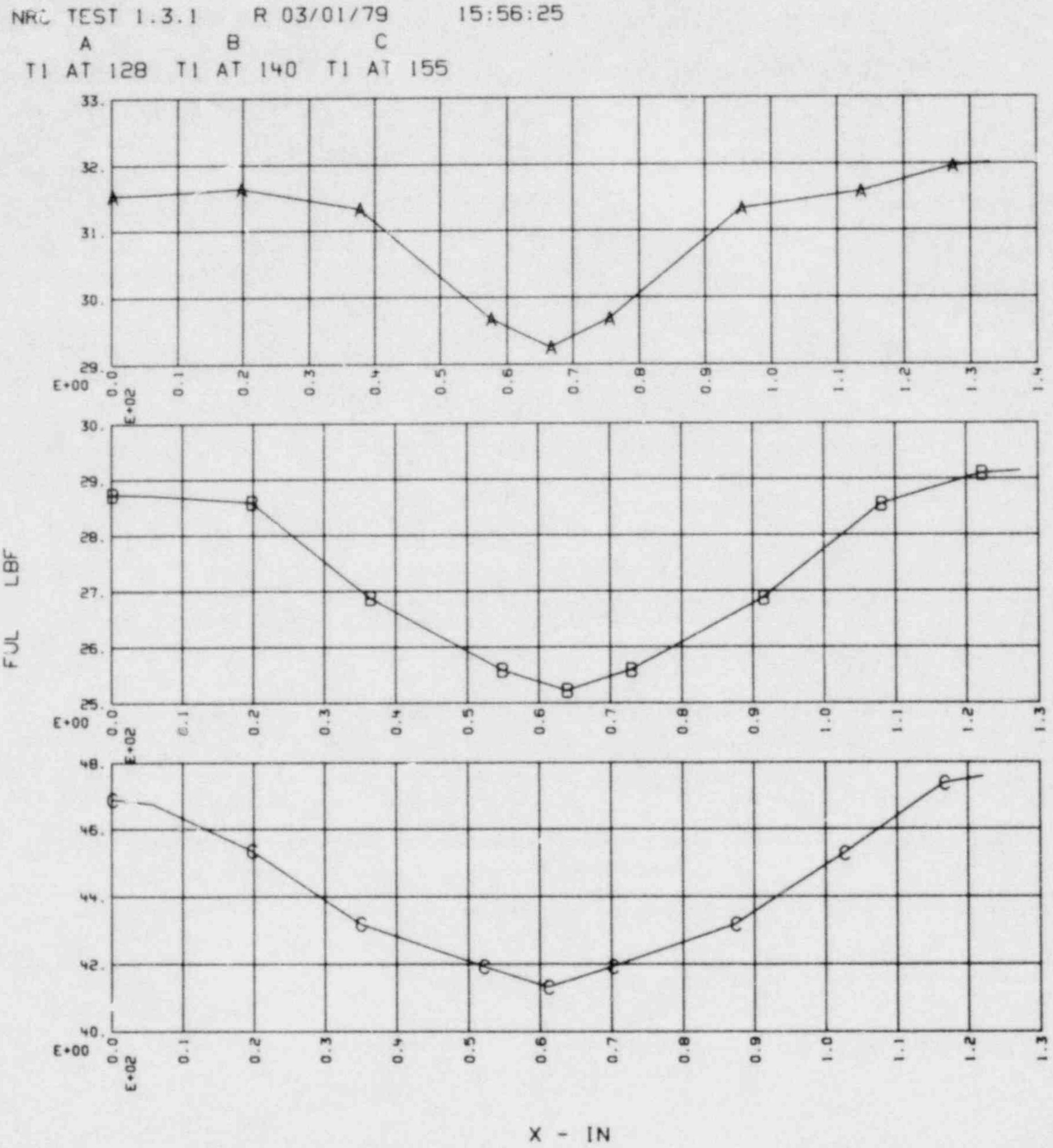

FIG. 1-13. Typical discrete plots of FUL versus axial position, test 1.3.1.

1.1.6. DISCUSSION OF RESULTS FROM THE BEST ESTIMATE HVLF ANALYSIS

The best estimate analysis of the hydrodynamic vertical load function is complete, and standard deviation estimates have been provided for the peak forces determined. A summary of the findings is provided in Table 1-5, including 45^{o}-sector peak force values, 2-D and 3-D peak force ratios, and associated standard deviations. A short description of the purpose of each test and the mean drywell pressurization rate of each test are also included in Table 1-5. Table 1-6 shows the 7.5^{o}-sector peak force values and associated standard deviations.

Study of the peak downloads and uploads developed from this work indicates that the previous HVLF calculations[1] conservatively overestimated the peak downloads by approximately 15 percent and the peak uploads by 9 percent. The ratios of peak forces have, however, remained relatively unchanged.

In general, we conclude that the 2-D (7.5^{o}) torus sector provides a useful test facility for prediction of peak down force because 3-D to 2-D down force ratios are near unity for all test conditions. This is not the case for prediction of peak upload, where this ratio approaches unity in only a limited number of cases, one of which includes the nominal condition tests. This further indicates that while the 2-D facility provides a valid geometrical average cell, it does not represent an average fluid dynamical system.

The accumulated HVLF errors are small, as expected based on previous study of the highly accurate pressure data.[4] The standard error on peak down forces ranges from 0.5 percent to 1.4 percent. The corresponding error on peak up forces ranges from 3.2 percent to 5.8 percent.

TABLE 1-5. Peak force results summary--hydrodynamic vertical load function (45° sector).

		T_1				T_2				T_3				T_4				
Test no.	$\bar{\dot{P}}dw$, psi/s	$\downarrow F$, lb$_f$	σ_F, lb$_f$	R^2	σ_R	$\downarrow F$, lb$_f$	σ_F, lb$_f$	R^2	σ_R	$\downarrow F$, lb$_f$	σ_F, lb$_f$	R^2	σ_R	$\uparrow F$, lb$_f$	σ_F, lb$_f$	R^2	σ_R	Test conditions
1.1	25.0	14760	193	0.87	0.01	7890	147	n.d.	-	10560	163	n.d.	-	7650	369	1.18	0.06	Nominal
1.3	26.0	16360	127	0.82	0.01	9700	133	n.d.	-	12640	146	n.d.	-	7470	414	1.29	0.08	Nominal
1.3.1	27.2	16880	132	1.03	0.01	10650	137	1.14	0.02	13450	148	1.02	0.01	8230	402	1.18	0.06	Nominal
1.4	18.4	13450	134	1.08	0.01	6760	137	0.96	0.02	10100	150	1.07	0.02	6980	328	1.03	0.05	Drywell p
1.5	30.0	18240	135	1.00	0.01	11840	141	1.05	0.02	14560	156	1.02	0.01	8630	425	1.11	0.06	Drywell p
1.6	34.9	16790	135	0.925	0.01	12790	141	1.08	0.02	15110	157	0.95	0.01	9110	491	1.23	0.07	Drywell p
2.1	28.7	n.d.	-	n.d.	-	n.d.	-	n.d.	-	12530	134	1.03	0.02	7160	331	1.10	0.05	Drywell Δp
2.2	25.7	n.d.	-	n.d.	-	n.d.	-	n.d.	-	9670	134	1.08	0.02	6340	299	1.18	0.06	Drywell Δp
2.3	26.6	n.d.	-	n.d.	-	n.d.	-	n.d.	-	9800	140	1.14	0.02	6190	321	1.20	0.07	Drywell Δp
2.4	24.3	16600	136	0.99	0.01	9200	143	1.07	0.02	12430	156	1.14	0.02	8370	395	1.30	0.07	Nominal
2.5	27.1	24760	128	1.08	0.01	7500	152	n.d.	-	11340	166	n.d.	-	9050	489	0.93	0.05	Pool level raised
2.6	25.4	n.d.	-	n.d.	-	9320	134	1.18	0.02	11490	136	1.14	0.02	5330	252	1.17	0.06	Pool level lowered
2.7	23.6	19580	132	1.06	0.01	8580	137	n.d.	-	13360	149	n.d.	-	9290	410	1.04	0.05	Downcomer extended
2.8	23.7	16390	128	1.02	0.01	11190	137	1.38	0.21	12280	146	1.02	0.02	8860	384	1.10	0.05	Downcomer extended/ pool lowered
2.9	16.1	14950	131	1.09	0.01	7230	137	1.15	0.03	11110	149	1.50	0.03	8190	380	1.12	0.06	Downcomer extended/pdw
2.10	27.9	21230	130	1.07	0.01	10880	135	1.12	0.02	15620	150	1.26	0.02	10300	524	1.10	0.06	Downcomer extended/pdw
2.11	29.9	22740	132	1.08	0.01	11780	138	1.13	0.02	17360	154	1.23	0.02	10840	518	1.12	0.06	Downcomer extended/pdw
3.1	28.9	16810	133	1.02	0.01	10180	141	1.12	0.02	14330	154	1.07	0.02	8170	439	1.21	0.07	Medium orifices
3.2	25.7	14560	136	0.94	0.01	9810	142	1.23	0.02	12510	160	0.98	0.02	9710	519	1.26	0.07	No orifices
3.3A	24.9	15690	133	1.01	0.01	6860	142	0.77	0.02	9120	154	0.73	0.01	6590	278	1.02	0.05	Right vent blocked
3.3B	24.9	15040	136	0.97	0.01	6260	145	0.78	0.02	7740	153	0.61	0.01	8920	281	1.36	0.05	Left vent blocked
3.4A	25.0	16940	134	1.05	0.01	8230	144	1.05	0.02	12180	162	1.00	0.02	7750	448	1.00	0.06	Right vent blocked
3.4B	22.6	15580	134	0.97	0.01	8510	144	1.02	0.02	10980	158	0.92	0.02	8092	435	1.02	0.06	Left vent blocked
3.5	25.6	16920	137	1.09	0.01	7260	148	0.77	0.02	12260	164	1.04	0.02	8600	439	1.22	0.06	Nominal

Legend: $\bar{\dot{P}}dw$ - mean drywell pressurization rate.
$\downarrow F$ - peak force (down).
$\uparrow F$ - peak force (up).
σ_F - standard deviation of force F.
R - ratio of 3-D force to six times 2-D force.
σ_R - standard deviation of ratio R.
n.d. - not determined.

TABLE 1-6. Peak force results summary--hydrodynamic vertical load function (7.5° sector).

		T_1		T_2		T_3		T_4	
Test	$\dot{\bar{P}}$dw, psi/s	↓F, lb_f	σ_F	↓F, lb_f	σ_F	↓F, lb_f	σ_F	↑F, lb_f	σ_F
1.1	25.0	2829	19	n.d.[a]	-	n.d.	-	1076	19
1.3	26.0	3305	19	n.d.[a]	-	n.d.	-	968	20
1.3.1	27.2	2728	19	1551	19	2208	19	1164	19
1.4	18.4	2082	19	1172	19	1570	19	1130	19
1.5	30.0	3037	19	1879	19	2383	19	1294	19
1.6	34.9	3384	19	1982	19	2663	19	1236	20
2.1	28.7	1905	19	1390	19	2021	19	1088	19
2.2	25.7	n.d.[a]	-	n.d.[a]	-	1494	19	894	19
2.3	26.6	n.d.[a]	-	n.d.[a]	-	1429	19	862	19
2.4	24.3	2794	19	1436	19	1813	19	1069	19
2.5	27.1	3810	19	n.d.[a]	-	n.d.[a]	-	1629	20
2.6	25.4	1659	19	1315	18	1685	19	761	18
2.7	23.6	3077	19	n.d.[a]	-	n.d.[a]	-	1487	20
2.8	23.7	2692	19	1350	19	2005	19	1343	19
2.9	16.1	2277	19	1047	19	1236	19	1218	19
2.10	27.9	3312	19	1628	19	2070	19	1567	20
2.11	29.9	3521	19	1741	19	2351	19	1607	20
3.1	28.9	2751	19	1515	19	2227	19	1126	20
3.2	25.7	2593	19	1332	19	2119	19	1281	20
3.3A	24.9	2583	19	1479	19	2085	19	1075	19
3.3B	24.9	2503	19	1421	19	2111	19	1093	19
3.4A	25.0	2693	19	1305	19	2019	19	1296	20
3.4B	22.6	2670	19	1384	19	1985	19	1320	20
3.5	25.6	2599	19	1574	19	1955	19	1176	19

[a] Not determined.

PART 2. EXTENDED ANALYSES AND CORRELATIONS

2.1 PEAK VERTICAL LOAD SENSITIVITIES

2.1.1 DETERMINATION OF PEAK FORCE SENSITIVITIES

As shown by the best estimate HVLF analysis discussed in Part 1, significant changes are effected in the peak forces by relatively small changes in test parameters. An important application of these results then is the determination of peak force sensitivity to the major parameters:

a) drywell pressurization rate,
b) drywell overpressure,
c) downcomer submergence.

Compared to the earlier,[1] less critical, analysis of the peak HVLF forces, the peak down forces are reduced approximately 15 percent and the peak up forces are reduced 9 percent. A key point of interest is the degree to which the earlier force sensitivities may have changed. In order to quantify this change and provide a complete update of the force sensitivity, an approach will be taken in which the sum of the weighted squares of the residuals are minimized as follows:

$$Q = \sum_i \omega_i \times \mathrm{res}_i^2 \quad . \tag{2-1}$$

The HVLF is assumed to be most sensitive to the drywell pressurization rate ($\dot{p}_{dw}$). Having determined this initial sensitivity for nominal case standard length downcomer tests (using tests 1.1, 1.3, 1.3.1, 1.4, 1.5, 1.6, 2.4, and 3.5), the peak forces for all tests using standard downcomers are normalized to the nominal pressurization rate of 27.4 psi/s. Tests 1.4, 1.5, and 1.6 are not normalized because these tests were, by definition in the final air text matrix, conducted at drywell pressurization rates other than the nominal 27.4 psi/s. This normalization is carried out for both 3-D and 2-D data. The peak force sensitivity to $\dot{p}_{dw}$, for extended downcomer tests, is determined in a similar manner using results from tests 2.7, 2.9, 2.10, and 2.11. The peak forces of test 2.7 and 2.8 are then normalized to the nominal pressurization rate of 27.4 psi/s.

2.1.2 REGRESSION OF PEAK FORCE ON DRYWELL PRESSURIZATION RATE

The peak forces (F) used here are taken from the best estimate analysis results (Tables 1-5 and 1-6). In earlier work[1] the F versus $\dot{p}_{dw}$ data were fitted to the line

$$y = \alpha_1 + \alpha_2 x \quad ; \quad y \rightarrow F \text{ and } x \rightarrow \dot{p}_{dw} \qquad (2\text{-}2)$$

with y and x (i.e., F and $\dot{p}_{dw}$, respectively) assumed to be free of all error and all weights of equal value, assumed to be unity. Now that the peak force standard errors have been established, nonequal weights are assigned to the forces as well as to the independent variable, $\dot{p}_{dw}$.* As discussed below, these weights are taken as a function of the reciprocal of the particular variance, that is, $w_{y_i} = 1/\sigma^2_{y_i}$ and $w_{x_i} = 1/\sigma^2_{x_i}$, in order to provide Q_{min}. The results of the multivariate regression of peak force on drywell pressurization rate for the 12 nominal tests (8 with standard length downcomers and 4 with the extended downcomers) provide 4 sets of sensitivity data for each of the downcomer lengths considered in the air test matrix. The results are presented in English units in the data plots of Figs. 2-1 and 2-2 and in Table 2-2, as is the estimated error for both α_1 and α_2 and the fitting coefficient, r^2.

2.1.3 MULTIVARIATE REGRESSION ANALYSIS METHOD

Due to experimental conditions, it was not possible to measure the peak force at a predetermined pressure rate. Therefore, part of the data analyses involved adjusting the peak force data to a common pressurization rate. Once this adjustment was made, the sensitivity of the peak force to variation in this rate could be determined.

In making the adjustment of peak force to a common pressurization rate (27.4 psi/s), it was assumed that a linear relationship

$$Y = \hat{\alpha}_1 + \hat{\alpha}_2 X \qquad (2\text{-}3)$$

---

*A complete tabulation of test-correlated independent variables, and their associated standard errors, are given in Table 2-1.

TABLE 2-1. Summary of independent variables with standard errors.

	Independent variable--standard deviation										Downcomer submergence/pool depth - inches								
	Drywell - psi/s				Ullage - psi				$p_{o_{dw}} - p_{o_{ull}}$		45° sector				7.5° sector				
Test	$\dot{\bar{p}}_{dw}$	$\sigma_{\dot{p}dw}$	$\bar{p}_{o_{dw}}$	$\sigma_{o_{dw}}$	$\bar{p}_o^{45^\circ}$	$\sigma_o^{45^\circ}$	$p_o^{7.5^\circ}$	$\sigma_o^{7.5^\circ}$	Δp, psi ($in.-H_2O$)	$\sigma_{\Delta p}$	D.C. subm., S^{45°	$\sigma_S^{45^\circ}$	Pool depth, L^{45°	$\sigma_L^{45^\circ}$	D.C. subm., $S^{7.5^\circ}$	$\sigma_S^{7.5^\circ}$	Pool depth, $L^{7.5^\circ}$	$\sigma_L^{7.5^\circ}$	Test
1.1	24.948	0.630	3.01	0.1421	3.01	0.01201	3.01	0.01302	0.	0.1427	9.6	0.104	34.8	0.1	9.6	0.104	35.1	0.1	1.1
1.3	25.962	0.322	2.934	0.0846	2.934	0.01491	2.934	0.01404	0.	0.0859	9.6	0.104	34.8	0.1	9.6	0.104	35.1	0.1	1.3
1.3.1	27.239	0.646	2.96	0.1611	2.96	0.01672	2.96	0.01480	0.	0.1619	9.6	0.104	34.8	0.1	9.6	0.104	35.1	0.1	1.3.1
1.4	18.400	0.156	2.94	0.1385	2.94	0.01600	2.94	0.01352	0.	0.1394	9.6	0.104	34.8	0.1	9.6	0.104	35.1	0.1	1.4
1.5	29.964	0.110	2.94	0.1576	2.94	0.0200	2.94	0.01215	0.	0.1585	9.6	0.104	34.8	0.1	9.6	0.104	35.1	0.1	1.5
1.6	34.876	0.953	2.95	0.1560	2.95	0.01470	2.95	0.01520	0.	0.1568	9.6	0.104	34.8	0.1	9.6	0.104	35.1	0.1	1.6
2.1	28.690	1.779	3.130	0.1636	2.96	0.01554	2.96	0.01065	0.170 (4.704)	0.1642	9.6	0.104	34.8	0.1	9.6	0.104	35.1	0.1	2.1
2.2	25.692	1.131	3.200	0.1520	2.94	0.01389	2.94	0.01480	0.26 (7.195)	0.1528	9.6	0.104	34.8	0.1	9.6	0.104	35.1	0.1	2.2
2.3	26.586	0.917	3.190	0.1459	2.93	0.01405	2.93	0.01563	0.26 (7.195)	0.1466	9.6	0.104	34.8	0.1	9.6	0.104	35.1	0.1	2.3
2.4	24.308	1.208	2.96	0.09380	2.96	0.01127	2.96	0.01525	0.	0.09475	9.6	0.104	34.8	0.1	9.6	0.104	35.1	0.1	2.4
2.5	27.095	1.044	2.96	0.09909	2.96	0.01263	2.96	0.01304	0.	0.09992	13.4	0.104	38.6	0.1	13.4	0.104	38.9	0.1	2.5
2.6	25.432	0.563	2.96	0.08751	2.96	0.01155	2.96	0.01452	0.	0.08849	5.8	0.104	31.0	0.1	5.8	0.104	31.3	0.1	2.6
2.7	23.566	1.249	2.94	0.09106	2.94	0.01318	2.94	0.01173	0.	0.09191	12.0	0.104	34.8	0.1	12.0	0.104	35.1	0.1	2.7
2.8	23.662	0.570	2.92	0.08605	2.92	0.01282	2.92	0.01448	0.	0.08713	9.6	0.104	32.4	0.1	9.9	0.104	33.0	0.1	2.8
2.9	16.136	0.422	2.94	0.08766	2.94	0.00991	2.94	0.01084	0.	0.08827	12.0	0.104	34.8	0.1	12.0	0.104	35.1	0.1	2.9
2.10	27.851	0.625	2.92	0.10302	2.92	0.01124	2.92	0.01706	0.	0.10403	12.0	0.104	34.8	0.1	12.0	0.104	35.1	0.1	2.10
2.11	29.933	1.625	2.94	0.09197	2.94	0.01167	2.94	0.01302	0.	0.09280	12.0	0.104	34.8	0.1	12.0	0.104	35.1	0.1	2.11
3.1	28.905	0.398	2.94	0.09482	2.94	0.01441	2.94	0.01360	0.	0.09585	9.6	0.104	34.8	0.1	9.6	0.104	35.1	0.1	3.1
3.2	25.728	0.379	2.97	0.09801	2.97	0.01395	2.97	0.01249	0.	0.09902	9.6	0.104	34.8	0.1	9.6	0.104	35.1	0.1	3.2
3.3A	24.898	0.551	2.92	0.08245	2.92	0.01347	2.92	0.01615	0.	0.08379	9.6	0.104	34.8	0.1	9.6	0.104	35.1	0.1	3.3A
3.3B	24.898	0.343	2.94	0.10253	2.94	0.01347	2.94	0.01010	0.	0.10322	9.6	0.104	34.8	0.1	9.6	0.104	35.1	0.1	3.3B
3.4A	25.004	0.494	2.94	0.08790	2.94	0.02360	2.94	0.01548	0.	0.09013	9.6	0.104	34.8	0.1	9.6	0.104	35.1	0.1	3.4A
3.4B	27.608	1.041	2.94	0.09378	2.94	0.01182	2.94	0.01373	0.	0.09465	9.6	0.104	34.8	0.1	9.6	0.104	35.1	0.1	3.4B
3.5	25.628	0.438	2.96	0.10191	2.96	0.01314	2.96	0.01637	0.	0.10298	9.6	0.104	34.8	0.1	9.6	0.104	35.1	0.1	3.5

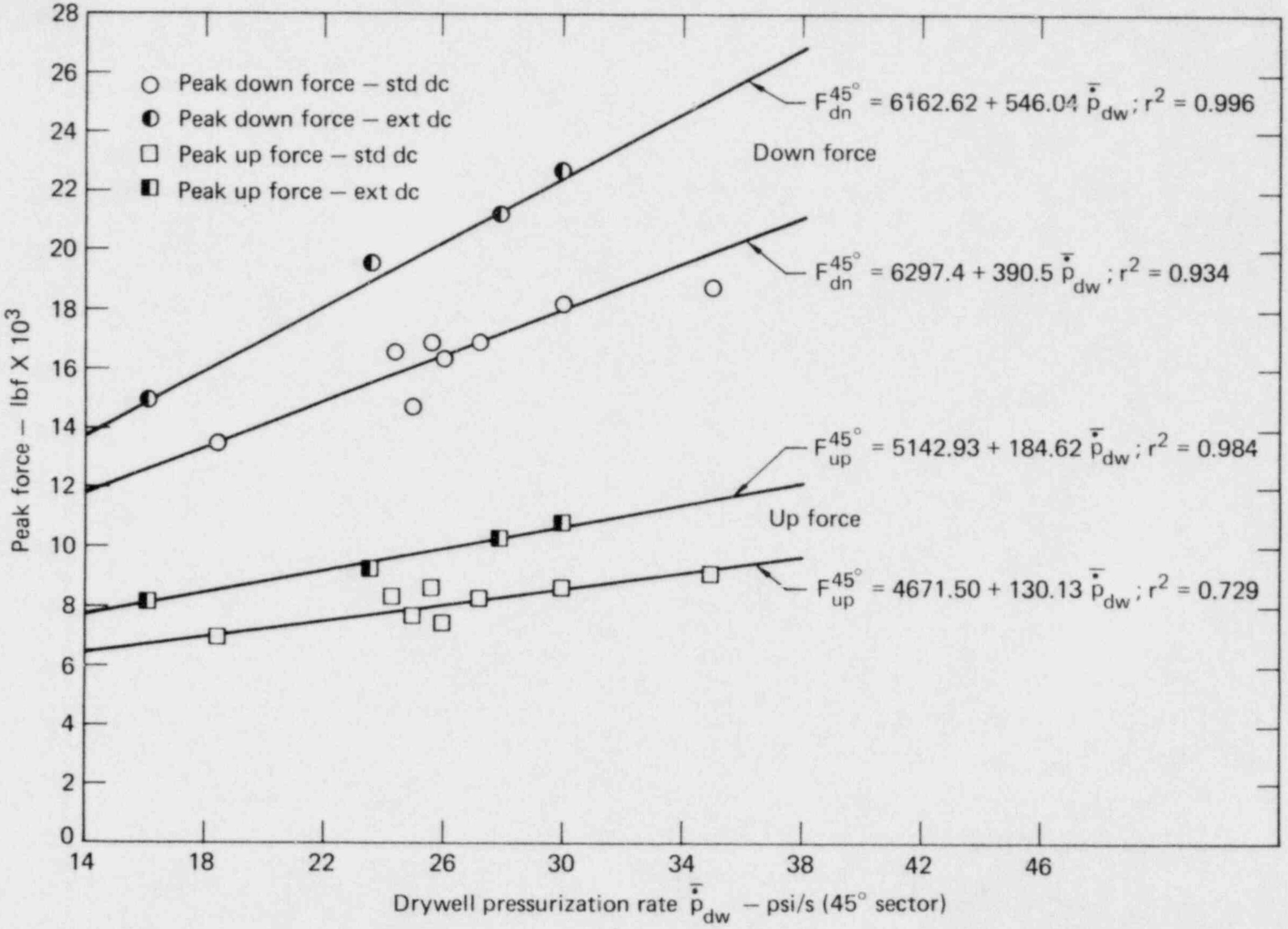

FIG. 2-1. Effect of drywell pressurization rate on peak hydrodynamic vertical force--45° sector.

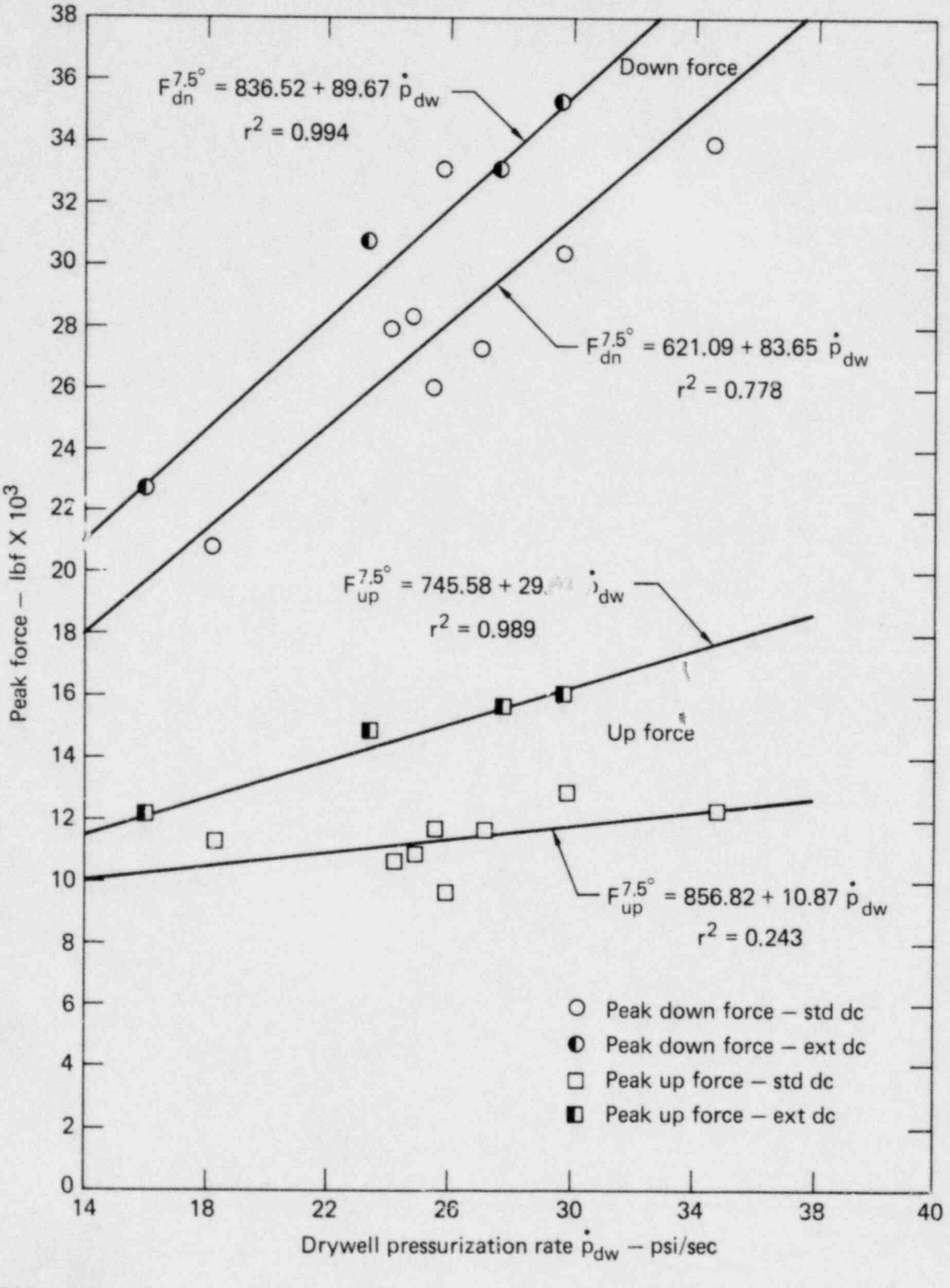

FIG. 2-2. Effect of drywell pressurization rate on peak hydrodynamic vertical force--7.5^0 sector.

TABLE 2-2. Least squares parameters[a]--peak force sensitivity to drywell pressurization rate, $\dot{p}_{dw}$.

	Standard downcomer length				Extended downcomer length			
	45^0 sector		7.5^0 sector		45^0 sector		7.5^0 sector	
	Down force	Up force	Down force	Up force	Down force	Up force	Down force	Up force
Intercept, $\alpha_1 (lb_f)$	6297.43	4671.50	621.09	856.82	6162.62	5142.93	836.52	745.58
Standard error, σ_{α_1} (lb_f)	411.68	839.38	65.72	43.73	766.04	1012.79	123.12	61.60
Slope, $\alpha_2 (lb_f/psi/s)$	390.54	130.13	83.65	10.87	546.04	184.62	89.67	29.62
Standard error, $\sigma_{\alpha_2} (lb_f/psi/s)$	15.95	32.46	2.55	1.65	35.32	43.53	5.70	2.70
Fit coefficient, r^2	0.934	0.729	0.778	0.243	0.996	0.984	0.994	0.989

[a] $F = \alpha_1 + \alpha_2 \dot{p}_{dw}$, where the data set $(F, \dot{p}_{dw})_i$ are associated with ordinate and abscissa error $(\sigma_F, \sigma_{\dot{p}})_i$, respectively.

exists between the actual (unobservable) pressure rate, X, and the actual (unobservable) peak force, Y. It was further assumed that the observed rate, x, and peak force, y, are corrected for any bias that may exist. Thus, for any set of experimental conditions,

$$x = X + \delta \tag{2-4}$$

$$y = Y + \varepsilon \ , \tag{2-5}$$

where ε, δ are random variables that

(a) have zero mean, i.e., $\mu_\varepsilon = \mu_\delta = 0$,

(b) have variances σ_ε^2 and σ_δ^2 which are not necessarily constant over all conditions, and are <u>known</u>,

(c) are uncorrelated, i.e., $\rho_{\varepsilon\delta,} = 0$.

It was further assumed that the adjustment made to the observed peak force, y, is based on the appropriate given value of the observed pressure rate, x. The correction, Δy, is determined from the model

$$\Delta y = \alpha_2 \Delta x \ , \tag{2-6}$$

where α_2 is an estimate of the slope, $\hat{\alpha}_2$, and $\Delta x = x - 27.4$ is the deviation of the observed pressure rate, x, from the common pressure rate 27.4 psi/sec. The adjusted peak force, $\tilde{y}$, is $\tilde{y} = y + \Delta y$ where y is the observed peak force.

The estimate, α_2, of the slope is based on a weighted least squares procedure developed as follows. Solving for (X,Y) in equations (2-4) and (2-5) and substituting into equation (2-3), the relationship between the observed pressure rate, x, and the peak force, y, is given by the model

$$Y = \hat{\alpha}_1 + \hat{\alpha}_2 \, x + (\varepsilon - \hat{\alpha}_2 \delta) \ . \tag{2-7}$$

where the bracketed term in equation (2-7) is a random variable with

(a) mean, $\mu = 0$

(b) variance, $\sigma_\varepsilon^2 + \hat{\alpha}_2^2 \, \sigma_\delta^2$.

When treating the observed pressure rates x_i as fixed constants, equation (2-7) is the usual regression model, except that the variance involves the unknown value of $\hat{\alpha}_2$. The estimation procedure was based on minimizing the weighted sum of squares, SSR$(\hat{\alpha}_1, \hat{\alpha}_2)$, where

$$\mathrm{SSR}\ (\hat{\alpha}_1, \hat{\alpha}_2) = \sum_{i=1}^{N} \omega_i (y_i - \alpha_1 - \alpha_2 x_i)^2 \ . \qquad (2\text{-}8)$$

The weights, ω_i, are assumed known and are

$$\omega_i = (\sigma_{\varepsilon_i} + a_2^2 \ \sigma_\delta^2 \ )^{-1} \ , \qquad (2\text{-}9)$$

where a_2, is an approximate value of α_2.

Based on this analysis, the estimates of $\hat{\alpha}_1$, and $\hat{\alpha}_2$ are

$$\alpha_1 = \bar{y}_\omega - \alpha_2 \bar{x}_\omega \qquad (2\text{-}10)$$

and

$$\alpha_2 = \sum_{i=1}^{N} \omega_i (x_i - \bar{x}_\omega)(y_i - \bar{y}_\omega) / \sum_{i=1}^{N} \omega_i (x_i - \bar{x}_\omega) \qquad (2\text{-}11)$$

where

$$\bar{x}_\omega = \sum_{i=1}^{N} \omega_i x_i / \sum_{i=1}^{N} \omega_i \ \text{and}\ \bar{y}_\omega = \sum_{i=1}^{N} \omega_i y_i / \sum_{i=1}^{N} \omega_i \ .$$

An approximation to the variance of α_2 is given by

$$\sigma_{\alpha_2}^2 = 1 / \sum_{i=1}^{N} \omega_i (x_i - \bar{x}_\omega)^2 \ . \qquad (2\text{-}12)$$

An initial estimate was made based on an unweighted least squares estimation. Since the weights in equation (2-9) are based on the use of an approximate value for the unknown $\hat{\alpha}_2$, the estimation scheme was made iterative with successively improved approximations being used. Iteration continued until successive estimates of α_2 were within 1 percent of each other.

2.1.4 COMPARISON TO EARLIER RESULTS

Table 2-3, reported in SI units, provides a comparison with the earlier work.[1] Because the original work was necessarily based on an assumption of error-free observations of y and x, the comparison results in Table 2-3 are likewise based on this assumption. On this error-free basis, the primary change, due to the more accurate force estimates, is a decrease in the standard downcomer length 3-D peak sensitivities (slope, a_1) of approximately 26 percent in down force and approximately 9 percent in up force. The extended downcomer results show a similar but smaller (approximately 13 percent) decrease in down force sensitivity but little change (approximately 1 percent) in up force sensitivity. No dramatic changes occurred in the 2-D sensitivities, with the exception of the peak up force sensitivity which increased nearly 30 percent. The peak down forces for the 3-D sector are, as before, approximately three times as sensitive to the drywell pressurization rate as the peak up forces, independent of downcomer extension length. In the case of the 7.5^0 sector, the trend is not as clear. With the standard downcomer length, the ratio of a_1's (down to up force), although reduced from the previous value of 8.9 to 1, is still anomalously high at a ratio of approximately 6.5 to 1. With the extended downcomer, the sensitivity ratio is still about 3 to 1, which is quite similar to the 90^0 sector findings. The small slope of the 7.5^0 sector up force curve for standard extension, which is approximately 7×10^{-3} kN/kPa/s, is of a different nature in the context of the overall data set.

2.1.5 NORMALIZATION OF PEAK FORCES

In order to provide a data base to determine the secondary parametric sensitivities (drywell overpressure and downcomer submergence) we used the slopes α_2 to normalize the relevant peak forces to the nominal pressurization rate of 27.4 psi/s

TABLE 2-3. Comparison of least squares parameters[a] (simple regression[b] on drywell pressurization rate).

	Standard downcomer length							
	90° sector				7.5° sector			
Item	[c]Down force	% change	[c]Up force	% change	[c]Down force	% change	[c]Up force	% change
Intercept, a_o(kN)	68.37	+2.7	43.18	-5.5	4.11	-0.77	3.75	-4.3
Slope, a_1(kN/kPa/s)	0.43	-26.6	0.16	-9.1	0.047	-5.9	0.0072	+29.1
Fit coefficient, r^2	0.83	- 5.5	0.69	-9.2	0.69	-7.3	0.27	+74.5
	Extended downcomer length							
Intercept, a_o(kN)	55.38	-10.0	44.81	-15.2	3.95	-2.2	3.46	+2.8
Slope, a_1(kN/kPa/s)	0.71	-13.5	0.24	+1.0	0.057	-1.6	0.0183	0.0
Fit coefficient, r^2	0.99	+1.7	0.98	+4.5	0.98	-1.0	0.97	-1.0

[a] Reference Table 15, UCRL-52371, Final Air Test Results.

[b] No error assigned to peak force (ordinate) or pressurization rate (abscissa).

[c] Based on Tables 1-5 and 1-6 of this report.

$$F_{nom} = F_{obs} + \alpha_2(\dot{p}_{nom} - \dot{p}_{obs}) \qquad (2\text{-}13)$$

where

F_{obs} = observed peak force, lbf
$\dot{p}_{obs}$ = observed drywell pressurization rate, psi/s
$\dot{p}_{nom}$ = nominal drywell pressurization rate of 27.4 psi/s
F_{nom} = peak force adjusted to the nominal pressurization rate.

Associated with each adjusted peak force is the variance

$$\sigma^2_{F_{nom}} = \sigma^2_{F_{obs}} + (\dot{p}_{nom} - \dot{p}_{obs})^2\,\sigma^2_{\alpha_2} + \alpha_2^2\,\sigma^2_{\dot{p}_{obs}} \quad , \qquad (2\text{-}14)$$

where

$\sigma_{F_{obs}}$ = standard error in F_{obs}
σ_{α_2} = standard error in α_2
$\sigma_{\dot{p}_{obs}}$ = standard error in $\dot{p}_{obs}$.

Applying both of these equations and the pertinent data from Tables 1-5, 1-6, 2-1, and 2-2 yields the desired normalized forces. The results of this treatment for the 45° torus sector and 7.5° torus sector forces and the associated standard errors are shown in Table 2-4.

2.1.6 SENSITIVITY OF PEAK FORCE TO DRYWELL OVERPRESSURE

The normalized peak force results of eight tests (1.1, 1.3, 1.3.1, 2.1, 2.2, 2.3, 2.4, and 3.5) were used to establish the sensitivity of peak force to drywell overpressure. The sensitivities evidenced by the 45° torus sector and 7.5° torus sector data were computed similarly, using multivariate regression with overvariance weighting. The results are tabulated in Table 2-5 and plotted in Fig. 2-3.

TABLE 2-4a. Tabulation of observed and normalized peak forces with standard errors--45° sector.

			HVLF--45° sector							
			Unnormalized				Normalized			
Air test no.	$\bar{P}_{dw}$ psi/s	$\sigma_{\bar{P}_{dw}}$	Down force	σ down	Up force	σ up	Down force	σ down	Up force	σ up
1.1	24.948	0.630	14763	135	7653	369	15721	283	7972	386
1.3	25.962	0.322	16363	127	7468	414	16925	180	7655	419
1.3.1	27.239	0.646	16882	132	8230	402	16945	285	8251	411
1.4	18.400	0.156	13451	134	6978	328	--	--	--	--
1.5	29.964	0.110	18236	135	8630	425	--	--	--	--
1.6	34.876	0.953	18789	135	9109	491	--	--	--	--
2.1	28.690	1.779	12526	133	7160	331	12022	708	6992	406
2.2	25.692	1.310	9667	134	6335	299	10334	530	6557	349
2.3	26.586	0.917	9804	140	6193	321	10122	385	6299	343
2.4	24.308	1.208	16596	136	8374	395	17804	493	8776	437
2.5	27.095	1.044	24761	128	9053	489	24880	427	9093	508
2.6	25.432	0.563	11489	136	5330	252	12258	260	5586	270
2.7	23.566	1.249	19579	132	9286	410	21673	708	9994	499
2.8	23.662	0.570	16392	128	8858	384	18433	362	9548	430
2.9	16.136	0.422	14948	131	8186	380	--	--	--	--
2.10	27.851	0.625	21229	130	10298	524	--	--	--	--
2.11	29.933	1.625	22740	131	10836	518	--	--	--	--
3.1	28.905	0.398	16810	133	8171	439	16222	206	7975	445
3.2	25.728	0.379	14555	136	9707	519	15208	203	9925	524
3.3A	24.898	0.551	15690	133	6593	278	16667	250	6919	298
3.3B	24.898	0.343	15038	136	8918	281	16015	195	9244	296
3.4A	25.004	0.494	16938	134	7754	448	17874	238	8066	459
3.4B	22.608	1.041	15578	134	8092	435	17449	435	8716	481
3.5	25.628	0.438	16919	137	8599	439	17611	221	8830	446

TABLE 2-4b. Tabulation of observed and normalized peak forces with standard errors--7.5° sector.

			HVLF--7.5° sector											
			Unnormalized				Normalized				Normalized compared to 45°			
Air test no.	$\bar{P}_{dw}$ psi/s	$\sigma_{\bar{P}_{dw}}$	Down force	σ down	Up force	σ_{up}	Down force	σ down	Up force	σ_{up}	Down force	σ down	Up force	σ_{up}
1.1	24.948	0.630	2829	19	1076	19	3034	56	1103	21	18205	338	6616	124
1.3	25.962	0.322	3305	19	968	20	3425	33	984	20	20552	199	5902	123
1.3.1	27.239	0.646	2728	19	1164	19	2741	57	1166	20	16449	344	6995	122
1.4	18.400	0.156	2082	19	1130	19	-	-	-	-	-	-	-	-
1.5	29.964	0.110	3037	19	1294	19	-	-	-	-	-	-	-	-
1.6	34.876	0.953	3384	19	1236	20	-	-	-	-	-	-	-	-
2.1	28.690	1.779	1905	19	1088	19	1797	150	1074	27	10783	900	6444	163
2.2	25.692	1.310	1189	18	894	19	1332	111	913	24	7991	667	5475	143
2.3	26.586	0.917	1429	19	862	19	1497	79	871	21	8983	474	5225	129
2.4	24.308	1.208	2794	19	1069	19	3053	103	1103	24	18316	617	6616	142
2.5	27.095	1.044	3818	19	1629	20	3844	89	1632	23	23061	536	9794	138
2.6	25.432	0.563	1685	19	761	18	1850	51	782	19	11098	306	4694	116
2.7	23.566	1.249	3077	19	1487	20	3421	116	1601	43	20525	694	9603	260
2.8	23.662	0.570	2692	19	1343	19	3027	59	1454	27	18163	351	8722	164
2.9	16.136	0.422	2277	19	1218	19	-	-	-	-	-	-	-	-
2.10	27.851	0.625	3312	19	1567	20	-	-	-	-	-	-	-	-
2.11	29.933	1.625	3521	19	1607	20	-	-	-	-	-	-	-	-
3.1	28.905	0.398	2571	19	1126	20	2445	39	1110	21	14671	231	6658	124
3.2	25.728	0.379	2593	19	1281	20	2733	37	1299	21	16397	223	7795	124
3.3A	24.898	0.551	2583	19	1075	19	2792	49	1102	20	16754	292	6613	122
3.3B	24.898	0.343	2583	19	1093	19	2792	35	1120	20	16754	210	6721	119
3.4A	25.004	0.494	2693	19	1296	20	2893	46	1322	21	17361	275	7932	126
3.4B	22.608	1.041	2670	19	1320	20	3071	90	1372	24	18425	540	8233	146
3.5	25.628	0.438	2599	19	1176	19	2747	42	1195	20	16483	249	7172	119

TABLE 2-5. Least squares parameters[a]--peak force sensitivity to drywell overpressure.

	45^0 sector		7.5^0 sector	
	Down force	Up force	Down force	Up force
Intercept, $\alpha_1(lb_f)$	17147.32	8293.01	3068.40	1095.53
Standard error, $\sigma_{\alpha_1}(lb_f)$	1316.66	404.49	315.36	34.66
Slope, $\alpha_2(lb_f/in.-H_2O)$	-981.36	-262.39	-235.49	-24.85
Standard error, $\sigma_{\alpha_2}(lb\ /in.-H_2O)$	420.09	119.88	100.63	10.87
Fit coefficient, r^2	0.956	0.754	0.877	0.455

[a] $F = \alpha_1 + \alpha_2 d$ where the data set $(F,d)_i$ is associated with ordinate and abscissa error $(\sigma_F, \sigma_d)_i$, respectively. In this regression analysis, the peak forces F_i (from tests 1.1, 1.3, 1.3.1, 2.1, 2.2, 2.3, 2.4, and 3.5), are normalized to the nominal $\dot{p}_{dw} = 27.4$ psi/s.

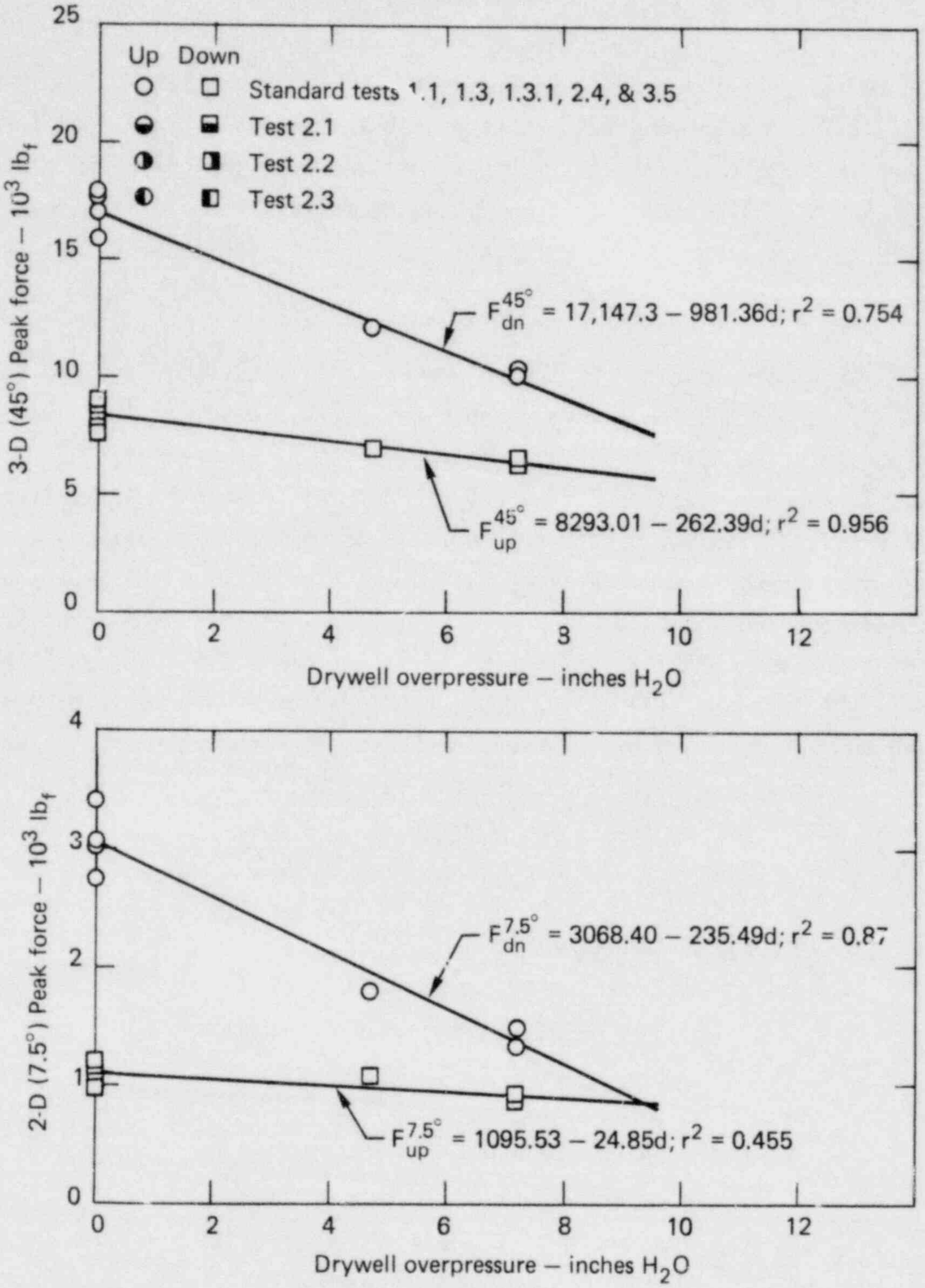

FIG. 2-3. Effect of drywell overpressure on normalized peak force ($\dot{p}_{dw}^{n}$ = 27.4 psi/s).

2.1.7 SENSITIVITY OF PEAK FORCE TO DOWNCOMER SUBMERGENCE

The normalized peak force results of nine tests (1.1, 1.3, 1.3.1, 2.4, 2.5, 2.6, 2.7, 2.8 and 3.5) were used to establish the sensitivity of peak force to downcomer submergence. The sensitivities evidenced by the 45° torus sector and 7.5° torus sector data were computed using multivariate regression with overvariance weighting. The results are tabulated in Table 2-6 and plotted in Fig. 2-4.

Table 2-7 shows a comparison of the computed sensitivities for the 3-D and 2-D sectors. In a perfect comparison between 3-D and 2-D data, we would expect the ratio of the sensitivities ($\alpha_2^{45^\circ}$ and $\alpha_2^{7.5^\circ}$) to be in the ratio of 6 to 1. As shown in Table 2-7, the ratios meet this expectation fairly closely for all cases considered, except for the case of up force sensitivity with standard downcomers, where the slope ratios are nearly twice the expected value. As compared to the earlier sensitivity analysis based on error-free regression analyses (Table 2-3), the slope ratios now better represent the trends in the data and again illustrate that down forces are well defined by both 3-D and 2-D facilities. However, up forces, particularly for nominal downcomer lengths, are rather nonconservatively defined by 2-D experiments.

TABLE 2-6. Least squares parameters[a]--peak force sensitivity to downcomer submergence.

	45° sector		7.5° sector	
	Down force	Up force	Down force	Up force
Intercept, $\alpha_1 (lb_f)$	2468.93	2449.58	380.66	56.91
Standard error, $\sigma_{\alpha_1} (lb_f)$	628.06	588.81	120.94	42.49
Slope, $\alpha_2 (lb_f/in.)$	1554.59	600.42	272.40	115.85
Standard error, $\sigma_{\alpha_2} (lb_f/in.)$	65.92	62.76	12.66	4.35
Fit coefficient, r^2	0.904	0.788	0.755	0.809

[a] $F = \alpha_1 + \alpha_2 s$, where the data set $(F, s)_i$ are associated with ordinate and abscissa error $(\sigma_F, \sigma_s)_i$, respectively. In this regression analysis, the peak forces, F_i (from tests 1.1, 1.3, 1.3.1, 2.4, 2.5, 2.6, 2.7, 2.8 and 3.5), are normalized to the nominal $\dot{p}_{dw} = 27.4$ psi/s.

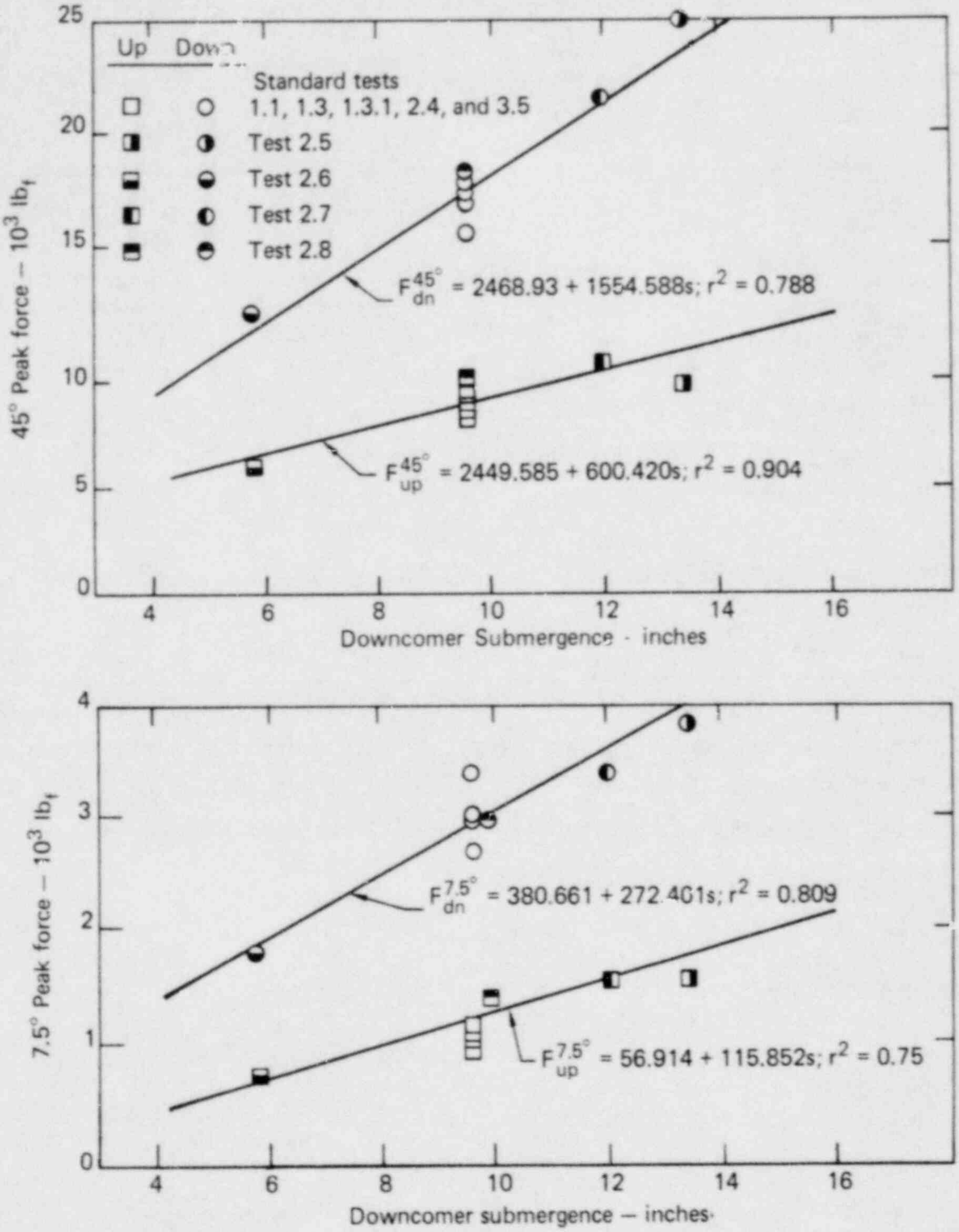

FIG. 2-4. Effect of downcomer submergence on normalized peak force ($\dot{p}_{dw}^{n}$ = 27.4 psi/s).

TABLE 2-7. Comparison of the 45° sector and 7.5° sector force sensitivities ($\alpha^{45^\circ}/\alpha^{7.5^\circ}$).

	Standard Downcomers		Extended Downcomers		Mix Downcomers	
Parameter	Down Force	Up Force	Down Force	Up Force	Down Force	Up Force
Drywell pressurization rate, $\dot{p}_{dw}$	4.67	11.97	6.09	6.22	--	--
Drywell overpressure, $\Delta p(d)$	4.17	10.56	--	--	--	--
Downcommer submergence, s	--	--	--	--	5.71	5.18

2.2 IMPULSE CHARACTERIZATION OF THE HYDRODYNAMIC VERTICAL LOAD FUNCTION

2.2.1 IMPULSE INTEGRATION

The primary purpose of the air transient test series was to determine the hydrodynamic vertical load function (HVLF) for both the three-dimensional and two-dimensional torus sectors. Significant insight into the consequences of a hypothetical loss-of-coolant accident (LOCA) was gained through characterization of the HVLF and specification of the associated peak vertical forces. Some understanding of the comparison between the spatially averaged 2-D sector and the complete 3-D sector has also been realized. In an effort to derive further information from the HVLFs, a short computer program was written to integrate the HVLF and to quantify both the negative impulse (that associated with the peak down force) and the positive impulse (that associated with the peak up force).

As defined here, and as shown in the schematic diagram in Fig. 2-5, the overall impulse integration begins at the initiation of drywell pressurization, $\overline{t}_o$,* and ends at the time of the second zero-crossing of the HVLF, t_{pos}. The negative impulse, I_{neg}, is defined at the $\int Fdt$ between $\overline{t}_o$ and the time of first zero crossing t_{neg}. I_{pos} is similarly defined by the impulse integral between t_{neg} and t_{pos}.

Typical results of the impulse calculations (from test 1.3.1) are shown in Figs. 2-6 and 2-7 for the 45^o and 7.5^o torus sectors, respectively. In general, the character of negative 2-D and 3-D impulses is the same and the corresponding integration limits ($\overline{t}_o$ to t_{neg}) are identical or nearly so. There are significant differences, however, between the 2-D and 3-D positive impulse results. In particular, the time of positive force is longer for the 7.5^o torus sector than the observable time in the 45^o torus sector, so that the relative impulse is greater in 2-D than in 3-D.

The results of preliminary benchtop tests, reported earlier by McCauley and Meier,[8] provide some insight into the differences between the 2-D and 3-D

---

*See Table 6 in Ref. 1.

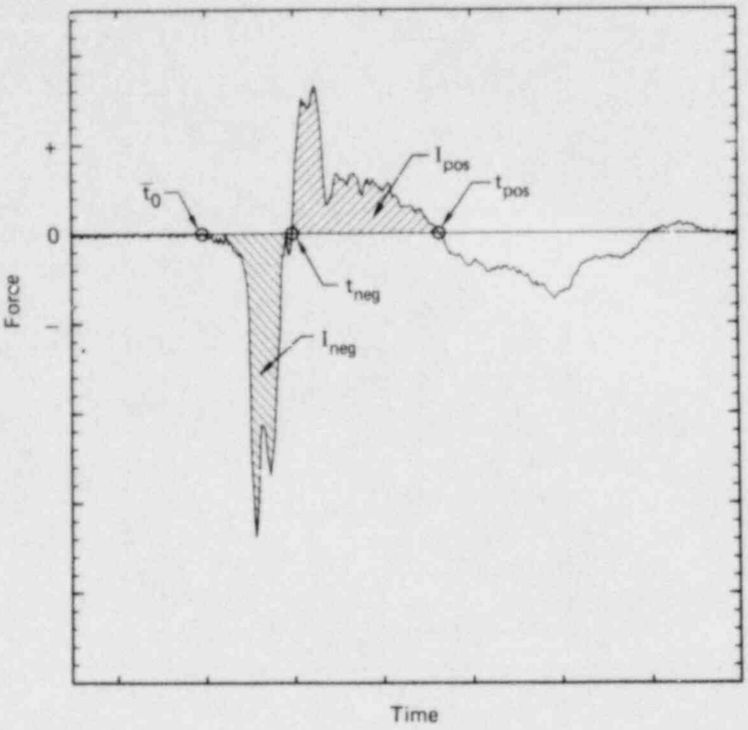

FIG. 2-5. Schematic diagram of the HVLF impulse.

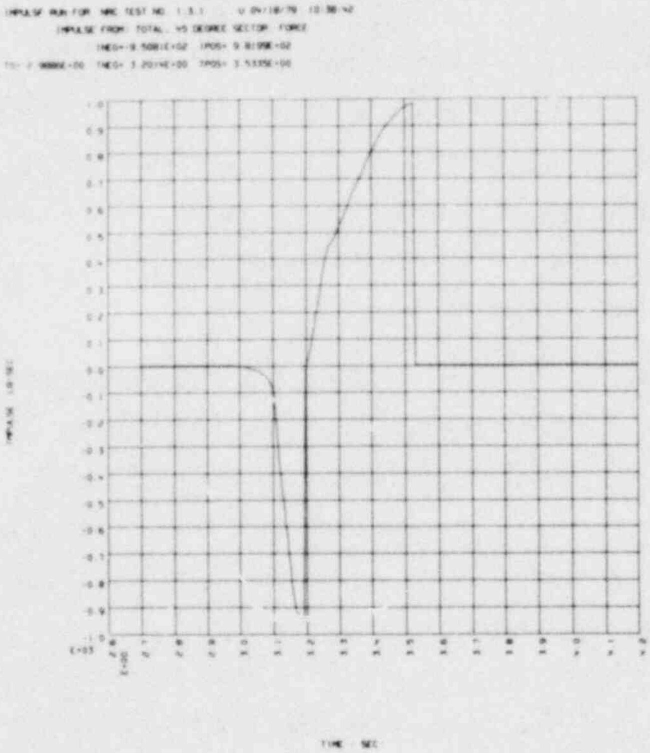

FIG. 2-6. Impulse run for test 1.3.1., 45° torus sector.

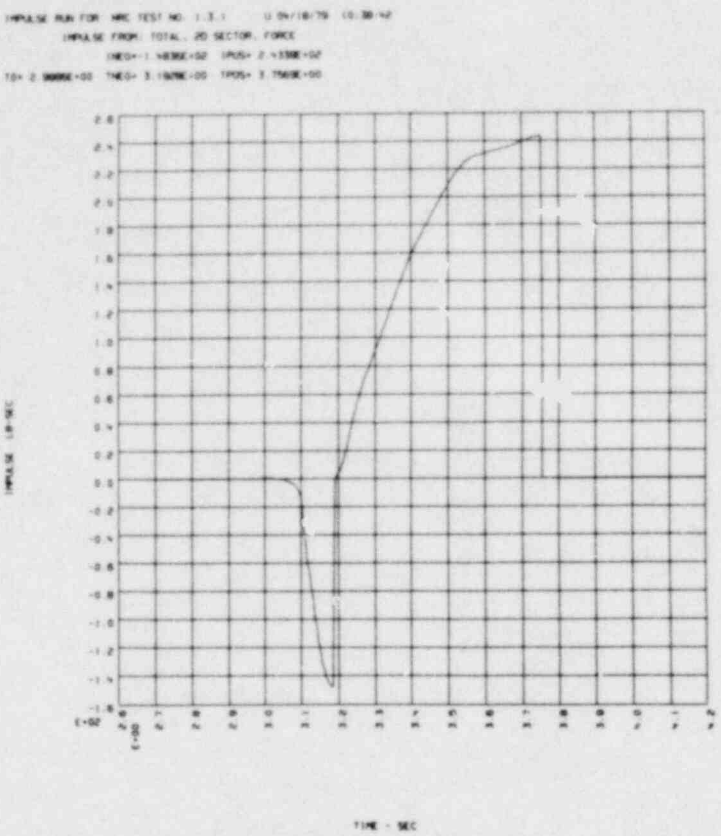

FIG. 2-7 Impulse run for test 1.3.1, 7.5^0 torus sector.

positive impulse results. In this experimental study (approximately 1/40-scale), a pair of downcomers was immersed in a rectangular tank containing water; spacing, immersion depth, bottom clearance, and side wall clearance approximated the Peach Bottom geometry. Axial boundary definition was provided by a pair of parallel, transparent plexiglas plates between which the downcomer pair was centered.

Several air injection tests were conducted to study bubble growth and pool swell, using plate spacings that ranged from below average to nearly free pool; the results were quantified from high speed film. For plate spacings that were sufficiently great (approximately 2 times average downcomer spacing), pool swell occurred with significant axial and transverse (radial), pool curvature centered around the downcomers through the time of breakthrough. For plate spacings in the range of average downcomer spacing, however, the pool swell character changed completely and essentially became one of slug flow, i.e., the pool surface moved upwards as a nearly planer unit. The observed differences between the 2-D and 3-D HVLFs, quantified by the impulse calculations, suggest that t_{pos} (2-D) may be greater than the corresponding t_{pos} (3-D), simply because slug flow behavior in the 7.5^{0} torus sector delays communication between the ullage and submembrane pressures. It appears likely that additional axial space between downcomer pairs (as found in the 3-D torus sector) allows equilibrium to occur at an earlier time. The net result of this effect in the 7.5^{0} sector is to distort the consequences of pool swell. This distortion is immediately apparent in a comparison of the 3-D (45^{0}) and 2-D (7.5^{0}) impulses.

To provide an unbiased basis of comparison between the 3-D and 2-D impulses, the 7.5^{0} torus sector HVLF impulse was also evaluated for all tests using the t_{pos} determined from the corresponding 45^{0} HVLF integration. An example of this is shown in Fig. 2-8 for test 1.3.1.

The results of the impulse analysis are presented in the following ways to increase their usefulness:

- Tabular results (Tables 2-8 through 2-13).

  The I_{neg}, t_{neg}, I_{pos}, and t_{pos} are listed for each test.

  In addition, the following computations were made:

  a. The ratio of I_{pos} to I_{neg} for the 45^{0} torus sector (3-D) and 7.5^{0} sector (2-D) HVLFs were computed, as was the ratio of I_{pos} to I_{neg} for the 2-D sector, using the shorter t_{pos} of the 3-D sector HVLF.

  b. The ratio of $I^{3-D}/(6 \times I^{2-D})$ was computed for both the negative and positive regions.

  An additional table (Table 2-14) is included. It provides an averaging of the results obtained from blocked-vent tests 3.3a, 3.3b (standard orifice) and 3.4a, 3.4b (no orifice).

- Graphical results (Figs. 2-9 through 2-11).

  a. The data of 1a and 1b are plotted for selected sets of tests, i.e., those concerned with drywell pressurization and drywell overpressure.

  b. The impulse history for each test is developed graphically for the 3-D (45^{0} torus sector) HVLF and the 2-D (7.5^{0} torus sector) HVLF. The latter is provided for both t_{pos} (2-D) and t_{pos} (3-D). This information is given in the microfiche (group 2) in Appendix E. The values of I_{neg}, t_{neg}, I_{pos}, and t_{pos} are listed as part of the heading of each plot along with the test start time, $\overline{t}_{0}$.

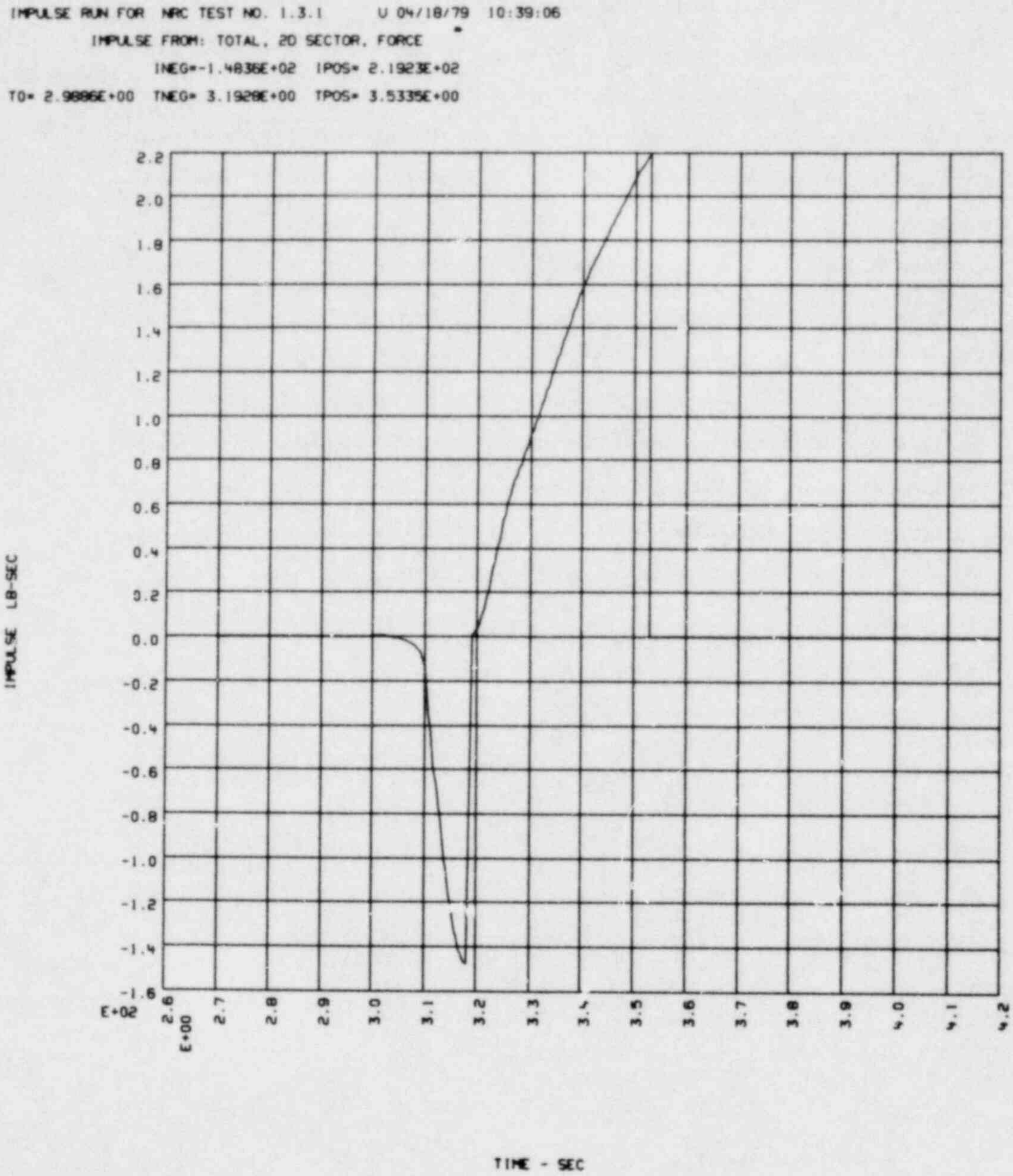

FIG. 2-8. HVLF impulse for 7.5^{0} torus sector (test 1.3.1).

TABLE 2-8. Impulse data summary (Tests 1.1, 1.3, 2.4, and 3.5).

Test no.	Sector	t_o--s	I_{neg} (lb-s)	t_{neg}--s	I_{pos} (lb-s)	t_{pos}--s	$\frac{I_{pos}}{I_{neg}}$	$\left(\frac{I^{45^o}}{6 \times I^{7.5^o}}\right)_{neg}$	$\left(\frac{I^{45^o}}{6 \times I^{7.5^o}}\right)_{pos}$
	45^o		-824.23	2.2021	1144.3	2.5743	1.388	--	--
1.1	7.5^o	1.9976	-125.94	2.2135	231.50	2.6316	1.838	1.091	0.824
	7.5^o		-125.94	2.2135	227.92	2.5743	1.810	1.091	0.837
	45^o		-938.87	2.8692	988.25	3.2071	1.053	--	--
1.3	7.5^o	2.6466	-140.23	2.8721	214.17	3.3274	1.527	1.116	0.769
	7.5^o		-140.23	2.8721	188.48	3.2071	1.344	1.116	0.874
	45^o		-891.52	3.0410	1190.8	3.4104	1.336	--	--
2.4	7.5^o	2.8159	-145.40	3.0381	246.79	3.6309	1.697	1.022	0.804
	7.5^o		-145.40	3.0381	222.24	3.4104	1.528	1.022	0.893
	45^o		-956.80	2.7461	1254.0	3.1155	1.311	--	--
3.5	7.5^o	2.5168	-142.06	2.7261	269.11	3.3160	1.894	1.122	0.777
	7.5^o		-142.06	2.7261	240.67	3.1155	1.694	1.122	0.868

TABLE 2-9. Impulse data summary (Tests 1.3.1, 1.4, 1.5, and 1.6).

Test no.	Sector	t_o--s	I_{neg} (lb-s)	t_{neg}--s	I_{pos} (lb-s)	t_{pos}--s	$\frac{I_{pos}}{I_{neg}}$	$\left(\frac{I^{45^o}}{6 \times I^{7.5^o}}\right)_{neg}$	$\left(\frac{I^{45^o}}{6 \times I^{7.5^o}}\right)_{pos}$
	45^o		-950.8	3.201	982.0	3.534	1.033	--	--
1.3.1	7.5^o	2.989	-148.4	3.193	243.4	3.757	1.640	1.068	0.672
	7.5^o		-148.4	3.193	219.2	3.534	1.478	1.068	0.746
	45^o		-751.7	1.873	967.5	2.211	1.287	--	--
1.4	7.5^o	1.645	-120.3	1.873	184.5	2.231	1.533	1.041	0.874
	7.5^o		-120.3	1.873	182.8	2.211	1.520	1.041	0.882
	45^o		-1015.9	2.843	1110.0	3.173	1.093	--	--
1.5	7.5^o	2.6342	-160.3	2.832	277.4	3.430	1.730	1.056	0.667
	7.5^o		-160.3	2.832	233.4	3.173	1.456	1.056	0.793
	45^o		-1064.8	1.707	972.7	2.019	0.913	--	--
1.6	7.5^o	1.500	-171.3	1.698	305.5	2.279	1.783	1.035	0.53
	7.5^o		-171.3	1.698	239.7	2.019	1.399	1.035	0.67

TABLE 2-10. Impulse data summary (Tests 2.1, 2.2, 2.3, and 3.1).

Test no.	Sector	t_o--s	I_{neg} (lb-s)	t_{neg}--s	I_{pos} (lb-s)	t_{pos}--s	$\frac{I_{pos}}{I_{neg}}$	$\left(\frac{I^{45^{\circ}}}{6 \times I^{7.5^{\circ}}}\right)_{neg}$	$\left(\frac{I^{45^{\circ}}}{6 \times I^{7.5^{\circ}}}\right)_{pos}$
2.1	45°	2.8602	-747.67	3.0238	818.41	3.3531	1.095	--	--
	7.5°		-121.60	3.0295	204.83	3.6939	1.684	1.025	0.666
	7.5°		-121.60	3.0295	179.49	3.3531	1.476	1.025	0.760
2.2	45°	2.5814	-627.18	2.7289	722.69	3.0554	1.152	--	--
	7.5°		-99.53	2.7347	177.61	3.2816	1.784	1.050	0.678
	7.5°		-99.53	2.7347	154.30	3.0554	1.550	1.050	0.781
2.3	45°	3.0188	-622.64	3.1699	717.31	3.4906	1.152	--	--
	7.5°		-95.57	3.1670	155.68	3.5335	1.629	1.086	0.768
	7.5°		-95.57	3.1670	149.45	3.4906	1.564	1.086	0.800
3.1	45°	3.1348	-996.89	3.3474	1223.6	3.7168	1.227	--	--
	7.5°		-159.51	3.3388	324.24	3.9688	2.033	1.042	0.629
	7.5°		-159.51	3.3388	268.61	3.7168	1.684	1.042	0.759

TABLE 2-11. Impulse data summary (Tests 2.5, 2.6, 2.8, and 3.2).

Test no.	Sector	t_o--s	I_{neg} (lb-s)	t_{neg}--s	I_{pos} (lb-s)	t_{pos}--s	$\frac{I_{pos}}{I_{neg}}$	$\left(\frac{I^{45^o}}{6 \times I^{7.5^o}}\right)_{neg}$	$\left(\frac{I^{45^o}}{6 \times I^{7.5^o}}\right)_{pos}$
	45°		-1184.0	2.9694	1172.9	3.3159	0.991	--	--
2.5	7.5°	2.7221	-188.70	2.9637	367.59	3.5421	1.948	1.046	0.532
	7.5°		-188.70	2.9637	292.93	3.3159	1.552	1.046	0.667
	45°		-561.89	3.4076	680.93	3.7799	1.212	--	--
2.6	7.5°	3.2446	-84.30	3.4047	151.61	3.8199	1.798	1.111	0.748
	7.5°		-84.30	3.4047	143.32	3.7799	1.700	1.111	0.792
	45°		-985.78	3.3790	1128.2	3.7598	1.144	--	--
2.8	7.5°	3.1622	-136.59	3.3732	249.93	3.8228	1.830	1.203	0.752
	7.5°		-136.59	3.3732	238.11	3.7598	1.743	1.203	0.790
	45°		-1019.3	3.1413	1601.5	3.5565	1.571	--	--
3.2	7.5°	2.9030	-161.10	3.1413	301.76	3.7541	1.873	1.054	0.884
	7.5°		-161.10	3.1413	271.79	3.5565	1.687	1.054	0.982

TABLE 2-12. Impulse data summary (Tests 2.7, 2.9, 2.10, and 2.11).

Test no.	Sector	t_o--s	I_{neg} (lb-s)	t_{neg}--s	I_{pos} (lb-s)	t_{pos}--s	$\frac{I_{pos}}{I_{neg}}$	$\left(\frac{I^{45^o}}{6 \times I^{7.5^o}}\right)_{neg}$	$\left(\frac{I^{45^o}}{6 \times I^{7.5^o}}\right)_{pos}$
2.7	45^o	3.2518	-1071.7	3.4935	1344.9	3.8715	1.255	--	--
	7.5^o		-167.33	3.5021	290.27	3.9688	1.735	1.067	0.772
	7.5^o		-167.33	3.5021	271.69	3.8715	1.624	1.067	0.825
2.9	45^o	1.3076	-930.0	1.5692	1190.1	1.9615	1.280	--	--
	7.5^o		-130.97	1.5721	242.62	1.9902	1.852	1.183	0.818
	7.5^o		-130.97	1.5721	240.33	1.9615	1.835	1.183	0.825
2.10	45^o	2.7266	-1250.3	2.9580	1488.5	3.3503	1.190	--	--
	7.5^o		-180.76	2.9580	320.98	3.4276	1.776	1.153	0.773
	7.5^o		-180.76	2.9580	305.47	3.3503	1.690	1.153	0.812
2.11	45^o	1.4312	-1316.0	1.6580	1598.1	2.0503	1.214	--	--
	7.5^o		-190.75	1.6580	371.35	2.2765	1.947	1.150	0.717
	7.5^o		-190.75	1.6580	328.44	2.0503	1.722	1.150	0.811

TABLE 2-13. Impulse data summary (Tests 3.3A, 3.3B, 3.4A, and 3.4B).

Test no.	Sector	t_o--s	I_{neg} (lb-s)	t_{neg}--s	I_{pos} (lb-s)	t_{pos}--s	$\frac{I_{pos}}{I_{neg}}$	$\left(\frac{I^{45^o}}{6 \times I^{7.5^o}}\right)_{neg}$	$\left(\frac{I^{45^o}}{6 \times I^{7.5^o}}\right)_{pos}$
3.3A	45^o	2.7786	-750.11	2.9895	925.89	3.3531	1.234	--	--
	7.5^o		-141.00	2.9895	302.76	3.6108	2.147	0.887	0.510
	7.5^o		-141.00	2.9895	242.98	3.3531	1.723	0.887	0.635
3.3B	45^o	2.9123	-673.08	3.1155	623.41	3.2444	0.926	--	--
	7.5^o		-140.33	3.1212	287.52	3.7340	2.049	0.800	0.361
	7.5^o		-140.33	3.1212	90.89	3.2444	0.648	0.800	1.143
3.4A	45^o	2.7964	-1036.0	3.0295	1231.3	3.3903	1.188	--	--
	7.5^o		-167.24	3.0181	336.14	3.6395	2.010	1.032	0.610
	7.5^o		-167.24	3.0181	286.39	3.3903	1.712	1.032	0.716
3.4B	45^o	2.2224	-892.99	2.4512	1148.9	2.7976	1.286	--	--
	7.5^o		-167.19	2.4483	341.47	3.1069	2.042	0.890	0.561
	7.5^o		-167.19	2.4483	279.04	2.7976	1.669	0.890	0.686

TABLE 2-14. Impulse data summary (average for blocked vent Tests 3.3 and 3.4).

Test no.	Sector	t_o--s[b]	$\hat{I}_{neg}$[a] (lb-s)	t_{neg}--s[b]	$\hat{I}_{pos}$[a] (lb-s)	t_{pos}--s[b]	$\frac{\hat{I}_{pos}}{\hat{I}_{neg}}$	$\left(\frac{\hat{I}^{45^\circ}}{6 \times \hat{I}^{7.5^\circ}}\right)_{neg}$	$\left(\frac{\hat{I}^{45^\circ}}{6 \times \hat{I}^{7.5^\circ}}\right)_{pos}$
	45°	0	-711.60	0.203 to 0.210	774.65	0.129 to 0.364	1.089	--	--
3.3	7.5°	0	-140.66	0.209 to 0.211	295.14	0.613 to 0.621	2.098	0.843	0.437
(Avg)	7.5°	0	-140.66	0.209 to 0.211	166.94	0.123 to 0.364	1.187	0.843	0.773
	45°	0	-964.50	0.229 to 0.233	1190.10	0.346 to 0.361	1.234	--	--
3.4	7.5°	0	-167.22	0.174 to 0.222	338.80	0.621 to 0.659	2.026	0.961	0.585
(Avg)	7.5°	0	-167.22	0.174 to 0.222	282.72	0.349 to 0.372	1.691	0.961	0.702

---

[a] $\hat{I}$ designates the average rather than the calculated mean.

[b] All times are referenced to the actual starting time of the particular tests, hence the indicated time ranges.

2.2.2 DISCUSSION OF THE IMPULSE RATIOS

Figure 2-9 plots the ratio of positive to negative impulse and the ratio of 3-D to 2-D impulse (negative and positive) versus drywell pressurization rate for each relevant case of the standard downcomer tests; Fig. 2-10 plots these ratios for extended downcomer tests. The notation "limited" in these graphs refers to the second 7.5° HVLF impulse evaluation, wherein the positive integration was stopped at $t_{pos}^{45^0}$.

The plots of I_{pos}/I_{neg} (curve a) vary significantly in the 3-D and 2-D tests. This ratio <u>decreases</u> with increasing pressurization rate in the 3-D tests. In the 2-D tests the impulse ratio shows substantial <u>increase</u> with increasing pressurization rate. A study of the components of the ratios shows that in the 3-D case the positive impulse (numerator) is little affected by a change in $\dot{p}_{dw}$, while the negative impulse (denominator) shows a uniform increase with the $\dot{p}_{dw}$ increase. The 2-D case exhibits a negative impulse behavior similar to the 3-D case. In the 2-D case, however, the positive impulse exhibits a strong dependence on $\dot{p}_{dw}$ so that as $\dot{p}_{dw}$ increases, the ratio of $(I_{pos}/I_{neg})_{2D}$ increases.

The lower set of plots on Figs. 2-9 and 2-10 shows the ratio of 3-D impulse to 2-D impulse. The negative impulse portion is essentially independent of pressurization rate and is near unity. This suggests that the 2-D geometrical model is capable of predicting the behavior of the 3-D system, confirming the previous study of peak downloads from the HVLFs. Because the decreasing ratios of positive impulse move further and further from unity with increasing $\dot{p}_{dw}$, however, it seems evident that there is a substantial difference in pool swell behavior between 2-D and 3-D systems.

The plots in Fig. 2-11 show the effects of drywell overpressure on impulse. For both 3-D and 2-D sectors, the impulse ratios (I_{pos}/I_{neg} and $I^{45^0}/(6 \times I^{7.5^0})$) are only a weak function of $\Delta\dot{p}_{dw}$. The effect of constrained pool swell in the 7.5° torus sector is pronounced, however, and causes the positive impulse effects in the 2-D sector to diverge from those observed in the 3-D sector. The negative impulse, however, is well-represented by both the 2-D and 3-D sectors.

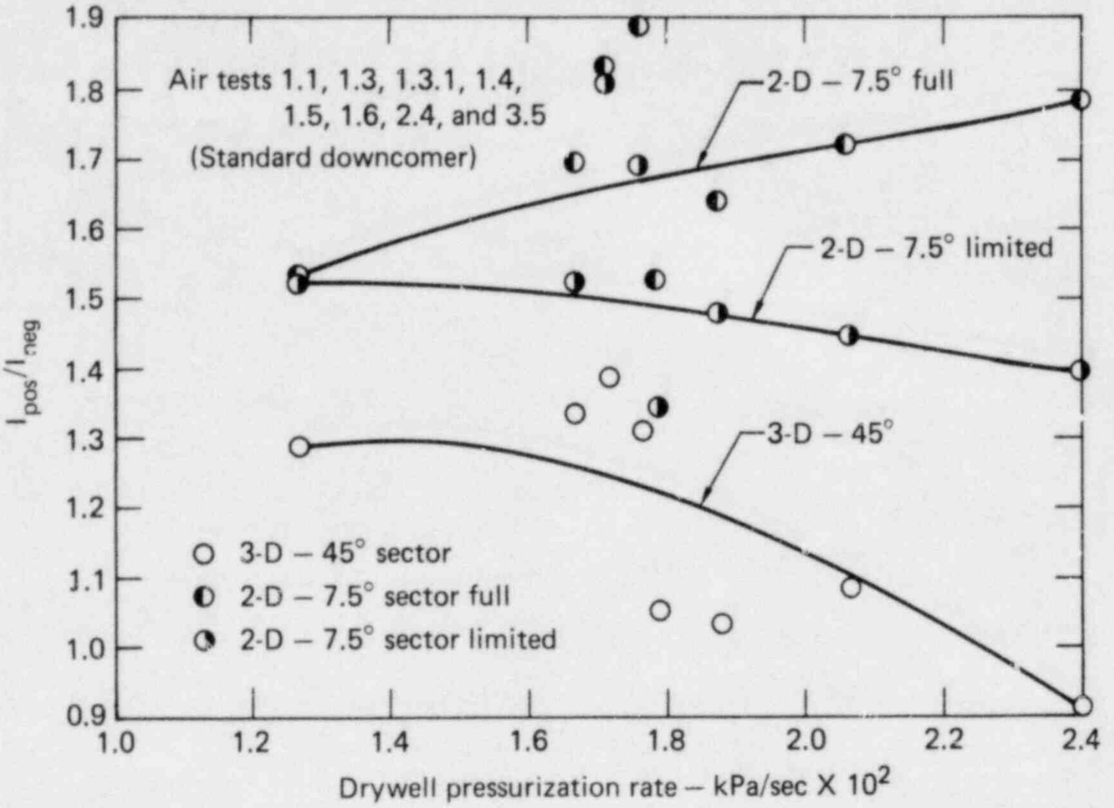

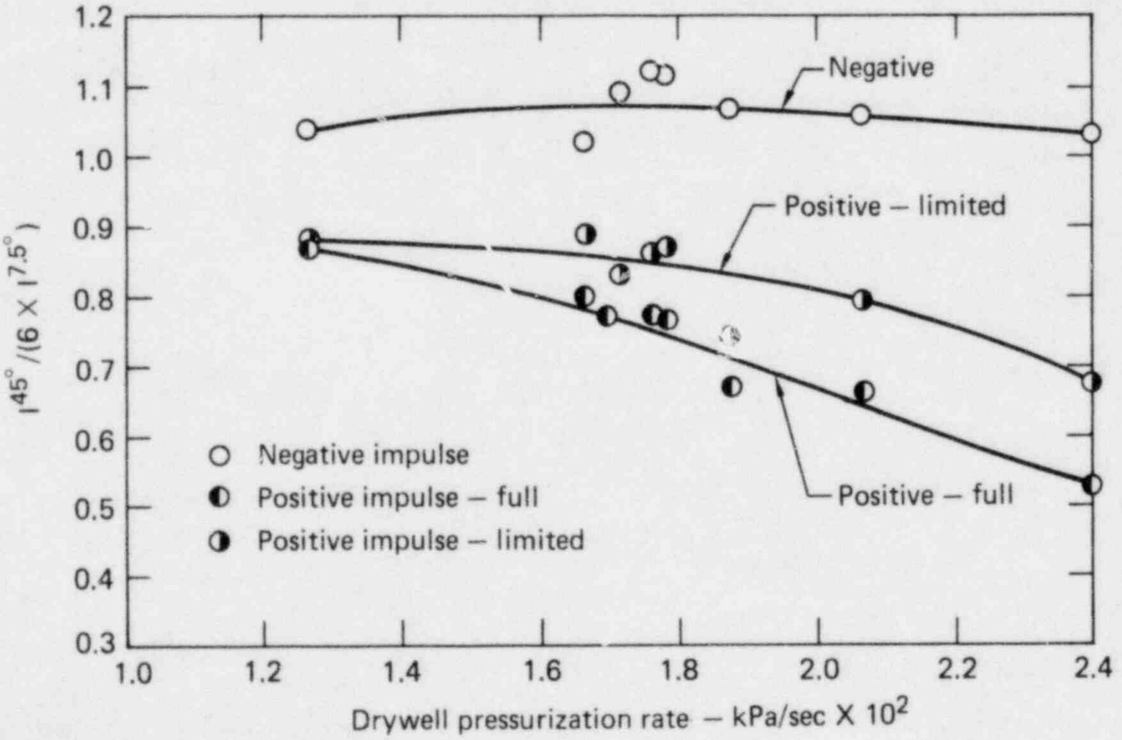

FIG. 2-9. Effect of drywell pressurization rate on HVLF impulse ratios. (standard length downcomer)

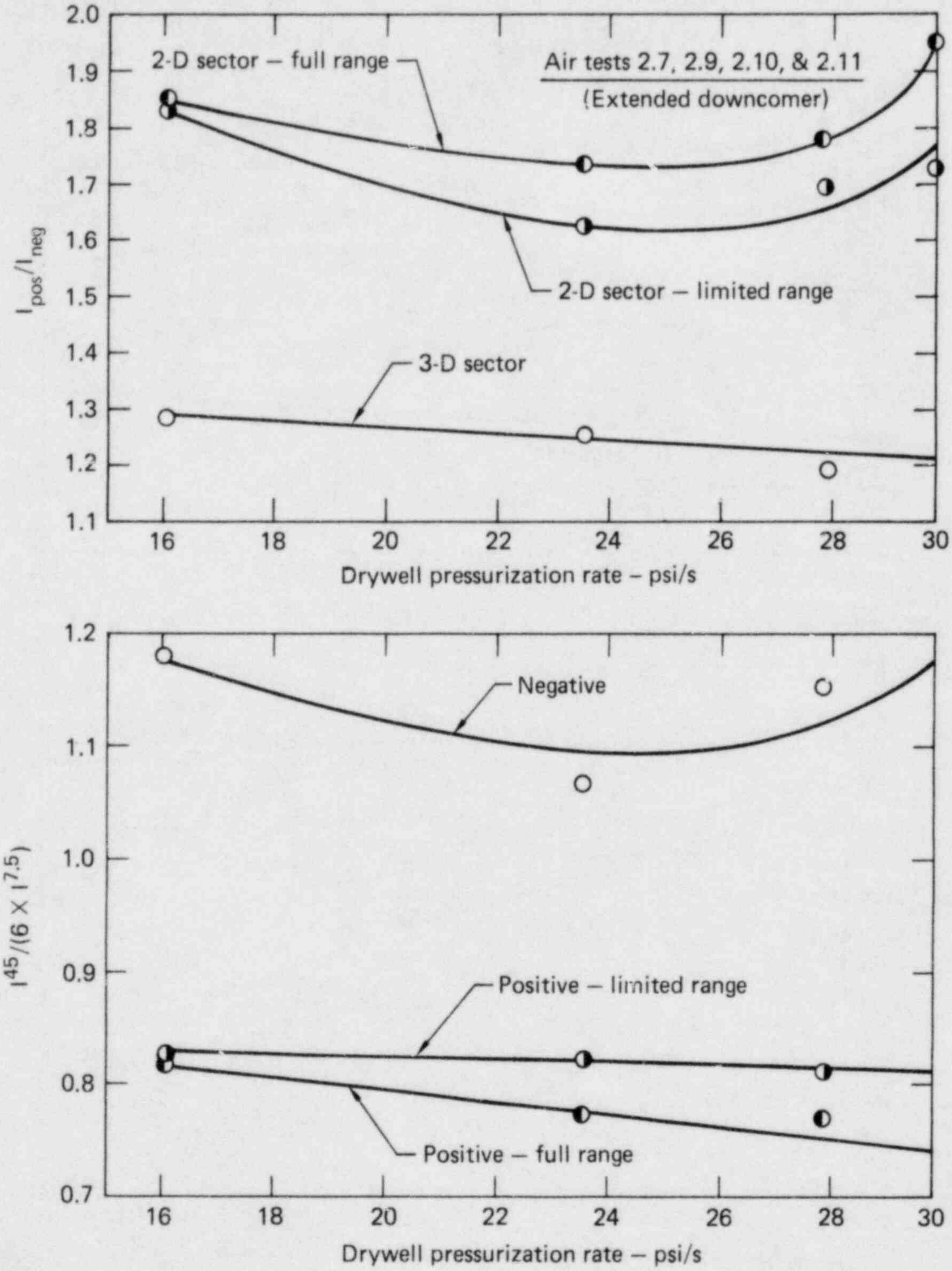

FIG. 2-10. Effect of drywell pressurization rate on HVLF impulse ratios. (extended length downcomer)

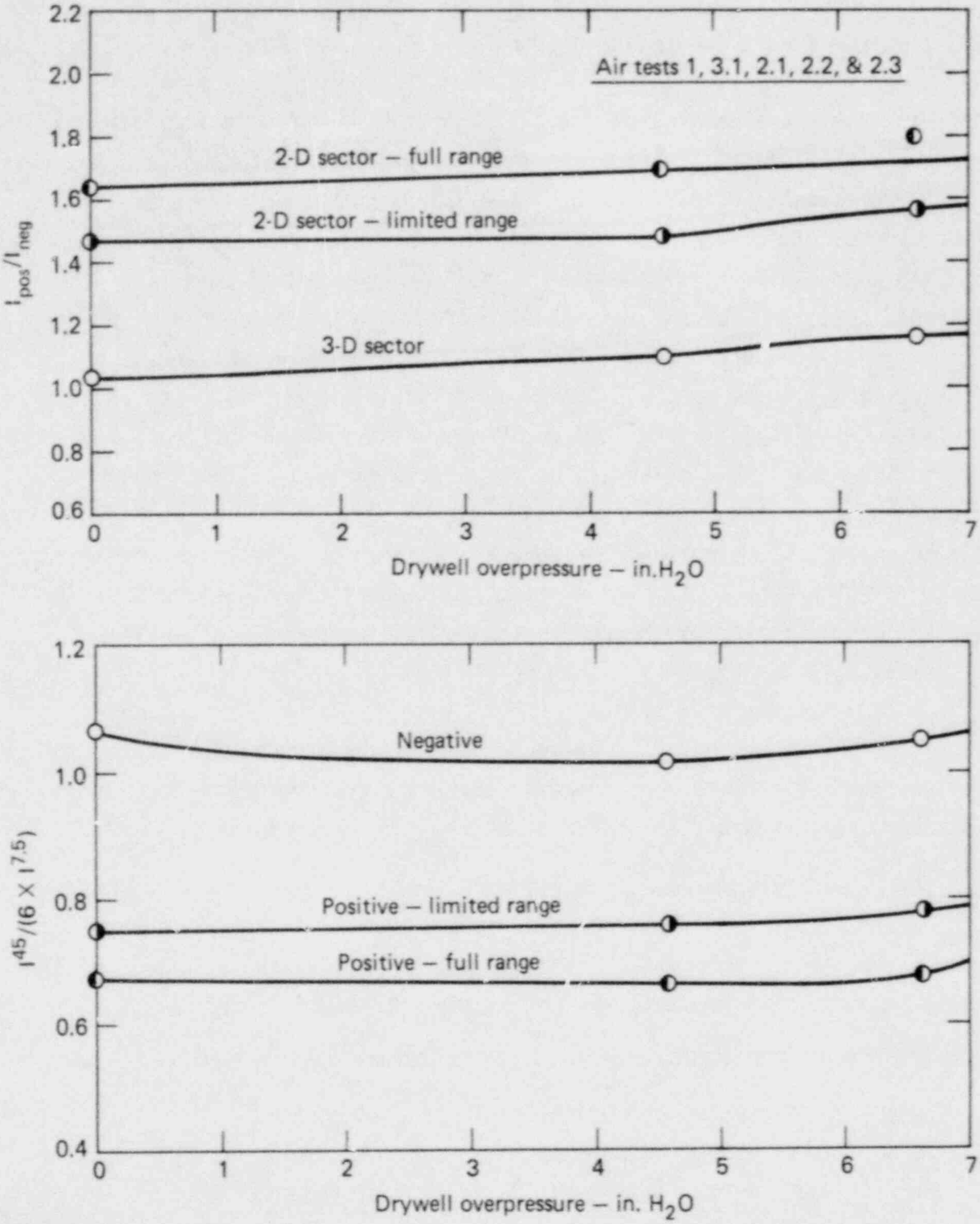

FIG. 2-11. Effect of drywell overpressure on HVLF impulse ratios.

2.3 STRUCTURAL INERTIAL EFFECTS STUDY

2.3.1 DYNAMIC MODELING OF THE RESPONSE VERTICAL LOAD FUNCTION

This section provides a dynamic modeling of the response vertical load function (RVLF) resulting from air test 1.3.1.[*] As input, the four internal ringheader strut load cell force histories and the computed hydrodynamic vertical load function (HVLF) of test 1.3.1 are used. These forces are applied to a finite element model of the 90^0 torus sector using the linear SAP4 finite-element code. This model,[9] makes use of beam elements which characterize the torsional and longitudinal stiffness of the torus shell. Three external torus sector supports carry the response measuring load cells. In the actual facility, the load cells are located on the strut at one end of the torus sector (LC-1), as well as on the outside and inside support trunnions of the torus sector midplane[†] (LC-4 and LC-5). In the finite element model, the strut and LC-1 are represented as a vertical Hooke's Law spring of stiffness k_1. The dual midplane support trunnions and their load cells are represented by the combination of a single vertical spring of stiffness k_2 and a clock spring of stiffness k_3.

The overall seven-node finite element model is shown in Fig. 2-12, as are the beam element properties, component weights, and spring constants. The component weights are distributed among the nodes as follows.

- At each of the five interior nodes (2 through 6), 1/6 of the water mass and 1/6 of the structure mass are applied.
- At the two end nodes (1 and 7), 1/12 of the water mass, 1/12 of the structure mass, and the entire end plate mass are applied.

The dynamic forces measured by the load cells are distributed as follows.

- LC-2--25 percent at node 1; 75 percent at node 2.
- LC-3--75 percent at node 3; 25 percent at node 4.
- LC-6--25 percent at node 4; 75 percent at node 5.
- LC-7--75 percent at node 6; 25 percent at node 7.

---

[*] See page 53 in Ref. 1 and Appendix E, fiche group 5.

[†] See Ref. 1, Fig. 9.

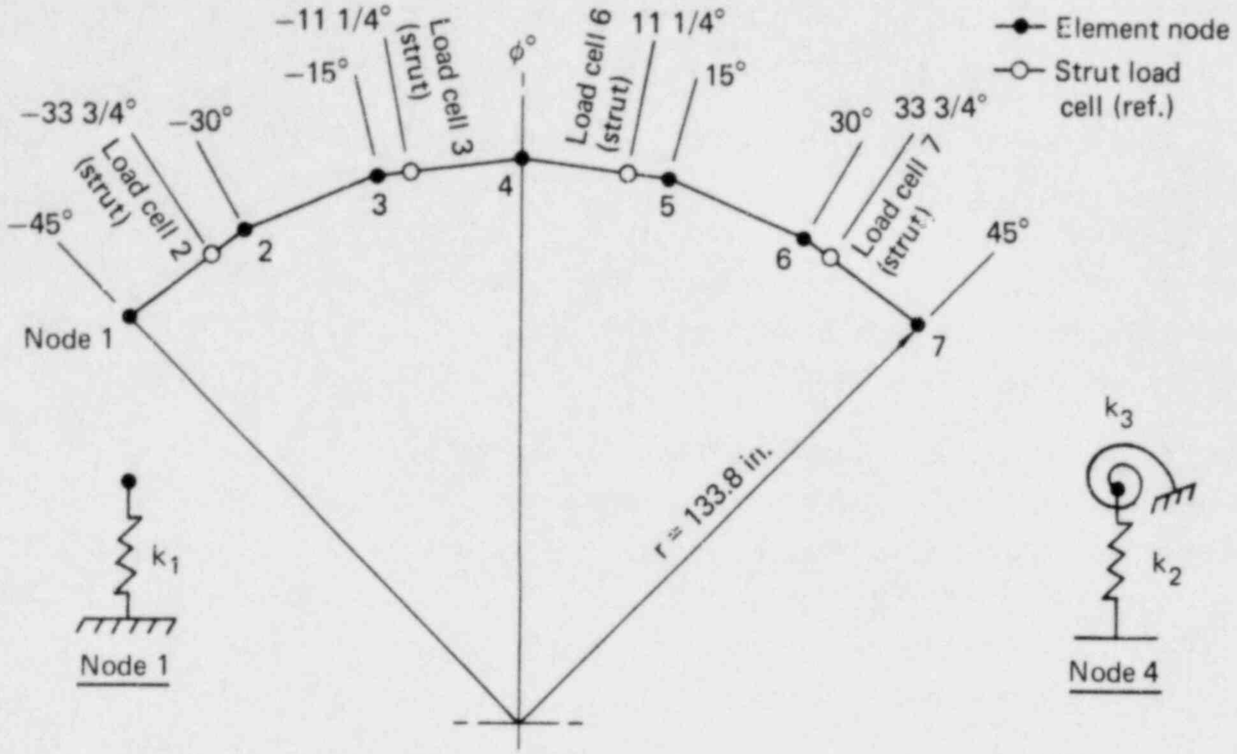

Beam elements: $E_y = 29 \times 10^6$ psi, $\nu = 0.27$
$I_b = 1.25 \times 10^5$ in.^{4}
$J = 2.50 \times 10^5$ in.^{4}
$A_s = 177.06$ in.^{2}
Cross section, circumference = 74.4" i.d.; t = 0.75 in.

Weight: Structure – 15,212 lb (W_s)
End plate – 4,594 lb(W_e)
Water – 15,340 lb (W_w)

Lumped mass: At nodes 1 and 7, $m = \frac{l}{g}\left(\frac{W_s}{12} + \frac{W_W}{12} + W_e\right) = 18.5 \frac{\text{lb-s}^2}{\text{in.}}$

At nodes 2 through 6, $m = \frac{l}{g}\left(\frac{W_s}{6} + \frac{W_w}{6}\right) = 13.2 \frac{\text{lb-s}^2}{\text{in.}}$

Springs: $k_1 = 1.88 \times 10^6$ lb/in.
$k_2 = 1.54 \times 10^7$ lb/in.
$k_3 = 3.26 \times 10^{10}$ in.-lb/rad.

FIG. 2-12. Finite element model of 90° torus.

The HVLF force is distributed as 1/12 at nodes 1 and 7 and 1/6 at each of nodes 2 through 6. The applied force histories for the force load cells (LC-2, LC-3, LC-6, LC-7) and the hydrodynamic load function are shown in Figs. 2-13 through 2-17.

Five cases were studied. The base case (1.3.1.0) used the conditions specified above. Case 1.3.1.+ increased each of the three spring constants k_1, k_2, and k_3 by a uniform 20 percent. Case 1.3.1.- decreased the spring constants by 20 percent. Case 1.3.1.2 modified the base case by increasing the water mass by 20 percent. The final case (1.3.1.3) increased the water mass by 30 percent. These conditions are listed in Table 2-15.

The 90^0 torus structure was experimentally studied earlier by M. Posehn,[10] who determined the natural frequencies of the water containing structure. A comparison of the measured response with the system modal content computed by the SAP4 code is shown in Table 2-16. In no case do these frequencies deviate from those measured by more than approximately 16 percent. The mode shapes of the three lowest modes of vertical vibration are shown in Fig. 2-18.

The dynamic calculations of the SAP4 code provide a vertical force history at node 1 and at node 4, as well as a moment history at node 4. The node 1 force history directly simulates the response of LC-1. In order to simulate the response of LC-4 and LC-5, it is necessary to transform the node 4 force and moment into an appropriate force couple. The geometry involved and the equations used are shown in Fig. 2-19.

The results of each case study include response force histories simulating LC-1, LC-4, and LC-5; their sum then simulates the observed RVLF. A summary of the results for the five cases considered here is given by Table 2-17. In this table, the peak vertical forces from each case are compared to those measured during test 1.3.1. The measured force histories for LC-1, LC-4A, LC-5B, and the RVLF are shown in Figs. 2-20 through 2-23.* A complete set of the four SAP-4 computed load histories simulating LC-1, LC-4, LC-5, and the

---

*In the actual PSE experiments, two load cell transducers were used at each location 4 and 5, providing redundant "A" and "B" measurements at these locations. For a discussion of the selection process for these measurements, see page 61 in Ref. 1.

RVLF for case 1.3.1.0 is included here as Figs. 2-24 through 2-27, respectively.

Finally, the frequency analysis of all measured forces histories (LC-1 through LC-7 and the RVLF) and the computed force histories for case 1.3.1.0 (LC-1, LC-4, LC-5, and the simulated RVLF) was performed. These results, along with all computed SAP4 load histories, are provided on microfiche in Appendix E.3. Figure 2-28 shows a typical result of the frequency analysis.

In all cases, the SAP4 model closely predicts the measured modal content of the structural system; in case 1.3.1.+, the computed frequencies are within 1 percent agreement with the measured frequencies.

The peak load cell forces, however, are underpredicted by the SAP4 model in all cases, except in the case of the simulated load cell 5 for which the maximum load is overpredicted. On the minimum load, the deviations range from 9 percent to 30 percent. The maximum load deviations range from a low of 5 percent at LC-5 to a high of 45 percent at LC-1. The simulated RVLF minimum load is underpredicted by 15 to 20 percent, and the corresponding maximum is underpredicted by 13 to 26 percent.

The simplified model used was adequate to demonstrate that the measured modal content of the experimental facility was correct. The analytical model was, however, inadequate to allow a highly accurate prediction of the response function. The high degree of consistency in the results leads to the conclusion that, overall, the facility is suitably designed for the intended hydrodynamic measurements and that these measurements are not compromised by structurally induced forces.

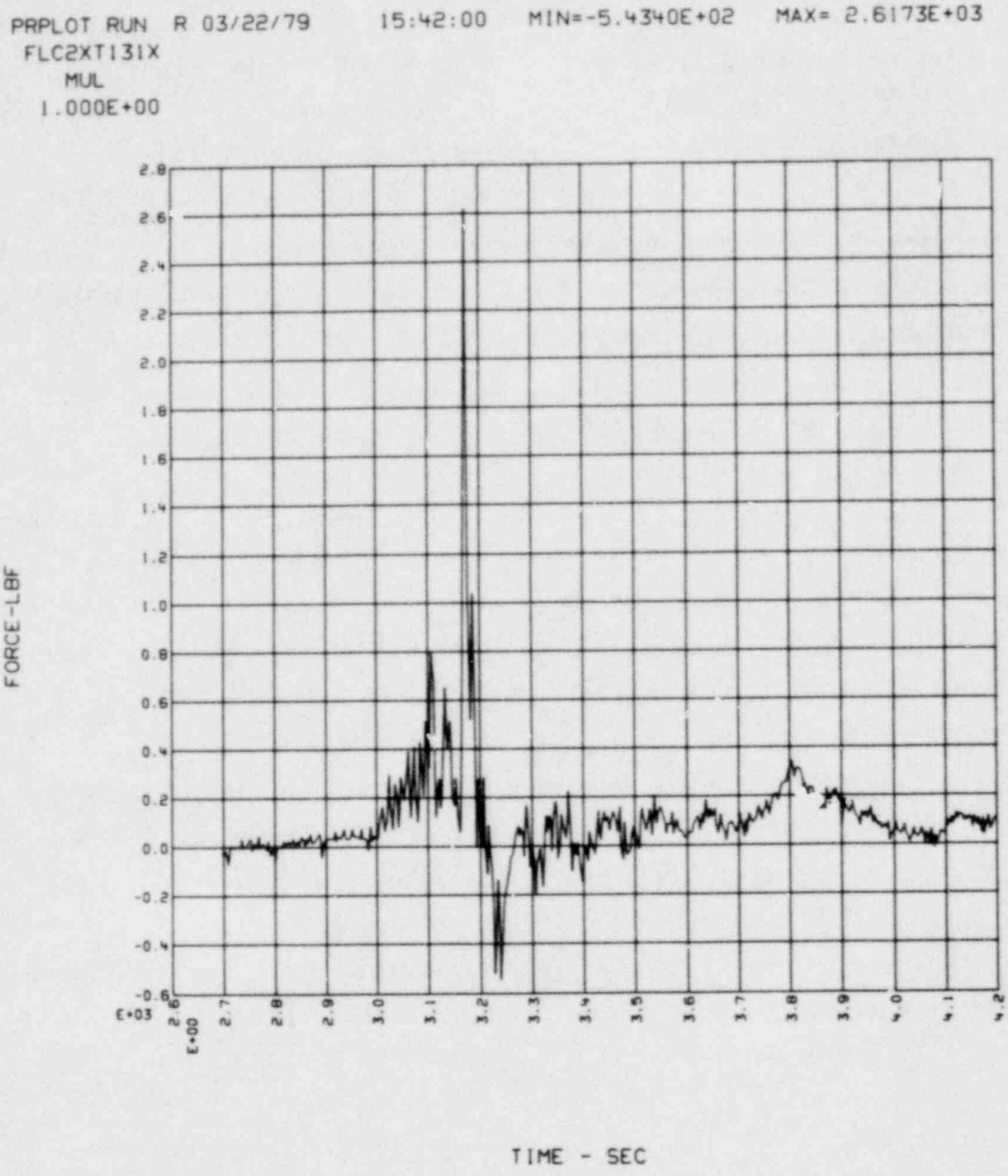

FIG. 2-13. Applied force history, load cell LC-2.

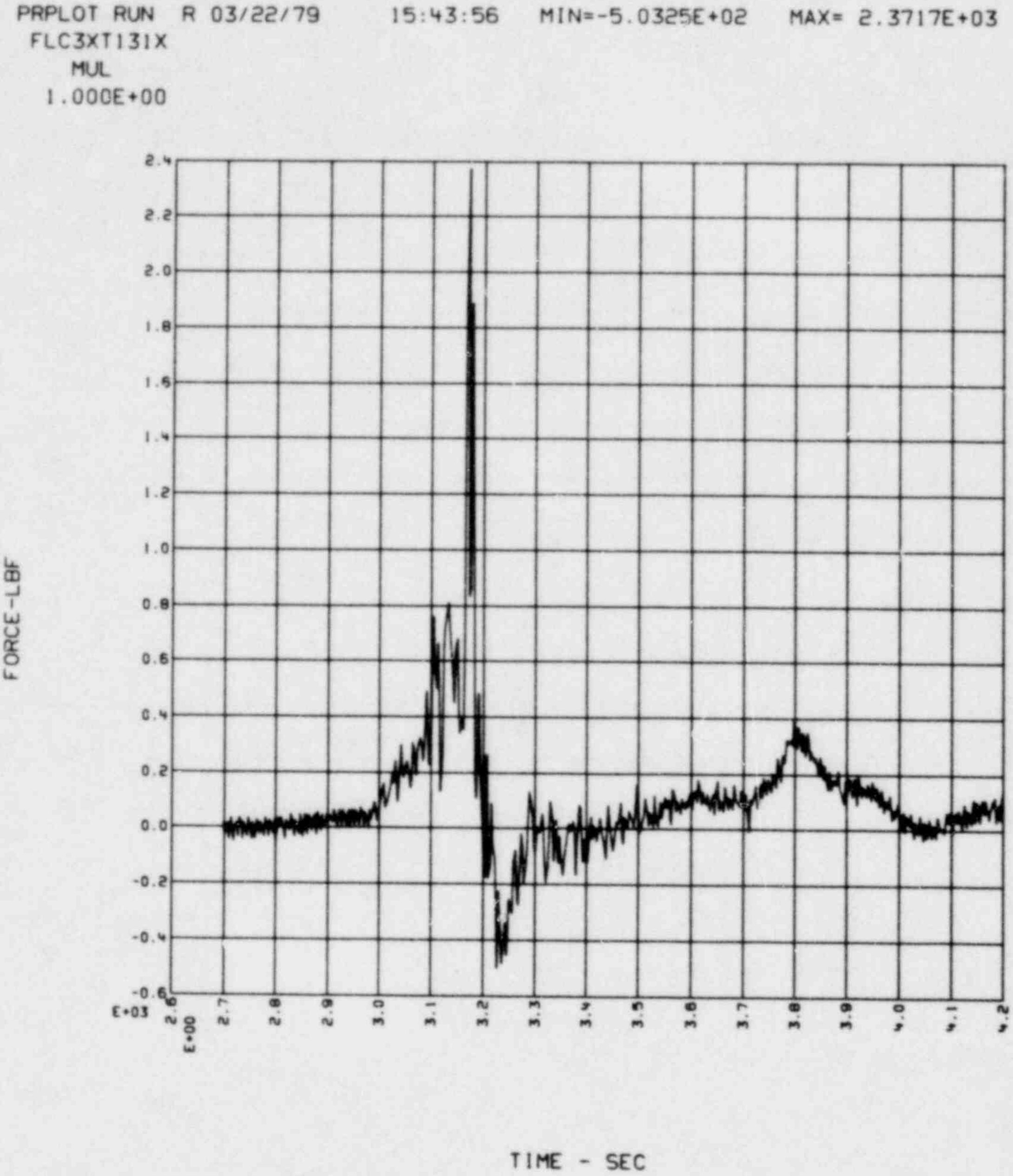

FIG. 2-14. Applied force history, load cell LC-3.

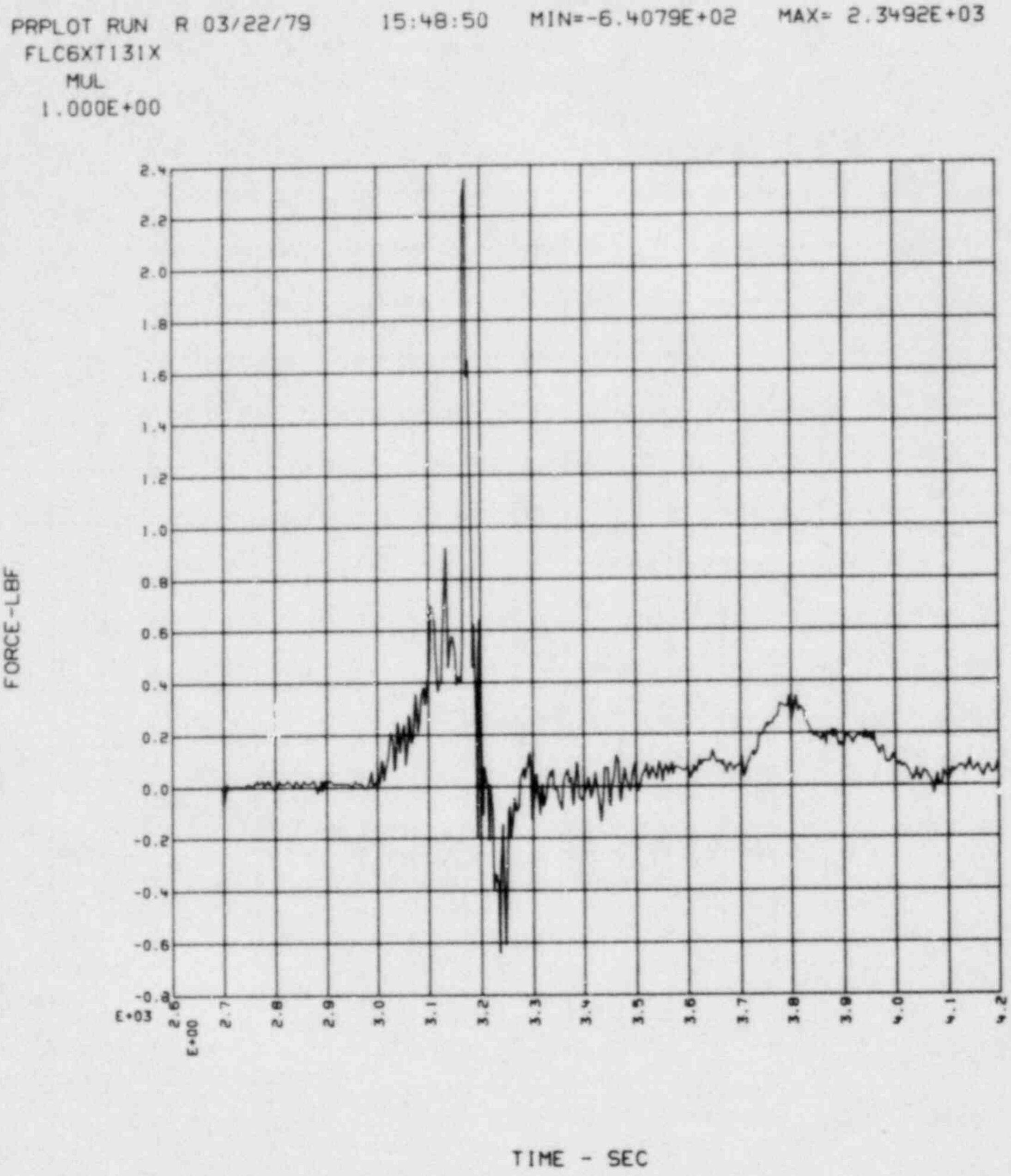

FIG. 2-15. Applied force history, load cell LC-6.

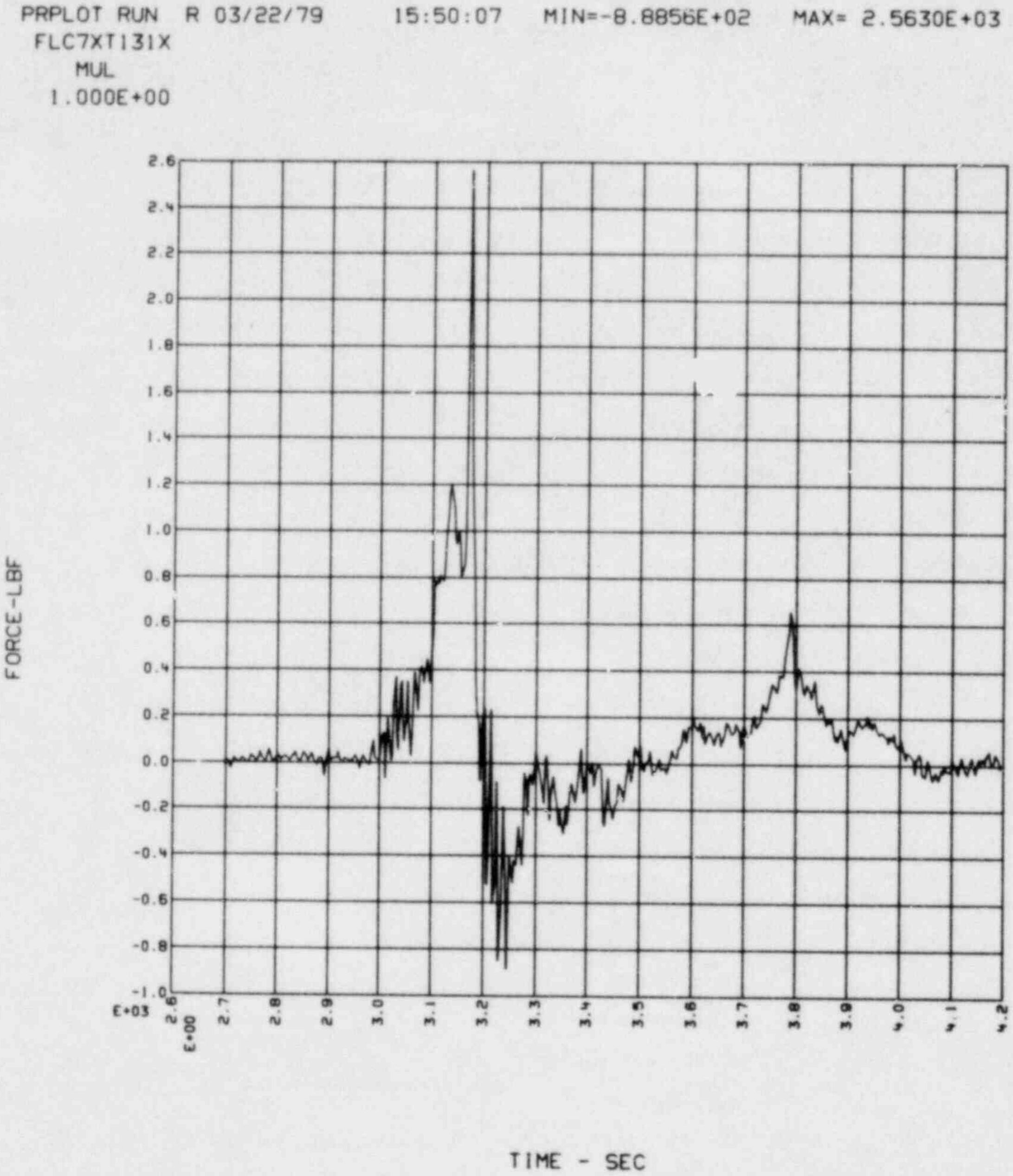

FIG. 2-16. Applied force history, load cell LC-7.

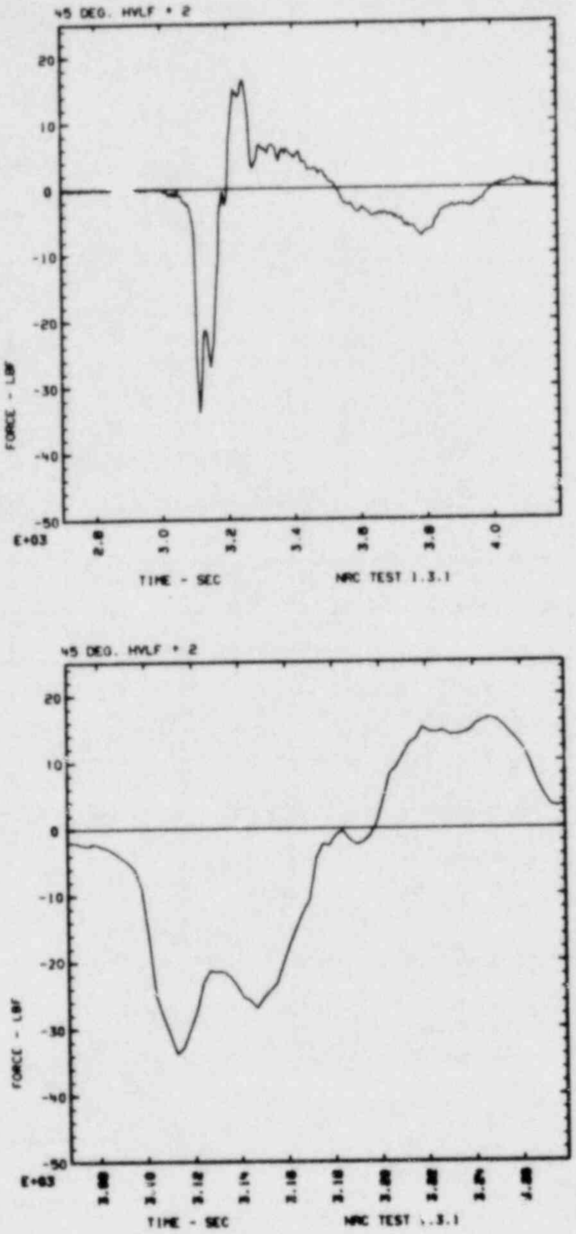

FIG. 2-17. Applied HVLF, 90° torus sector.

TABLE 2-15. Basic problem conditions.

	Spring constants			
Problem number	k_1 (lb/in.)	k_2 (lb./in)	k_3 (in.-lb/rad)	Water mass (lb-s^2/in.)
1.3.1.0	1.88×10^6	1.54×10^7	3.26×10^{10}	39.75
1.3.1.+	2.256×10^6	1.848×10^7	3.912×10^{10}	39.75
1.3.1.-	1.504×10^6	1.232×10^7	2.608×10^{10}	39.75
1.3.1.2	1.88×10^6	1.54×10^7	3.26×10^{10}	47.70
1.3.1.3	1.88×10^6	1.54×10^7	3.26×10^{10}	51.68

TABLE 2-16. Experimental and analytical natural frequencies (torus with water).

	SAP4 analytical model--Hz				
Hammer blow tests--Hz	Case .0	Case .+	Case .-	Case .2	Case .3
25.9	23.8	25.6	21.7	23.1	22.8
59.8	55.1	59.3	50.3	53.4	52.6
--	135.8	143.0	127.1	130.6	128.5

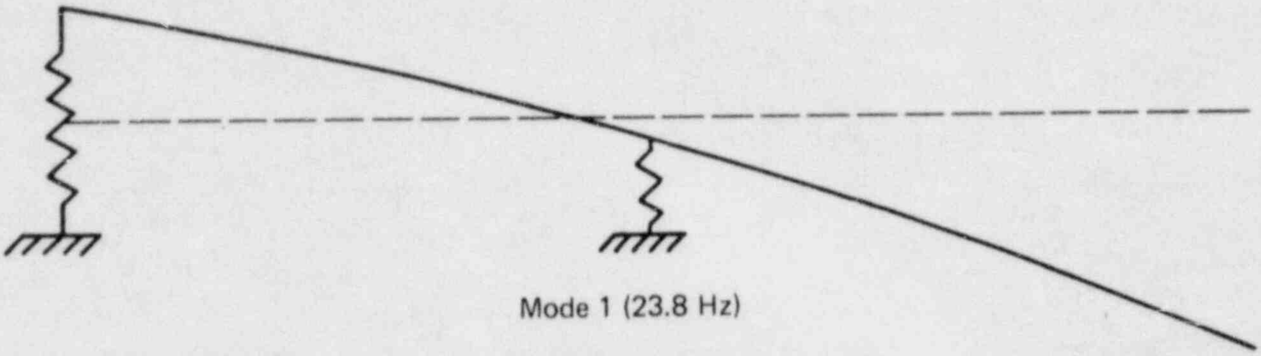

Mode 1 (23.8 Hz)

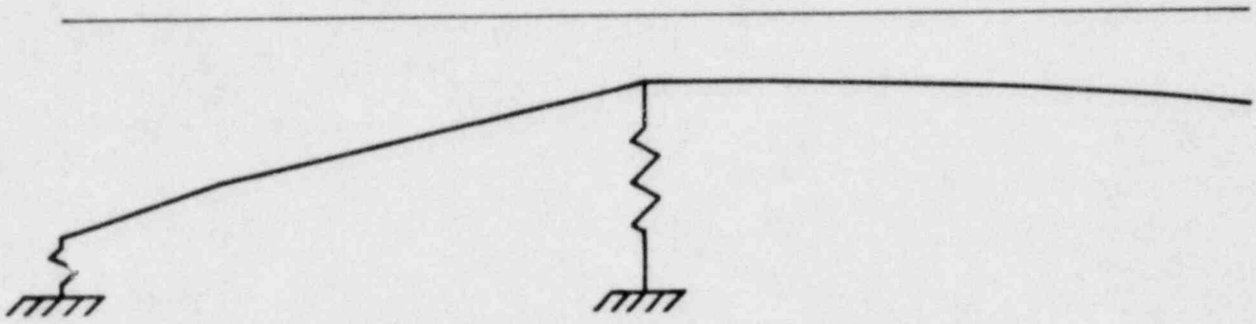

Mode 2 (55.8 Hz)

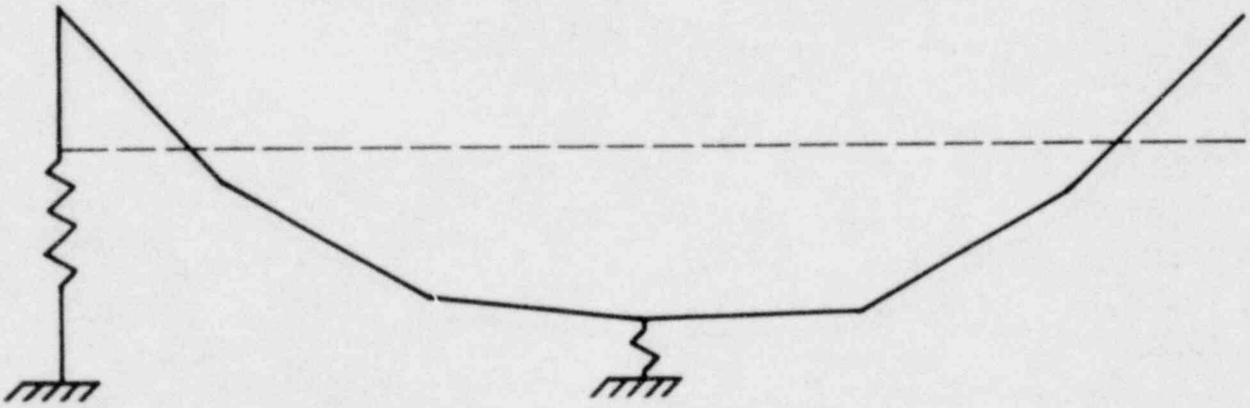

Mode 3 (135.8 Hz)

FIG. 2-18. Mode shapes of lowest three modes of vertical vibration.

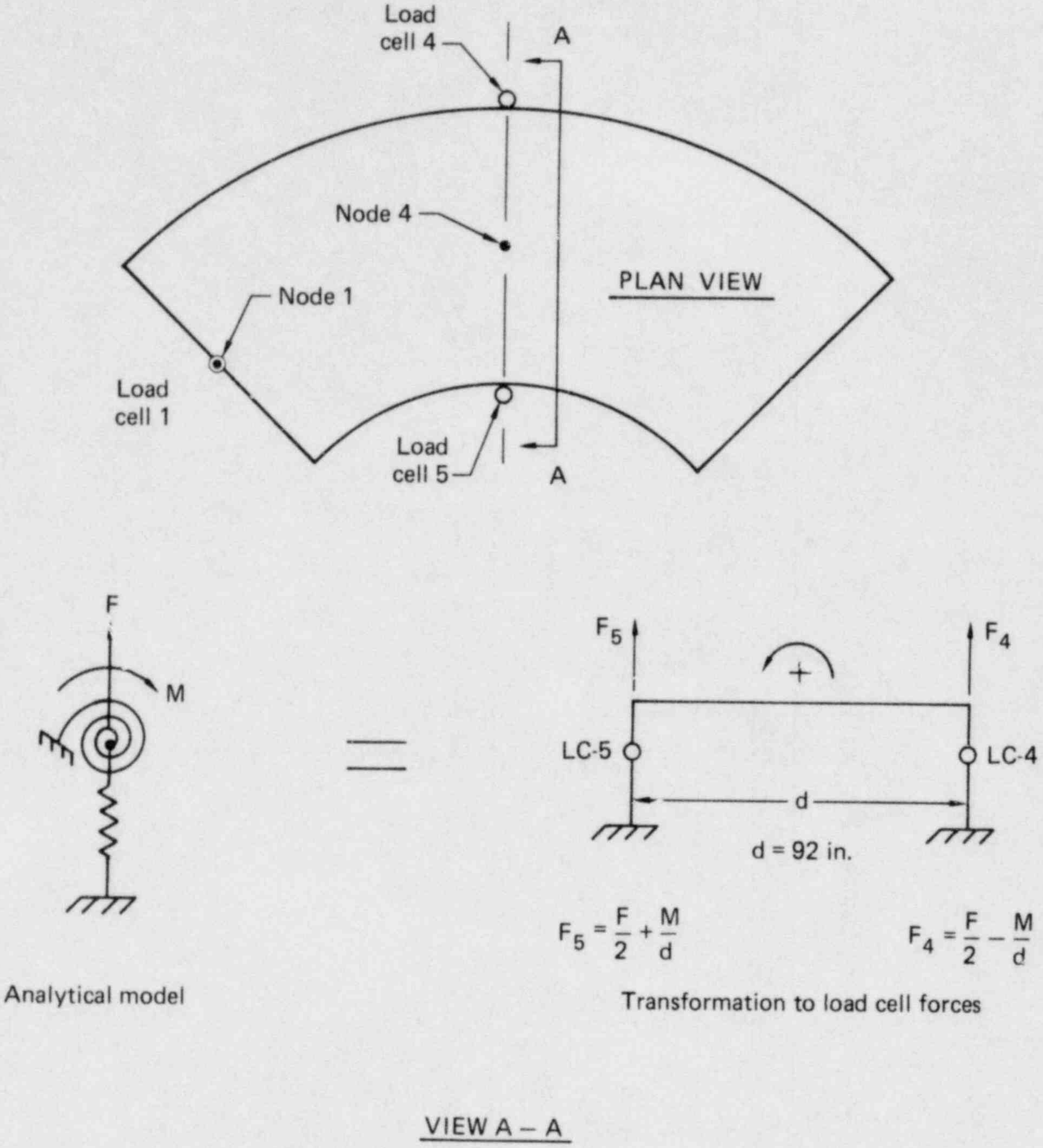

FIG. 2-19. Transformation of analytical model force and moment to load cell forces.

TABLE 2-17. Experimental and analytical natural frequencies (torus with water).

Load cell	Measured		Case .0		Case .+		Case .-		Case .2		Case .3	
	Min.	Max.	Min.	Max.	Min.	Max.	Min.	Max.	Min.	Max.	Min.	Max.
1	-7440	8620	-5790	5400	-5200	4730	-5560	4990	-5925	5490	-5950	5485
4	-16120	6580	-11640	5530	-11340	5830	-11970	5120	-11775	5465	-11825	5415
5	-24250	11950	-21930	14500	-21900	14740	-22340	12570	-22100	14150	-22165	13945
RVLF[a] (sum)	-42000	19530	-34280	16080	-33200	16920	-35540	14490	-34710	15610	-34900	15370

[a] Times of peak loads on load cells 1, 4, and 5 do not occur at the same time so that the RVLF sum $\neq \Sigma$LC-1, 4 and 5.

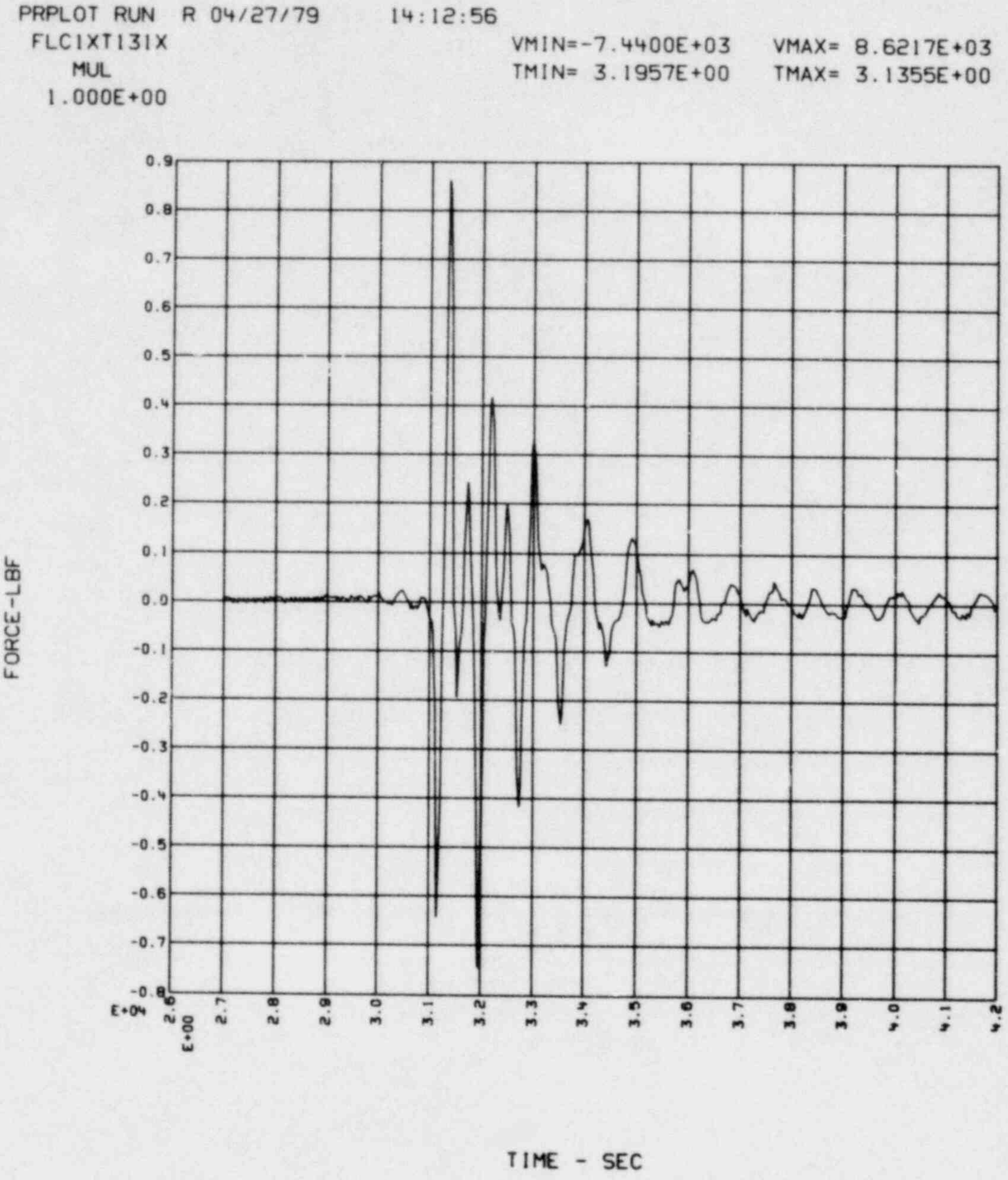

FIG. 2-20. Measured force history, load cell LC-1.

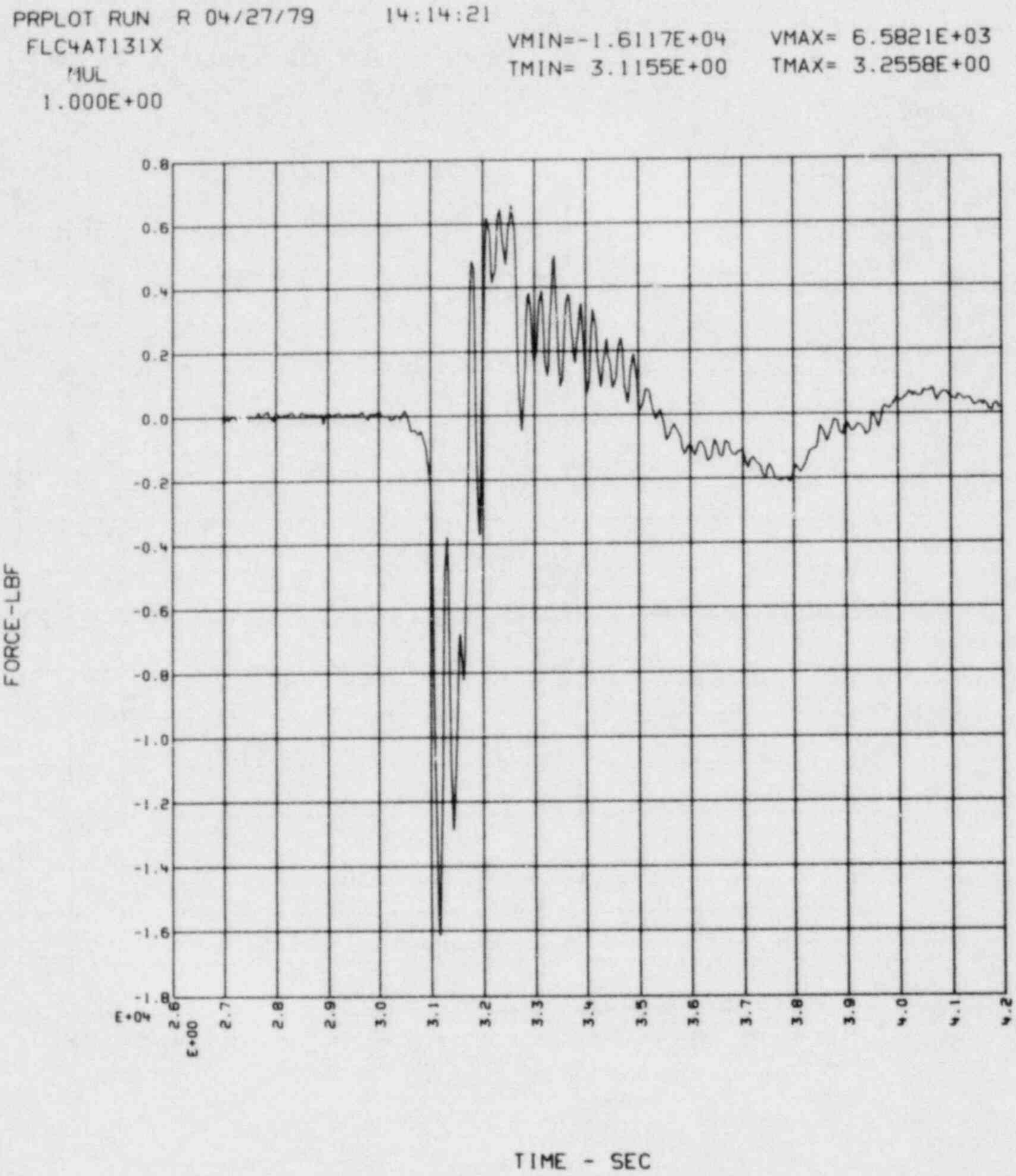

FIG. 2-21. Measured force history, load cell LC-4A.

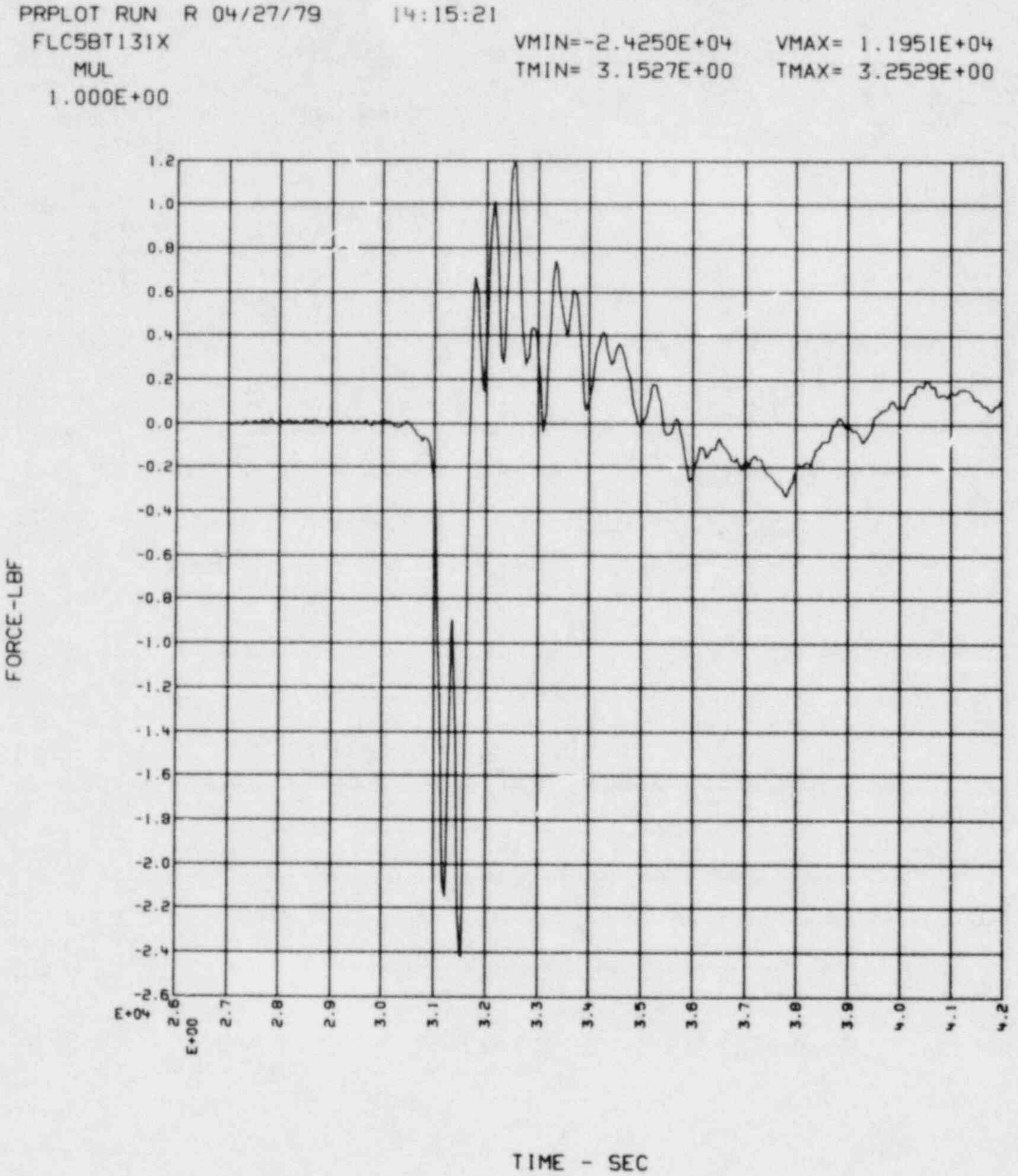

FIG. 2-22. Measured force history, load cell LC-5B.

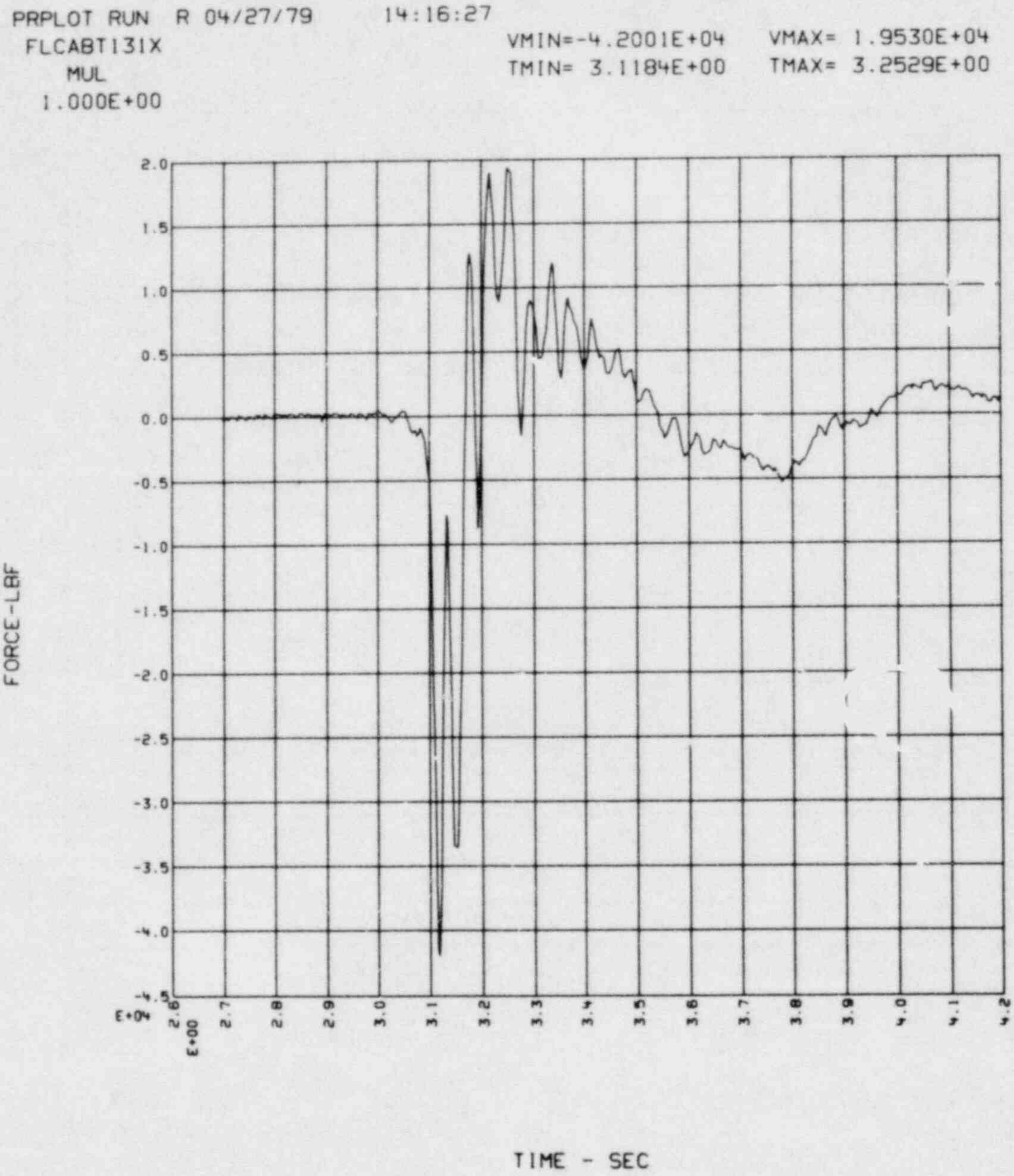

FIG. 2-23. Measured response vertical load function (RVLF).

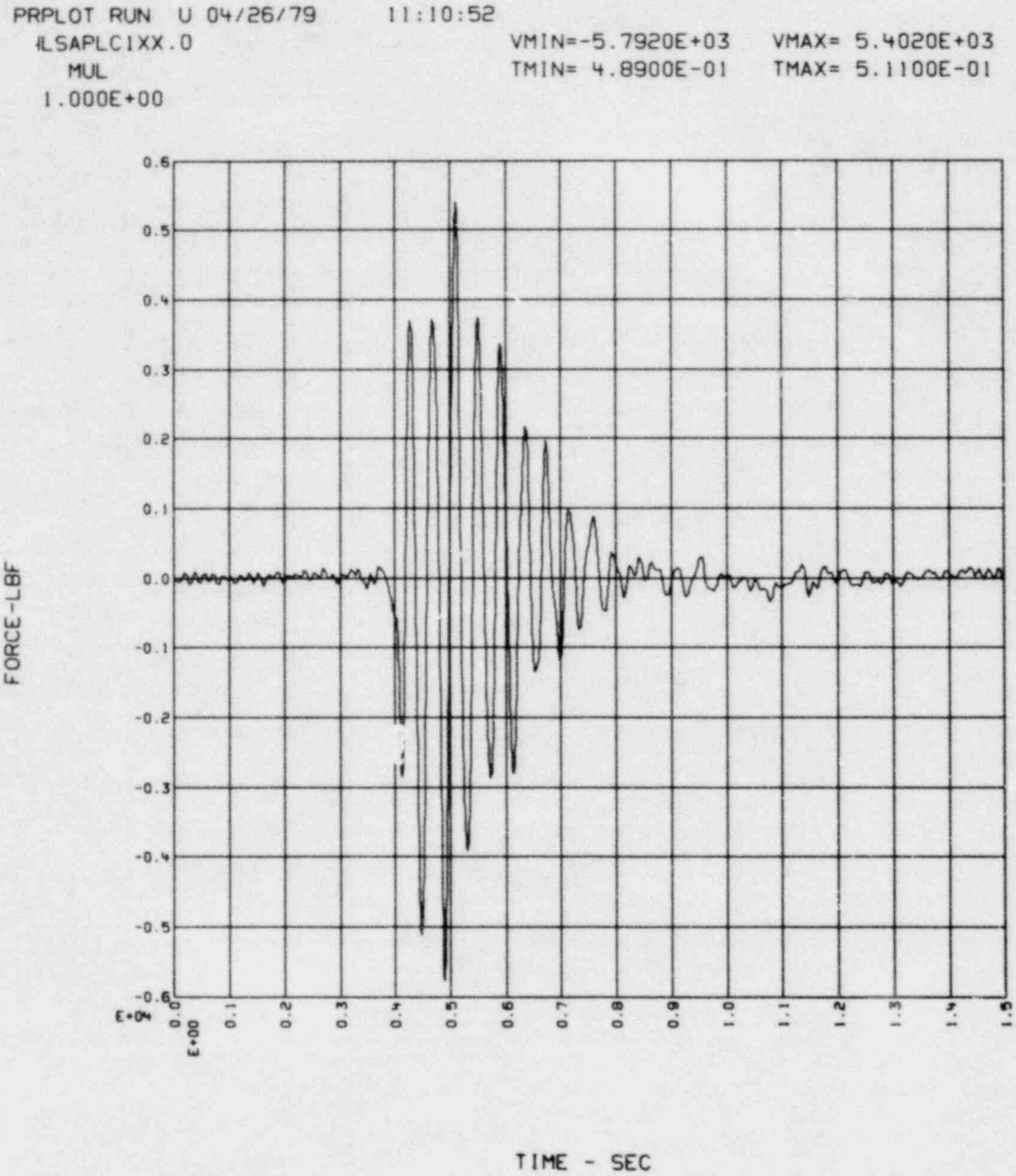

FIG. 2-24. Computed force history, case 1.3.1.0, load cell LC-1.

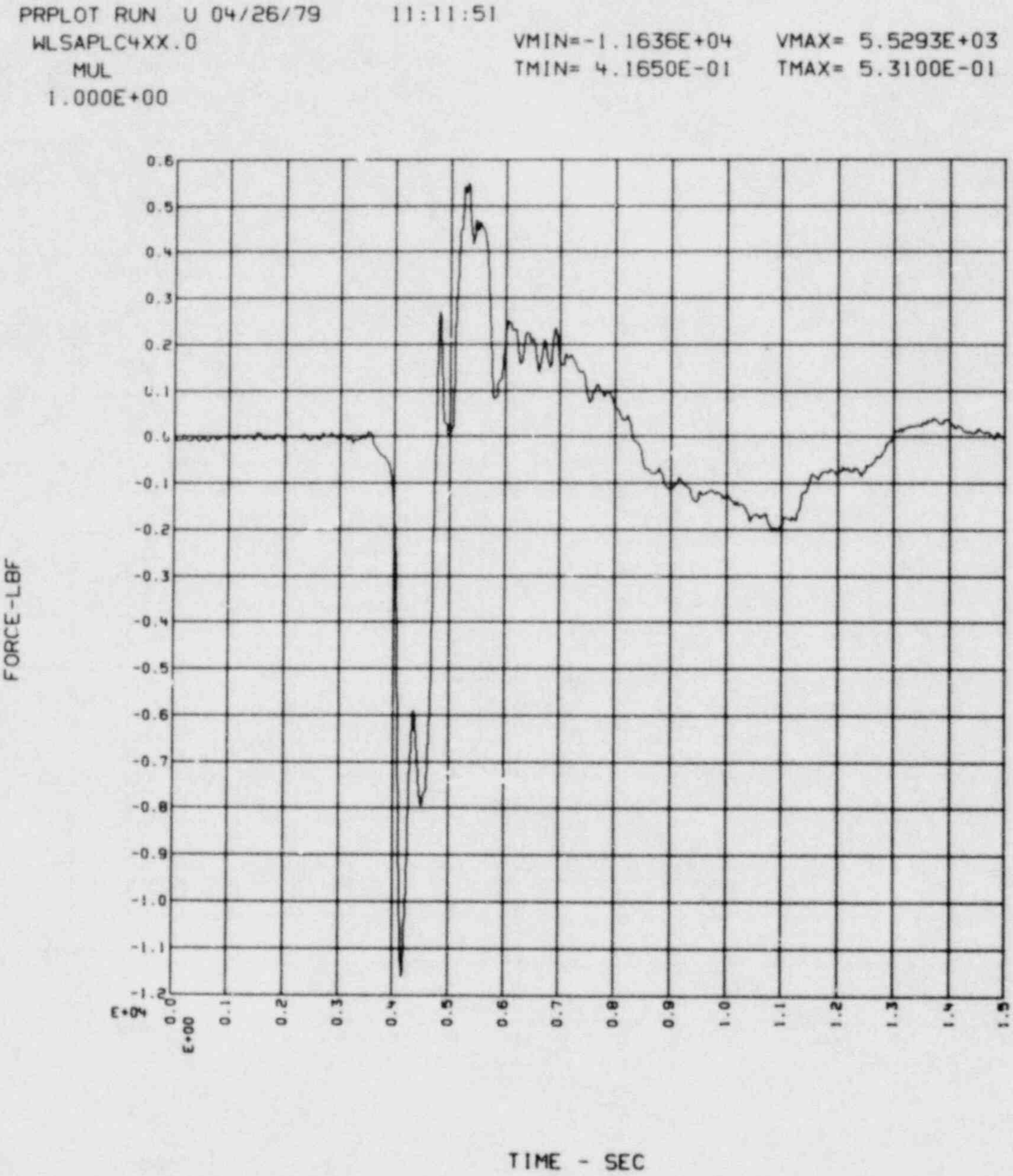

FIG. 2-25. Computed force history, case 1.3.1.0, load cell LC-4.

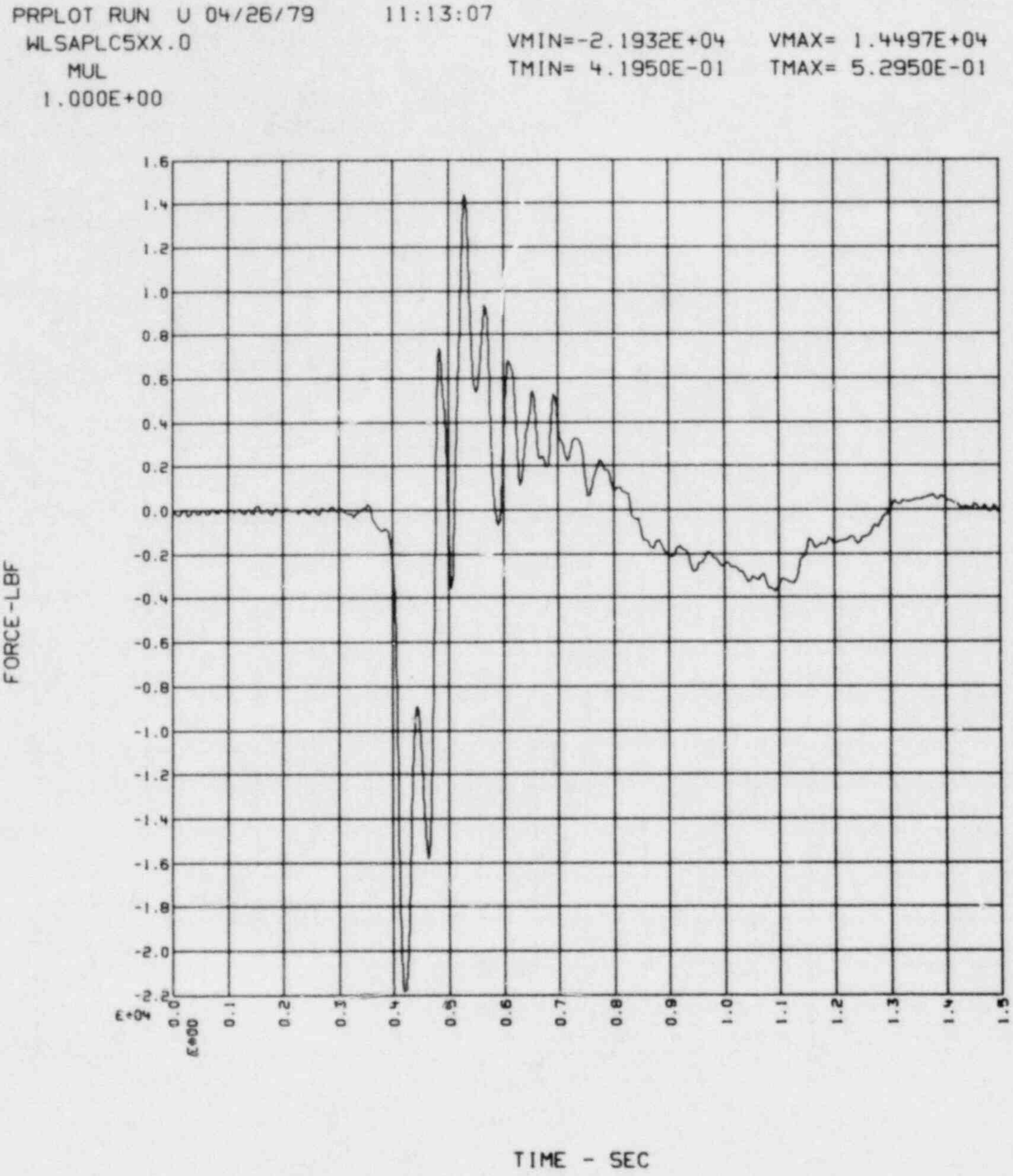

FIG. 2-26. Computed force history, case 1.3.1.0, load cell LC-5.

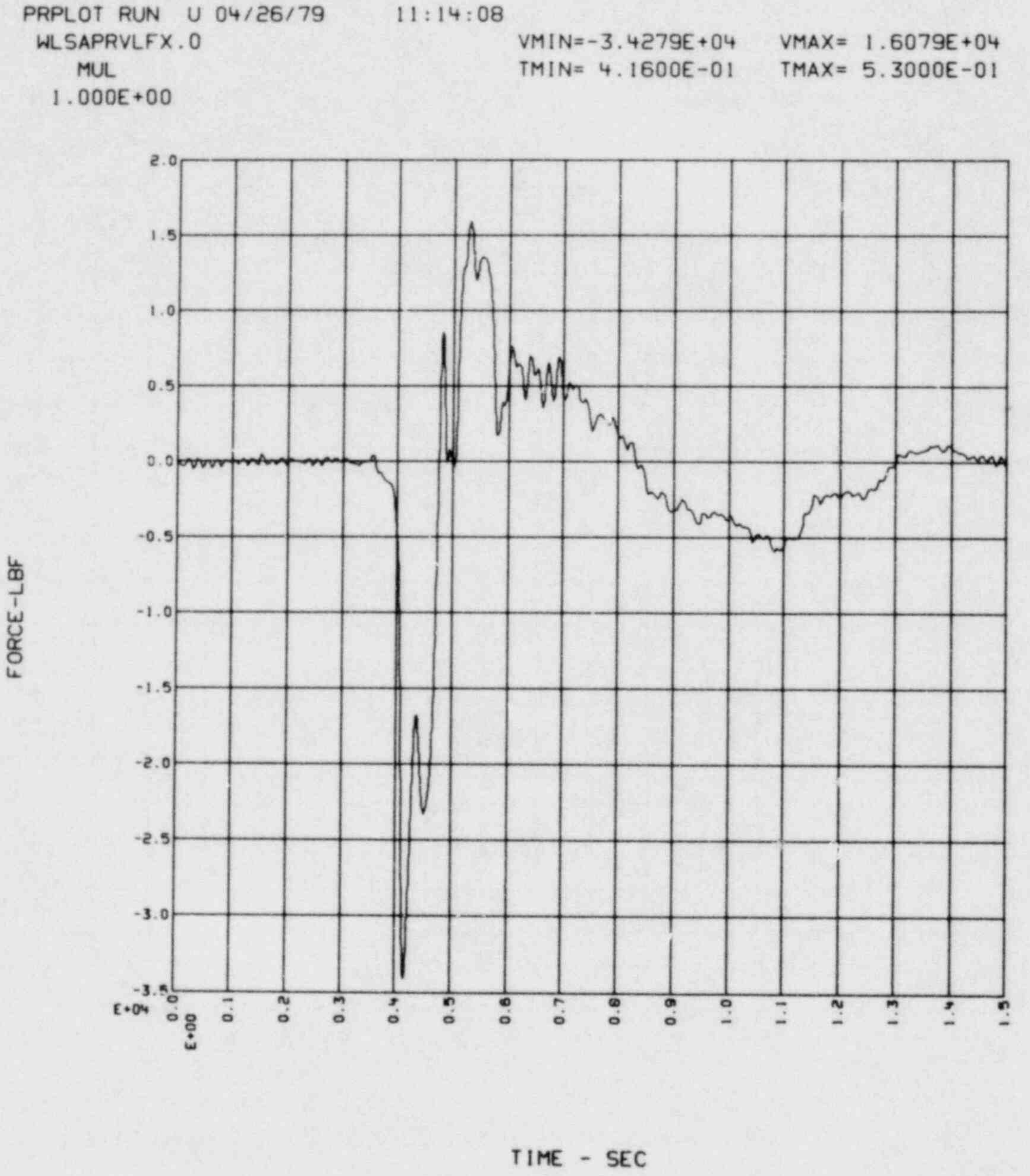

FIG. 2-27. Computed RVLF, case 1.3.1.0.

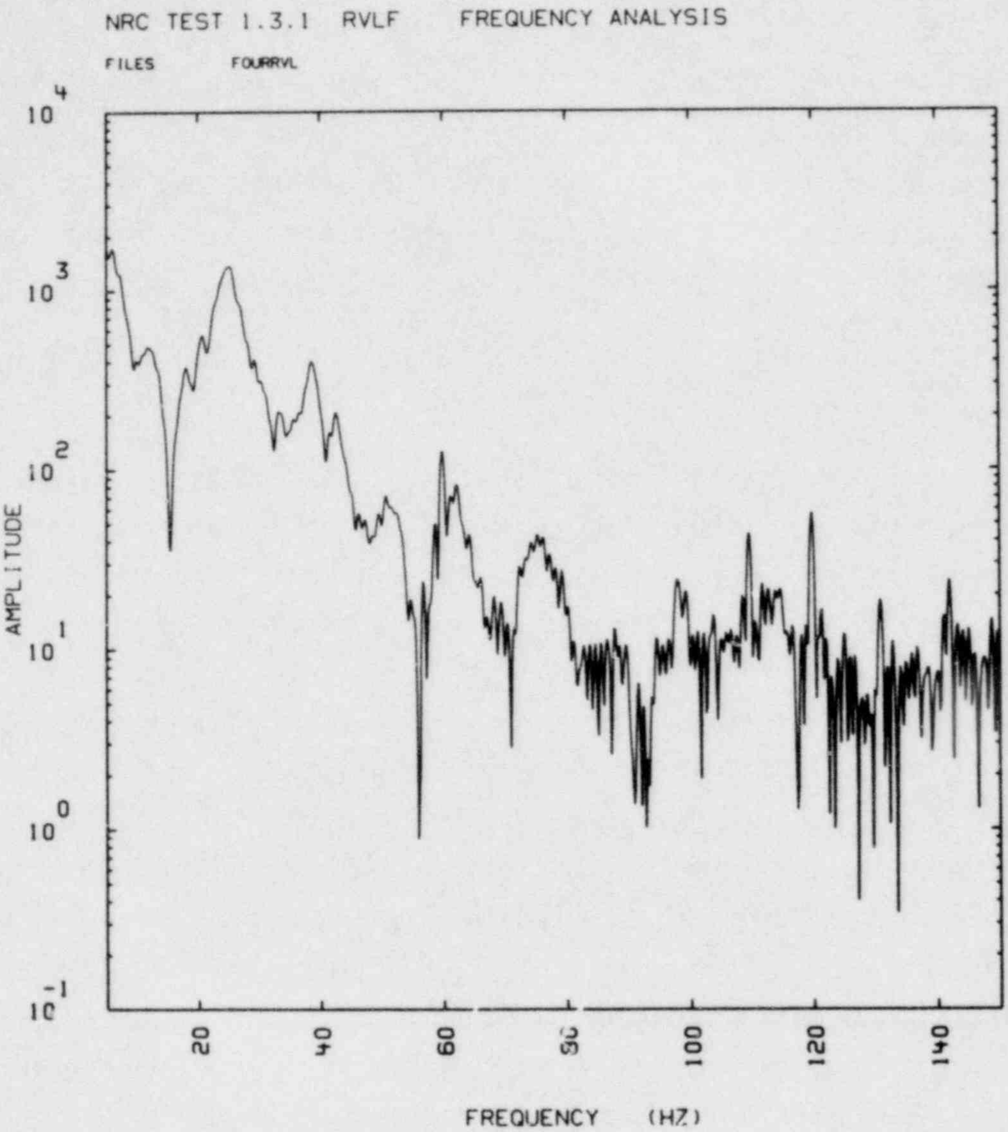

FIG. 2-28. Typical frequency analysis of computed force history.

2.4 CALCULATION OF ENTHALPY FLUX

2.4.1 METHODOLOGY

As part of the extended analysis of data from the 1/5-scale Mark I boiling water reactor pressure suppression experiment (PSE), enthalpy flux into the two test sections was calculated for each of 24 air blowdown tests. Enthalpy flux is calculated by convoluting time-dependent mass flow (m) and temperature (T) data according to the relationship

$$\dot{m}h = \dot{m}c_pT \qquad (2\text{-}15)$$

where c_p denotes the constant pressure specific heat of the working fluid. For ideal gas nitrogen, the specific heat is essentially constant for the temperature range evaluated in the PSE. Mass flows for the single 7.5° (2-D) and the two 45° (3-D) test section vent pipes were calculated by Pitts[11] shortly after the completion of the final air test series, using the pressure differential data recorded during each test. Temperatures were measured directly at each of the three vent pipes.

The results of the mass flow calculations, which are essential in the calculation of enthalpy flux, were retained in graphic form, both as hardcopy plots[11] and as computerized graphics ("FR80") files. Unfortunately, the corresponding mass flow data were not saved in digital form as required for the enthalpy flux calculations. We were, therefore, forced to consider three alternate methods for recovery of the mass flow data.

- Regeneration of the mass flows from the original PSE raw data tapes.
- "Hand" digitization of the hardcopy mass flow plots, based on available hard- and software techniques in use at LLL.
- Using the available computerized graphics files, i.e., unpacking the coordinate data directly and converting to engineering units; no software existed at LLL to accomplish this task.

The regeneration of the mass flow from the original data tapes was not viewed as practical within the time constraints for completion of the PSE extended analyses. Attempts were made to hand-digitize the mass flow curves in Ref. 11

using PPLOT,[12,13] a computer routine that interfaces a mechanical stylus with the CDC 7600 computer, but this effort proved to be too time consuming and tedious for practical production purposes. Therefore, the necessary computer software was developed by Blair[14] to extract coordinate information directly from the available graphics computer files. As indicated by Figs. 2-29 and 2-30 excellent replication of the original mass flow data was achieved. Details about the recovery of mass flow data can be found in Ref. 15.

2.4.2 CALCULATION OF THE TIME-DEPENDENT ENTHALPY FLUX

After the mass flow data were recovered, calculation of enthalpy flux was straightforward. A typical enthalpy flux calculation is outlined by Figs. 2-31 through 2-33. Using the newly-developed computer routine ENFLUX, recovered mass flow data (Fig. 2-31) and unfiltered temperature transducer data (Fig. 2-32) are combined according to equation (2-15) to yield enthalpy flux as shown in Fig. 2-33. A number of enthalpy flux calculations were also performed using temperature data that had been passed through a simple numerical filter (Fig. 2-34); these results (Fig. 2-35) were essentially identical to those obtained using unfiltered temperature data. All final enthalpy flux calculations were calculated, therefore, using unfiltered temperature data.

Enthalpy fluxes calculated for all tests* are included in Appendix E.5. Corresponding mass flow and temperature data used for the calculations are also given in Appendix E.5.

The maximum enthalpy flux calculated in each case is tabulated in Table 2-18; a representation of the total enthalpy input to each test sector is also provided. The total enthalpy is calculated by a trapezoidal integration between a start time that is 0.2 s prior to the calculated test zero time (i.e., $t_{start} = \bar{t}_0 - 0.2$ s) and the calculated time t_{pos}, which represents the time of second zero crossing of the positive 3-D HVLF as

---

*Enthalpy fluxes for test 1.2 are not included because no corresponding HVLF has been calculated.

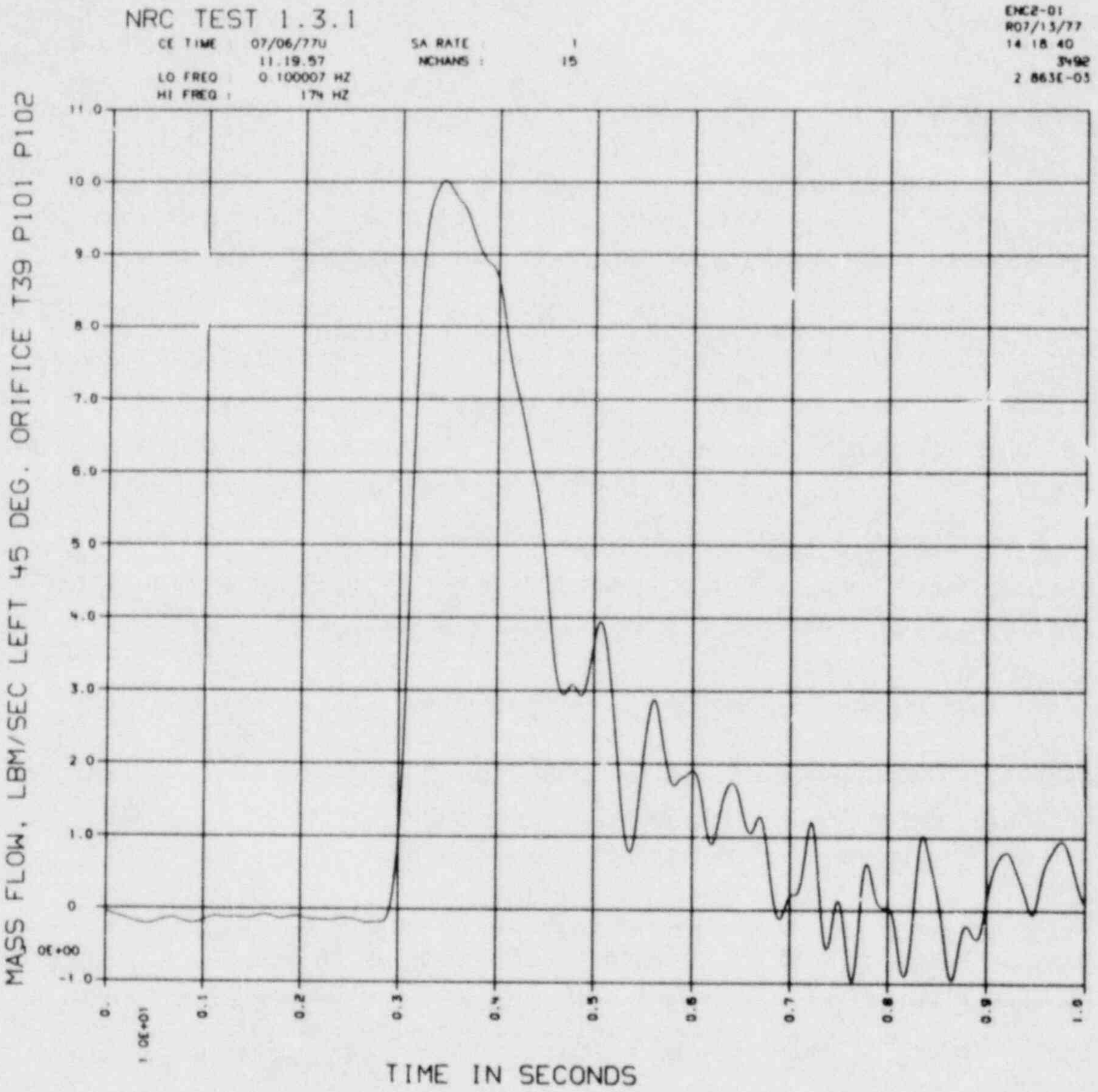

FIG. 2-29. Time-dependent mass flow in left 3-D vent pipe, test 1.3.1.

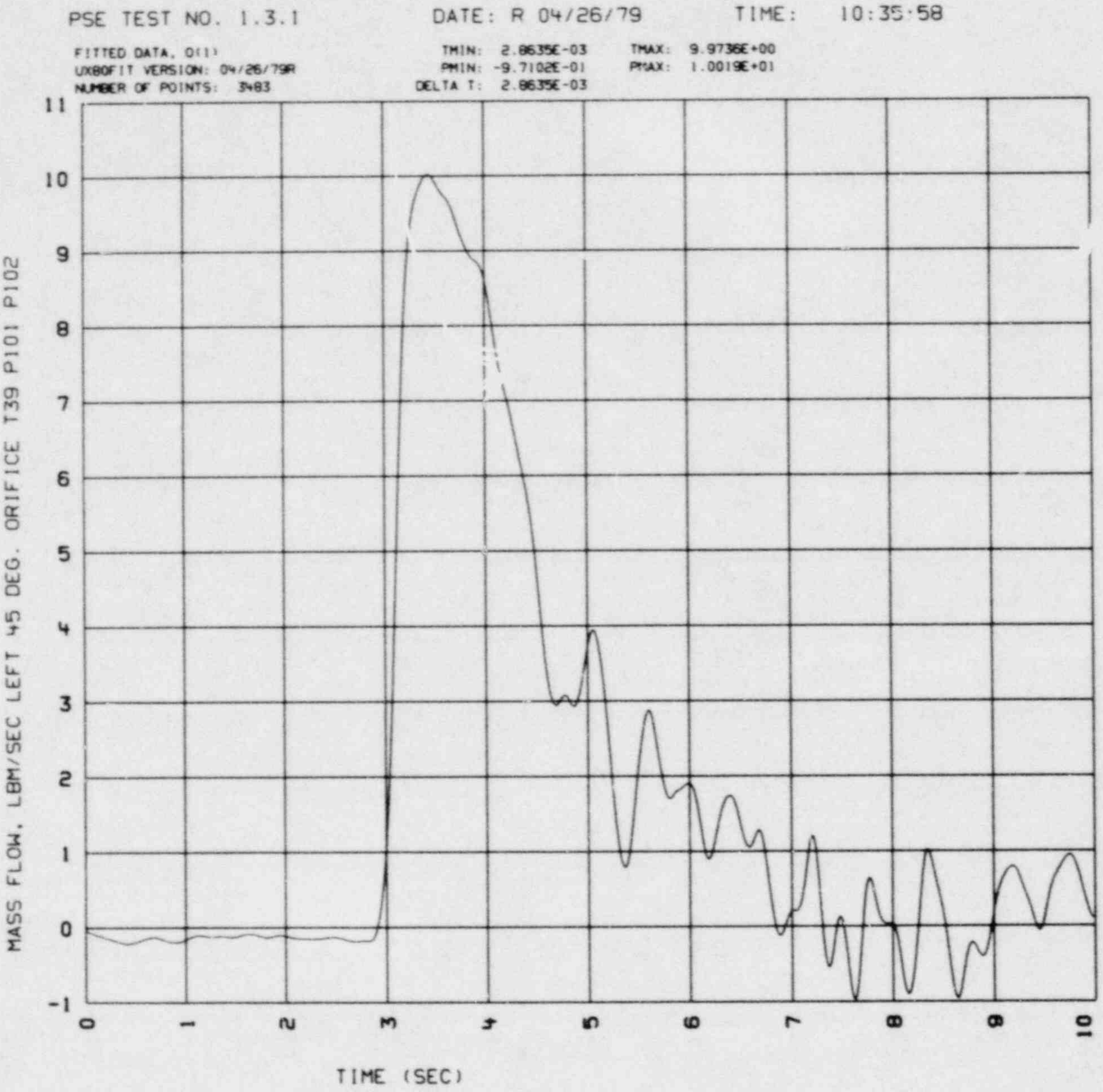

FIG. 2-30. Data recovered from Fig. 2-29 and fit using standard uniform PSE time step (2.8635 ms).

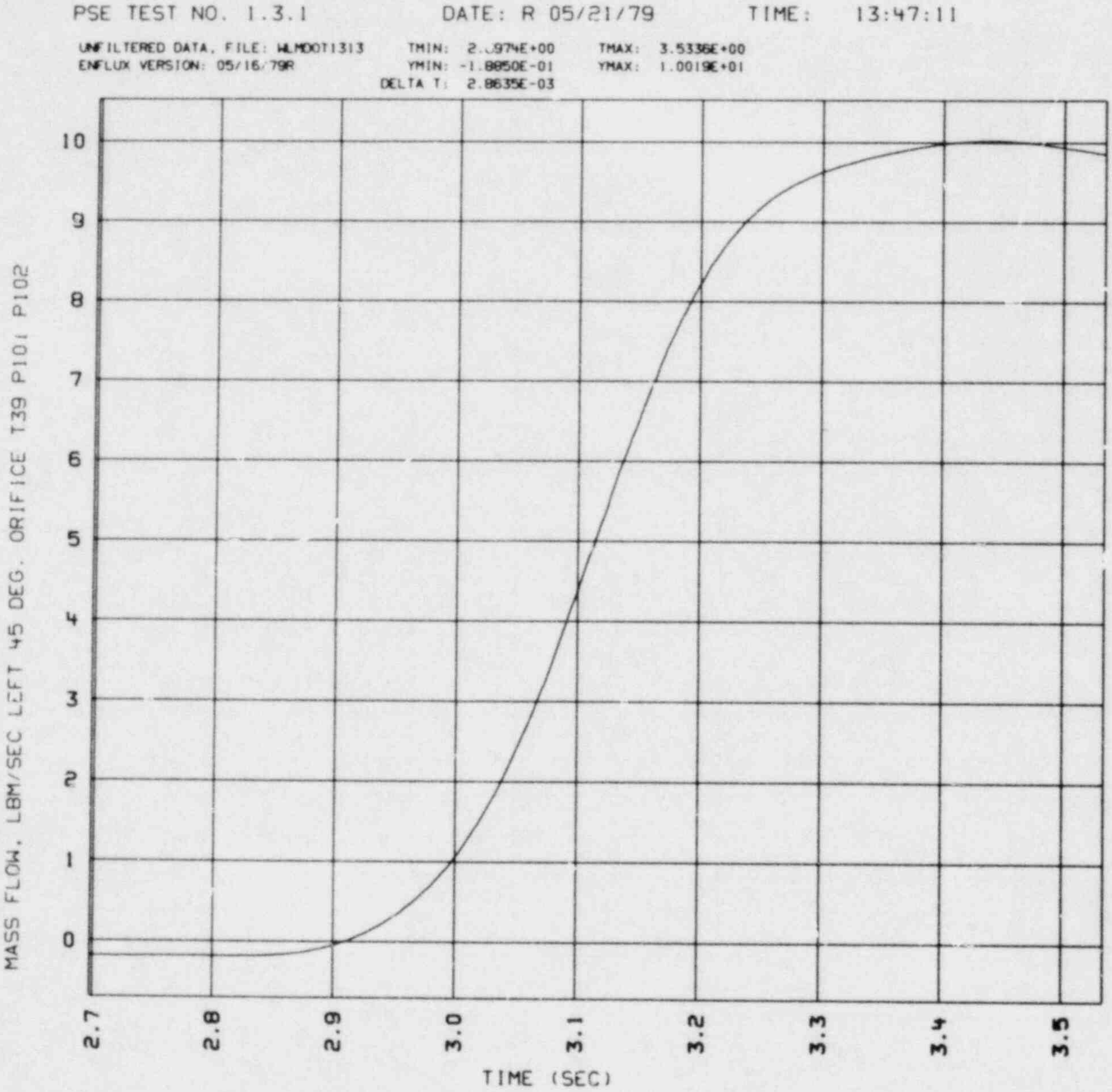

FIG. 2-31. Recovered mass flow data, test 1.3.1 (left 3-D vent pipe).

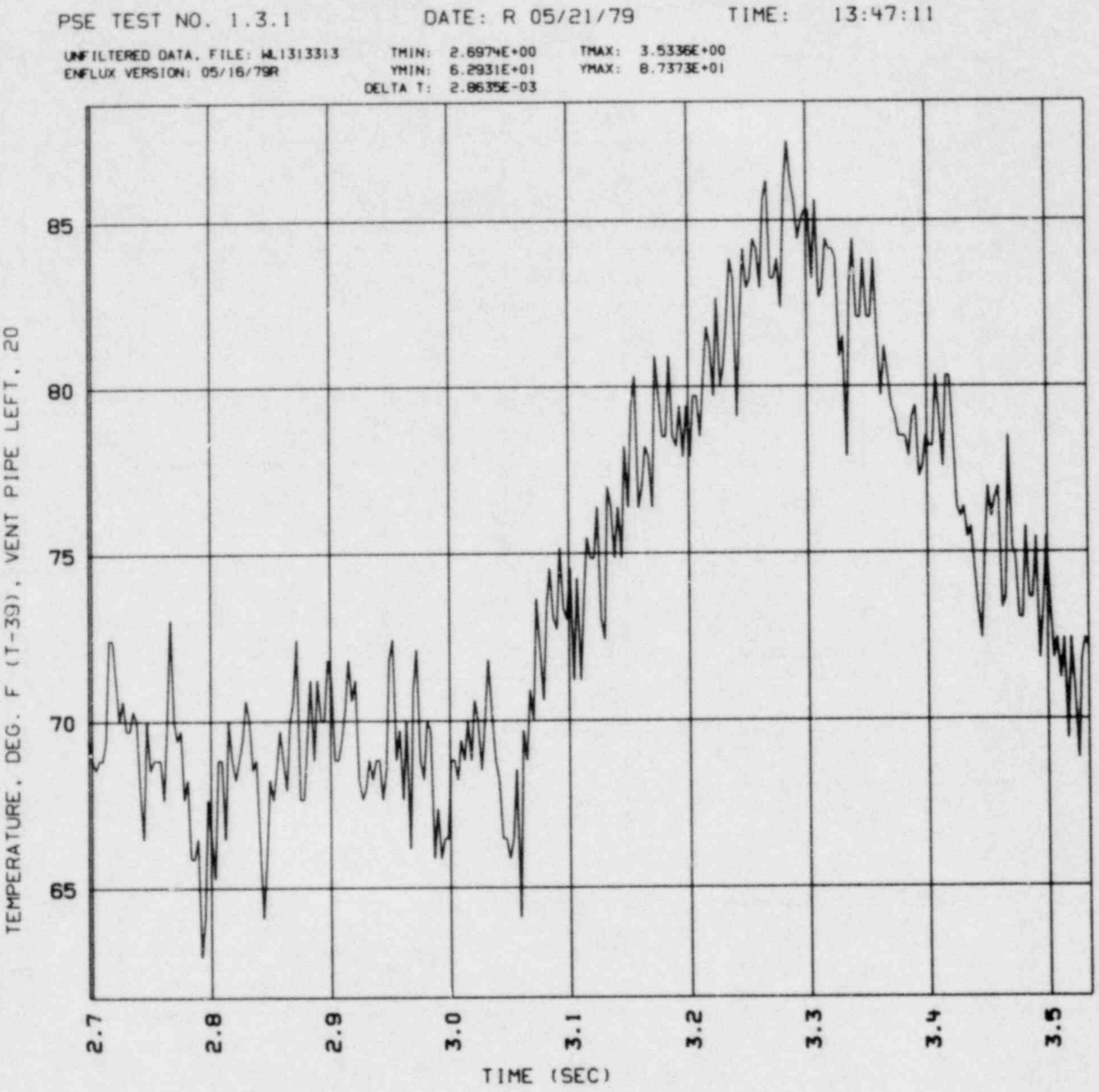

FIG. 2-32. Unfiltered temperature data, test 1.3.1 (left 3-D vent pipe).

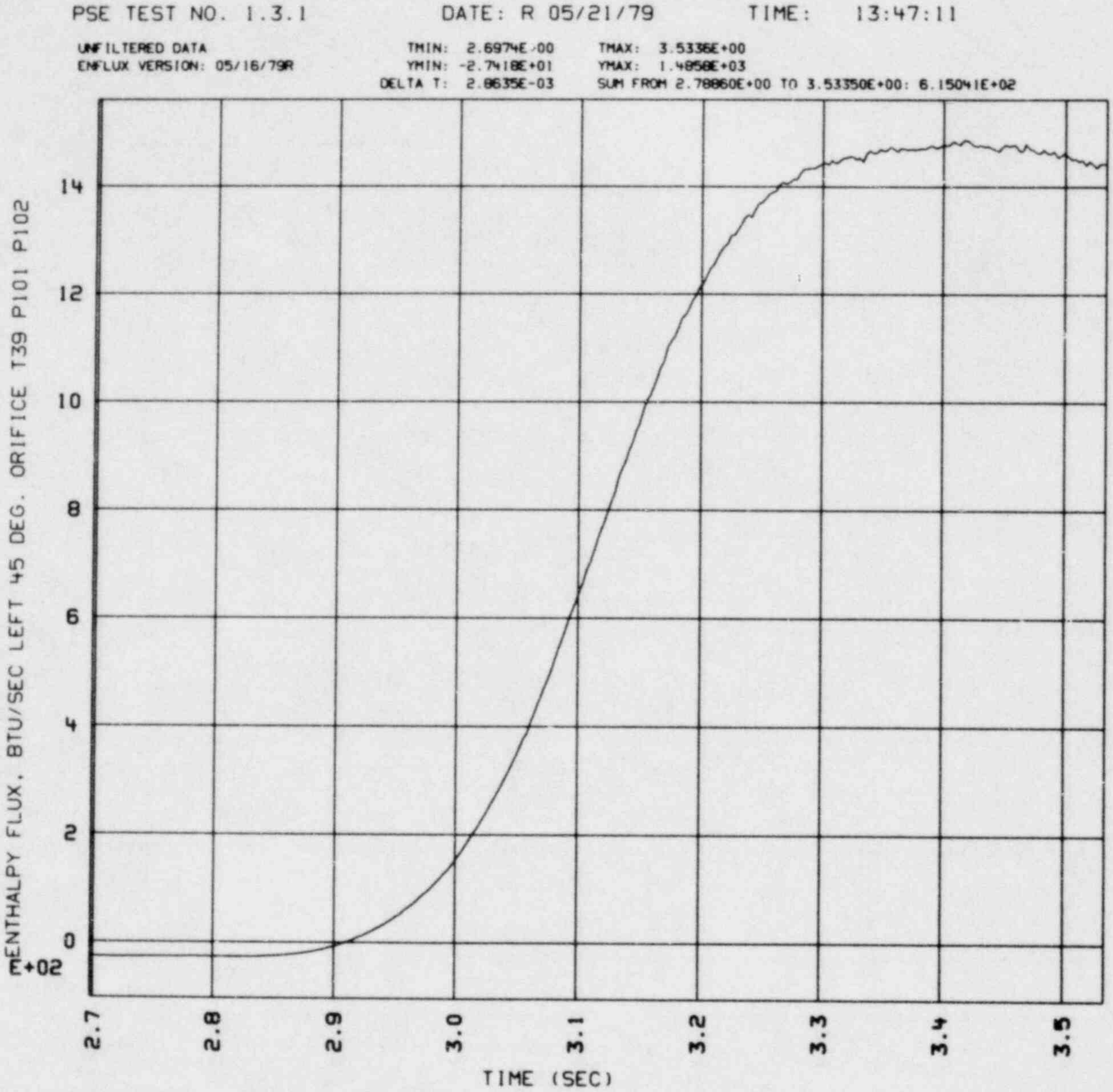

FIG. 2-33. Enthalpy flux calculated using data in Fig. 2-31 and Fig. 2-32.

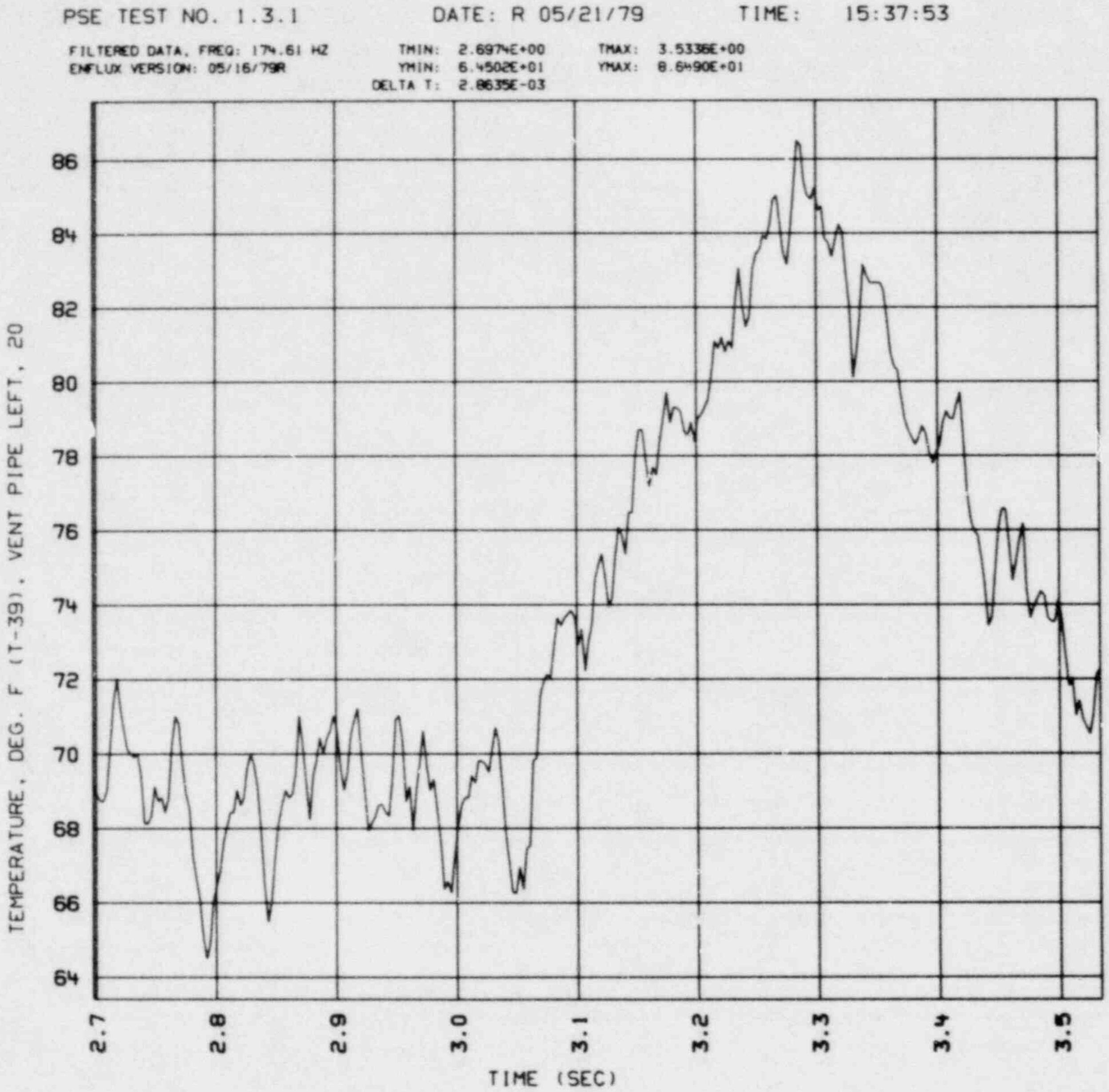

FIG. 2-34. Temperature data filtered to 174.6 Hz, test 1.3.1 (left 3-D vent).

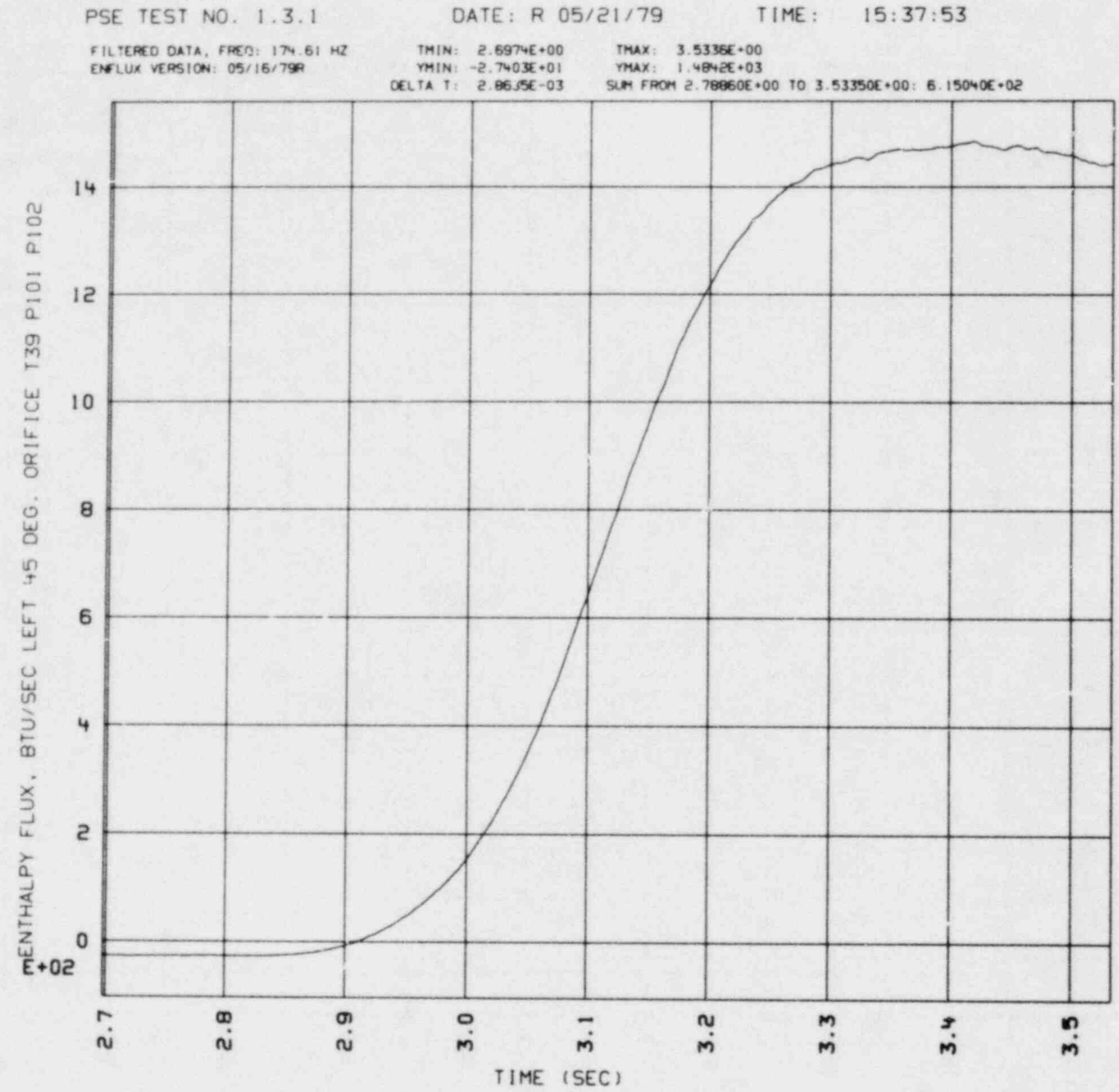

FIG. 2-35. Enthalpy flux calculated using data from Fig. 2-31 and Fig. 2-34.

TABLE 2-18. Results of enthalpy flux calculations.

Test	Sector	Start[a] second	t_{zero}[b] second	t_{pos}[c] second	$\dot{m}h_{max}$[d] Btu/second	$\int \dot{m}h$[e] Btu
1.1	2D	1.7	1.7976	2.5743	270.9	115.3
	45R				1683.1	717.4
	45L				1731.0	737.1
1.3	2D	2.4	2.4466	3.2071	229.9	92.06
	45R				1420.9	594.4
	45L				1466.9	603.0
1.3.1	2D	2.7	2.7886	3.5335	262.5	104.7
	45R				1479.4	606.8
	45L				1485.8	615.0
1.4	2D	1.4	1.4452	2.2106	206.9	83.20
	45R				1024.7	411.5
	45L				1032.8	420.5
1.5	2D	2.4	2.4342	3.1727	287.8	115.0
	45R[f]				1619.9	644.2
	45L				1592.1	655.6
1.6	2D	1.2	1.2999	2.0188	313.3	118.6
	45R[f]				1748.5	677.6
	45L				1781.0	686.5
2.1	2D	2.5	2.6602	3.3531	249.1	92.87
	45R[f]				1427.6	527.1
	45L				1465.4	549.8
2.2	2D	2.3	2.3814	3.0554	191.6	52.63
	45R[f]				1408.0	487.1
	45L				1420.8	506.0
2.3	2D	2.7	2.8188	3.4906	241.6	88.64
	45R[f]				1349.8	501.9
	45L				1377.1	520.2
2.4	2D	2.5	2.6159	3.4104	251.1	111.1
	45R				1561.5	657.6
	45L				1571.9	667.0
2.5	2D	2.5	2.5221	3.3159	253.3	108.9
	45R				1507.4	628.6
	45L				1542.8	657.5
2.6	2D	2.9	3.0446	3.7799	252.1	101.3
	45R				1492.5	586.4
	45L				1505.4	597.1
2.7	2D	3.0	3.0518	3.8715	247.4	109.7
	45R				1470.8	659.2
	45L				1501.3	681.2
2.8	2D	2.9	2.9622	3.7598	233.6	104.4
	45R				1433.8	630.0
	45L				1433.4	643.3

TABLE 2-18. (Continued).

Test	Sector	Start[a] second	t_{zero}[b] second	t_{pos}[c] second	$\dot{m}h_{max}$[d] Btu/second	$\int\dot{m}h$[e] Btu
2.9	2D	1.0	1.1076	1.9615	173.3	77.48
	45R				1054.4	483.0
	45L				1075.4	490.2
2.10	2D	2.4	2.5266	3.3503	254.5	116.5
	45R				1582.7	703.0
	45L				1604.6	731.7
2.11	2D	1.1	1.2312	2.0503	283.1	129.6
	45R				1740.1	777.4
	45L				1756.0	802.4
3.1	2D	2.8	2.9348	3.7168	278.0	119.2
	45R				1527.3	665.8
	45L				1555.3	694.4
3.2	2D	2.6	2.7030	3.5565	240.2	107.1
	45R				1452.7	687.5
	45L				2140.5	1152.7
3.3A	2D	2.5	2.5786	3.3531	287.6	117.0
	45R				g	g
	45L				2264.2	867.3
3.3B	2D	2.6	2.7123	3.2444	270.8	50.47
	45R				1775.3	346.6
	45L				g	g
3.4A	2D	2.5	2.5964	3.3903	288.9	112.5
	45R				g	g
	45L				2449.6	1100.0
3.4B	2D	1.9	2.0224	2.7976	287.4	111.1
	45R				1878.7	776.8
	45L				g	g
3.5	2D	2.2	2.3168	3.1155	231.8	104.1
	45R				1394.2	612.1
	45L				1478.4	653.1

[a] 75--point (1.5 s time window) HVLF start time.

[b] Test zero time ($\bar{t}_0$) less 0.2 s.

[c] Positive impulse time of last zero crossing from impulse calculations for 3-D sector.

[d] Maximum calculated enthalpy flux.

[e] Total enthalpy input over the time interval t_{zero} to t_{pos}.

[f] Used T-39 temperature data (left vent header) for the right vent header because temperature transducer T-38 was unavailable.

[g] Vent line blocked.

determined by the impulse analyses described in Section 2.2. The 0.2 s precursor on $\bar{t}_0$ was used to account for early ($t<\bar{t}_0$) mass flux which is an artifact of the noninstantaneous start of drywell pressurization. The choice of 0.2 s was arbitrary and is viewed as a conservative method of treating the "extra" (albeit small--typically less than 1 percent of the total) enthalpy injected prior to $\bar{t}_0$.

The total enthalpy results for the 3-D sector indicate near equality between the total energy flow in the left and right vent pipes, although a slight (typically split about 51 percent-49 percent) preferential flow through the left vent pipe is consistently indicated.

2.4.3 INFERRED ENTHALPY FLUX AT DOWNCOMERS

Both the inferred enthalpy flux at downcomer pairs and comparison of enthalpy flux at individual downcomers are based on local pressure-temperature (p-T) products and, where temperature data are not available, local pressures alone. To represent the local weighting of enthalpy flux in the simplest manner possible, the integral summation of each local parameter is used. This summation is calculated by a simple trapezoidal integration similar to that used for the total enthalpy at each vent pipe. This approach neglects any time-dependency of the local resistance to mass flow and, by implication, any time-dependency of local enthalpy flux weighting.

Pressure and temperature tranducer locations in the 3-D test section (see Fig. 2-36) are not sufficiently complete to allow comparisons of enthalpy flux weighting on the preferred basis of integral p-T products. However, if we compare the calculated enthalpy flux curves in Appendix E.5 with the corresponding mass flow and temperature data in Appendix E.5, the curve shapes indicate that mass flow is clearly the dominant parameter influencing enthalpy flux. Therefore, it can be reasonably argued that integral local pressures alone should provide a sufficient basis for weighting inferred enthalpy flux between individual downcomers in a given instrumentation plane and between symmetrical instrumentation planes (for example, between planes 11 and 20, if end effects are assumed to be negligible) when suitable temperature data are unavailable.

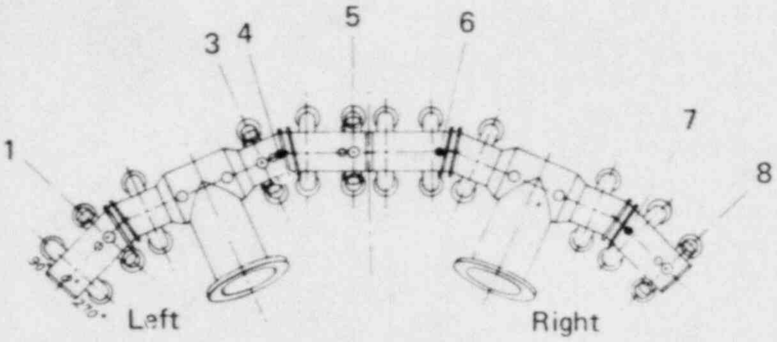

Plan view

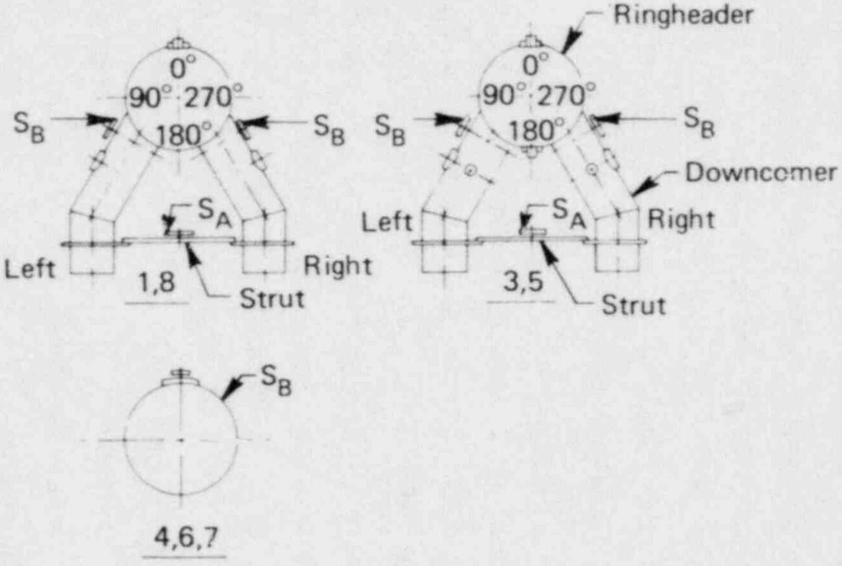

Sections

Ringheader									
		Transducer No.							
		Section							
Location	Type of XDCR	1	2	3	4	5	6	7	8
0°	P	58		61		65			70
	T	15		16		20			25
	S_B				7		11	12	
180°	P			62		66			
	T			17		21			

Downcomer									
		Transducer No.							
		Section							
Location	Type of XDCR	1	2	3	4	5	6	7	8
LEFT	P	59		63		67			71
	T			18		22			
	S_B	1		4		8			13
RIGHT	P	60		64		68			72
	T			19		23			
	S_B	2		5		9			14
STRUT	S_A	3		6		10			15

P = Pressure
T = Thermocouple, fluid
S_A = Strain, axial
S_B = Strain, bending

FIG. 2-36. Instrumentation locations for ringheader/downcomer (90^0 torus).

On this basis, the following calculations are performed for the 3-D sector:

- Ring header symmetry between planes 11 and 20 (sections 5 and 8 in Fig. 2-36) is checked by comparing integral p-T products at 0°.
- Ring header symmetry is recalculated using integral pressure data alone as a check on the feasibility of using pressure data alone to infer enthalpy flux.
- Integral p-T products are compared between downcomers in plane 11 (section 5).
- Integral pressure data are compared between downcomers in plane 11 and are then used to infer local enthalpy flux weighting.
- Integral pressure data are compared between downcomers in plane 20 and are then used to infer local enthalpy flux weighting.
- Integral pressure data are compared among the four downcomers in planes 11 and 20.
- Integral pressure data for the downcomers in planes 11 and 20 are weighted by the calculated ring header distribution and are then compared.
- Weighted pressure data are used to calculate the final enthalpy flux distribution among the downcomers in planes 11 and 20.

Calculations for the 7.5° sector are performed as follows:

- Integral p-T products are compared between downcomers (see Fig. 2-37).
- Integral pressures are compared between downcomers and are used to calculate the inferred enthalpy flux distribution.

Integral p-T products and integral pressures are presented both as absolute and as normalized (or weighted) parameters. For an arbitrary "left-right" set of p-T products, the left and right weights (w_L^{PT} and w_R^{PT}, respectively) are defined by:

$$w_L^{PT} = \frac{\sum p_L T_L}{\sum p_L T_L + \sum p_R T_R} \qquad (2\text{-}16)$$

$$w_R^{PT} = \frac{\sum p_R T_R}{\sum p_L T_L + \sum p_R T_R} \qquad (2\text{-}17)$$

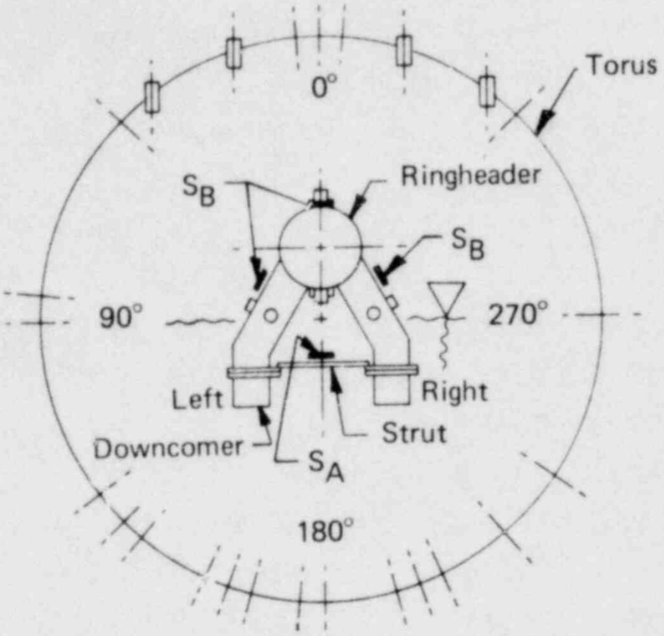

Torus			
Location	Type of XDCR	Transducer No.	
0°	P		Air
5°	T		
18°	PS		
37°	PS	9	
45°	P	75	
85°	T		
90°	P		
128°	P	76	Water
135°	T		
140°	P		
155°	P	77	
160°	P	78	
165°	P	79	
175°	T	30	
180°	P	80	
195°	P	81	
200°	P	82	
205°	P	83	
220°	P	84	
235°	P	85	
270°	P		
315°	P	86	Air
323°	PS	10	
342°	PS		
355°	T	202	

Downcomer		
Location	Type of XDCR	Transducer No.
Left	P	89
	T	33
	S$_B$	17
	S$_A$	
Right	P	90
	T	34
	S$_B$	18
	S$_A$	
Strut	P	
	T	
	S$_B$	
	S$_A$	19

Ringheader		
Location	Type of XDCR	Transducer No.
0°	P	87
	T	31
	S$_B$	16
	S$_A$	
180°	P	88
	T	32
	S$_B$	
	S$_A$	

P = Pressure
T = Thermocouple
PS = Pool swell
S$_A$ = Strain, axial
S$_B$ = Strain, bending

FIG. 2-37. Instrumentation locations for torus and ringheader/downcomer (7.5^0 sector).

Similarly, if integral pressures alone are considered, the weights are defined by:

$$w_L^P = \frac{\sum p_L}{\sum p_L + \sum p_R} \tag{2-18}$$

$$w_R^P = \frac{\sum p_R}{\sum p_L + \sum p_R}$$

Note that in both cases the sum of the weights is equal to unity.

If a local integral pressure characterizes a resistance to mass flow at that location, the inferred enthalpy flux distribution is given by

$$w_L^H = \frac{1/\sum p_L}{1/\sum p_L + \sum 1/\sum p_R} \tag{2-20}$$

$$w_R^H = \frac{1/\sum p_R}{1/\sum p_L + 1/\sum p_R} \; , \tag{2-21}$$

where w_L^H and w_R^H are the normalized "left" and "right" enthalpy fluxes respectively. Distribution of electric current between parallel resistors provides a useful analog here. For data pairs it can be shown that

$$w_L^H = w_R^P \tag{2-22}$$

$$w_R^H = w_L^P \; . \tag{2-23}$$

If more than two locations are considered, for example, comparison among all downcomers in both sections 5 and 8 (planes 11 and 20), then the individual weights of integral pressures are given by:

$$w_{5L}^P = \frac{\sum p_{5L}}{\sum p_{5L} + \sum p_{5R} + \sum p_{8L} + \sum p_{8R}} \tag{2-24}$$

$$w_{5R}^P = \frac{\sum p_{5R}}{\sum p_{5L} + \sum p_{5R} + \sum p_{8L} + \sum p_{8R}} \tag{2-25}$$

$$w_{8L}^{P} = \frac{\sum p_{8L}}{\sum p_{5L} + \sum p_{5R} + \sum p_{8L} + \sum p_{8R}} \qquad (2\text{-}26)$$

$$w_{8R}^{P} = \frac{\sum p_{8R}}{\sum p_{5L} + \sum p_{5R} + \sum p_{8L} + \sum p_{8R}} \qquad (2\text{-}27)$$

Similarly, again considering the parallel resistor analog, the inferred enthalpy flux weights are given by:

$$w_{5L}^{H} = \frac{1/\sum p_{5L}}{1/\sum p_{5L} + 1/\sum p_{5R} + 1/\sum p_{8L} + 1/\sum p_{8R}} \qquad (2\text{-}28)$$

$$w_{5R}^{H} = \frac{1/\sum p_{5R}}{1/\sum p_{5L} + 1/\sum p_{5R} + 1/\sum p_{8L} + 1/\sum p_{8R}} \qquad (2\text{-}29)$$

$$w_{8L}^{H} = \frac{1/\sum p_{8L}}{1/\sum p_{5L} + 1/\sum p_{5R} + 1/\sum p_{8L} + 1/\sum p_{8R}} \qquad (2\text{-}30)$$

$$w_{8R}^{H} = \frac{1/\sum p_{8R}}{1/\sum p_{5L} + 1/\sum p_{5R} + 1/\sum p_{8L} + 1/\sum p_{8R}} \qquad (2\text{-}31)$$

Up to this point in the development of the inferred enthalpy flux distribution scheme, it has been assumed that all locations at which pressure integrals are determined are connected to a common source. For the calculation of inferred enthalpy flux distribution among the four downcomers in planes 11 and 20, this assumption is valid only if enthalpy flux is evenly distributed between the right and left sides of the ring header. Since in general this is not the case, the final estimation of the downcomer enthalpy flux distribution must take into account the ring header distribution. This is done as follows:

$$(w_{5L}^{H})' = w_{5L}^{H} \cdot (w_{5}^{H})_{rnghdr}/0.50 \qquad (2\text{-}32)$$

$$(w_{5R}^{H})' = w_{5R}^{H} \cdot (w_{5}^{H})_{rnghdr}/0.50 \qquad (2\text{-}33)$$

$$(w^H_{8L})' = w^H_{8L} \cdot (w^H_8)_{rnghdr}/0.50 \qquad (2\text{-}34)$$

$$(w^H_{8R})' = w^H_{8R} \cdot (w^H_8)_{rnghdr}/0.50 \qquad (2\text{-}35)$$

where $(w^H_5)_{rnghdr}$ and $(w^H_8)_{rnghdr}$ represent the inferred enthalpy flux weighting calculated for the left and right (section 5 and section 8) sides of the ring header respectively.

Calculation of the inferred enthalpy flux distribution in the 3-D test section was initially performed for test 1.3.1. The results of these calculations, outlined in Figs. 2-38a through 2-38g, indicate the following:

- Enthalpy flux distributions inferred by comparing integral pressures are essentially identical to those inferred by integral pressure-temperature products, both between planes 11 and 20 in the ring header and between downcomers in plane 11. It is therefore implied that the substitution of pressure alone for pressure-temperature products is valid for the enthalpy flux calculation.
- Enthalpy flux is almost equally split between the left (plane 11) and right (plane 20) sides of the ring header, with a slight preferential flow to the left side. This result is consistent with that calculated for the left and right vent pipes.
- Enthalpy flux is distributed essentially evenly between the right and left (inboard and outboard, respectively) downcomers in both plane 11 and plane 20.

Calculation of inferred enthalpy flux was also performed for the 7.5° test sector downcomer pair (see Figs. 2-39a and b). As indicated in Fig. 2-39b, a slight preferential flow (split about 51.5 percent to 48.5 percent) was indicated for the left downcomer.

Inferred enthalpy flux calculations were completed for the remaining PSE tests (except for test 1.2). The resulting ring header distributions and the downcomer distributions weighted by the ring header distributions are presented in Table 2-19. The distribution of enthalpy flux between the left

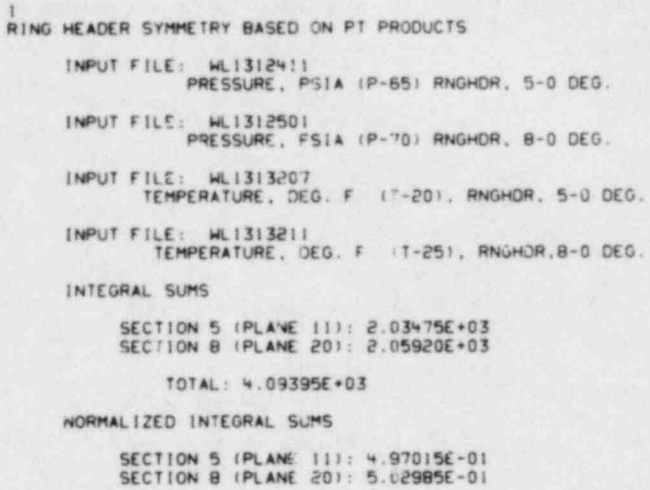

```
1
RING HEADER SYMMETRY BASED ON PT PRODUCTS

     INPUT FILE:  WL1312411
                PRESSURE, PSIA (P-65) RNGHDR, 5-0 DEG.

     INPUT FILE:  WL1312501
                PRESSURE, PSIA (P-70) RNGHDR, 8-0 DEG.

     INPUT FILE:  WL1313207
            TEMPERATURE, DEG. F  (T-20), RNGHDR, 5-0 DEG.

     INPUT FILE:  WL1313211
             TEMPERATURE, DEG. F  (T-25), RNGHDR,8-0 DEG.

     INTEGRAL SUMS

          SECTION 5 (PLANE 11): 2.03475E+03
          SECTION 8 (PLANE 20): 2.05920E+03

              TOTAL: 4.09395E+03

     NORMALIZED INTEGRAL SUMS

          SECTION 5 (PLANE 11): 4.97015E-01
          SECTION 8 (PLANE 20): 5.02985E-01
```

FIG. 2-38a. Ring header symmetry based on p-T products (test 1.3.1).

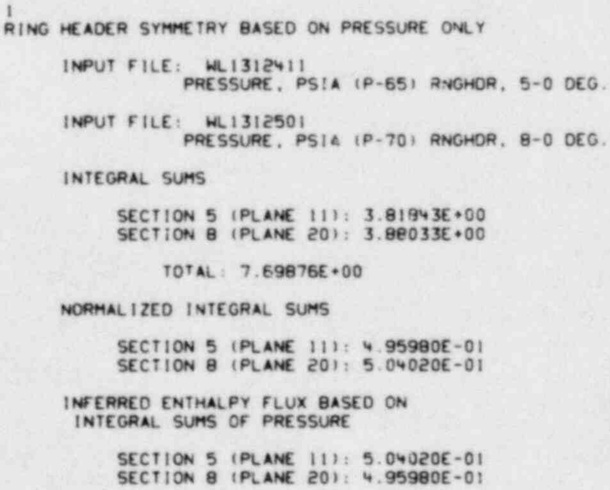

```
1
RING HEADER SYMMETRY BASED ON PRESSURE ONLY

     INPUT FILE:  WL1312411
                PRESSURE, PSIA (P-65) RNGHDR, 5-0 DEG.

     INPUT FILE:  WL1312501
                PRESSURE, PSIA (P-70) RNGHDR, 8-0 DEG.

     INTEGRAL SUMS

          SECTION 5 (PLANE 11): 3.81843E+00
          SECTION 8 (PLANE 20): 3.88033E+00

              TOTAL: 7.69876E+00

     NORMALIZED INTEGRAL SUMS

          SECTION 5 (PLANE 11): 4.95980E-01
          SECTION 8 (PLANE 20): 5.04020E-01

     INFERRED ENTHALPY FLUX BASED ON
      INTEGRAL SUMS OF PRESSURE

          SECTION 5 (PLANE 11): 5.04020E-01
          SECTION 8 (PLANE 20): 4.95980E-01
```

FIG. 2-38b. Ring header symmetry based on integral pressure only (test 1.3.1).

```
1
SECTION 5 (PLANE 11) DOWNCOMER SYMMETRY BASLD ON PT PRODUCTS

     INPUT FILE:  WL1312413
               PRESSURE, PSIA (P-67) DOWNCOMER LEFT, 5

     INPUT FILE:  WL1312414
               PRESSURE, PSIA (P-68) DOWNCOMER RIGHT, 5

     INPUT FILE:  WL1313209
            TEMPERATURE, DEG. F  (T-22), DOWNCOMER LEFT, 5

     INPUT FILE:  WL1313210
           TEMPERATURE, DEG. F  (T-23), DOWNCOMER RIGHT, 5

     INTEGRAL SUMS

             LEFT,5: 1.99869E+03
            RIGHT,5: 2.01727E+03

              TOTAL: 4.01596E+03

     NORMALIZED INTEGRAL SUMS

             LEFT,5: 4.97686E-01
            RIGHT,5: 5.02314E-01
```

FIG. 2-38c. Plane 11 downcomer symmetry [illegible]ed on [illegible]-T products (test 1.3.1).

```
1
SECTION 5 (PLANE 11) DOWNCOMER SYMMETRY BASED ON PRESSURE ONLY

     INPUT FILE:  WL1312413
               PRESSURE, PSIA (P-67) DOWNCOMER LEFT, 5

     INPUT FILE:  WL1312414
               PRESSURE, PSIA (P-68) DOWNCOMER RIGHT, 5

     INTEGRAL SUMS

             LEFT,5: 3.75141E+00
            RIGHT,5: 3.78507E+00

              TOTAL: 7.53648E+00

     NORMALIZED INTEGRAL SUMS

             LEFT,5: 4.97767E-01
            RIGHT,5: 5.02233E-01

     INFERRED ENTHALPY FLUX BASED ON
      INTEGRAL SUMS OF PRESSURE

             LEFT,5: 5.02233E-01
            RIGHT,5: 4.97767E-01
```

FIG. 2-38d. Plane 11 downcomer symmetry based on integral pressures only (test 1.3.1).

```
1
SECTION 8 (PLANE 20) DOWNCOMER SYMMETRY BASED ON PRESSURE ONLY

     INPUT FILE:  WL1312502
              PRESSURE, PSIA (P-71) DOWNCOMER LEFT, 8

     INPUT FILE:  WL1312415
              PRESSURE, PSIA  (P-72), DOWNCOMER RT., 8

     INTEGRAL SUMS

             LEFT,8: 3.78258E+00
            RIGHT,8: 3.75419E+00

              TOTAL: 7.53676E+00

     NORMALIZED INTEGRAL SUMS

             LEFT,8: 5.01883E-01
            RIGHT,8: 4.98117E-01

     INFERRED ENTHALPY FLUX BASED ON
      INTEGRAL SUMS OF PRESSURE

             LEFT,8: 4.98117E-01
            RIGHT,8: 5.01883E-01
```

FIG. 2-38e. Plane 20 downcomer symmetry based on integral pressures only (test 1.3.1).

```
1
SECTIONS 5 & 8 (PLANES 11 & 20) WEIGHTING BASED ON PRESSURE ONLY

     INPUT FILE:  WL1312413
              PRESSURE, PSIA (P-67) DOWNCOMER LEFT, 5

     INPUT FILE:  WL1312414
              PRESSURE, PSIA (P-68) DOWNCOMER RIGHT, 5

     INPUT FILE:  WL1312502
              PRESSURE, PSIA (P-71) DOWNCOMER LEFT, 8

     INPUT FILE:  WL1312415
              PRESSURE, PSIA  (P-72), DOWNCOMER RT., 8

     INTEGRAL SUMS

             LEFT,5: 3.75141E+00
            RIGHT,5: 3.78507E+00

             LEFT,8: 3.78258E+00
            RIGHT,8: 3.75419E+00

              TOTAL: 1.50732E+01

     NORMALIZED INTEGRAL SUMS

             LEFT,5: 2.48879E-01
            RIGHT,5: 2.51112E-01

             LEFT,8: 2.50946E-01
            RIGHT,8: 2.49063E-01
```

FIG. 2-38f. Inferred downcomer symmetry, planes 11 and 20, no allowance for ring header flux distribution (test 1.3.1).

```
1
SECTIONS 5 & 8 (PLANES 11 & 20) WEIGHTING BASED ON PRESSURE
 WEIGHTED BY CALCULATED VENT HEADER WEIGHTING

     INPUT FILE:  WL1312413
              PRESSURE, PSIA (P-67) DOWNCOMER LEFT, 5

     INPUT FILE:  WL1312414
              PRESSURE, PSIA (P-68) DOWNCOMER RIGHT, 5

     INPUT FILE:  WL1312502
              PRESSURE, PSIA (P-71) DOWNCOMER LEFT, 8

     INPUT FILE:  WL1312415
              PRESSURE, PSIA  (P-72), DOWNCOMER RT., 8

     INTEGRAL SUMS

             LEFT,5: 3.75141E+00
            RIGHT,5: 3.78507E+00

             LEFT,8: 3.78258E+00
            RIGHT,8: 3.75419E+00

              TOTAL: 1.50732E+01

     NORMALIZED INTEGRAL SUMS

             LEFT,5: 2.46878E-01
            RIGHT,5: 2.49093E-01

             LEFT,8: 2.52964E-01
            RIGHT,8: 2.51065E-01

     INFERRED ENTHALPY FLUX BASED ON
      INTEGRAL SUMS OF PRESSURE

             LEFT,5: 2.53135E-01
            RIGHT,5: 2.50884E-01

             LEFT,8: 2.47058E-01
            RIGHT,8: 2.48924E-01
```

FIG. 2-38g. Inferred enthalpy flux distribution, planes 11 and 20, including allowance for ring header distribution (test 1.3.1).

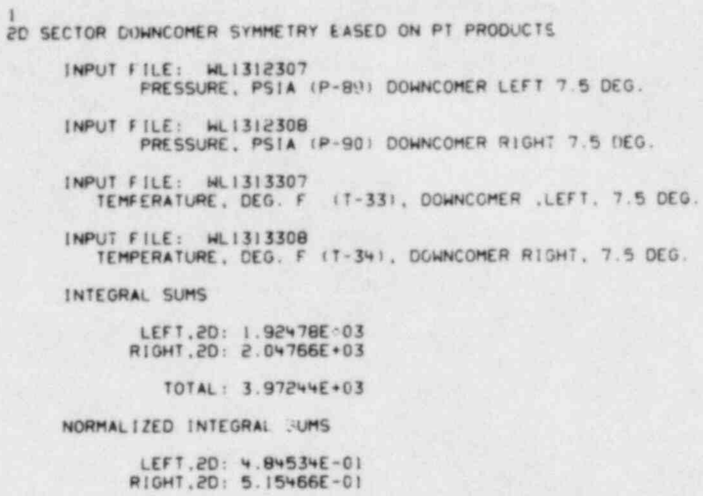

```
1
2D SECTOR DOWNCOMER SYMMETRY EASED ON PT PRODUCTS

     INPUT FILE:  WL1312307
            PRESSURE, PSIA (P-89) DOWNCOMER LEFT 7.5 DEG.

     INPUT FILE:  WL1312308
            PRESSURE, PSIA (P-90) DOWNCOMER RIGHT 7.5 DEG.

     INPUT FILE:  WL1313307
        TEMPERATURE, DEG. F  (T-33), DOWNCOMER .LEFT, 7.5 DEG.

     INPUT FILE:  WL1313308
        TEMPERATURE, DEG. F (T-34), DOWNCOMER RIGHT, 7.5 DEG.

     INTEGRAL SUMS

             LEFT,2D: 1.92478E+03
            RIGHT,2D: 2.04766E+03

               TOTAL: 3.97244E+03

     NORMALIZED INTEGRAL SUMS

             LEFT,2D: 4.84534E-01
            RIGHT,2D: 5.15466E-01
```

FIG. 2-39a. 7.5° sector downcomer symmetry based on p-T products (test 1.3.1).

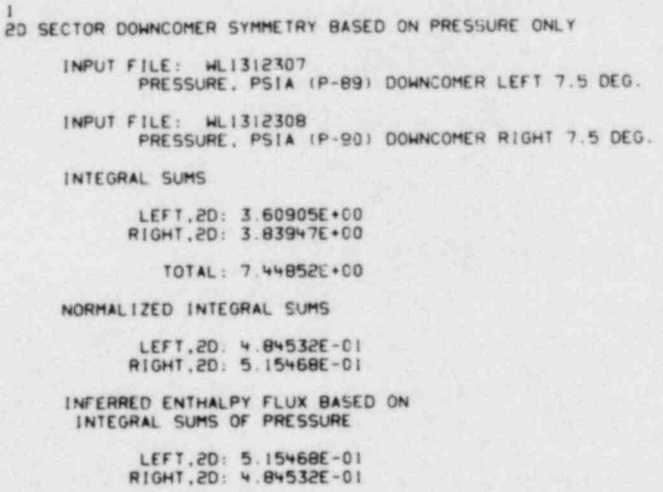

```
1
2D SECTOR DOWNCOMER SYMMETRY BASED ON PRESSURE ONLY

     INPUT FILE:  WL1312307
            PRESSURE, PSIA (P-89) DOWNCOMER LEFT 7.5 DEG.

     INPUT FILE:  WL1312308
            PRESSURE, PSIA (P-90) DOWNCOMER RIGHT 7.5 DEG.

     INTEGRAL SUMS

             LEFT,2D: 3.60905E+00
            RIGHT,2D: 3.83947E+00

               TOTAL: 7.44852E+00

     NORMALIZED INTEGRAL SUMS

             LEFT,2D: 4.84532E-01
            RIGHT,2D: 5.15468E-01

     INFERRED ENTHALPY FLUX BASED ON
      INTEGRAL SUMS OF PRESSURE

             LEFT,2D: 5.15468E-01
            RIGHT,2D: 4.84532E-01
```

FIG. 2-39b. Inferred enthalpy flux distribution, 7.5° sector (test 1.3.1).

TABLE 2-19. Inferred enthalpy flux in 90° sector ring header and at individual downcomers.

	90° ring header[a]		Plane 11[b]		Plane 20[b]		7.5° sector	
Test	Left vent	Right vent	Left	Right	Left	Right	Left	Right
1.1	0.5015	0.4985	0.2495	0.2519	0.2486	0.2499	0.5201	0.4799
1.3	0.4994	0.5006	0.2492	0.2501	0.2505	0.2502	0.5165	0.4835
1.3.1	0.5040	0.4960	0.2531	0.2509	0.2471	0.2489	0.5155	0.4845
1.4	0.5027	0.4973	0.2507	0.2520	0.2511	0.2462	0.5315	0.4685
1.5	0.5008	0.4992	0.2501	0.2507	0.2507	0.2485	0.5094	0.4906
1.6	0.5013	0.4987	0.2522	0.2492	0.2511	0.2476	0.5069	0.4931
2.1	0.5032	0.4968	0.2514	0.2517	0.2488	0.2480	0.5280	0.4720
2.2	0.4995	0.5005	0.2491	0.2504	0.2493	0.2512	0.4973	0.5027
2.3	0.5008	0.4992	0.2505	0.2503	0.2489	0.2503	0.5076	0.4924
2.4	0.5017	0.4983	0.2496	0.2521	0.2451	0.2533	0.5032	0.4968
2.5	0.5007	0.4993	0.2493	0.2513	0.2483	0.2510	0.5096	0.4904
2.6	0.5099	0.4901	0.2514	0.2585	0.2309	0.2592	0.4748	0.5252
2.7	0.5053	0.4947	0.2513	0.2540	0.2402	0.2549	0.5059	0.4941
2.8	0.5014	0.4986	0.2509	0.2505	0.2501	0.2485	0.5096	0.4904
2.9	0.5018	0.4982	0.2513	0.2505	0.2443	0.2539	0.4996	0.5004
2.10	0.5065	0.4935	0.2522	0.2543	0.2455	0.2480	0.5181	0.4819
2.11	0.4988	0.5012	0.2491	0.2498	0.2538	0.2474	0.5222	0.4778
3.1	0.5004	0.4996	0.2487	0.2517	0.2479	0.2516	0.4969	0.5031
3.2	0.5014	0.4986	0.2489	0.2525	0.2436	0.2549	0.4944	0.5056
3.3A	0.4947	0.5053	0.2468	0.2478	0.2581	0.2473	0.5108	0.4892
3.3B	0.5159	0.4841	0.2569	0.2591	0.2443	0.2397	0.4966	0.5034
3.4A	0.4997	0.5003	0.2515	0.2482	0.2471	0.2531	0.4997	0.5003
3.4B	0.5244	0.4756	0.2620	0.2624	0.2405	0.2352	0.5167	0.4833
3.5	0.5023	0.4977	0.2497	0.2526	0.2473	0.2505	0.5029	0.4971

---

[a] "Right" and "left" are defined relative to an observer at the drywell centerline (see Fig. 2-38).

[b] "Right" and "left" refer to the inboard and outboard downcomers respectively for each instrumentation plane (see Fig. 2-38).

and right sides of the ring header was very nearly equal in each test, with a slight preferential flow to the left side in almost every case. As with test 1.3.1, this is consistent with the result of the vent pipe enthalpy flux calculations. The distribution of enthalpy flux among the four downcomers in planes 11 and 10 is typically uniform within a few percent.

No definite flow preference was indicated by the results of calculations for the 7.5^{0} sector. For all cases, the distribution of enthalpy flux between downcomers was within 5 percent of being evenly split.

2.4.4 ENTHALPY FLUX UNCERTAINTY ANALYSIS

The relative standard deviation in the vent pipe enthalpy flux calculations is estimated using the standard relationship for relative error propagation together with equation (2-15) as follows:

$$\frac{\sigma_{\dot{m}h}}{\dot{m}h} = \left[\left(\frac{\sigma_{\dot{m}}}{\dot{m}}\right)^2 + \left(\frac{\sigma_T}{T}\right)^2\right]^{1/2} \qquad (2\text{-}36)$$

The typical uncertainty in the mass flows for the representative tests considered in Ref. (11) was on the order of 7 percent for tests in which the pressure differential across the orifice was used to calculate the mass flow, and approximately 11 percent when the annubar static rake was used. For all tests, the temperature uncertainty was determined to be on the order of 1 percent. When used in equation (2-36), these values yield relative standard deviations in enthalpy flux of approximately 7 and 11 percent, depending on the particular device (orifice or static rake) used to measure vent pipe pressure differentials.

Error due to integer arithmetic roundoff in the recovery of mass flow data from the computer graphics files is approximately two orders of magnitude less than the relative standard deviation in the mass flow calculations and, therefore, is not regarded as significant.

2.5 POOL SWELL EVALUATION

2.5.1 METHODOLOGY

Several high speed cameras (HYCAM), providing viewing in the wetwell airspace and subpool,[5] were used during the LOCA tests to provide a visual record of events corresponding to transducer signal characteristics. Although it is easy to correlate ring header impact timing with strut load cell signals, it is more difficult to arrive at a pool surface history. This section provides a description of the impact time measurement reduction method and its results. A description of the method used to determine the pool surface history along one line of the outer surface of the downcomer is also included.

The focus of this evaluation is placed on the 16 mm film record obtained through port 4-60 of the test facility.* This record, filmed from a point well above the initial water level and near plane 4, shows the ring header, header strut, and downcomer from the miter joint to the flange.

Each film sequence shows that, as a result of pool surface impact, the splash comes from beneath the ring header. Though no measurement of time between impact and initial sighting of the splash is possible, due to restricted viewing angle, a subjective estimate of between 1 ms and 1.5 ms was obtained using the film speed of approximately 1 frame per ms. Relating the timing of this visual event to strut load transducer history requires incorporation of two features into the HYCAM record: timing marks along one edge of the film and a zero time mark along the other. Since the equipment for recording the zero time was received only after several tests were completed, selection of a test sequence for pool surface measurements has been restricted to later tests. Tests 2.7, 2.9, 2.10, and 2.11 were chosen for this study because they were conducted under identical conditions except for changes in pressurization rates.

The zero time mark records a green light-emitting diode which has an electric pulse of 5 ms duration. The leading edge of this pulse corresponds to the

---

*See Fig. 2 in Ref. [5].

leading edge of the pulse that is used to open the bleed-down solenoid valve at the beginning of each test.[*] Because the light-emitting diode is positioned five frames ahead of the film exposure aperture, a zero time offset of five frames must be added to the frame count between the zero time mark and the frame of interest. When segments of the PCM-recorded transducer signals are transferred to computer-compatible tape, zero time also coincides with the leading edge of the solenoid pulse. Therefore this method establishes a correlation of zero time between film records and transducer data records.

Timing marks are recorded along the film edge opposite to the zero time record. These marks are recorded using a red light-emitting diode that is controlled by an oscillator that separates each successive mark by 1 ms. Since the HYCAMs were run at a nominal rate of 1000 frames per second, there is approximately one timing mark per frame. The number of elapsed frames from zero mark to the first frame showing a splash (i.e., from initial pool surface to header impact) is counted using a film transport with a frame counter. Concurrently, the difference between the number of timing marks and the number of frames is counted visually. Correcting the frame count, using the zero time offset and the discrepancy in splash time that is indicated by the timing marks yields the splash time in seconds. Table 2-20 shows the results of this procedure. Because the splash time is very close to the time of peak vertical force, it is interesting to compare them (see Table 2-21). The plot of the response of a typical ring header strut load cell, shown in Fig. 2-40, also aids in this comparison.

Table 2-22 shows a more critical comparison by displaying the data of Table 2-21 using the film splash time for each experiment as the reference time.

The time difference shown by these results, between the film splash time and load cell peaks is greatest for tests 2.7 and 2.10, yet the pressurization rates are relatively close together. Also, the time delay from zero to splash for tests 2.7 and 2.10 is roughly twice that for test 2.11. The apparent reason for these discrepancies lies in the nonuniform start time from test to test and the fact that timing error, based on frame counting, develops at a rate of approximately 1 percent. The relative time differences are shown in Table 2-22, and are clarified by the later Fig. 2-56.

---

[*] See Fig. 13 in Ref. [1].

TABLE 2-20. Development of pool swell frame timing.

Test	Splash frame	Discrepancy (ms)	Offset (ms)	Splash time (s)
2.7	3502	-56.5	+5	3.4505
2.9	1563	-26.25	+5	1.5418
2.10	2957	-50.2	+5	2.9118
2.11	1638	-27.25	+5	1.6158

TABLE 2-21. Comparison of absolute event times (load cell peak force to splash).

		Test			
Transducer	Plane	2.7	2.9	2.10	2.11
LC-2	2	3.4677	1.5492	2.9294	1.6265
LC-3	3	3.4648	1.5434	2.9236	1.6236
Film	4	3.4505	1.5418	2.9118	1.6158
LC-6	5	3.4648	1.5434	2.9236	1.6207
LC-7	6	3.4648	1.5492	2.9265	1.6236
Pressurization rate (psi/s)		23.6	16.1	27.9	29.9

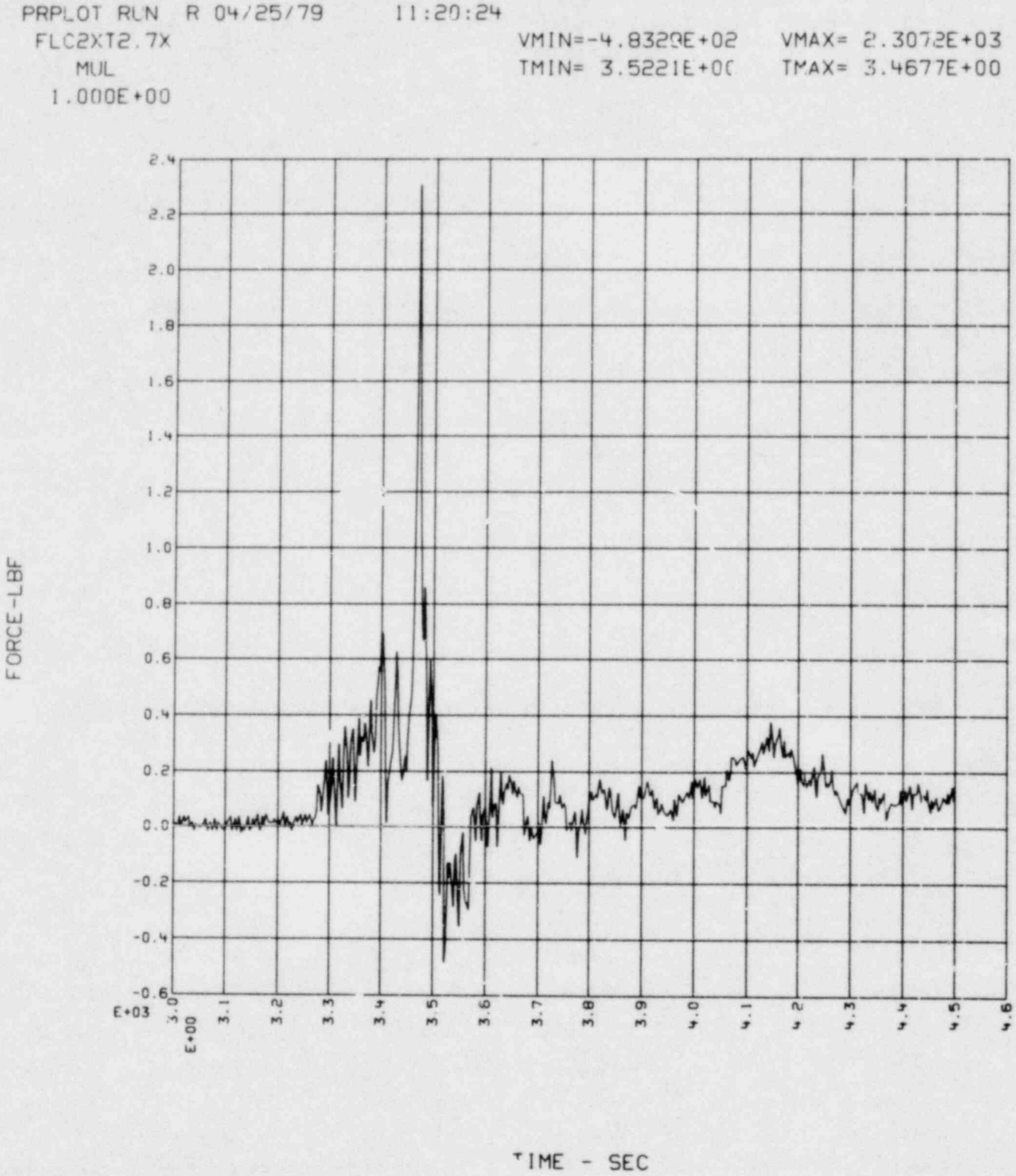

FIG. 2-40. Force history, load cell 2 (test 2.7).

TABLE 2-22. Comparison of relative event times (in seconds).

		Test			
Transducer	Plane	2.7	2.9	2.10	2.11
LC-2	2	+0.0172	+0.0074	+0.0176	+0.0107
LC-3	3	+0.0143	+0.0016	+0.0118	+0.0078
FILM	4	0	0	0	0
LC-6	5	+0.0143	+0.0016	+0.0118	+0.0049
LC-7	6	+0.0143	+0.0074	+0.0147	+0.0078
Pressurization rate (psi/s)		23.6	16.1	27.9	29.9

2.5.2 POOL SURFACE MOTION

2.5.2.1 Description of Film

The 16 mm film from the camera positioned at port 4-60 was analyzed to obtain a measure of pool surface position as a function of time for tests 2.7, 2.9, 2.10, and 2.11.

As can be seen in the frame reproduced as Fig. 2-41, the lighting reveals the curved line along which the pool surface meets the downcomer of plane 4. In successive frames, this line rises until it becomes obscured by the lower lighting level resulting from motion in other parts of the pool and by motion blur resulting from finite frame exposure time (approximately 0.4 ms).

Four white marks that were spray-painted onto the outer surface of the downcomer through a stencil are also visible in Fig. 2-41. Next to each mark is a two-digit numeral indicating the vertical distance from the mark to the face of the downcomer flange.* Although the numerals indicate that the marks are equidistant, the distances appear to vary considerably, even to the naked eye. The reasons for this discrepancy are as follows:

- The stencil provides a gage which is based on visual judgment rather than mensuration.
- The camera view is through a 1-inch-thick quartz port, which results in considerable distortion.

In principle, measurement of the pool surface line in a selected set of frames should provide sufficient data for determining the pool surface history. However, the stenciled lines provided significant ambiguity. To resolve this problem of measuring the pool position accurately, a scale marked in quarter-inch-units was devised. This scale was then attached to the downcomer and the same camera and lens used to expose a strip of 16 mm film from a position nearly identical to that of the test films. The new scale was easily read on the film and resulted in more accurate readings.

---

*See Fig. A-1, Appendix A.

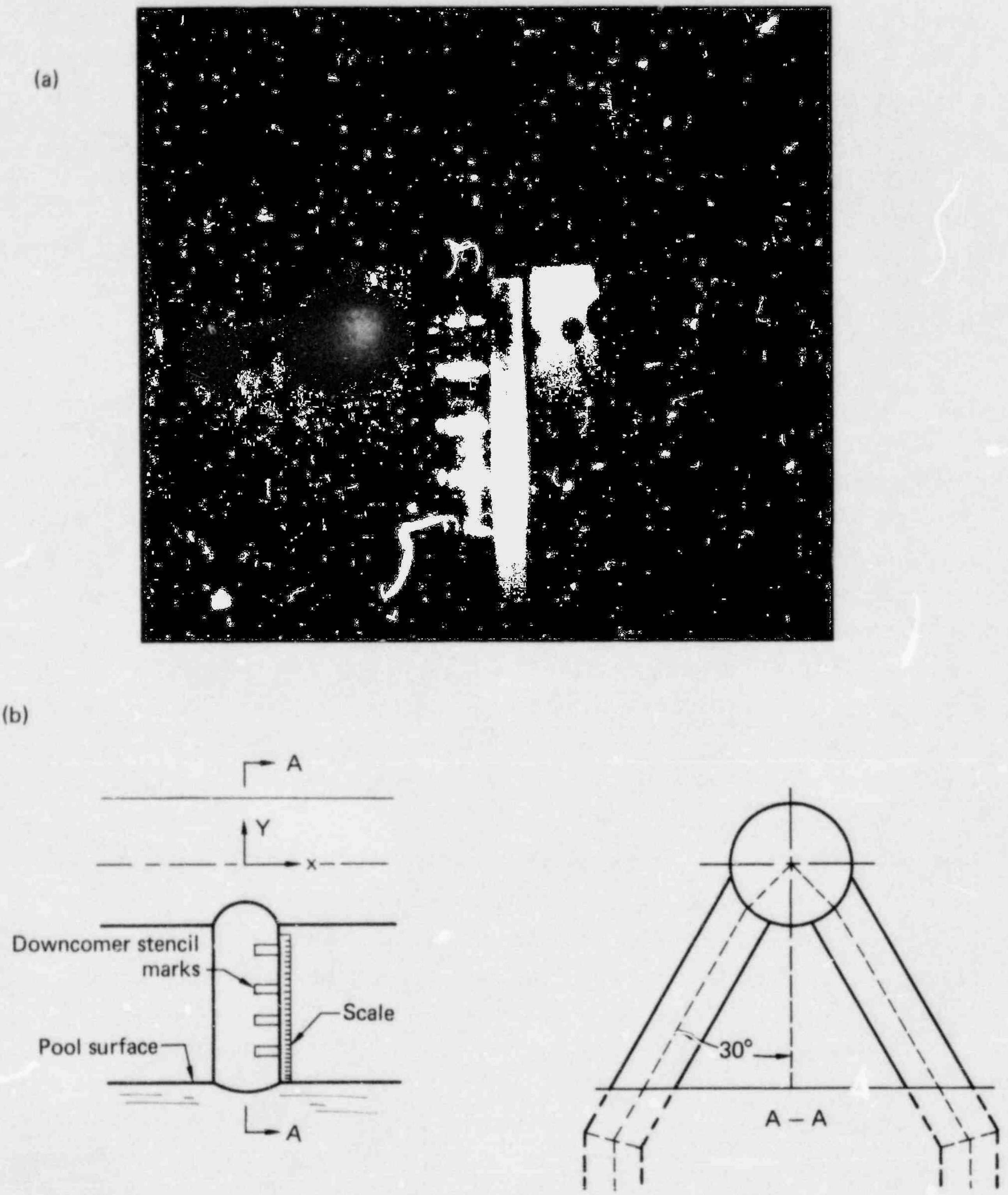

FIG. 2-41. Photograph (a) and sketch (b) of downcomer view at plane 4-60^0, showing downcomer stencil marks and placement of linear scale.

Although the camera frame rate is fairly uniform after reaching operating speed (~1000 frames/s), it is not accurately governed, and is therefore inadequate for time measurements. To overcome this problem, as discussed earlier, a device in each camera records a sequence of 1 ms pulses which are accurate to within one percent, along one edge of the film. Because no greater precision was available using the cameras and no external trigger output was provided, the influence of this inaccuracy was taken into account when interpreting the results. A second pulse that responded to an external trigger was also recorded for each test along the opposite edge of the film. This pulse allowed cross-timing with the load cell and other transducer recordings.

2.5.2.2 Mensuration

A set of six to eight frames was selected for measurement from the film strip of each test. The first frame in each set was selected before any pool surface motion had occurred, the last frame was taken as late as possible in the test sequence such that both the pool surface-downcomer line and the upper downcomer stencil mark could still be seen. The line of intersection, along which the pool surface meets the downcomer, was digitized for each frame, defining it as <x,y> cartesian coordinate pairs (see Fig. 2-41). Similarly, the lower edge of each white stencil mark visible on the downcomer above the pool surface was digitized, so that the point farthest left coincided with the extreme lower left corner of the mark. A frame of the film strip showing the scale marked in quarter-inch divisions was also digitized in the same manner.

The coordinate data sets corresponding to each selected test frame, as well as the scale-frame data set for each test, were produced using a Vanguard Motion Analyzer, Model M-16CD. Because there was excessive clearance in the registration pin of the analyzer, it was necessary to provide a special procedure in order to compensate for this problem. This consisted of the first two steps in the following overall data reduction procedure.

2.5.2.3 Data Reduction

The reduction of the digital data for each test was accomplished in the following steps which resulted in values of pool height and corresponding time for each frame.

The first two steps in the data reduction procedure establish the <x,y> coordinates corresponding to each of the white stencil marks on the outside of the downcomer. Nominally, the coordinates indicated for a given stencil mark in each of the six to eight frames analyzed for each test should be the same; however, the slight imprecision in coordinate determination, introduced by the excessive clearance in the Vanguard registration pin, made it necessary to establish a mean <x,y> value for each of the stencil marks, averaged over the frames analyzed for a given test. This was accomplished as follows:

1. Using all of the six to eight frame data sets for a given test (except for the scale-frame), a mean value for the location of each stencil mark is computed.
2. A vertical offset correction factor is defined for each frame by adjusting each frame in the vertical (y) direction so that the mean square vertical deviation of stencil points with respect to the corresponding mean location determined in Step 1 is a minimum.

These two steps establish a common reference frame for all of the film frames analyzed for a given test. The scale attached to the side of the downcomer is then mapped onto the downcomer stencil marks as follows:

3. Using the coordinates of the point at the extreme left of each stencil mark over all tests frames, a straight line fit is computed in the least squares sense.
4. Similarly, using the coordinates of the point at the extreme left of each quarter-inch division mark on the attached scale, a straight-line fit is computed, again in the least square sense.
5. The scale-frame is then translated in the horizontal (x) direction so that the straight lines computed in steps 3 and 4 coincide. Since, in general, the slopes of these lines are different, the scale line is rotated as necessary to establish coincidence.

6. The <x,y> coordinate pairs defining the entire lower edge of each stencil mark in each film frame are determined. These coordinate pairs for each stencil mark are then collected over <u>all</u> film frames and used to compute a parabolic fit in the least squares sense that defines the lower edge of each corresponding stencil mark.

7. Two reference frames may now be considered to exist, one overlaid on the other. One of these, the "A" frame, contains the scale points computed in step 4 together with the <x,y> coordinate pairs used in step 6. The second reference frame, the "B" frame, contains the parabolic fits determined in step 6. The "A" frame (i.e., the scale frame) is now translated along the direction defined by the coincident straight lines (step 5) until the mean square vertical deviation taken over all of the <x,y> coordinate pairs from step 6 is a minimum with respect to the fixed "B" frame parabolas from step 6.
8. Using the adjusted coordinates determined in step 7, a straight line fit to points at the extreme left of the scale divisions, is computed in the least square sense.
9. The final <x,y> coordinate pairs, against which the pool surface height is measured, are then established for each division of the scale from the straight line computed in step 8. The points of this scale cover the full range of pool surface height; typical points computed for test 2.7 are shown in Fig. 2-42.

This last step completes the mapping of the accurate scale (which is divided into quarter-inch divisions) onto the line defined by the left edges of the downcomer stencil marks. Using the reference scale defined in this manner, the pool surface position for each test frame is determined as follows:

10. In the least square sense and for each frame, a parabolic fit is computed to the points defining the intersection of the pool surface and the downcomer. Fig. 2-43 shows the set of points for all eight pool surface lines for test 2.7; Fig. 2-44 shows the corresponding parabolic fits. Note in Fig. 2-44 that the fit for the initial pool surface line is displayed as a dotted curve to distinguish it from the others and also that portions of the line defining the initial pool surface lie above the subsequent pool surface line labeled "A". This is believed to be an artifact of uncertainty in tracing the pool surface line and not of any physical phenomena.
11. For each parabolic fit of step 10, the point of intersection with the scale straight line from step 8 is determined and the point used to evaluate the distance along the outer edge of the downcomer by linear interpolation between the nearest two scale points computed in step 9.

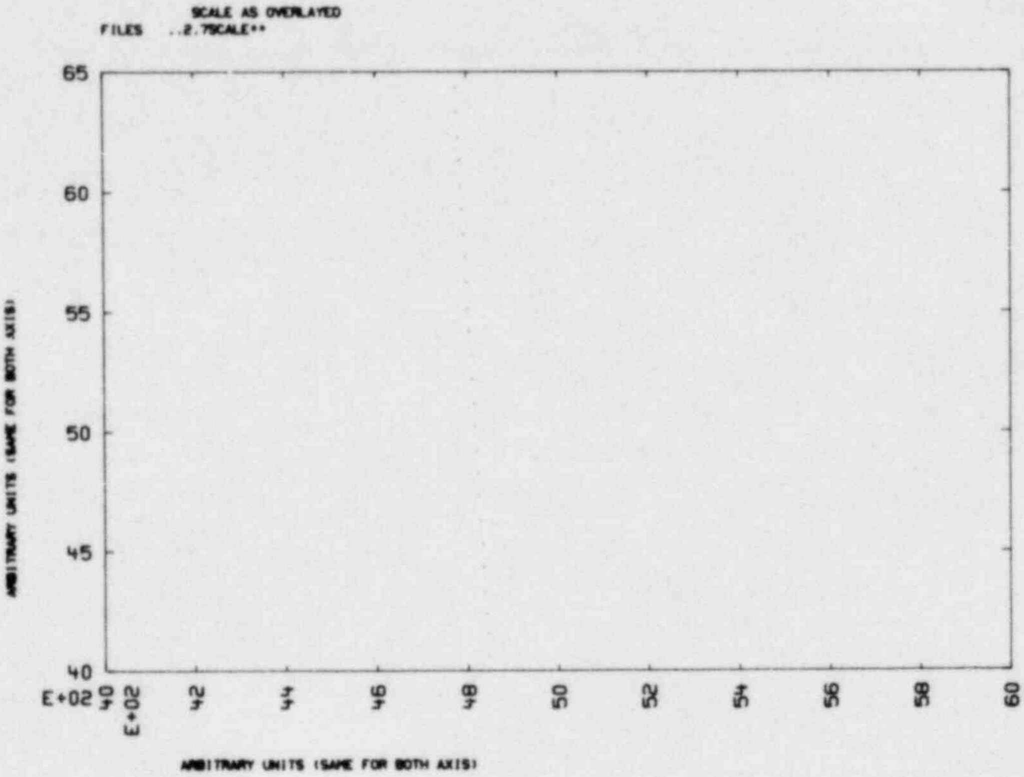

FIG. 2-42. Range of pool surface height, test 2.7.

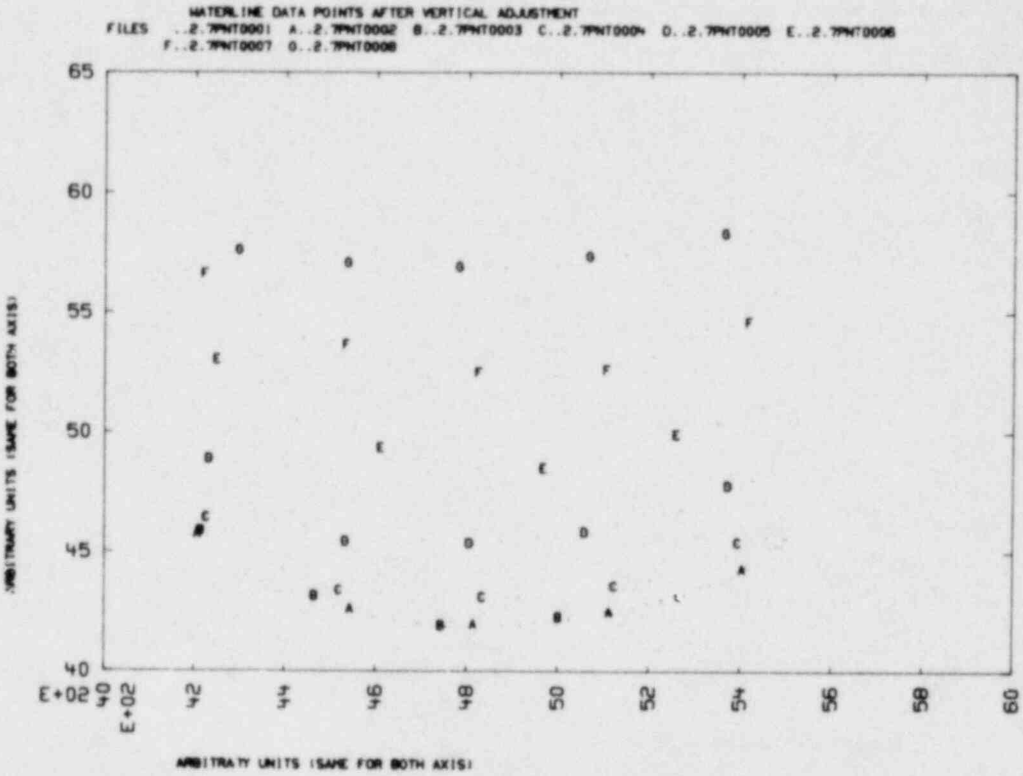

FIG. 2-43. Points defining pool surface lines, test 2.7.

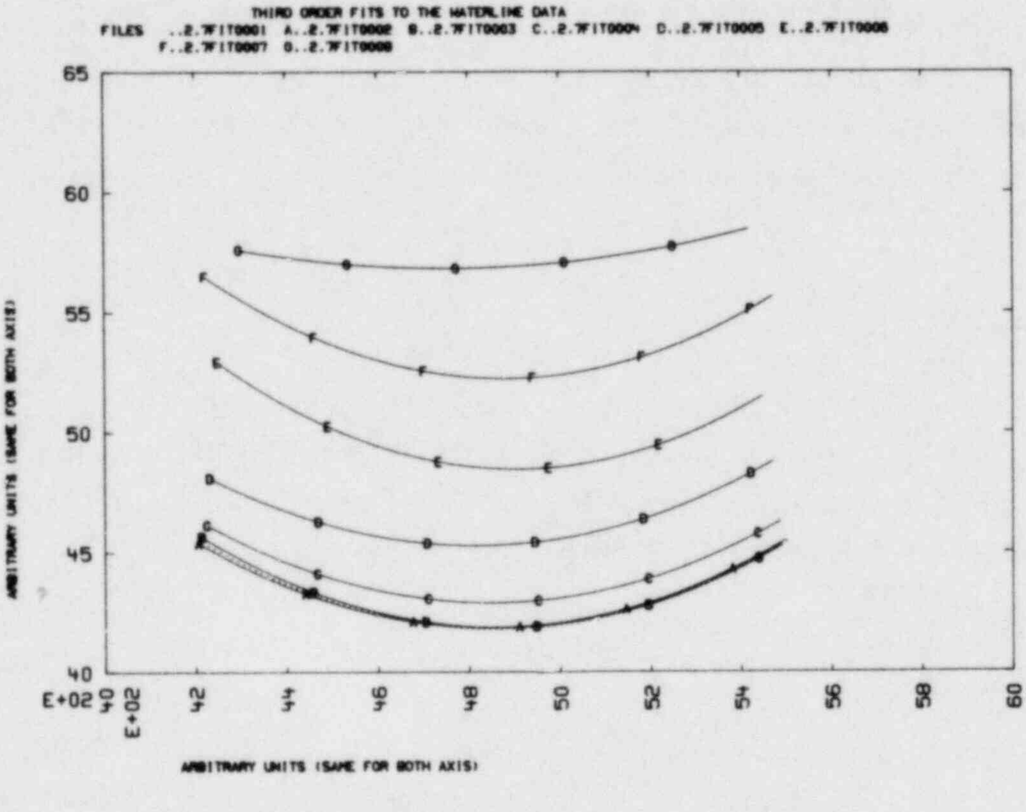

FIG. 2-44. Parabolic fit to points defining each pool surface height, test 2.7.

12. Since step 11 results in determining the relative distance along the downcomer, this result is multiplied by cos 30^{0} to obtain the vertical height. The height obtained for the first frame, which represents the initial pool surface level, is subtracted from all of the others to obtain relative height above the initial pool surface.

13. Since the zero time mark on the film strip corresponds to the zero time mark for the other recorded data from transducers, it is necessary only to count the timing marks from zero time to the selected frame to determine the time associated with that frame.

Figure 2-45 shows the results of generating a natural cubic spline passing through the eight computed points in test 2.7. The fit includes both end points; the inner points are designated by a "Z" patterned interruption of the fit and are located precisely at the intersection of the center of the pattern and the imaginary continuous spline.

2.5.2.4 Results

Figures 2-46 through 2-48 show the pool surface line parabolic fits for tests 2.9, 2.10, and 2.11, respectively. Figures 2-49 through 2-51 are the pool height versus time for tests 2.9, 2.10, and 2.11, respectively. In addition, the following tabulations of pool height versus time are given for the calculated points:

TEST 2.7		TEST 2.9	
height(meters)	time(seconds)	0.	1.2975
0.	3.2515	0.5514e-03	1.3713
.43167e-03	3.3010	5.9045e-03	1.4451
.76368e-03	3.3490	31.599e-03	1.4795
13.521e-03	3.3980	90.390e-03	1.5090
40.063e-03	3.4217	167.62e-03	1.5336
77.491e-03	3.4355	231.61e-03	1.5482
118.70e-03	3.4503		
167.38e-03	3.4650		

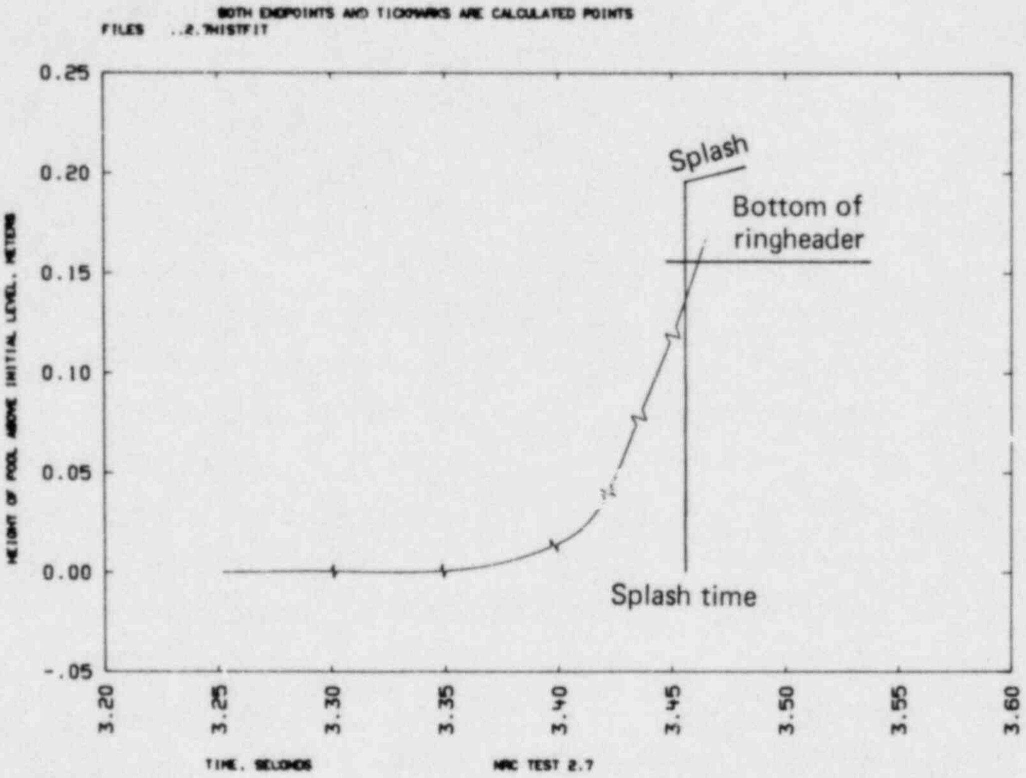

FIG. 2-45. Pool surface elevation along linear scale, test 2.7.

TEST 2.10

height(meters)	time(seconds)
0.	2.7514
4.7198e-03	2.8007
22.291e-03	2.8498
91.813e-03	2.8841
168.95e-03	2.8990
230.74e-03	2.9088

TEST 2.11

0	1.4163
0.0509e-03	1.4654
4.6262e-03	1.5145
30.188e-03	1.5636
96.357e-03	1.5932
153.34e-03	1.6079
213.78e-03	1.6187

Note that in Figs. 2-45 and 2-49 through 2-51 there is a horizontal line near the upper right end of the curve indicating the approximate height of the ring header bottom, and a vertical line designating the time the first splash from pool surface-ring header impact is seen. Because this latter time is taken from the same film as used for the pool surface measurements, the maximum time error is only 1 percent of the time interval between pool surface-ring header impact and the time being compared at a point on the curve.[*] For example, the time interval to splash from the first frame digitized in test 2.7 is 0.199 s ± 0.002 s.

Comparison of times of events which depend upon cross-timing and the zero time mark of the film is much more difficult. Figure 2-52 is a plot of all four test pool surface history curves. Because the test films are independently timed, each has an independent error. Thus, e.g., the maximum error in time correlation between tests 2.7 and 2.11 is measured by the total time, $(3.5 + 2.8) \times 0.01 = 0.063$s rather than the difference $(3.5 - 2.8) \times 0.01 = 0.007$s. This lack of close correlation makes it possible to determine the coincidence of header strut load cell and pool height or splash observation only in a very rough sense.

Figure 2-53 can be used to compare pool surface motion shapes; offsets in both time and height have been introduced to bring the plots into proximity without overplotting.

---

[*] Recall that the timing error based on frame counting develops at a rate of approximately 1 percent.

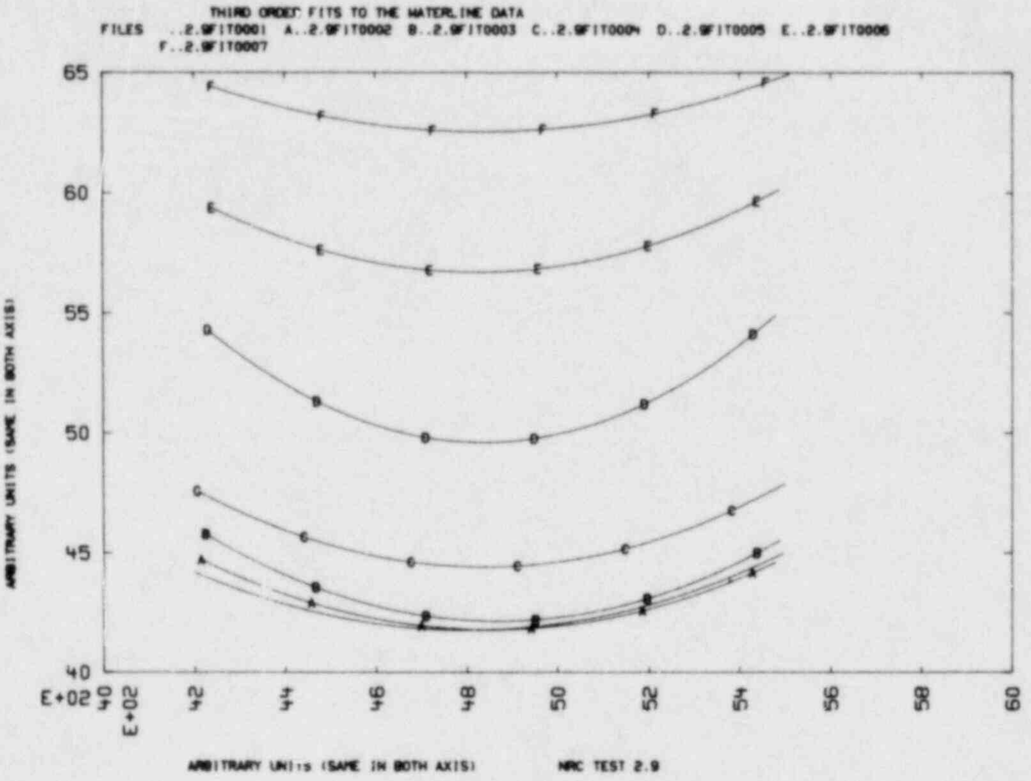

FIG. 2-46. Parabolic fit to points defining each pool surface height, test 2.9.

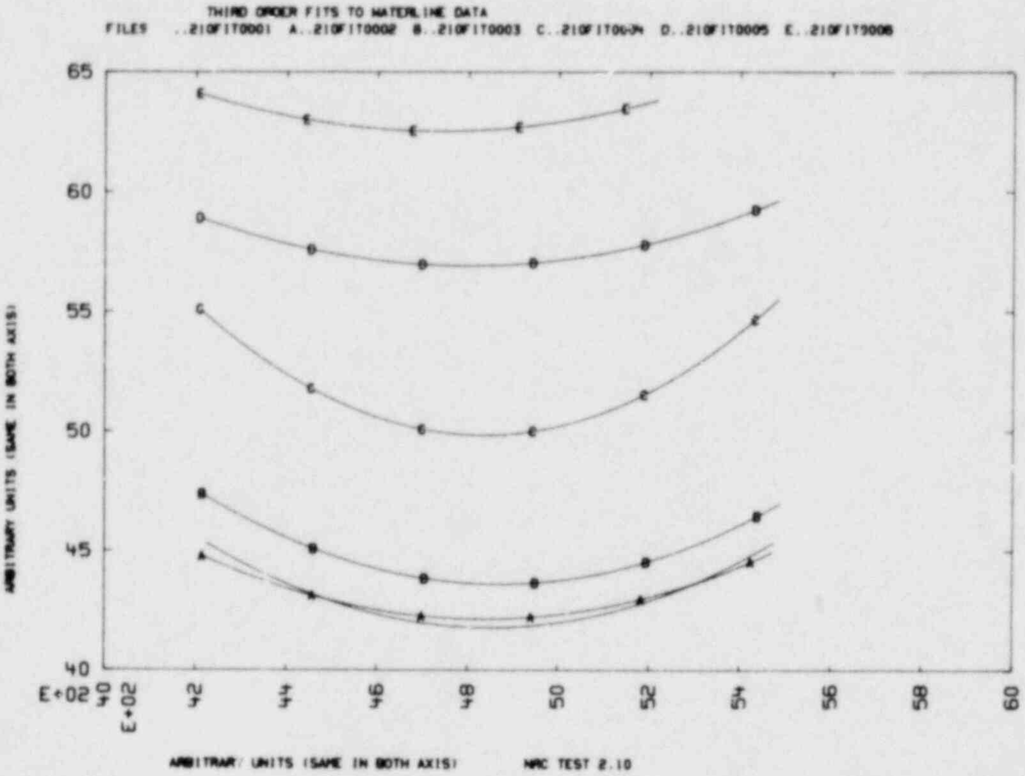

FIG. 2-47. Parabclic fit to points defining each pool surface height, test 2.10.

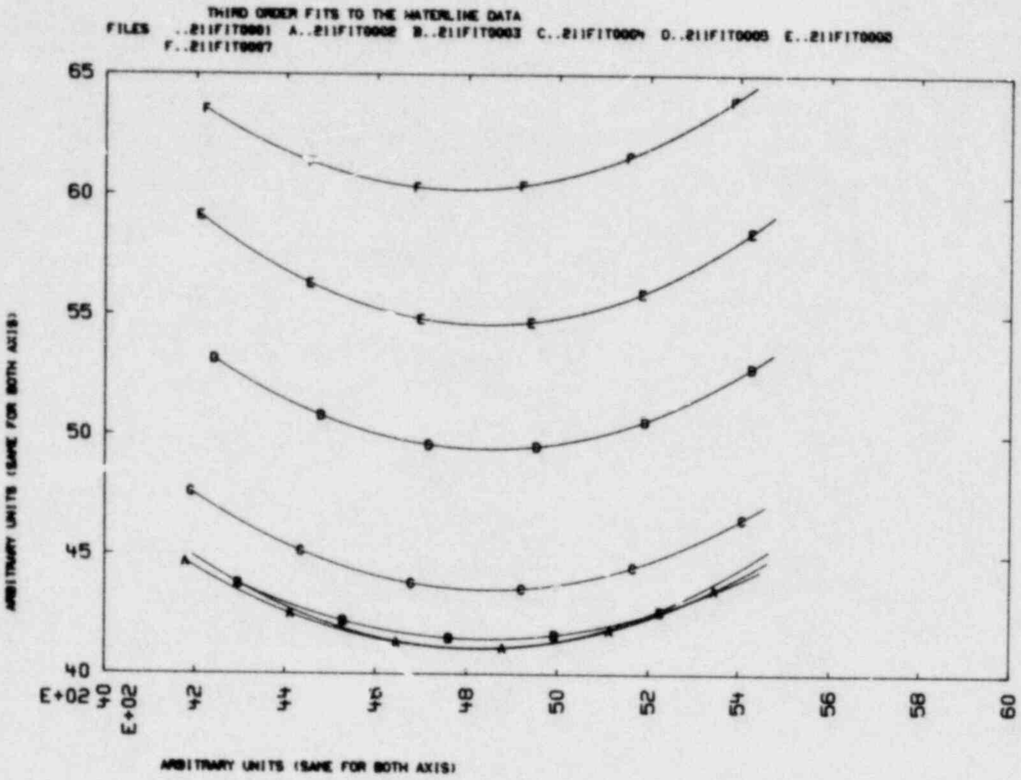

FIG. 2-48. Parabolic fit to points defining each pool surface height, test 2.11.

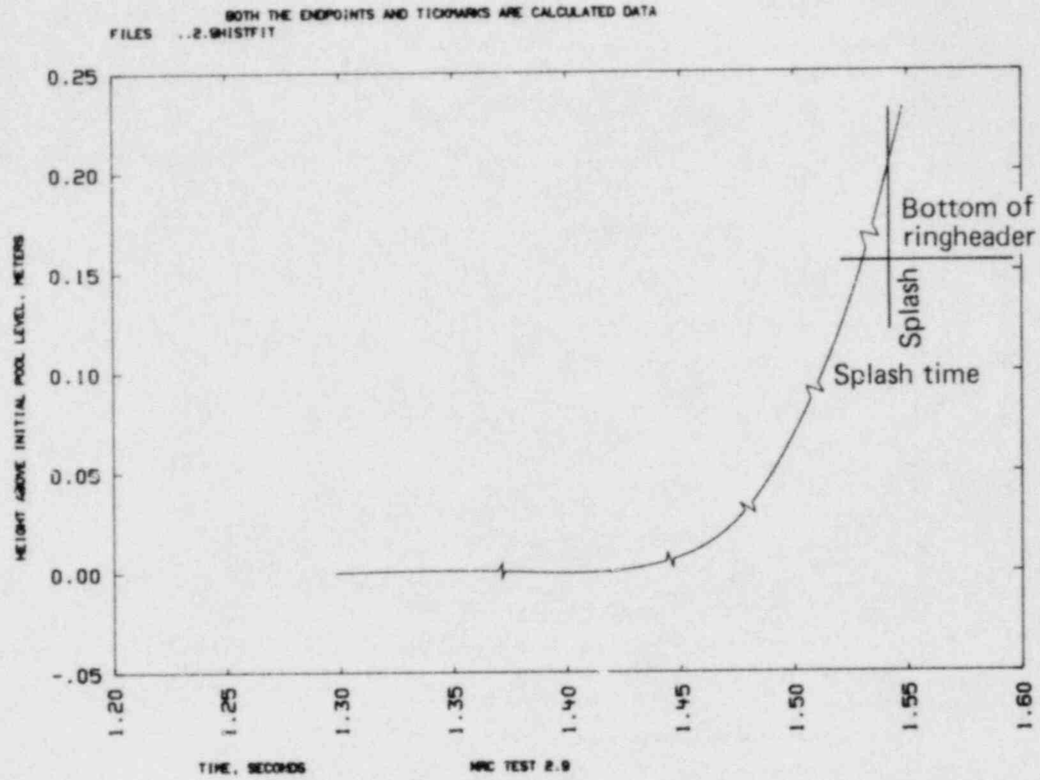

FIG. 2-49. Pool surface elevation along linear scale, test 2.9.

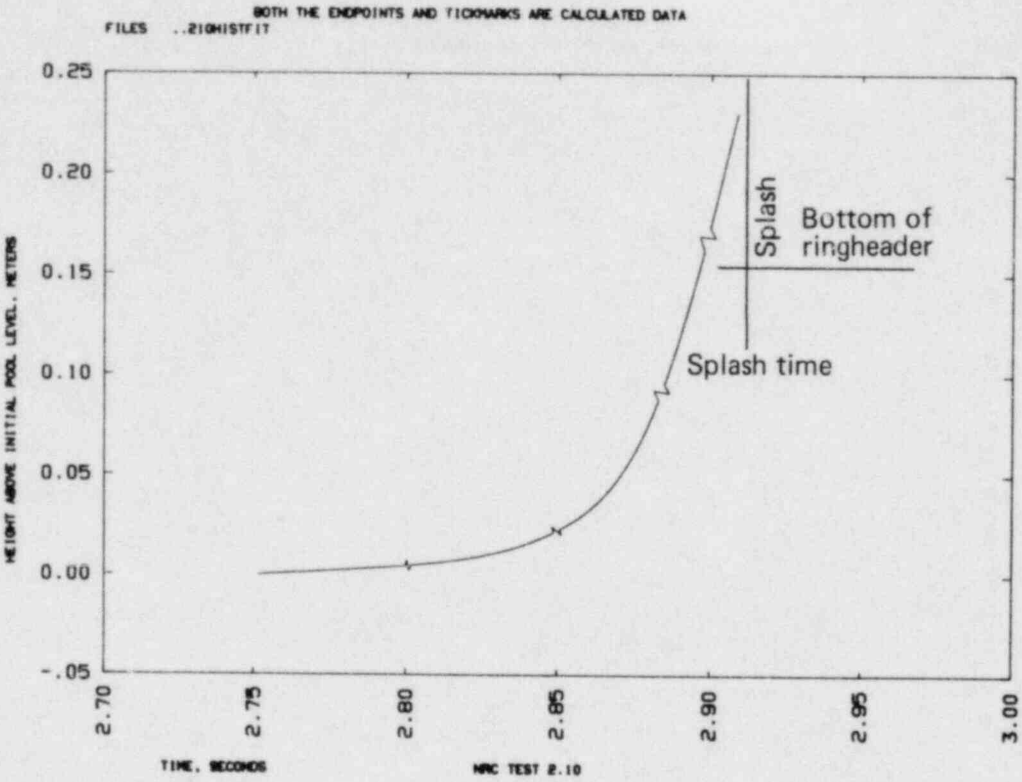

FIG. 2-50. Pool surface elevation along linear scale, test 2.10.

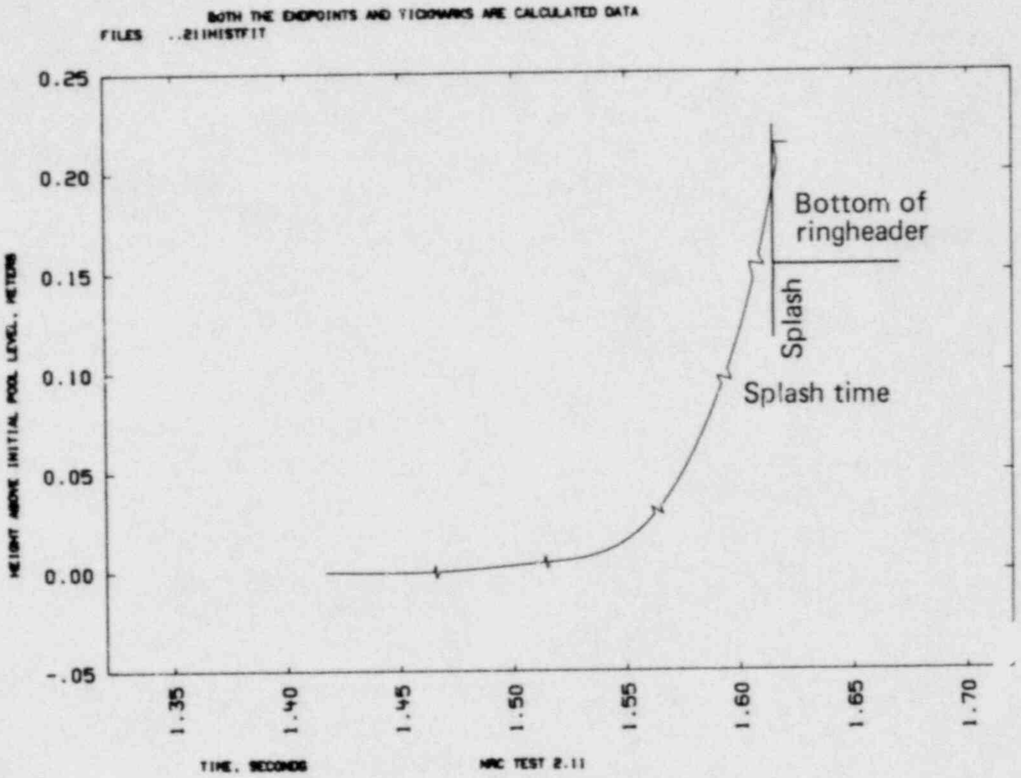

FIG. 2-51. Pool surface elevation along linear scale, test 2.11.

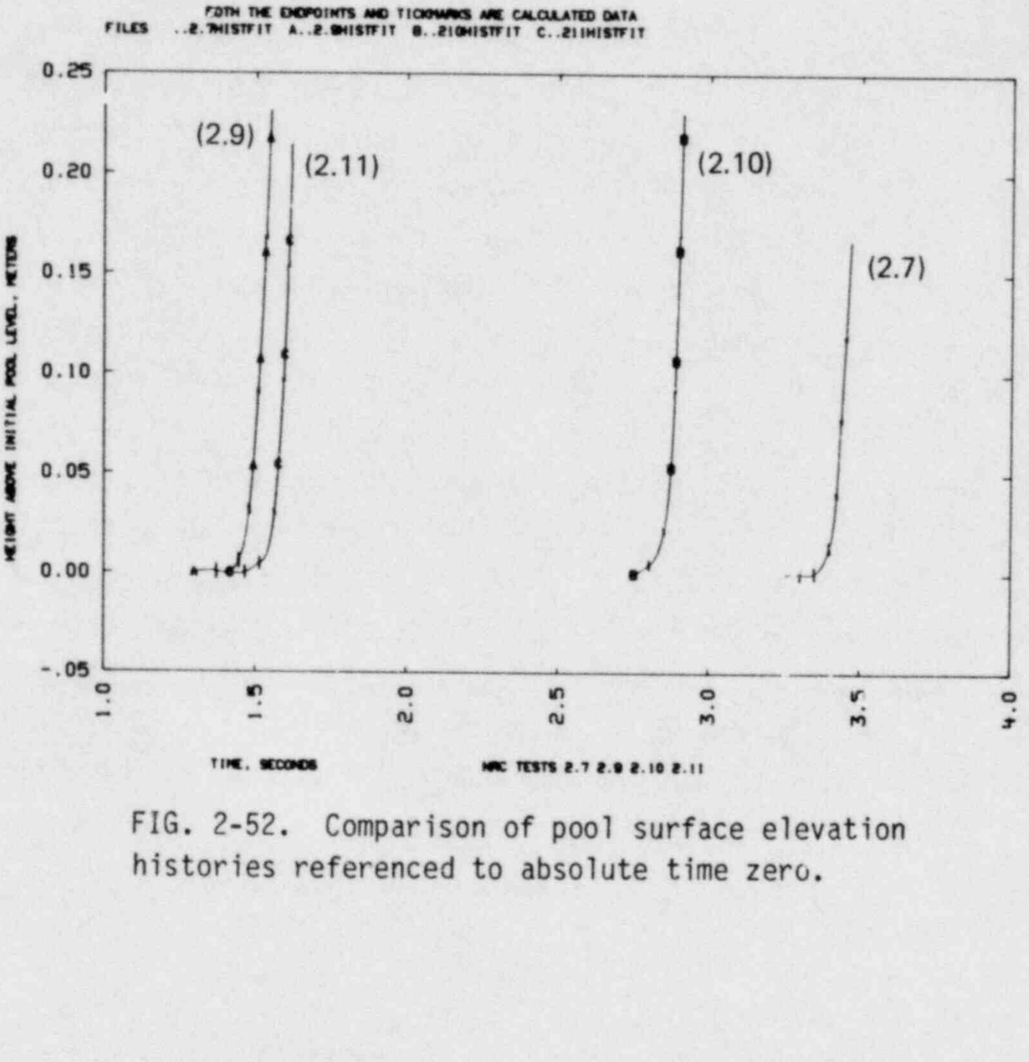

FIG. 2-52. Comparison of pool surface elevation histories referenced to absolute time zero.

Figures 2-54 and 2-55 are pool surface history curves showing the time relative to the start of drywell pressurization. Vertical offsets of 0.1 m are used for clarity in Fig. 2-54. Again, time is established through use of zero mark cross-timing and large time errors are likely associated with these curves.

2.5.3 POOL SURFACE VELOCITY

Figures 2-56 through 2-59 are time derivatives (in units of m/s) of Figs. 2-45, 2-49, 2-50 and 2-51 respectively. If the pool surface were absolutely level, these figures would represent vertical pool surface velocity, but this is not the case. These figures represent the vertical rate of rise at the point where pool surface and downcomer outer edge intersect. Since both a horizontal velocity component and a surface inclination may contribute to this rise, it is not recommended that the derivative information be used directly to compare one test with another, nor with data acquired from other experimental installations. Comparisons of these tests should be confined to pool history along a line comparable to the outer downcomer edge.

The following procedure is used to provide an estimate of vertical velocity histories on the torus centerline beneath the center of the ring header; the results should only be used with the above cautions in mind. When pool surface ring-header impact splash is first observed, the height of the pool surface at the downcomer line is read from the pool surface history plots. As shown schematically in Fig. 2-60, a parabolic curve is generated through the two points, the impact point $<0,Y_{imp}>$ and the height on the downcomer line $<z_L,y_L>$, by evaluating a and b in the expression,

$$y = az^2 + b \quad . \tag{2-36}$$

It is assumed that the shape of the pool surface does not deviate significantly from this parabola during pool swell. Therefore, the plane 4 pool swell velocity history may be represented by,

$$y = (az^2 + b)\ U(t) \tag{2-37}$$

where U(t) is a function of time. For each of the calculated pool heights versus time, the value of U(t) is computed from the quantity bU(t), which

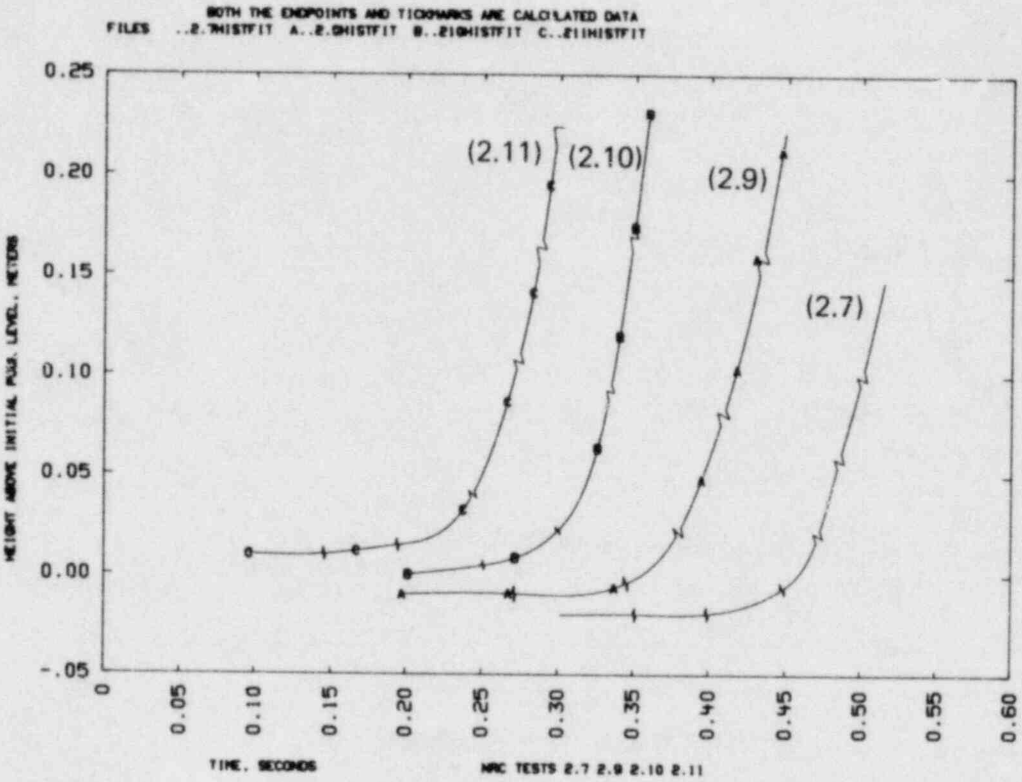

FIG. 2-53. Comparison of pool surface elevation histories using arbitrary vertical and horizontal scale offsets.

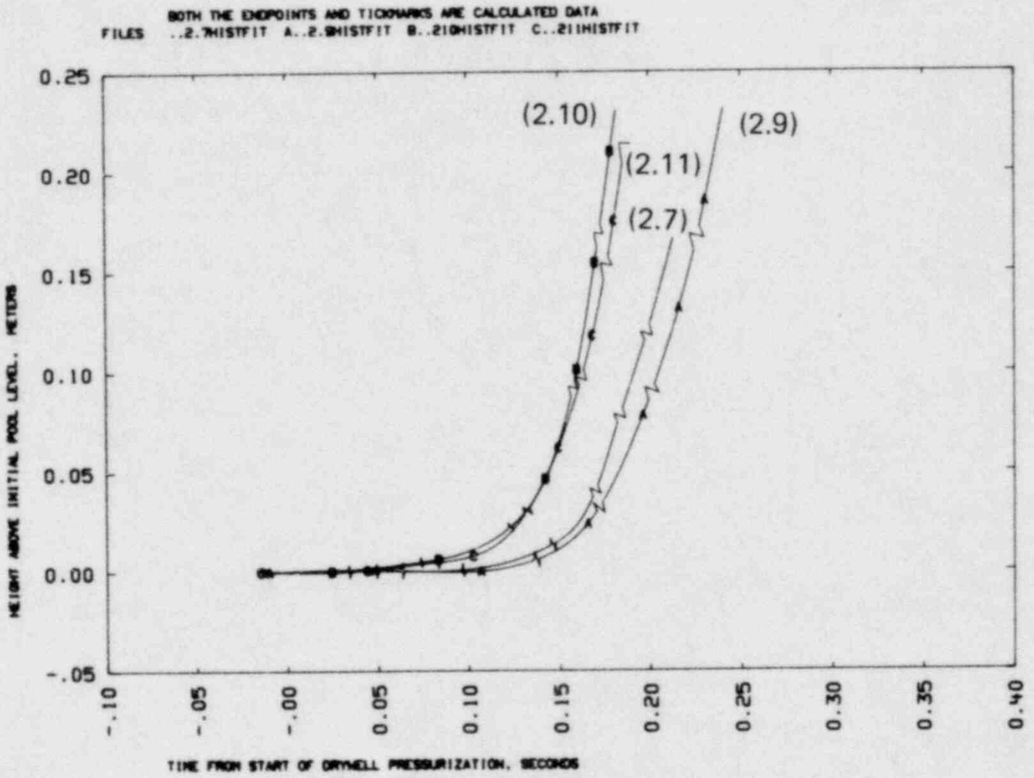

FIG. 2-54. Comparison of pool surface elevation histories referenced to start of drywell pressurization for each test.

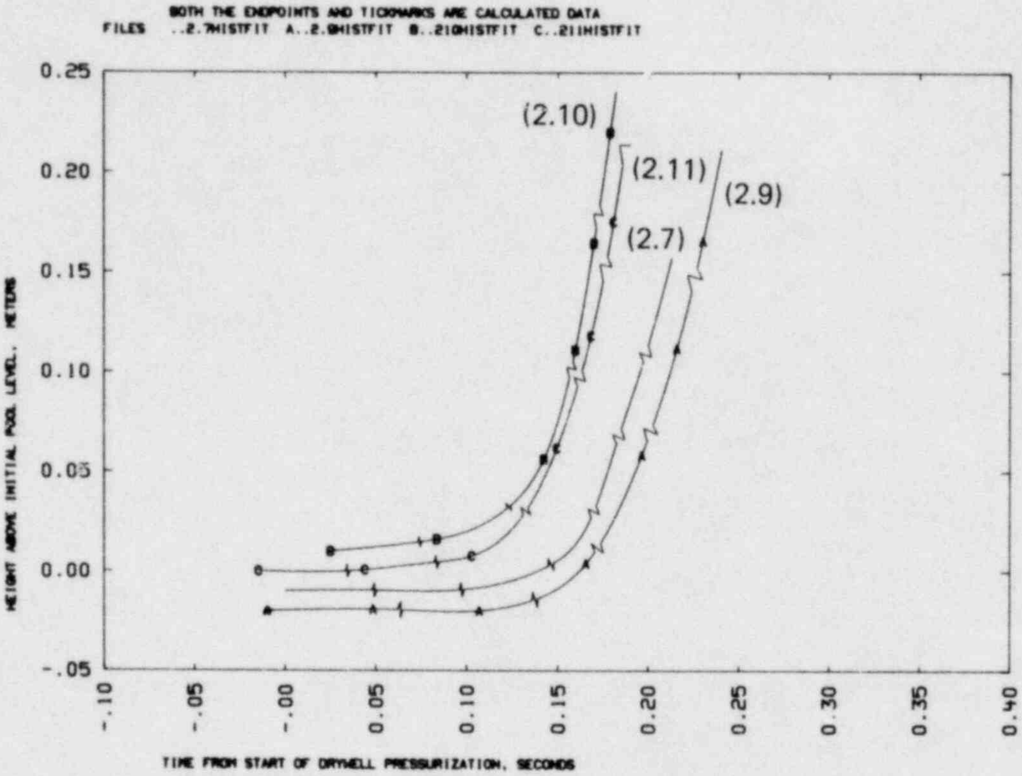

FIG. 2-55. Comparison of pool surface elevation histories referenced to start of drywell pressurization for each test, vertical offsets added for clarity.

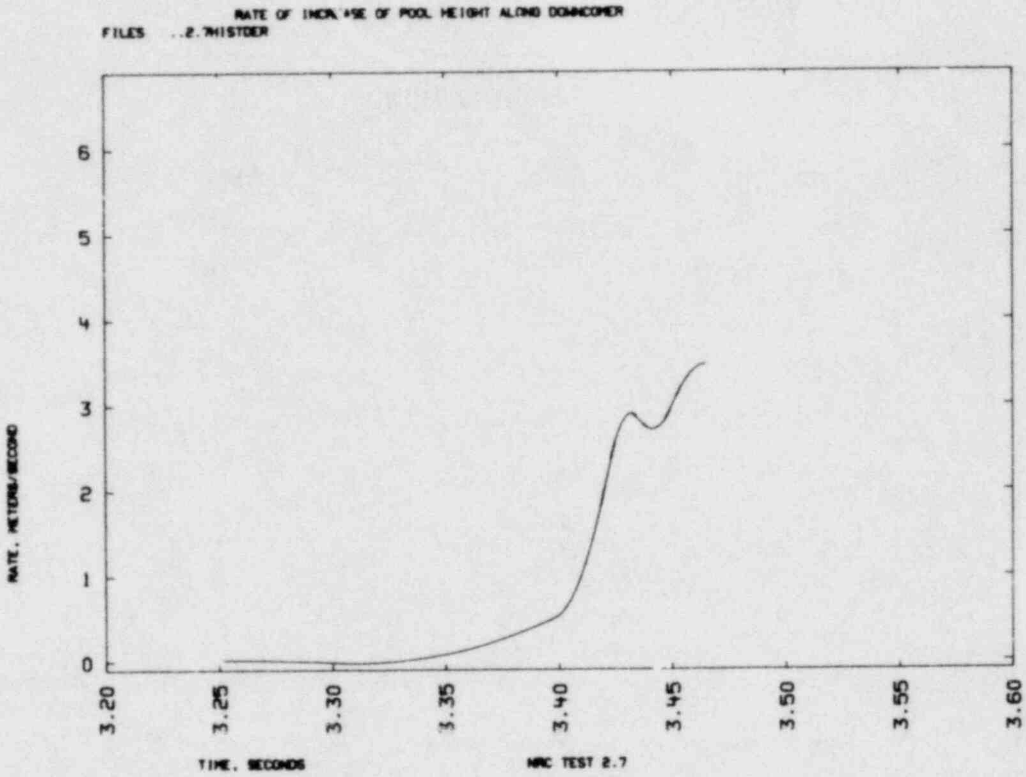

FIG. 2-56. Rate of increase in pool height along downcomer, test 2.7.

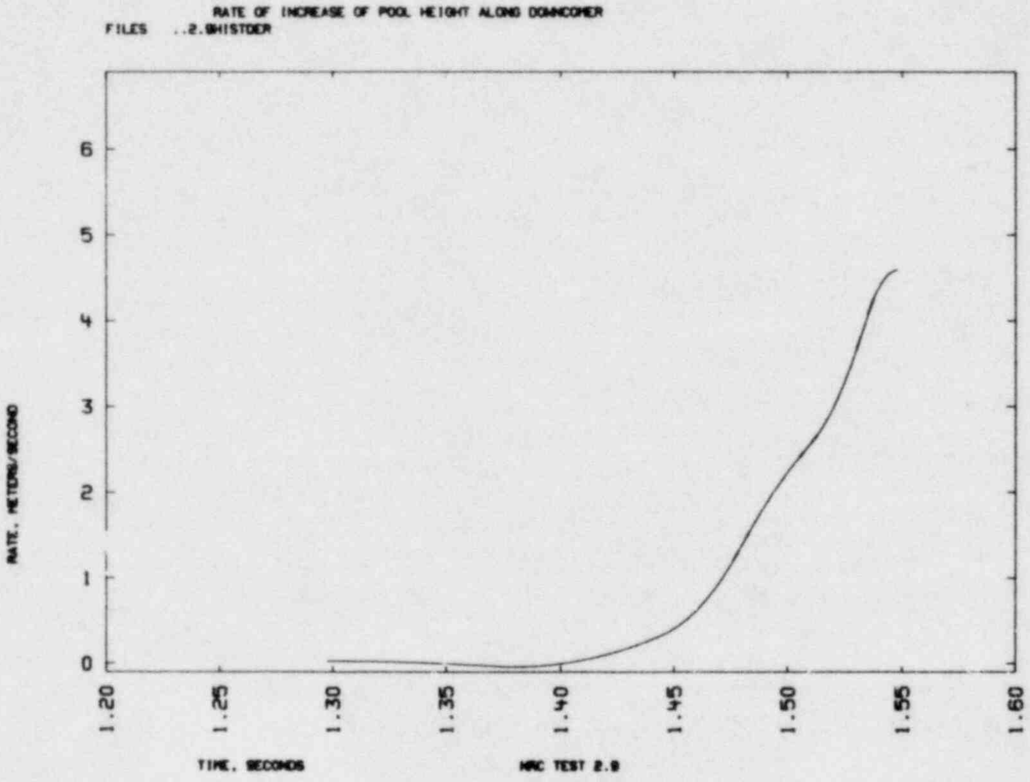

FIG. 2-57. Rate of increase in pool height along downcomer, test 2.9.

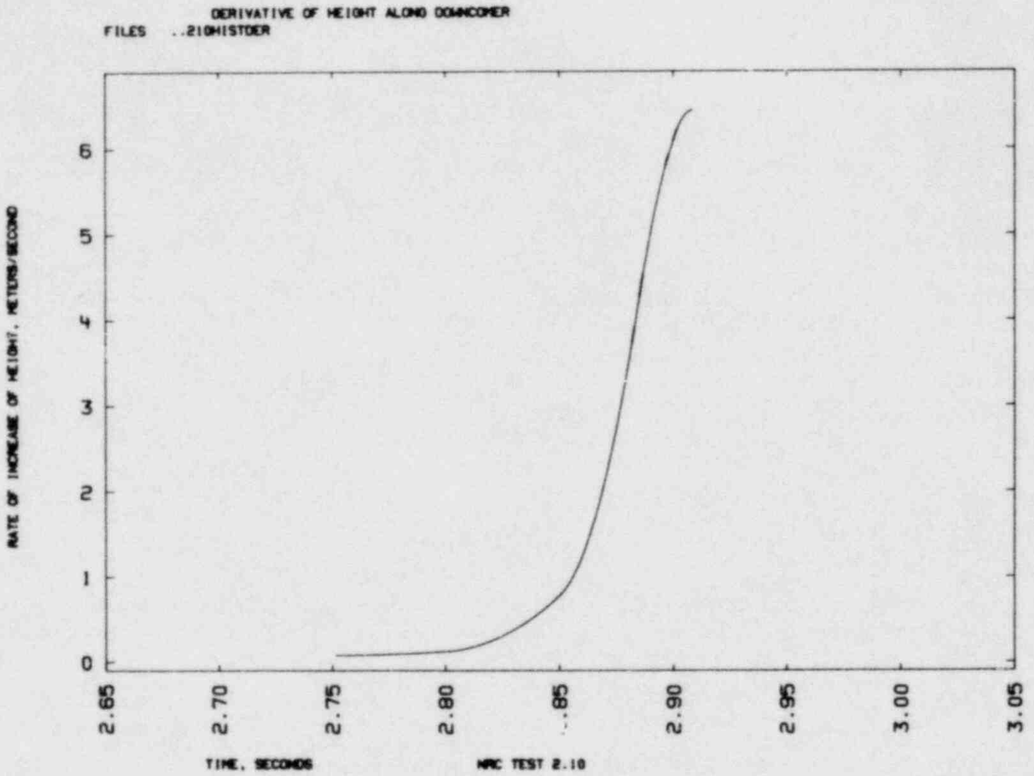

FIG. 2-58. Rate of increase in pool height along downcomer, test 2.10.

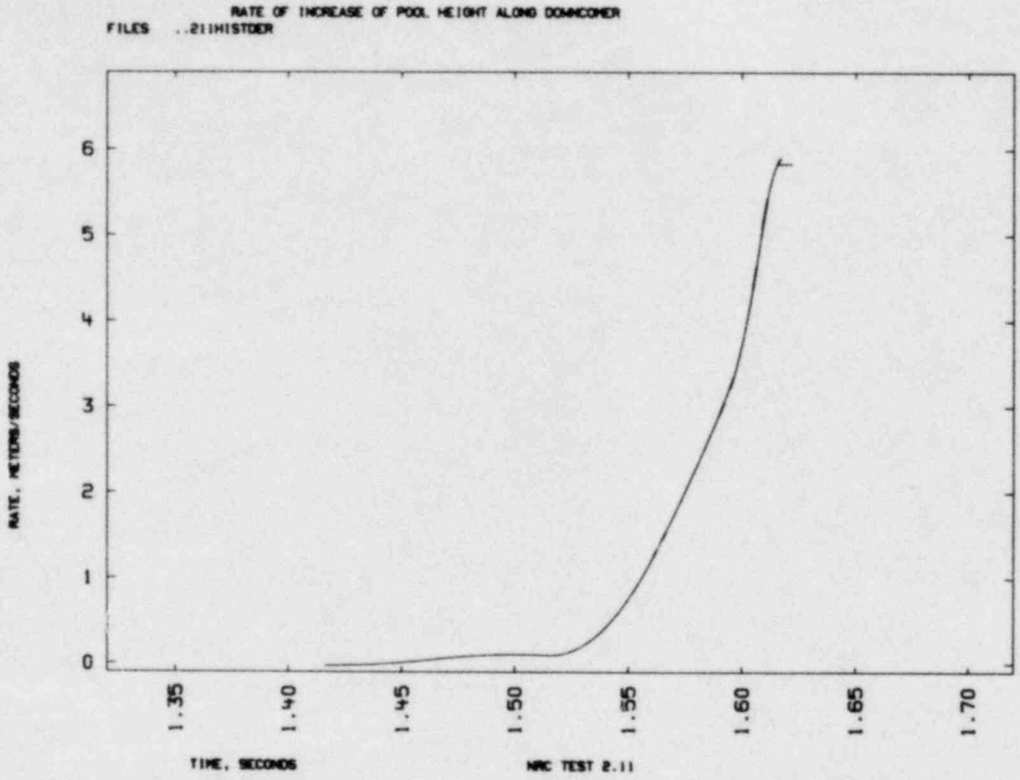

FIG. 2-59. Rate of increase in pool height along downcomer, test 2.11.

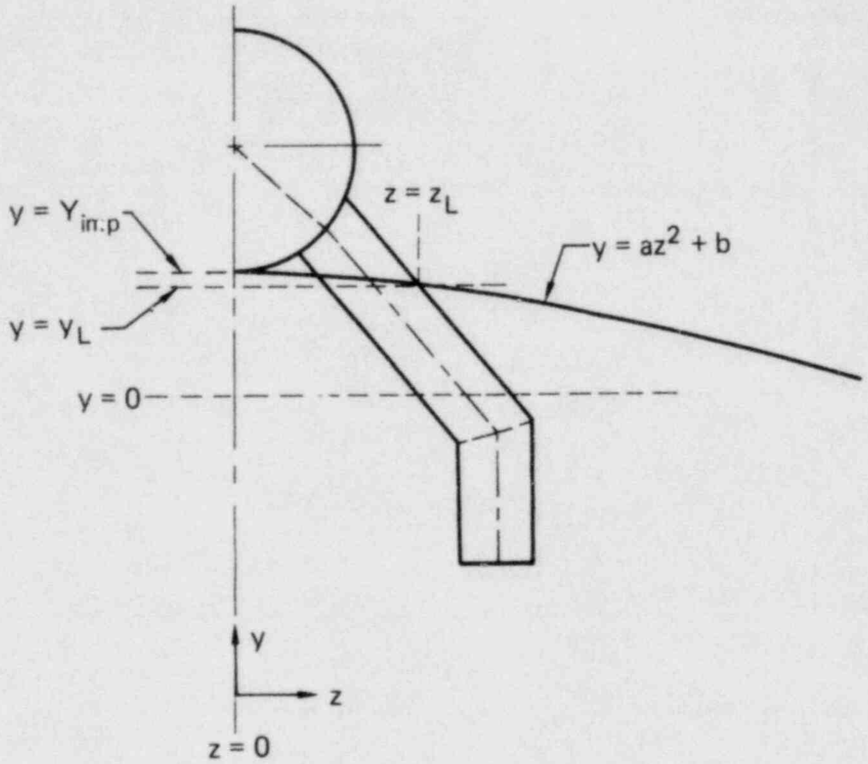

FIG. 2-60. Schematic diagram of ring header/downcomer cross-section for pool swell velocity calculation.

represents the estimated pool surface height along the torus vertical centerline. Figures 2-61 through 2-64 are plots of these heights with a natural cubic spline fitted through them. Figures 2-65 through 2-68 are plots of the derivatives of these splines, and can be considered estimated vertical velocities of the pool surface along the torus vertical centerline.

Results of the vertical pool surface motion evaluations, both along the downcomer and the torus centerline are tabulated for the time of ring header impact in Table 2-23. These data are correlated to the drywell pressurization rate ($\dot{p}_{dw}$) in Figs. 2-69. As shown in Fig. 2-69a there appears to be a strong linear correlation between the time interval to header impact and $\dot{p}_{dw}$. Such uniform results are not, however, evidenced by the motion plots of Fig. 2-69b. The vertical motion estimates, both from along-downcomer evaluation as well as along torus centerline, evidence an unexplained minima from the data of test 2.7; omission of that point suggests a more reasonable linear relationship as observed in the time-to-impact correlation.

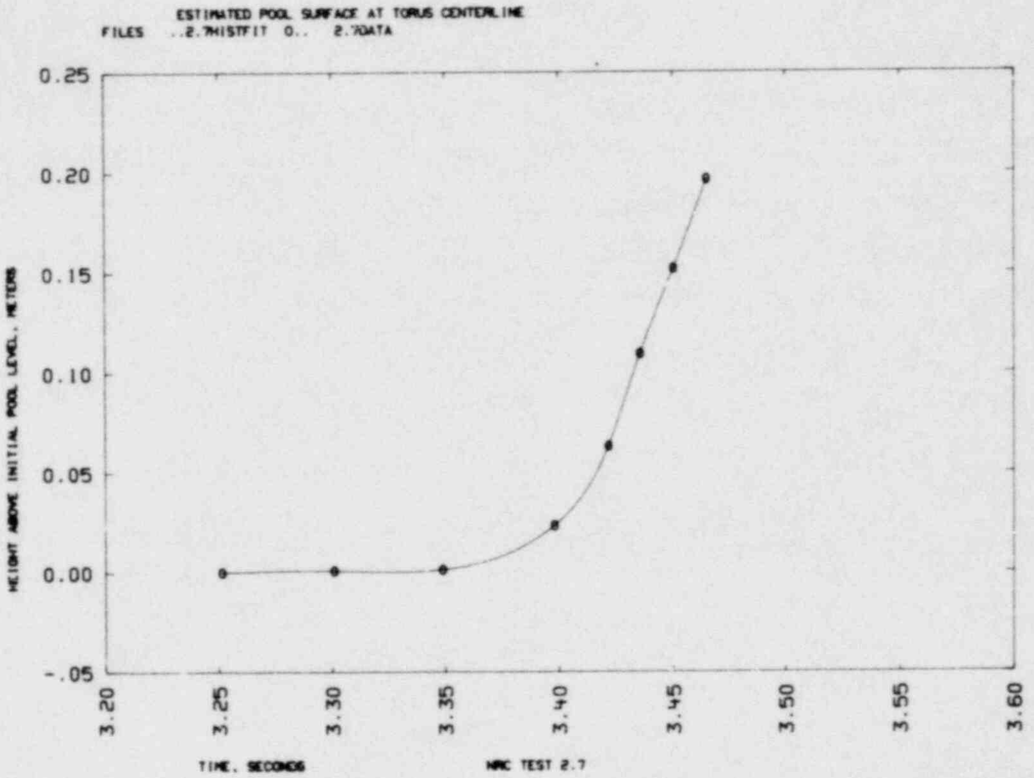

FIG. 2-61. Estimated pool surface height along torus vertical centerline, test 2.7.

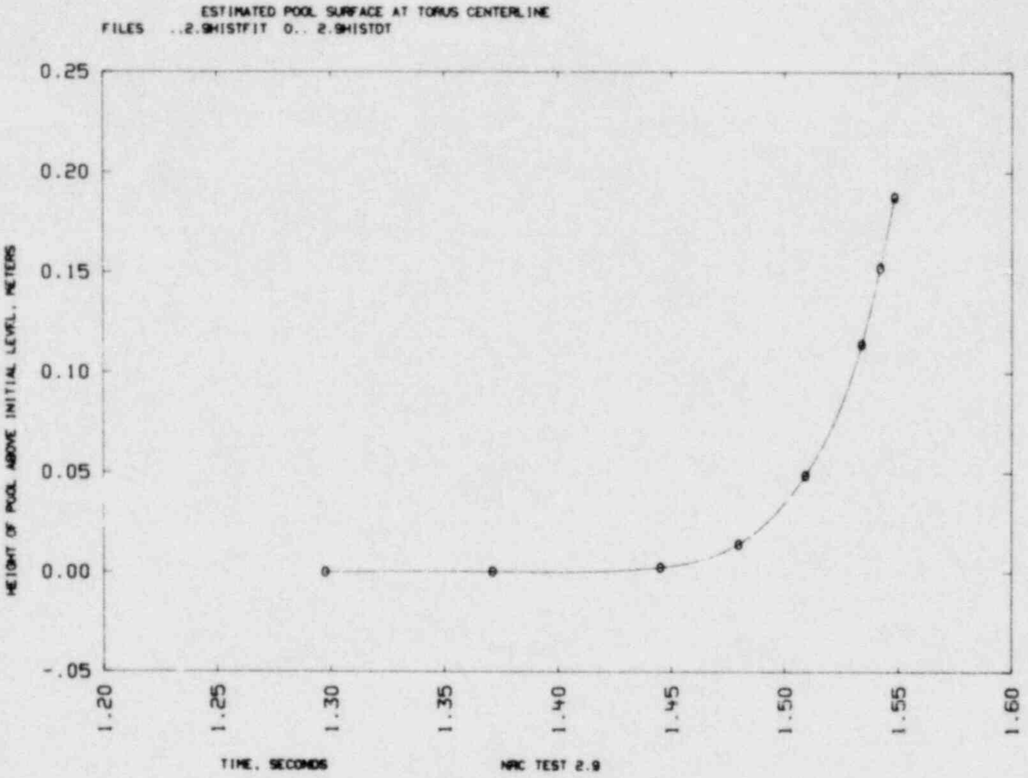

FIG. 2-62. Estimated pool surface height along torus vertical centerline, test 2.9.

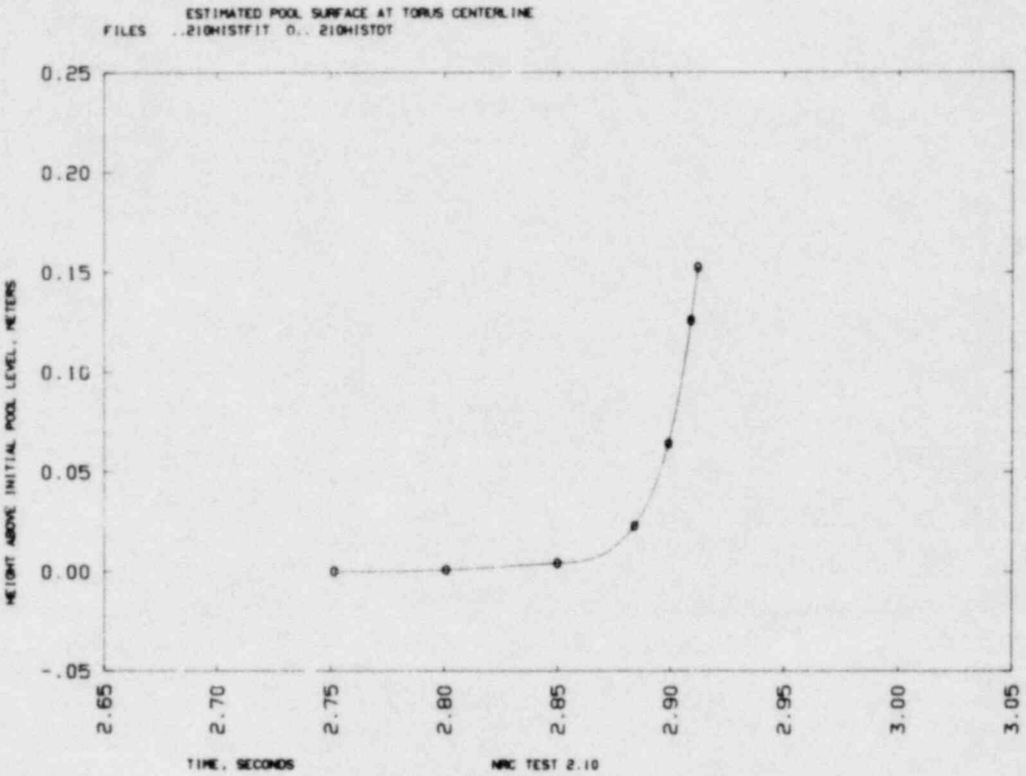

FIG. 2-63. Estimated pool surface height along torus vertical centerline, test 2.10.

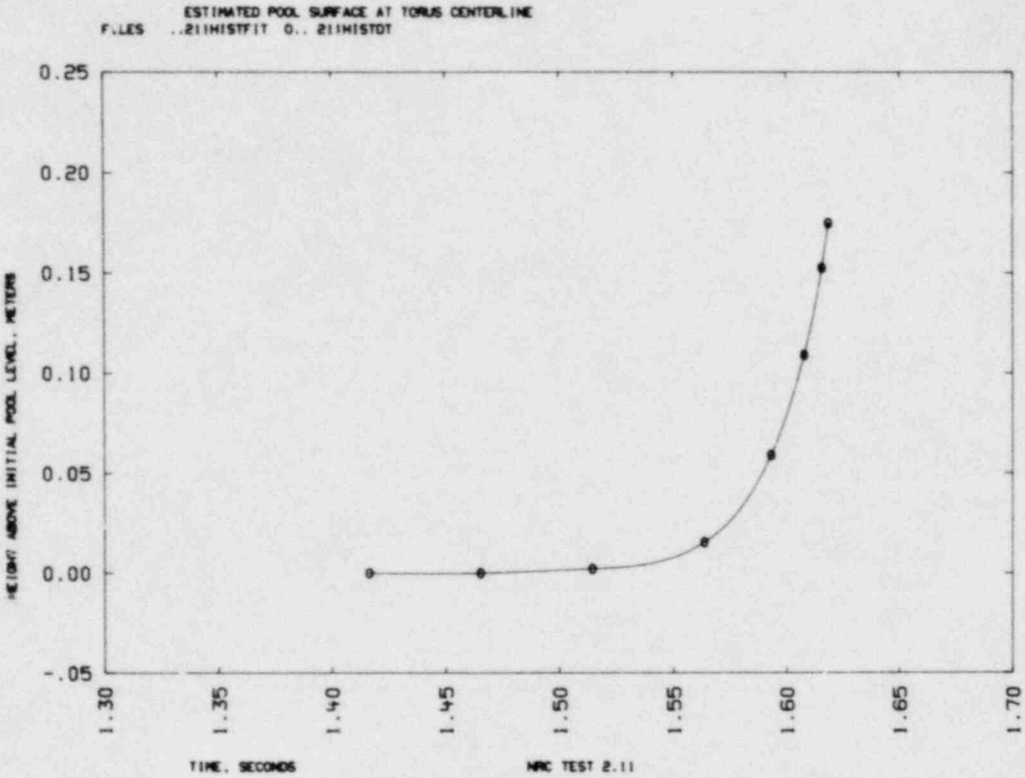

FIG. 2-64. Estimated pool surface height along torus vertical centerline, test 2.11.

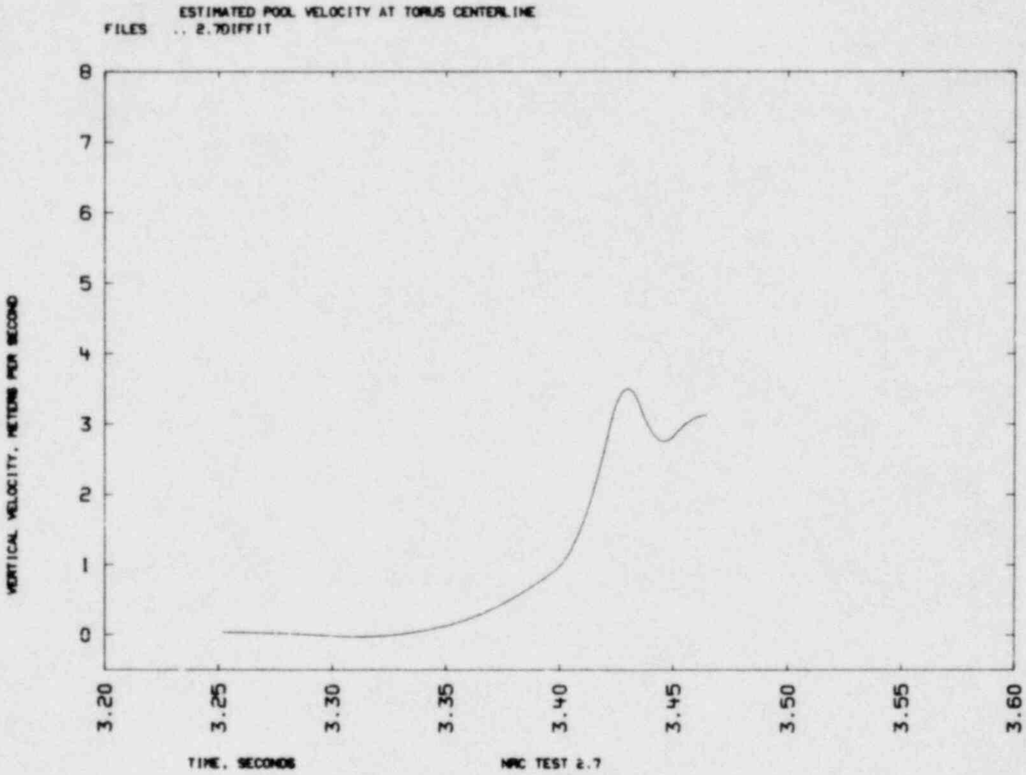

FIG. 2-65. Estimated pool surface velocity along torus vertical centerline, test 2.7.

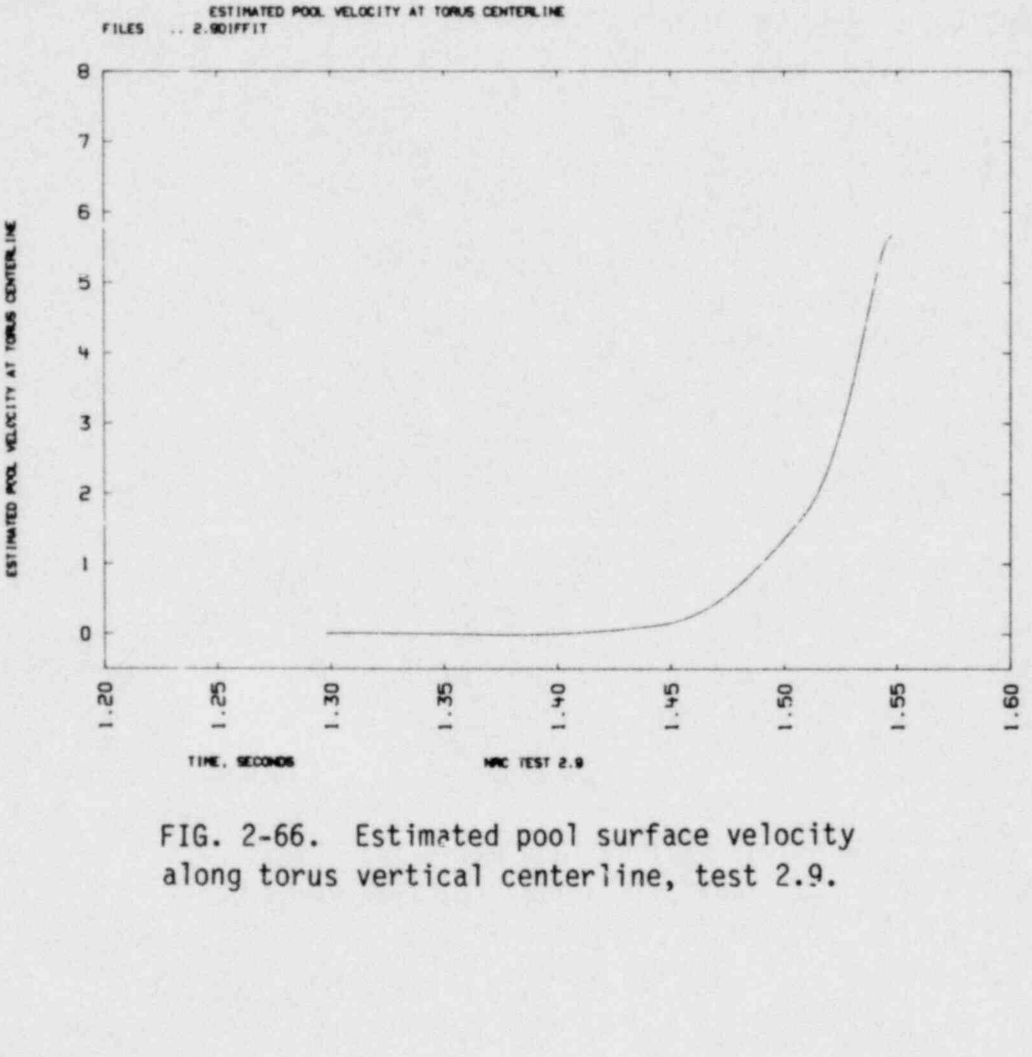

FIG. 2-66. Estimated pool surface velocity along torus vertical centerline, test 2.9.

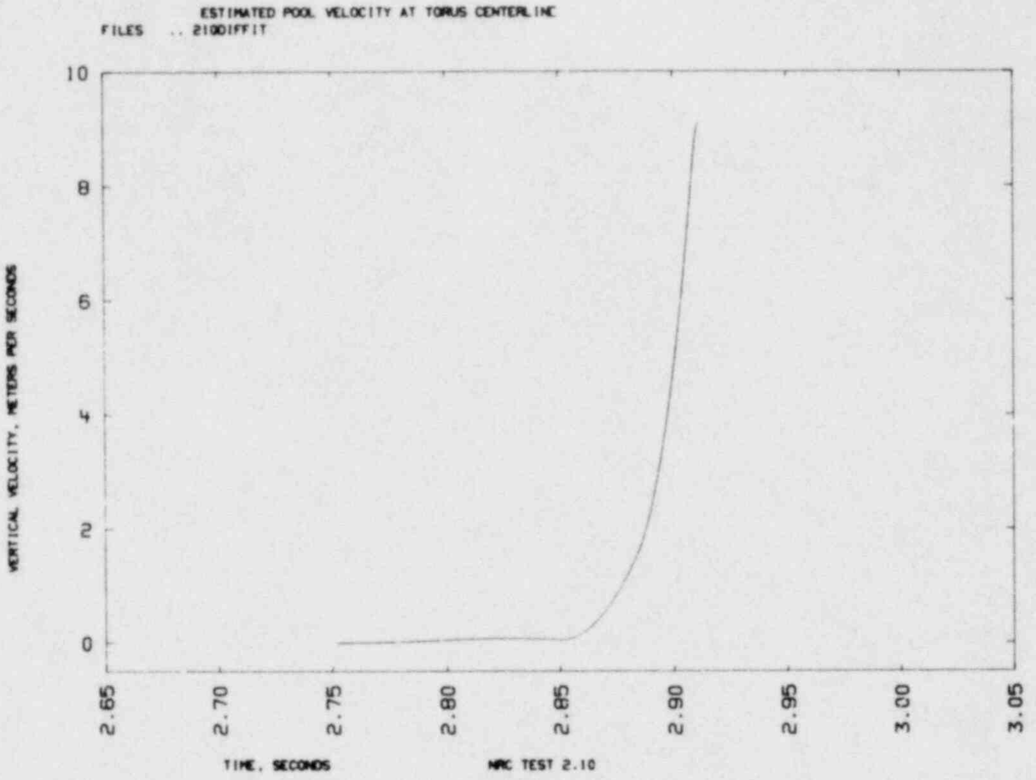

FIG. 2-67. Estimated pool surface velocity along torus vertical centerline, test 2.10.

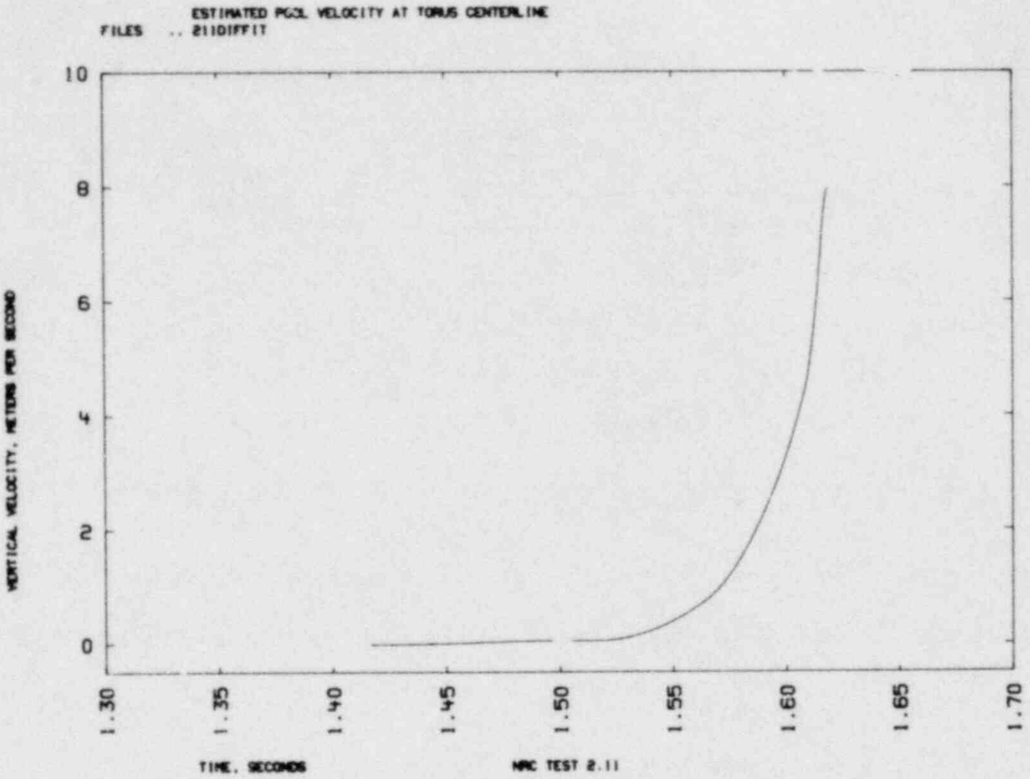

FIG. 2-6 . Estimated pool surface velocity along torus vertical centerline, test 2.11.

TABLE 2-23. Estimated vertical pool surface motion at time of ring header impact.

Test	t_{imp}	V_{imp}^{d}	V_{imp}^{c}	$\bar{\dot{p}}_{dw}$	$\bar{t}_o$
	sec	m/s	m/s	psi/s	sec
2.7	3.455	3.22	3.00	23.566	3.2518
2.9	1.542	4.45	5.14	15.136	1.3076
2.10	2.912	6.45	9.12	27.851	2.7266
2.11	1.616	5.84	7.00	29.933	1.4312

t_{imp} = time of vent header impact.

V_{imp}^{d} = vertical velocity of pool surface measured along downcomer.

V_{imp}^{c} = vertical impact velocity of pool surface measured along vertical centerline.

$\bar{\dot{p}}_{dw}$ = drywell pressurization rate.

$\bar{t}_o$ = time of start of drywell pressurization.

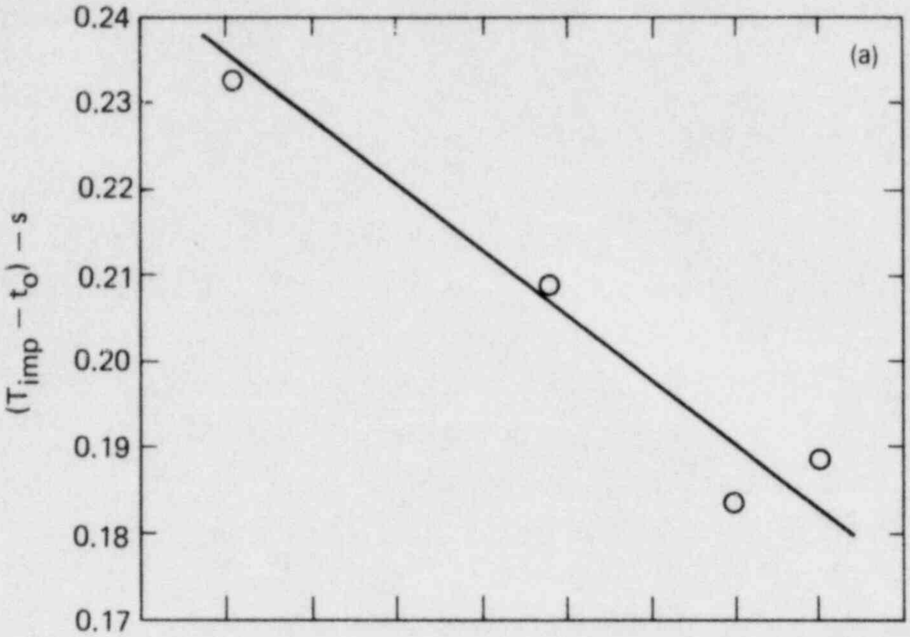

FIG. 2.69a. Effect of drywell pressurization rate on time to pool surface-ring header impact.

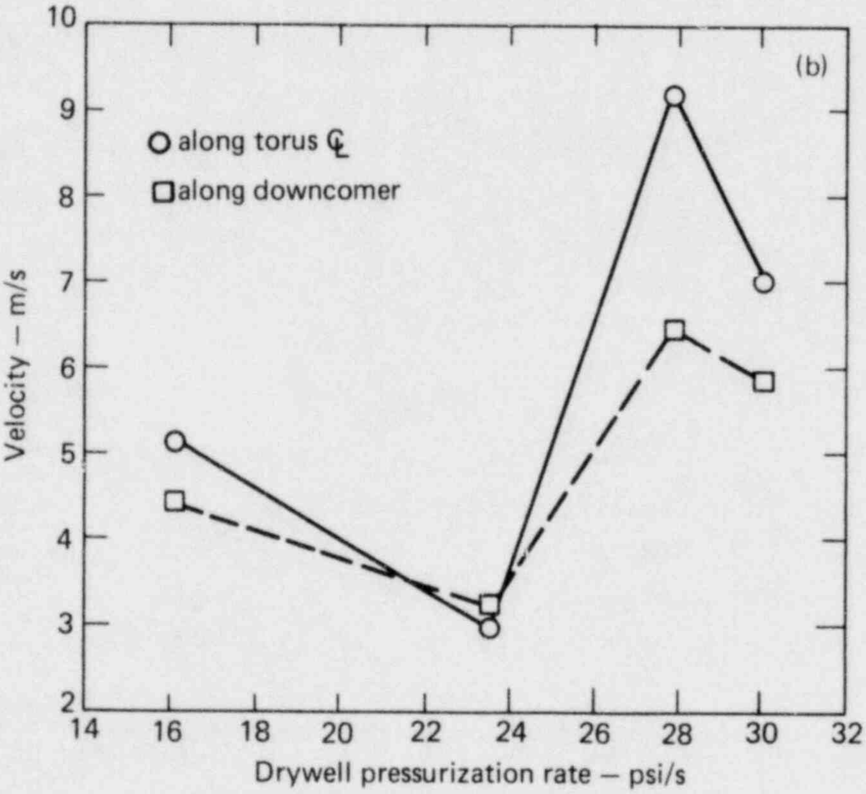

FIG. 2.69b. Estimated pool surface velocity.

2.6 SUMMARY

2.6.1 RESULTS OF THE PSE EXTENDED ANALYSES

The best estimate analysis of the hydrodynamic vertical load function has been completed and standard deviation estimates for the peak forces have been determined. The accumulated HVLF errors are small, as expected from previous study of highly accurate data acquired from some 70 pressure transducers.[4] The standard error on peak down forces ranges from 0.5 percent to 1.4 percent; the corresponding error on peak up forces ranges from 3.2 percent to 5.8 percent.

From the development of the best-estimate HVLF discussed in Part I of this report, it was concluded that the 2-D (7.5°) torus sector provides a useful test facility for prediction of peak down force; 3-D to 2-D down force ratios are nearly unity for all test conditions. This is not the case for prediction of peak upload. In only a limited number of cases, and in none of the nominal condition tests, does that ratio approach unity. These data indicate that while the 2-D facility provides a valid geometrical average cell, it does not represent a fluid dynamical average system. The following review of the overall results of the extended analyses supports this basic conclusion.

2.6.1.1 Force Sensitivity

For "perfect" comparison between 3-D and 2-D data we would expect the ratio of the sensitivities ($\alpha_2^{45^{\circ}}$ and $\alpha_2^{7.5^{\circ}}$) to be in the ratio of 6 to 1. As shown in Table 2-7, the ratios meet this expectation fairly closely for all cases considered except for the case of up force sensitivity with standard downcomers, where the slope ratios are nearly twice the expected value. As compared to the earlier sensitivity analysis based on error-free regression analyses (Table 2-3), the slope ratios now better represent the trends in the data. These ratios again point out that down forces are well defined by both 3-D and 2-D facilities, but that up forces, particularly for nominal downcomer lengths, are nonconservatively defined by 2-D experiments.

2.6.1.2 HVLF Impulse

Integration of the hydrodynamic vertical load function ($\int Fdt$) for determination of the negative impulse (down force region) and positive impulse (up force region) has shown that the 2-D facility produces peak down forces consistent with those observed in the 3-D facility. The event times, particularly the time of transition from down force to up force is highly consistent in data from both facilities. The time of up force is, however, always somewhat longer in the 2-D facility than in the 3-D sector. The effect of this observable was studied by comparison of the total impulse ratio I_{pos}/I_{neg} from each torus sector. It was found that the ratio decreases with increasing pressurization rate in the 3-D facility while increasing in the 2-D facility. Study of the components of the ratios shows that in the 3-D case the positive impulse (numerator) is little affected by a change in $\dot{p}_{dw}$ while the negative impulse (denominator) shows uniform increase with $\dot{p}_{dw}$ increase. The 2-D case exhibits negative impulse behavior similar to the 3-D case; however, the positive impulse exhibits a strong dependence on $\dot{p}_{dw}$ so that as $\dot{p}_{dw}$ increases, the ratio of $(I_{pos}/I_{neg})_{2-D}$ increases.

The ratio of 3-D impulse to 2-D impulse was also studied. The ratios of negative impulse are essentially independent of pressurization rate and are near unity. This suggests that the 2-D geometrical model is capable of predicting behavior of the 3-D system, as has been previously confirmed by study of peak downloads from the HVLFs. The decreasing ratios of positive impulse in this comparison of 3-D to 2-D impulse, by tending further and further from unity with increasing $\dot{p}_{dw}$, provide further evidence that there apparently is a substantial difference in pool swell behavior between 2-D and 3-D systems.

Similar studies were made to quantify the effects of drywell overpressure on impulse. For both 3-D and 2-D sectors, the impulse ratios (I_{pos}/I_{neg} and $I^{45^0}/(6 \times I^{7.5^0})$) are only a weak function of $\Delta\dot{p}_{dw}$. Again, however, the effect of constrained pool swell in the 7.5^0 torus sector is pronounced, causing the positive impulse effects in 2-D to diverge from those observed in the 45^0 torus sector. The negative impulse, however, remains well represented by both the 2-D and 3-D sectors.

2.6.1.3 Structural Aspects of the PSE Experimental Facility

Structural analysis results show that the SAP4 analytical model developed for facility design by Arthur[9] accurately predicts the measured modal content of the structural system. However, the peak load cell forces are underpredicted by the SAP4 model in all cases except for the simulated load cell 5 which overpredicts the maximum load. From these results we conclude that the simplified model used was adequate to demonstrate that the measured modal content of the experimental facility was correct. The high degree of consistency in the results leads us to conclude that overall, the facility is suitably designed for the intended hydrodynamic measurements and that these measurements are not compromised by structurally induced forces.

2.6.1.4 Enthalpy Flux

The total enthalpy results for the 3-D sector indicate near equality between the total energy flow in the left and right vent pipes, although a slight (typically split 51 percent-49 percent) preferential flow through the left vent pipe is consistently indicated. The total energy flow into the 2-D sector is typically in the order of one-sixth that of each 45° sector, which implies comparable energy input per downcomer for both 2-D and 3-D test sections. Not surprisingly, considering the dominant influence of mass flow on enthalpy flux, this result is consistent with the mass flows per downcomer calculated by Pitts.[11]

Calculations of inferred enthalpy flux at locations other than the vent pipes indicate (for the 3-D test sectors) that the distribution of enthalpy flux between the left and right sides of the ring header was very nearly equal, with a slight preferential flow to the left side in almost every case. As with test 1.3.1, this is consistent with the results of the vent pipe enthalpy flux calculations. The distribution of enthalpy flux among the four downcomers in planes 11 and 20 is typically uniform within a few percent.

No definite flow preference was indicated by the results of calculations for the 7.5° sector. For all cases, the distribution of enthalpy flux between downcomers was within 5 percent of being evenly split.

The results of the inferred enthalpy flux calculations therefore indicate the validity of the assumption of uniform distribution among downcomers implicit in the comparison of 2-D and 3-D for both mass flow per dowmcomer and enthalpy flux per downcomer.

2.6.1.5 Pool Swell

Using available photographic data, an estimate vertical pool motion was developed for the extended downcomer test series. Results correlated to drywell pressurization rate ($\dot{p}_{dw}$) indicate that the time to ring header impact is nearly linearly dependent on the pressurization rate. The estimates of the vertical pool swell velocity at the torus center, however, exhibit an anomalous strong minima in an otherwise linear increase with $\dot{p}_{dw}$. Due to the lack of an alternative basis for pool swell velocity evaluation it is conjectured that this effect is due either to unsuspected inaccuracies in the evaluations or possibly to a significant change in pool curvature which invalidates the simple assumption of a uniform parabolic pool surface shape.

ACKNOWLEDGEMENTS

We would like to thank Robert Cudlin and Chris Grimes (U.S. NRC), John Ranlet (Brookhaven National Laboratory), and Don Arthur of this Laboratory for their many helpful discussions and suggestions during the course of this work. In addition, we wish to recognize the important contributions that Lee Richards made during the initial development of the TORUS code. Particular appreciation is directed to Dick Mensing for his innovative and effective development of the multivariate regression analysis used here, and to Mark Blair for his responsive and clever solution to the problem of digitizing mass flows directly from computer graphics files. Finally, we wish to acknowledge Shelly Calvert and Carol Meier for their patience and devotion during manuscript preparation, as well as the editing efforts of Cathy Brown (EG&G) in developing the final report.

REFERENCES

1. W. Lai and E. K. Collins, ed., Final Air Test Results for the 1/5-Scale Mark I Boiling Water Reactor Pressure Suppression Experiment, Lawrence Livermore Laboratory, Livermore, CA, UCRL-52371 (1977).
2. R. G. Altes, J. H. Pitts, R. F. Ingraham, and E. K. Collins, Mark I 1/5-Scale Boiling Water Reactor Pressure Suppression Experiment Facility Report, Lawrence Livermore Laboratory, Livermore, CA, UCRL-52340 (1977).
3. W. Lai and E. W. McCauley, Air Scaling and Modeling Studies for the 1/5-Scale Mark I Boiling Water Reactor Pressure Suppression Experiment, Lawrence Livermore Laboratory, Livermore CA, UCRL-523183 (1977).
4. W. M. Shay, W. G. Brough and T. B. Miller, Instrumenting a Pressure Suppression Experiment for a MKI Boiling Water Reactor--Another Measurements Engineering Challenge, Lawrence Livermore Laboratory, Livermore, CA, UCRL-52314 (July 14, 1977).
5. W. Lai and R. Ingraham, ed., Photographic and Video Techniques Used in the 1/5-Scale Mark I Pressure Suppression Experiment, Lawrence Livermore Laboratory, Livermore, CA, UCRL-52367 (Rev. 1) (1977).
6. W. Lai and E. W. McCauley, Data Processing for the Mark I 1/5-Scale Boiling Water Reactor Pressure Suppression Experiment, Lawrence Livermore Laboratory, Livermore, CA, UCRL-52384 (1977).
7. M. E. Hummell and H. F. Finn, SOCKITTOME Image Processing, Lawrence Livermore Laboratory, Livermore, CA, UCID-17100 (1978).
8. E. W. McCauley and J. K. Meier, A Preliminary Investigation into Effects of Downcomer Spacing, Lawrence Livermore Laboratoary, Livermore, CA, UCID-17676 (1977).
9. D. Arthur, Dynamic Response Analysis of the PSE Torus, Lawrence Livermore Laboratory, Livermore, CA, UCID-17594 (1977).
10. M. R. Poesehn, Modal Analysis of the NRC Pressure Suppression Experimental Facility, Lawrence Livermore Laboratory, Livermore, CA, UCID-17494 (1977).
11. J. H. Pitts, Mass Flowrates through the Vent Lines During Air Tests of the 1/5-Scale Mark I BWR Pressure Suppression System, Lawrence Livermore Laboratory, Livermore, CA, UCID-17601 (1977).

12. R. E. Aley, PPLOT Program, EG&G Technical Note, San Ramon, Ca, SRO TN -12 (1974).

13. O. R. Mowrey, PPLOT User's Guide, Mechanical Engineering Department Engineering Note, Lawrence Livermore Laboratory, Livermore, CA, ENN 79-13 (1979) (Internal Document).

14. M. D. Blair, PSECLUGE, Undocumented Computer Routine for Digitizing PSE UXdd80 Files, Lawrence Livermore Laboratory, Livermore, CA, (1979)

15. G. S. Holman and E. W. McCauley, Computer-aided Digitization of Mass Flow Data from the 1/5-Scale Mark I BWR Pressure Suppression Experiment, Lawrence Livermore Laboratory, Livermore, CA, (in preparation).

16. R. Potter et al., The ORDER System, Lawrence Livermore Laboratory, Livermore, CA, LTSS-202 (1974)

17. G. S. Holman, PSEPLOT: A Controller for Plotting Data from the Mark I Boiling Water Reactor Pressure Suppression Experiment, Lawrence Livermore Laboratory, Livermore, CA, UCRL-52501 (1978).

CB:rls

APPENDIX A

DRYWELL AND TORUS VOLUMES AND POOL AREAS

DRYWELL AND TORUS VOLUMES AND POOL AREAS

This appendix tabulates drywell and torus volumes along with the torus pool areas. These parameters are established by the particular pool level position and downcomer type (normal or extended) used for each test.[1] With the exception of three air transient tests the pool level was maintained at its nominal level below the torus center line (H_{90} = 2.4 in. and $H_{7.5}$ = 2.1 in.). The reader is reminded that due to a manufacturing error, the 7.5^0 torus sector header/downcomer assembly was located 0.3 in. higher than intended so that all pool levels in that sector were 0.3 in. higher than in the 90^0 torus sector.

In test 2.5, the torus water level was raised above the horizontal center line. In tests 2.6 and 2.8, the water level was lowered below the nominal position. Tables A-1 and A-2 provide both a summary of all tests of pool level and downcomer submergence information for the 90^0 sector and 7.5^0 sector, respectively. Included is the vertical distance (D) from the torus sector horizontal center line to the downcomer exit. Figure A-1 provides a geometrical summary of downcomer placement in the two torus sectors.

From the data of Tables A-1 and A-2, the torus pool volume (VP) and ullage volume (VU) were calculated along with other such relevant parameters as pool volume per downcomer (VP/VU), pool area (AP), and pool area per downcomer (AP/DC). These data are listed for all tests in Table A-3 for the 90^0 sector and in Table A-4 for the 7.5^0 sector; corresponding drywell volumes are also indicated.

TABLE A-1. Pool level and downcomer submergence (90° torus sector).

Test no. DC-type	H-in.[a]	D-in.[b]	Subm.-in.	
1.1	2.4	12.0	9.6	std
1.3	2.4	12.0	9.6	std
1.3.1	2.4	12.0	9.6	std
1.4	2.4	12.0	9.6	std
1.5	2.4	12.0	9.6	std
1.6	2.4	12.0	9.6	std
2.1	2.4	12.0	9.6	std
2.2	2.4	12.0	9.6	std
2.3	2.4	12.0	9.6	std
2.4	2.4	12.0	9.6	std
2.5	-1.4	12.0	13.4	std
2.6	6.2	12.0	5.8	std
2.7	2.4	14.4	12.0	ext
2.8	4.8	14.4	9.6	ext
2.9	2.4	14.4	12.0	ext
2.10	2.4	14.4	12.0	ext
2.11	2.4	14.4	12.0	ext
3.1	2.4	12.0	9.6	std
3.2	2.4	12.0	9.6	std
3.3A	2.4	12.0	9.6	std
3.3B	2.4	12.0	9.6	std
3.4A	2.4	12.0	9.6	std
3.4B	2.4	12.0	9.6	std
3.5	2.4	12.0	9.6	std

[a] H = Vertical distance, torus center to pool surface; below center is positive.

[b] D = Vertical distance, torus center to downcomer exit.

TABLE A-2. Pool level and downcomer submergence (7.5^{o} torus sector).

Test no. DC-type	H-in.[a]	D-in.[b]	Subm.-in.	
1.1	2.1	11.7	9.6	std
1.3	2.1	11.7	9.6	std
1.3.1	2.1	11.7	9.6	std
1.4	2.1	11.7	9.6	std
1.5	2.1	11.7	9.6	std
1.6	2.1	11.7	9.6	std
2.1	2.1	11.7	9.6	std
2.2	2.1	11.7	9.6	std
2.3	2.1	11.7	9.6	std
2.4	2.1	11.7	9.6	std
2.5	-1.7	11.7	13.4	std
2.6	5.9	11.7	5.8	std
2.7	2.1	14.1	12.0	ext
2.8	4.2	14.1	9.9	ext
2.9	2.1	14.1	12.0	ext
2.10	2.1	14.1	12.0	ext
2.11	2.1	14.1	12.0	ext
3.1	2.1	11.7	9.6	std
3.2	2.1	11.7	9.6	std
3.3A	2.1	11.7	9.6	std
3.3B	2.1	11.7	9.6	std
3.4A	2.1	11.7	9.6	std
3.4B	2.1	11.7	9.6	std
3.5	2.1	11.7	9.6	std

[a] H = Vertical distance, torus center to pool surface; below center is positive.

[b] D = Vertical distance, torus center to downcomer exit.

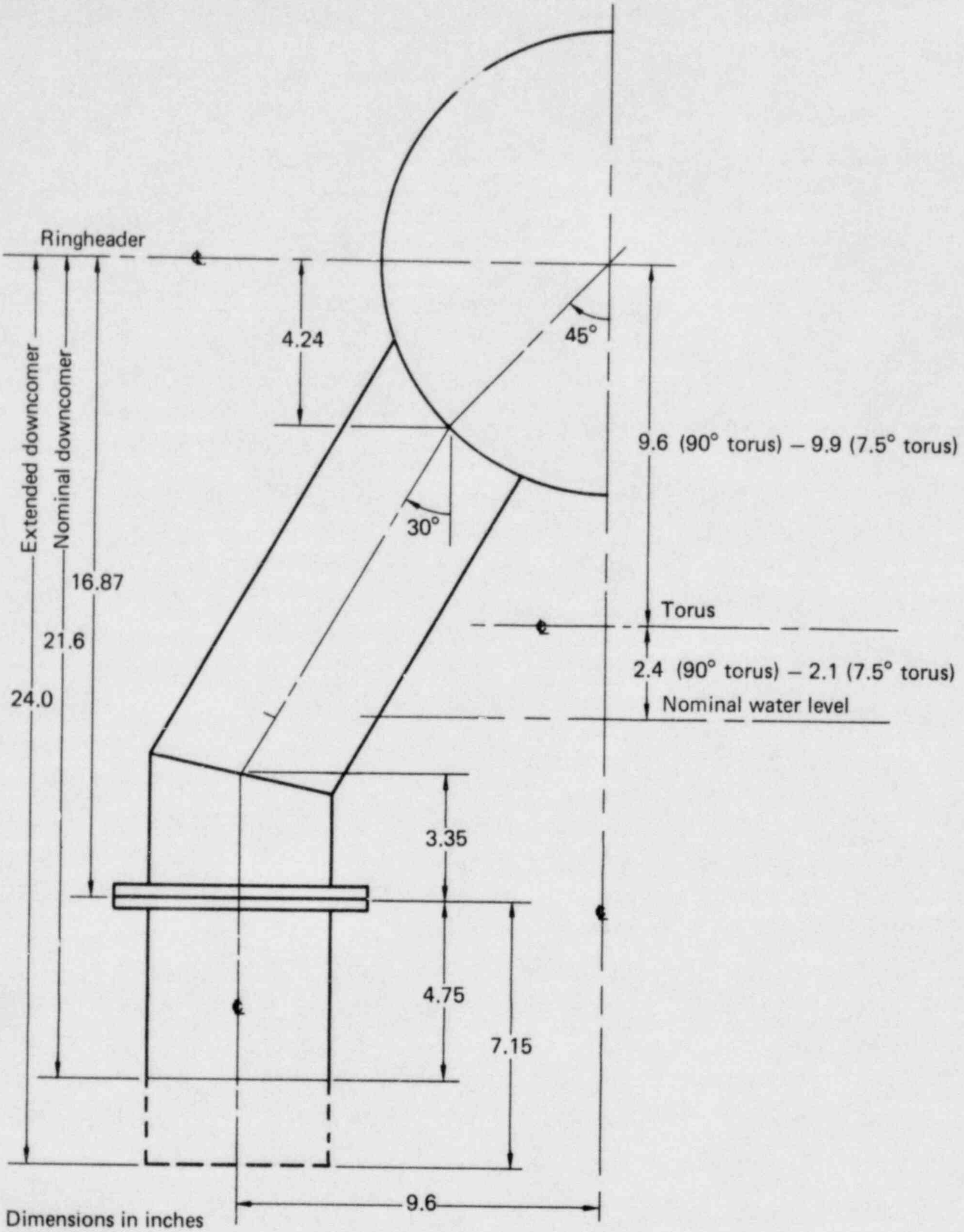

FIG. A-1. As-built ring header/downcomer geometry (1/5-scale MK I BWR-Peach Bottom).

TABLE A-3. Drywell and torus volumes and pool areas (90° torus sector).

	Volume-ft^3				Area-ft^2	
Test no.	Pool-VP	VP/DC	Ullage-VU	VP/VU	Pool-AP	AP/DC
1.1	2.459E+02	1.024E+01	2.898E+02	8.483E-01	1.098E+02	4.574E+00
1.3	2.459E+02	1.024E+01	2.898E+02	8.483E-01	1.098E+02	4.574E+00
1.3.1[a]	2.459E+02	1.024E+01	2.898E+02	8.483E-01	1.098E+02	4.574E+00
1.4[a]	2.459E+02	1.024E+01	2.898E+02	8.483E-01	1.098E+02	4.574E+00
1.5[a]	2.459E+02	1.024E+01	2.898E+02	8.483E-01	1.098E+02	4.574E+00
1.6[a]	2.459E+02	1.024E+01	2.898E+02	8.483E-01	1.098E+02	4.574E+00
2.1[a]	2.459E+02	1.024E+01	2.898E+02	8.483E-01	1.098E+02	4.574E+00
2.2[a]	2.459E+02	1.024E+01	2.898E+02	8.483E-01	1.098E+02	4.574E+00
2.3[a]	2.459E+02	1.024E+01	2.898E+02	8.483E-01	1.098E+02	4.574E+00
2.4[a]	2.459E+02	1.024E+01	2.898E+02	8.483E-01	1.098E+02	4.574E+00
2.5[a]	2.807E+02	1.169E+01	2.550E+02	1.101E+00	1.099E+02	4.580E+00
2.6[a]	2.113E+02	8.803E+00	3.244E+02	6.512E-01	1.085E+02	4.519E+00
2.7	2.459E+02	1.024E+01	2.898E+02	8.483E-01	1.098E+02	4.574E+00
2.8	2.240E+02	9.332E+00	3.117E+02	7.185E-01	1.091E+02	4.545E+00
2.9	2.459E+02	1.024E+01	2.898E+02	8.483E-01	1.098E+02	4.574E+00
2.10	2.459E+02	1.024E+01	2.898E+02	8.483E-01	1.098E+02	4.574E+00
2.11	2.459E+02	1.024E+01	2.898E+02	8.483E-01	1.098E+02	4.574E+00
3.1[a]	2.459E+02	1.024E+01	2.898E+02	8.483E-01	1.098E+02	4.574E+00
3.2	2.459E+02	1.024E+01	2.898E+02	8.483E-01	1.098E+02	4.574E+00
3.3A	2.459E+02	1.024E+01	2.898E+02	8.483E-01	1.098E+02	4.574E+00
3.3B	2.459E+02	1.024E+01	2.898E+02	8.483E-01	1.098E+02	4.574E+00
3.4A	2.459E+02	1.024E+01	2.898E+02	8.483E-01	1.098E+02	4.574E+00
3.4B	2.459E+02	1.024E+01	2.898E+02	8.483E-01	1.098E+02	4.574E+00
3.5	2.459E+02	1.024E+01	2.898E+02	8.483E-01	1.098E+02	4.574E+00

[a] Drywell volume = 296 ft^3, all other tests had a drywell volume = 348.6 ft^3.

TABLE A-4. Drywell and torus volumes and pool areas (7.5^{0} torus sector).

	Volume-ft^3				Area-ft^2	
Test no.	Pool-VP	VP/DC	Ullage-VU	VP-VU	Pool-AP	AP/DC
1.1	2.062E+01	1.031E+01	2.381E+01	8.660E-01	9.110E+00	4.555E+00
1.3	2.062E+01	1.031E+01	2.381E+01	8.660E-01	9.110E+00	4.555E+00
1.3.1[a]	2.062E+01	1.031E+01	2.381E+01	8.660E-01	9.110E+00	4.555E+00
1.4[a]	2.062E+01	1.031E+01	2.381E+01	8.660E-01	9.110E+00	4.555E+00
1.5[a]	2.062E+01	1.031E+01	2.381E+01	8.660E-01	9.110E+00	4.555E+00
1.6[a]	2.062E+01	1.031E+01	2.381E+01	8.660E-01	9.110E+00	4.555E+00
2.1[a]	2.062E+01	1.031E+01	2.381E+01	8.660E-01	9.110E+00	4.555E+00
2.2[a]	2.062E+01	1.031E+01	2.381E+01	8.660E-01	9.110E+00	4.555E+00
2.3[a]	2.062E+01	1.031E+01	2.381E+01	8.660E-01	9.110E+00	4.555E+00
2.4[a]	2.062E+01	1.031E+01	2.381E+01	8.660E-01	9.110E+00	4.555E+00
2.5[a]	2.351E+01	1.175E+01	2.092E+01	1.124E+00	9.115E+00	4.557E+00
2.6[a]	1.775E+01	8.874E+00	2.668E+01	6.652E-01	9.009E+00	4.504E+00
2.7	2.062E+01	1.031E+01	2.381E+01	8.660E-01	9.110E+00	4.555E+00
2.8	1.903E+01	9.514E+00	2.540E+01	7.491E-01	9.066E+00	4.533E+00
2.9	2.062E+01	1.031E+01	2.381E+01	8.660E-01	9.110E+00	4.555E+00
2.10	2.062E+01	1.031E+01	2.381E+01	8.660E-01	9.110E+00	4.555E+00
2.11	2.062E+01	1.031E+01	2.381E+01	8.660E-01	9.110E+00	4.555E+00
3.1[a]	2.062E+01	1.031E+01	2.381E+01	8.660E-01	9.110E+00	4.555E+00
3.2	2.062E+01	1.031E+01	2.381E+01	8.660E-01	9.110E+00	4.555E+00
3.3A	2.062E+01	1.031E+01	2.381E+01	8.660E-01	9.110E+00	4.555E+00
3.3B	2.062E+01	1.031E+01	2.381E+01	8.660E-01	9.110E+00	4.555E+00
3.4A	2.062E+01	1.031E+01	2.381E+01	8.660E-01	9.110E+00	4.555E+00
3.4B	2.062E+01	1.031E+01	2.381E+01	8.660E-01	9.110E+00	4.555E+00
3.5	2.062E+01	1.031E+01	2.381E+01	8.660E-01	9.110E+00	4.555E+00

[a] Drywell volume = 296 ft^3, all other tests had a drywell volume = 348.6 ft^3.

APPENDIX B

PRESSURE TRANSDUCER LOCATION DIMENSIONS

(Δx and Δz)

B.1 DXDZ2.7 (nominal pool level)
B.2 DXDZ2.5 (pool level raised)
B.3 DXDZ2.6 (pool level lowered)
B.4 DXDZ2.8 (pool level lowered)

B.1 DXDZ2.7 (nominal pool level)

```
NRC TEST   2.7      H90 =  2.40      H7 5 =  2.10
PLANE AND AXIAL LOCATIONS
          THETA            XT            DELZT
PLANE =    1
TOTAL ULLAGE WIDTH   =      7.4245E+01
TOTAL POOL WIDTH   =      7.4245E+01
             45.0000   1.0818E+01    5.6250E+00
             12.0000   2.9388E+01    5.6250E+00
            348.0000   4.4857E+01    5.6250E+00
            315.0000   6.3427E+01    5.6250E+00
            270.0000   7.4245E+01  . 5.6250E+00
            128.0000   7.8085E+00    5.6250E+00
            140.0000   1.3211E+01    5.6250E+00
            155.0000   2.1401E+01    5.6250E+00
            160.0000   2.4399E+01    5.6250E+00
            165.0000   2.7494E+01    5.6250E+00
            180.0000   3.7122E+01    5.6250E+00
            195.0000   4.6751E+01    5.6250E+00
            200.0000   4.9846E+01    5.6250E+00
            205.0000   5.2844E+01    5.6250E+00
            220.0000   6.1034E+01    5.6250E+00
            235.0000   6.7595E+01    5.6250E+00
            269.0000   7.4245E+01    5.6250E+00
              0.       0.            0.
PLANE =    3
TOTAL ULLAGE WIDTH   =      7.4413E+01
TOTAL POOL WIDTH   =      7.4618E+01
             45.0000   1.0818E+01    1.4000E+01
             12.0000   2.9388E+01    1.4000E+01
            348.0000   4.4857E+01    1.4000E+01
            315.0000   6.3594E+01    1.2750E+01
            270.0000   7.4413E+01    1.1500E+01
            128.0000   7.8085E+00    1.4000E+01
            140.0000   1.3211E+01    1.4000E+01
            155.0000   2.1401E+01    1.4000E+01
            160.0000   2.4399E+01    1.4000E+01
            165.0000   2.7494E+01    1.4000E+01
            180.0000   3.7122E+01    1.4000E+01
            195.0000   4.6751E+01    1.4000E+01
            200.0000   4.9846E+01    1.4000E+01
            205.0000   5.2844E+01    1.4000E+01
            220.0000   6.1407E+01    1.2750E+01
            235.0000   6.7968E+01    1.1500E+01
            269.0000   7.4618E+01    1.1500E+01
              0.       0.            0.
PLANE =    4
TOTAL ULLAGE WIDTH   =      7.5700E+01
TOTAL POOL WIDTH   =      7.5700E+01
             45.0000   1.1030E+01    1.7631E+01
             12.0000   2.9964E+01    1.4708E+01
            348.0000   4.5736E+01    1.1323E+01
            315.0000   6.4669E+01    9.1875E+00
            270.0000   7.5700E+01    7.5147E+00
            128.0000   7.9615E+00    1.7930E+01
            140.0000   1.3470E+01    1.6616E+01
            155.0000   2.1820E+01    1.5265E+01
            160.0000   2.4877E+01    1.4152E+01
            165.0000   2.8033E+01    1.3546E+01
            180.0000   3.7850E+01    1.2280E+01
            195.0000   4.7666E+01    1.0365E+01
```

```
              200.0000   5.0822E+01   9.0998E+00
              205.0000   5.3879E+01   8.4938E+00
              220.0000   6.2230E+01   8.6311E+00
              235.0000   6.8919E+01   8.4140E+00
              269.0000   7.5700E+01   7.1001E+00
                0.       0.           0.
PLANE =   4A
TOTAL ULLAGE WIDTH   =      7.4245E+01
TOTAL POOL WIDTH   =     7.4245E+01
               45.0000   1.0818E+01   1.9589E+01
               12.0000   2.9388E+01   1.6666E+01
              348.0000   4.4857E+01   1.3281E+01
              315.0000   6.3427E+01   9.8958E+00
              270.0000   7.4245E+01   6.9729E+00
              128.0000   7.8085E+00   1.9889E+01
              140.0000   1.3211E+01   1.8575E+01
              155.0000   2.1401E+01   1.7223E+01
              160.0000   2.4399E+01   1.6110E+01
              165.0000   2.7494E+01   1.5504E+01
              180.0000   3.7122E+01   1.4239E+01
              195.0000   4.6751E+01   1.2324E+01
              200.0000   4.9846E+01   1.1058E+01
              205.0000   5.2844E+01   1.0452E+01
              220.0000   6.1034E+01   9.3394E+00
              235.0000   6.7595E+01   7.8723E+00
              269.0000   7.4245E+01   6.5584E+00
                0.       0.           0.
PLANE =    5
TOTAL ULLAGE WIDTH   =      7.4245E+01
TOTAL POOL WIDTH   =     7.4245E+01
               45.0000   1.0818E+01   9.0000E+00
               12.0000   2.9388E+01   9.0000E+00
              348.0000   4.4857E+01   9.0000E+00
              315.0000   6.3427E+01   9.0000E+00
              270.0000   7.4245E+01   9.0000E+00
              128.0000   7.8085E+00   9.0000E+00
              140.0000   1.3211E+01   9.0000E+00
              155.0000   2.1401E+01   9.0000E+00
              160.0000   2.4399E+01   9.0000E+00
              165.0000   2.7494E+01   9.0000E+00
              180.0000   3.7122E+01   9.0000E+00
              195.0000   4.6751E+01   9.0000E+00
              200.0000   4.9846E+01   9.0000E+00
              205.0000   5.2844E+01   9.0000E+00
              220.0000   6.1034E+01   9.0000E+00
              235.0000   6.7595E+01   9.0000E+00
              269.0000   7.4245E+01   9.0000E+00
                0.       0.           0.
PLANE =    6
TOTAL ULLAGE WIDTH   =      7.4245E+01
TOTAL POOL WIDTH   =     7.4245E+01
               45.0000   1.0818E+01   9.0000E+00
               12.0000   2.9388E+01   9.0000E+00
              348.0000   4.4857E+01   9.0000E+00
              315.0000   6.3427E+01   9.0000E+00
              270.0000   7.4245E+01   9.0000E+00
              128.0000   7.8085E+00   9.0000E+00
              140.0000   1.3211E+01   9.0000E+00
              155.0000   2.1401E+01   9.0000E+00
              160.0000   2.4399E+01   9.0000E+00
```

```
            165.0000   2.7494E+01   9.0000E+00
            180.0000   3.7122E+01   9.0000E+00
            195.0000   4.6751E+01   9.0000E+00
            200.0000   4.9846E+01   9.0000E+00
            205.0000   5.2844E+01   9.0000E+00
            220.0000   6.1034E+01   9.0000E+00
            235.0000   6.7595E+01   9.0000E+00
            269.0000   7.4245E+01   9.0000E+00
              0.       0.           0.
PLANE =   8
TOTAL ULLAGE WIDTH   =     7.5700E+01
TOTAL POOL WIDTH   =     7.5700E+01
             45.0000   1.1030E+01   1.9589E+01
             12.0000   2.9964E+01   1.6666E+01
            348.0000   4.5736E+01   1.3281E+01
            315.0000   6.4669E+01   9.8958E+00
            270.0000   7.5700E+01   6.9729E+00
            128.0000   7.9615E+00   1.9889E+01
            140.0000   1.3470E+01   1.8575E+01
            155.0000   2.1820E+01   1.7223E+01
            160.0000   2.4877E+01   1.6110E+01
            165.0000   2.8033E+01   1.5504E+01
            180.0000   3.7850E+01   1.4239E+01
            195.0000   4.7666E+01   1.2324E+01
            200.0000   5.0822E+01   1.1058E+01
            205.0000   5.3879E+01   1.0452E+01
            220.0000   6.2230E+01   9.3394E+00
            235.0000   6.8919E+01   7.8723E+00
            269.0000   7.5700E+01   6.5584E+00
              0.       0.           0.
PLANE =   9
TOTAL ULLAGE WIDTH   =     7.4413E+01
TOTAL POOL WIDTH   =     7.4618E+01
             45.0000   1.0818E+01   1.7631E+01
             12.0000   2.9388E+01   1.4708E+01
            348.0000   4.4857E+01   1.1323E+01
            315.0000   6.3594E+01   9.1875E+00
            270.0000   7.4413E+01   7.5147E+00
            128.0000   7.8085E+00   1.7930E+01
            140.0000   1.3211E+01   1.6616E+01
            155.0000   2.1401E+01   1.5265E+01
            160.0000   2.4399E+01   1.4152E+01
            165.0000   2.7494E+01   1.3546E+01
            180.0000   3.7122E+01   1.2280E+01
            195.0000   4.6751E+01   1.0365E+01
            200.0000   4.9846E+01   9.0998E+00
            205.0000   5.2844E+01   8.4938E+00
            220.0000   6.1407E+01   8.6311E+00
            235.0000   6.7968E+01   8.4140E+00
            269.0000   7.4618E+01   7.1001E+00
              0.       0.           0.
PLANE =  11
TOTAL ULLAGE WIDTH   =     7.4245E+01
TOTAL POOL WIDTH   =     7.4245E+01
             45.0000   1.0818E+01   1.4000E+01
             12.0000   2.9388E+01   1.4000E+01
            348.0000   4.4857E+01   1.4000E+01
            315.0000   6.3427E+01   1.2750E+01
            270.0000   7.4245E+01   1.1500E+01
            128.0000   7.8085E+00   1.4000E+01
```

```
           140.0000   1.3211E+01   1.4000E+01
           155.0000   2.1401E+01   1.4000E+01
           160.0000   2.4399E+01   1.4000E+01
           165.0000   2.7494E+01   1.4000E+01
           180.0000   3.7122E+01   1.4000E+01
           195.0000   4.6751E+01   1.4000E+01
           200.0000   4.9846E+01   1.4000E+01
           205.0000   5.2844E+01   1.4000E+01
           220.0000   6.1034E+01   1.2750E+01
           235.0000   6.7595E+01   1.1500E+01
           269.0000   7.4245E+01   1.1500E+01
             0.        0.           0.
PLANE =  2D
TOTAL ULLAGE WIDTH  =     7.4281E+01
TOTAL POOL WIDTH  =    7.4281E+01
            45.0000   1.0836E+01   1.7660E+01
            12.0000   2.9406E+01   1.7660E+01
           348.0000   4.4875E+01   1.7660E+01
           315.0000   6.3445E+01   1.7660E+01
           270.0000   7.4281E+01   1.7660E+01
           128.0000   7.8267E+00   1.7660E+01
           140.0000   1.3229E+01   1.7660E+01
           155.0000   2.1419E+01   1.7660E+01
           160.0000   2.4418E+01   1.7660E+01
           165.0000   2.7513E+01   1.7660E+01
           180.0000   3.7141E+01   1.7660E+01
           195.0000   4.6769E+01   1.7660E+01
           200.0000   4.9864E+01   1.7660E+01
           205.0000   5.2862E+01   1.7660E+01
           220.0000   6.1052E+01   1.7660E+01
           235.0000   6.7613E+01   1.7660E+01
           269.0000   7.4281E+01   1.7660E+01
            -7.5000
        UNCLASSIFIED                                    FILM ONLY              10:42   11/21/79R
```

B.2 DXDZ2.5 (pool level raised)

```
NRC TEST   2.5      H90 =  1.40      H7.5 =  1.70
PLANE AND AXIAL LOCATIONS
          THETA           XT            DELZT
PLANE =    1
TOTAL ULLAGE WIDTH   =     7.4347E+01
TOTAL POOL WIDTH   =     7.4347E+01
            45.0000   1.0869E+01   5.6250E+00
            12.0000   2.9439E+01   5.6250E+00
           348.0000   4.4908E+01   5.6250E+00
           315.0000   6.3478E+01   5.6250E+00
           270.0000   7.4347E+01   5.6250E+00
           128.0000   7.8596E+00   5.6250E+00
           140.0000   1.3262E+01   5.6250E+00
           155.0000   2.1452E+01   5.6250E+00
           160.0000   2.4450E+01   5.6250E+00
           165.0000   2.7546E+01   5.6250E+00
           180.0000   3.7174E+01   5.6250E+00
           195.0000   4.6802E+01   5.6250E+00
           200.0000   4.9897E+01   5.6250E+00
           205.0000   5.2895E+01   5.6250E+00
           220.0000   6.1085E+01   5.6250E+00
           235.0000   5.7646E+01   5.6250E+00
           269.0000   7.4347E+01   5.6250E+00
             0.       0.            0.
PLANE =    3
TOTAL ULLAGE WIDTH   =     7.4515E+01
TOTAL POOL WIDTH   =     7.4720E+01
            45.0000   1.0869E+01   1.4000E+01
            12.0000   2.9439E+01   1.4000E+01
           348.0000   4.4908E+01   1.4000E+01
           315.0000   6.3646E+01   1.2750E+01
           270.0000   7.4515E+01   1.1500E+01
           128.0000   7.8596E+00   1.4000E+01
           140.0000   1.3262E+01   1.4000E+01
           155.0000   2.1452E+01   1.4000E+01
           160.0000   2.4450E+01   1.4000E+01
           165.0000   2.7546E+01   1.4000E+01
           180.0000   3.7174E+01   1.4000E+01
           195.0000   4.6802E+01   1.4000E+01
           200.0000   4.9897E+01   1.4000E+01
           205.0000   5.2895E+01   1.4000E+01
           220.0000   6.1458E+01   1.2750E+01
           235.0000   6.8019E+01   1.1500E+01
           269.0000   7.4720E+01   1.1500E+01
             0.       0.            0.
PLANE =    4
TOTAL ULLAGE WIDTH   =     7.5804E+01
TOTAL POOL WIDTH   =     7.5804E+01
            45.0000   1.1082E+01   1.7636E+01
            12.0000   3.0016E+01   1.4708E+01
           348.0000   4.5788E+01   1.1323E+01
           315.0000   6.4722E+01   9.1926E+00
           270.0000   7.5804E+01   7.5197E+00
           128.0000   8.0136E+00   1.7935E+01
           140.0000   1.3522E+01   1.6616E+01
           155.0000   2.1873E+01   1.5265E+01
           160.0000   2.4930E+01   1.4152E+01
           165.0000   2.8085E+01   1.3546E+01
           180.0000   3.7902E+01   1.2280E+01
           195.0000   4.7719E+01   1.0365E+01
```

```
              200.0000   5.0874E+01   9.0998E+00
              205.0000   5.3931E+01   8.4938E+00
              220.0000   6.2282E+01   8.6362E+00
              235.0000   6.8971E+01   8.4242E+00
              269.0000   7.5804E+01   7.1052E+00
                0.       0.           0.
PLANE =  4A
TOTAL ULLAGE WIDTH  =    7.4347E+01
TOTAL POOL WIDTH  =    7.4347E+01
               45.0000   1.0869E+01   1.9594E+01
               12.0000   2.9439E+01   1.6666E+01
              348.0000   4.4908E+01   1.3281E+01
              315.0000   6.3478E+01   9.8958E+00
              270.0000   7.4347E+01   6.9678E+00
              128.0000   7.8596E+00   1.9894E
              140.0000    .3262E+01   1.8575   1
              155.0000   2.1452E+01   1.7223E+01
              160.0000   2.4450E+01   1.6110E+01
              165.0000   2.7546E+01   1.5504E+01
              180.0000   3.7174E+01   1.4239E+01
              195.0000   4.6802E+01   1.2324E+01
              200.0000   4.9897E+01   1.1058E+01
              205.0000   5.2895E+01   1.0452E+01
              220.0000   6.1085E+01   9.3394E+00
              235.0000   6.7646E+01   7.8723E+00
              269.0000   7.4347E+01   6.5533E+00
                0.       0.           0.
PLANE =   5
TOTAL ULLAGE WIDTH  =    7.4347E+01
TOTAL POOL WIDTH  =    7.4347E+01
               45.0000   1.0869E+01   9.0000E+00
               12.0000   2.9439E+01   9.0000E+00
              348.0000   4.4908E+01   9.0000E+00
              315.0000   6.3478E+01   9.0000E+00
              270.0000   7.4347E+01   9.0000E+00
              128.0000   7.8596E+00   9.0000E+00
              140.0000   1.3262E+01   9.0000E+00
              155.0000   2.1452E+01   9.0000E+00
              160.0000   2.4450E+01   9.0000E+00
              165.0000   2.7546E+01   9.0000E+00
              180.0000   3.7174E+01   9.0000E+00
              195.0000   4.6802E+01   9.0000E+00
              200.0000   4.9897E+01   9.0000E+00
              205.0000   5.2895E+01   9.0000E+00
              220.0000   6.1085E+01   9.0000E+00
              235.0000   6.7646E+01   9.0000E+00
              269.0000   7.4347E+01   9.0000E+00
                0.       0.           0.
PLANE =   6
TOTAL ULLAGE WIDTH  =    7.4347E+01
TOTAL POOL WIDTH  =    7.4347E+01
               45.0000   1.0869E+01   9.0000E+00
               12.0000   2.9439E+01   9.0000E+00
              348.0000   4.4908E+01   9.0000E+00
              315.0000   6.3478E+01   9.0000E+00
              270.0000   7.4347E+01   9.0000E+00
              128.0000   7.8596E+00   9.0000E+00
              140.0000   1.3262E+01   9.0000E+00
              155.0000   2.1452E+01   9.0000E+00
              160.0000   2.4450E+01   9.0000E+00
```

```
               165.0000   2.7546E+01   9.0000E+00
               180.0000   3.7174E+01   9.0000E+00
               195.0000   4.6802E+01   9.0000E+00
               200.0000   4.9897E+01   9.0000E+00
               205.0000   5.2895E+01   9.0000E+00
               220.0000   6.1085E+01   9.0000E+00
               235.0000   6.7646E+01   9.0000E+00
               269.0000   7.4347E+01   9.0000E+00
                  0.      0.           0.
PLANE =    8
TOTAL ULLAGE WIDTH   =     7.5804E+01
TOTAL POOL WIDTH   =     7.5804E+01
                45.0000   1.1082E+01   1.9594E+01
                12.0000   3.0016E+01   1.6666E+01
               348.0000   4.5788E+01   1.3281E+01
               315.0000   6.4722E+01   9.8958E+00
               270.0000   7.5804E+01   6.9678E+00
               128.0000   8.0136E+00   1.9894E+01
               140.0000   1.3522E+01   1.8575E+01
               155.0000   2.1873E+01   1.7223E+01
               160.0000   2.4930E+01   1.6110E+01
               165.0000   2.8085E+01   1.5504E+01
               180.0000   3.7902E+01   1.4239E+01
               195.0000   4.7719E+01   1.2324E+01
               200.0000   5.0874E+01   1.1058E+01
               205.0000   5.3931E+01   1.0452E+01
               220.0000   6.2282E+01   9.3394E+00
               235.0000   6.8971E+01   7.8723E+00
               269.0000   7.5804E+01   6.5533E+00
                  0.      0.           0.
PLANE =    9
TOTAL ULLAGE WIDTH   =     7.4515E+01
TOTAL POOL WIDTH   =     7.4720E+01
                45.0000   1.0869E+01   1.7636E+01
                12.0000   2.9439E+01   1.4708E+01
               348.0000   4.4908E+01   1.1323E+01
               315.0000   6.3646E+01   9.1926E+00
               270.0000   7.4515E+01   7.5197E+00
               128.0000   7.8596E+00   1.7935E+01
               140.0000   1.3262E+01   1.6616E+01
               155.0000   2.1452E+01   1.5265E+01
               160.0000   2.4450E+01   1.4152E+01
               165.0000   2.7546E+01   1.3546E+01
               180.0000   3.7174E+01   1.2280E+01
               195.0000   4.6802E+01   1.0365E+01
               200.0000   4.9897E+01   9.0998E+00
               205.0000   5.2895E+01   8.4938E+00
               220.0000   6.1458E+01   8.6362E+00
               235.0000   6.8019E+01   8.4242E+00
               269.0000   7.4720E+01   7.1052E+00
                  0.      0.           0.
PLANE =  11
TOTAL ULLAGE WIDTH   =     7.4347E+01
TOTAL POOL WIDTH   =     7.4347E+01
                45.0000   1.0869E+01   1.4000E+01
                12.0000   2.9439E+01   1.4000E+01
               348.0000   4.4908E+01   1.4000E+01
               315.0000   6.3478E+01   1.2750E+01
               270.0000   7.4347E+01   1.1500E+01
               128.0000   7.8596E+00   1.4000E+01
```

```
          140.0000   1.3262E+01   1.4000E+01
          155.0000   2.1452E+01   1.4000E+01
          160.0000   2.4450E+01   1.4000E+01
          165.0000   2.7546E+01   1.4000E+01
          180.0000   3.7174E+01   1.4000E+01
          195.0000   4.6802E+01   1.4000E+01
          200.0000   4.9897E+01   1.4000E+01
          205.0000   5.2895E+01   1.4000E+01
          220.0000   6.1085E+01   1.2750E+01
          235.0000   6.7646E+01   1.1500E+01
          269.0000   7.4347E+01   1.1500E+01
            0.         0.           0.
PLANE =  2D
TOTAL ULLAGE WIDTH  =     7.4322E+01
TOTAL POOL WIDTH  =     7.4322E+01
           45.0000   1.0857E+01   1.7660E+01
           12.0000   2.9427E+01   1.7660E+01
          348.0000   4.4895E+01   1.7660E+01
          315.0000   6.3466E+01   1.7660E+01
          270.0000   7.4322E+01   1.7660E+01
          128.0000   7.8471E+00   1.7660E+01
          140.0000   1.3249E+01   1.7660E+01
          155.0000   2.1440E+01   1.7660E+01
          160.0000   2.4438E+01   1.7660E+01
          165.0000   2.7533E+01   1.7660E+01
          180.0000   3.7161E+01   1.7660E+01
          195.0000   4.6789E+01   1.7660E+01
          200.0000   4.9884E+01   1.7660E+01
          205.0000   5.2883E+01   1.7660E+01
          220.0000   6.1073E+01   1.7660E+01
          235.0000   6.7634E+01   1.7660E+01
          269.0000   7.4322E+01   1.7660E+01
           -7.5000
        UNCLASSIFIED                              FILM ONLY          10:43   11/21/79R
```

B.3 DXDZ2.6 (pool level lowered)

```
NRC TEST   2.6      H90 =  6.20       H7.5 =  5.90
PLANE AND AXIAL LOCATIONS
         THETA           XT            DELZT
PLANE =   1
TOTAL ULLAGE WIDTH   =      7.3359E+01
TOTAL POOL WIDTH   =     7.3359E+01
           45.0000    1.0375E+01    5.6250E+00
           12.0000    2.8945E+01    5.6250E+00
          348.0000    4.4414E+01    5.6250E+00
          315.0000    6.2984E+01    5.6250E+00
          270.0000    7.3359E+01    5.6250E+00
          128.0000    7.3657E+00    5.6250E+00
          140.0000    1.2768E+01    5.6250E+00
          155.0000    2.0958E+01    5.6250E+00
          160.0000    2.3957E+01    5.6250E+00
          165.0000    2.7052E+01    5.6250E+00
          180.0000    3.6680E+01    5.6250E+00
          195.0000    4.6308E+01    5.6250E+00
          200.0000    4.9403E+01    5.6250E+00
          205.0000    5.2401E+01    5.6250E+00
          220.0000    6.0591E+01    5.6250E+00
          235.0000    6.7152E+01    5.6250E+00
          269.0000    7.3359E+01    5.6250E+00
            0.        0.            0.
PLANE =   3
TOTAL ULLAGE WIDTH   =      7.3527E+01
TOTAL POOL WIDTH   =     7.3732E+01
           45.0000    1.0375E+01    1.4000E+01
           12.0000    2.8945E+01    1.4000E+01
          348.0000    4.4414E+01    1.4000E+01
          315.0000    6.3152E+01    1.2750E+01
          270.0000    7.3527E+01    1.1500E+01
          128.0000    7.3657E+00    1.4000E+01
          140.0000    1.2768E+01    1.4000E+01
          155.0000    2.0958E+01    1.4000E+01
          160.0000    2.3957E+01    1.4000E+01
          165.0000    2.7052E+01    1.4000E+01
          180.0000    3.6680E+01    1.4000E+01
          195.0000    4.6308E+01    1.4000E+01
          200.0000    4.9403E+01    1.4000E+01
          205.0000    5.2401E+01    1.4000E+01
          220.0000    6.0964E+01    1.2750E+01
          235.0000    6.7525E+01    1.1500E+01
          269.0000    7.3732E+01    1.1500E+01
            0.        0.            0.
PLANE =   4
TOTAL ULLAGE WIDTH   =      7.4797E+01
TOTAL POOL WIDTH   =     7.4797E+01
           45.0000    1.0579E+01    1.7587E+01
           12.0000    2.9512E+01    1.4708E+01
          348.0000    4.5284E+01    1.1323E+01
          315.0000    6.4218E+01    9.1434E+00
          270.0000    7.4797E+01    7.4706E+00
          128.0000    7.5100E+00    1.7886E+01
          140.0000    1.3018E+01    1.6616E+01
          155.0000    2.1369E+01    1.5265E+01
          160.0000    2.4426E+01    1.4152E+01
          165.0000    2.7582E+01    1.3546E+01
          180.0000    3.7398E+01    1.2280E+01
          195.0000    4.7215E+01    1.0365E+01
```

```
                  200.0000    5.0371E+01    9.0998E+00
                  205.0000    5.3428E+01    8.4938E+00
                  220.0000    6.1778E+01    8.5870E+00
                  235.0000    6.8468E+01    8.3259E+00
                  269.0000    7.4797E+01    7.0561E+00
                    0.        0.            0.
 PLANE =  4A
 TOTAL ULLAGE WIDTH  =     7.3359E+01
 TOTAL POOL WIDTH  =     7.3359E+01
                   45.0000    1.0375E+01    1.9545E+01
                   12.0000    2.8945E+01    1.6666E+01
                  348.0000    4.4414E+01    1.3281E+01
                  315.0000    6.2984E+01    9.8958E+00
                  270.0000    7.3359E+01    7.0170E+00
                  128.0000    7.3657E+00    1.9845E+01
                  140.0000    1.2768E+01    1.8575E+01
                  155.0000    2.0958E+01    1.7223E+01
                  160.0000    2.3957E+01    1.6110E+01
                  165.0000    2.7052E+01    1.5504E+01
                  180.0000    3.6680E+01    1.4239E+01
                  195.0000    4.6308E+01    1.2324E+01
                  200.0000    4.9403E+01    1.1058E+01
                  205.0000    5.2401E+01    1.0452E+01
                  220.0000    6.0591E+01    9.3394E+00
                  235.0000    6.7152E+01    7.8723E+00
                  269.0000    7.3359E+01    6.6024E+00
                    0.        0.            0.
 PLANE =   5
 TOTAL ULLAGE WIDTH  =     7.3359E+01
 TOTAL POOL WIDTH  =     7.3359E+01
                   45.0000    1.0375E+01    9.0000E+00
                   12.0000    2.8945E+01    9.0000E+00
                  349.0000    4.4414E+01    9.0000E+00
                  315.0000    6.2984E+01    9.0000E+00
                  270.0000    7.3359E+01    9.0000E+00
                  128.0000    7.3657E+00    9.0000E+00
                  140.0000    1.2768E+01    9.0000E+00
                  155.0000    2.0958E+01    9.0000E+00
                  160.0000    2.3957E+01    9.0000E+00
                  165.0000    2.7052E+01    9.0000E+00
                  180.0000    3.6680E+01    9.0000E+00
                  195.0000    4.6308E+01    9.0000E+00
                  200.0000    4.9403E+01    9.0000E+00
                  205.0000    5.2401E+01    9.0000E+00
                  220.0000    6.0591E+01    9.0000E+00
                  235.0000    6.7152E+01    9.0000E+00
                  269.0000    7.3359E+01    9.0000E+00
                    0.        0.            0.
 PLANE =   6
 TOTAL ULLAGE WIDTH  =     7.3359E+01
 TOTAL POOL WIDTH  =     7.3359E+01
                   45.0000    1.0375E+01    9.0000E+00
                   12.0000    2.8945E+01    9.0000E+00
                  348.0000    4.4414E+01    9.0000E+00
                  315.0000    6.2984E+01    9.0000E+00
                  270.0000    7.3359E+01    9.0000E+00
                  128.0000    7.3657E+00    9.0000E+00
                  140.0000    1.2768E+01    9.0000E+00
                  155.0000    2.0958E+01    9.0000E+00
                  160.0000    2.3957E+01    9.0000E+00
```

```
            165.0000   2.7052E+01   9.0000E+00
            180.0000   3.6680E+01   9.0000E+00
            195.0000   4.6308E+01   9.0000E+00
            200.0000   4.9403E+01   9.0000E+00
            205.0000   5.2401E+01   9.0000E+00
            220.0000   6.0591E+01   9.0000E+00
            235.0000   6.7152E+01   9.0000E+00
            269.0000   7.3359E+01   9.0000E+00
              0.       0.           0.
PLANE =    8
TOTAL ULLAGE WIDTH   =     7.4797E+01
TOTAL POOL WIDTH   =     7.4797E+01
             45.0000   1.0579E+01   1.9545E+01
             12.0000   2.9512E+01   1.6666E+01
            348.0000   4.5284E+01   1.3281E+01
            315.0000   6.4218E+01   9.8958E+00
            270.0000   7.4797E+01   7.0170E+00
            128.0000   7.5100E+00   1.9845E+01
            140.0000   1.3018E+01   1.8575E+01
            155.0000   2.1369E+01   1.7223E+01
            160.0000   2.4426E+01   1.6110E+01
            165.0000   2.7582E+01   1.5504E+01
            180.0000   3.7398E+01   1.4239E+01
            195.0000   4.7215E+01   1.2324E+01
            200.0000   5.0371E+01   1.1058E+01
            205.0000   5.3428E+01   1.0452E+01
            220.0000   6.1778E+01   9.3394E+00
            235.0000   6.8468E+01   7.8723E+00
            269.0000   7.4797E+01   6.6024E+00
              0.       0.           0.
PLANE =    9
TOTAL ULLAGE WIDTH   =     7.3527E+01
TOTAL POOL WIDTH   =     7.3732E+01
             45.0000   1.0375E+01   1.7587E+01
             12.0000   2.8945E+01   1.4708E+01
            348.0000   4.4414E+01   1.1323E+01
            315.0000   6.3152E+01   9.1434E+00
            270.0000   7.3527E+01   7.4706E+00
            128.0000   7.3657E+00   1.7886E+01
            140.0000   1.2768E+01   1.6616E+01
            155.0000   2.0958E+01   1.5265E+01
            160.0000   2.3957E+01   1.4152E+01
            165.0000   2.7052E+01   1.3546E+01
            180.0000   3.6680E+01   1.2280E+01
            195.0000   4.6308E+01   1.0365E+01
            200.0000   4.9403E+01   9.0998E+00
            205.0000   5.2401E+01   8.4936E+00
            220.0000   6.0964E+01   8.5870E+00
            235.0000   6.7525E+01   8.3259E+00
            269.0000   7.3732E+01   7.0561E+00
              0.       0.           0.
PLANE =   11
TOTAL ULLAGE WIDTH   =     7.3359E+01
TOTAL POOL WIDTH   =     7.3359E+01
             45.0000   1.0375E+01   1.4000E+01
             12.0000   2.8945E+01   1.4000E+01
            348.0000   4.4414E+01   1.4000E+01
            315.0000   6.2984E+01   1.2750E+01
            270.0000   7.3359E+01   1.1500E+01
            128.0000   7.3657E+00   1.4000E+01
```

```
            140.0000    1.2768E+01    1.4000E+01
            155.0000    2.0958E+01    1.4000E+01
            160.0000    2.3957E+01    1.4000E+01
            165.0000    2.7052E+01    1.4000E+01
            180.0000    3.6680E+01    1.4000E+01
            195.0000    4.6308E+01    1.4000E+01
            200.0000    4.9403E+01    1.4000E+01
            205.0000    5.2401E+01    1.4000E+01
            220.0000    6.0591E+01    1.2750E+01
            235.0000    6.7152E+01    1.1500E+01
            269.0000    7.3359E+01    1.1500E+01
              0.        0.            0.
PLANE =  2D
TOTAL ULLAGE WIDTH  =     7.3458E+01
TOTAL POOL WIDTH  =     7.3458E+01
             45.0000   1.0425E+01    1.7660E+01
             12.0000   2.8995E+01    1.7660E+01
            348.0000   4.4463E+01    1.7660E+01
            315.0000   6.3034E+01    1.7660E+01
            270.0000   7.3458E+01    1.7660E+01
            128.0000   7.4151E+00    1.7660E+01
            140.0000   1.2817E+01    1.7660E+01
            155.0000   2.1008E+01    1.7660E+01
            160.0000   2.4006E+01    1.7660E+01
            165.0000   2.7101E+01    1.7660E+01
            180.0000   3.6729E+01    1.7660E+01
            195.0000   4.6357E+01    1.7660E+01
            200.0000   4.9452E+01    1.7660E+01
            205.0000   5.[illegible]E+01    1.7660E+01
            220.0000   6.0641E+01    1.7660E+01
            235.000[illegible]   6.7202E+01    1.7660E+01
            269.00[illegible]0   7.3458E+01    1.7660E+01
             -7.50[illegible]
         UNCLASSIFIED                                     FILM ONLY            10:43    11/21/79R
```

B.4 DXDZ2.8 (pool level lowered)

```
NRC TEST   2.8     H90 =  4.80      H7.5 =  4.20
PLANE AND AXIAL LOCATIONS
             THETA            XT            DELZT
PLANE =   1
TOTAL ULLAGE WIDTH  =     7.3778E+01
TOTAL POOL WIDTH  =     7.3778E+01
             45.0000   1.0585E+01    5.6250E+00
             12.0000   2.9155E+01    5.6250E+00
            348.0000   4.4623E+01    5.6250E+00
            315.0000   6.3193E+01    5.6250E+00
            270.0000   7.3776E+01    5.6250E+00
            128.0000   7.5750E+00    5.6250E+00
            140.0000   1.2977E+01    5.6250E+00
            155.0000   2.1168E+01    5.6250E+00
            160.0000   2.4166E+01    5.6250E+00
            165.0000   2.7261E+01    5.6250E+00
            180.0000   3.6889E+01    5.6250E+00
            195.0000   4.6517E+01    5.6250E+00
            200.0000   4.9612E+01    5.6250E+00
            205.0000   5.2610E+01    5.6250E+00
            220.0000   6.0801E+01    5.6250E+00
            235.0000   6.7361E+01    5.6250E+00
            269.0000   7.3778E+01    5.6250E+00
              0.       0.            0.
PLANE =   3
TOTAL ULLAGE WIDTH  =     7.3946E+01
TOTAL POOL WIDTH  =     7.4151E+01
             45.0000   1.0585E+01    1.4000E+01
             12.0000   2.9155E+01    1.4000E+01
            348.0000   4.4623E+01    1.4000E+01
            315.0000   6.3361E+01    1.2750E+01
            270.0000   7.3946E+01    1.1500E+01
            128.0000   7.5750E+00    1.4000E+01
            140.0000   1.2977E+01    1.4000E+01
            155.0000   2.1168E+01    1.4000E+01
            160.0000   2.4166E+01    1.4000E+01
            165.0000   2.7261E+01    1.4000E+01
            180.0000   3.6889E+01    1.4000E+01
            195.0000   4.6517E+01    1.4000E+01
            200.0000   4.9612E+01    1.4000E+01
            205.0000   5.2610E+01    1.4000E+01
            220.0000   6.1174E+01    1.2750E+01
            235.0000   6.7735E+01    1.1500E+01
            269.0000   7.4151E+01    1.1500E+01
              0.       0.            0.
PLANE =   4
TOTAL ULLAGE WIDTH  =     7.5223E+01
TOTAL POOL WIDTH  =     7.5223E+01
             45.0000   1.0792E+01    1.7608E+01
             12.0000   2.9726E+01    1.4708E+01
            348.0000   4.5498E+01    1.1323E+01
            315.0000   6.4431E+01    9.1642E+00
            270.0000   7.5223E+01    7.4914E+00
            128.0000   7.7234E+00    1.7907E+01
            140.0000   1.3232E+01    1.6616E+01
            155.0000   2.1582E+01    1.5265E+01
            160.0000   2.4639E+01    1.4152E+01
            165.0000   2.7795E+01    1.3546E+01
            180.0000   3.7612E+01    1.2280E+01
            195.0000   4.7428E+01    1.0365E+01
```

```
          200.0000   5.0584E+01   9.0998E+00
          205.0000   5.3641E+01   8.4938E+00
          220.0000   6.1992E+01   8.6078E+00
          235.0000   6.8681E+01   8.3676E+00
          269.0000   7.5223E+01   7.0769E+00
            0.       0.           0.
PLANE =  4A
TOTAL ULLAGE WIDTH  =    7.3778E+01
TOTAL POOL WIDTH  =    7.3778E+01
           45.0000   1.0585E+01   1.9566E+01
           12.0000   2.9155E+01   1.6666E+01
          348.0000   4.4623E+01   1.3281E+01
          315.0000   6.3193E+01   9.8958E+00
          270.0000   7.3778E+01   6.9962E+00
          128.0000   7.5750E+00   1.9865E+01
          140.0000   1.2977E+01   1.8575E+01
          155.0000   2.1168E+01   1.7223E+01
          160.0000   2.4166E+01   1.6110E+01
          165.0000   2.7261E+01   1.5504E+01
          180.0000   3.6889E+01   1.4239E+01
          195.0000   4.6517E+01   1.2324E+01
          200.0000   4.9612E+01   1.1058E+01
          205.0000   5.2610E+01   1.0452E+01
          220.0000   6.0801E+01   9.3394E+00
          235.0000   6.7361E+01   7.8723E+00
          269.0000   7.3778E+01   6.5816E+00
            0.       0.           0.
PLANE =   5
TOTAL ULLAGE WIDTH  =    7.3778E+01
TOTAL POOL WIDTH  =    7.3778E+01
           45.0000   1.0585E+01   9.0000E+00
           12.0000   2.9155E+01   9.0000E+00
          348.0000   4.4623E+01   9.0000E+00
          315.0000   6.3193E+01   9.0000E+00
          270.0000   7.3778E+01   9.0000E+00
          128.0000   7.5750E+00   9.0000E+00
          140.0000   1.2977E+01   9.0000E+00
          155.0000   2.1168E+01   9.0000E+00
          160.0000   2.4166E+01   9.0000E+00
          165.0000   2.7261E+01   9.0000E+00
          180.0000   3.6889E+01   9.0000E+00
          195.0000   4.6517E+01   9.0000E+00
          200.0000   4.9612E+01   9.0000E+00
          205.0000   5.2610E+01   9.0000E+00
          220.0000   6.0801E+01   9.0000E+00
          235.0000   6.7361E+01   9.0000E+00
          269.0000   7.3778E+01   9.0000E+00
            0.       0.           0.
PLANE =   6
TOTAL ULLAGE WIDTH  =    7.3778E+01
TOTAL POOL WIDTH  =    7.3778E+01
           45.0000   1.0585E+01   9.0000E+00
           12.0000   2.9155E+01   9.0000E+00
          348.0000   4.4623E+01   9.0000E+00
          315.0000   6.3193E+01   9.0000E+00
          270.0000   7.3778E+01   9.0000E+00
          128.0000   7.5750E+00   9.0000E+00
          140.0000   1.2977E+01   9.0000E+00
          155.0000   2.1168E+01   9.0000E+00
          160.0000   2.4166E+01   9.0000E+00
```

```
            165.0000   2.7261E+01   9.0000E+00
            180.0000   3.6889E+01   9.0000E+00
            195.0000   4.6517E+01   9.0000E+00
            200.0000   4.9612E+01   9.0000E+00
            205.0000   5.2610E+01   9.0000E+00
            220.0000   6.0801E+01   9.0000E+00
            235.0000   6.7361E+01   9.0000E+00
            269.0000   7.3778E+01   9.0000E+00
              0.       0.           0.
PLANE =    8
TOTAL ULLAGE WIDTH  =     7.5223E+01
TOTAL POOL WIDTH  =     7.5223E+01
             45.0000   1.0792E+01   1.9566E+01
             12.0000   2.9726E+01   1.6666E+01
            348.0000   4.5498E+01   1.3281E+01
            315.0000   6.4431E+01   9.8958E+00
            270.0000   7.5223E+01   6.9962E+00
            128.0000   7.7234E+00   1.9865E+01
            140.0000   1.3232E+01   1.8575E+01
            155.0000   2.1582E+01   1.7223E+01
            160.0000   2.4639E+01   1.6110E+01
            165.0000   2.7795E+01   1.5504E+01
            180.0000   3.7612E+01   1.4239E+01
            195.0000   4.7428E+01   1.2324E+01
            200.0000   5.0584E+01   1.1058E+01
            205.0000   5.3641E+01   1.0452E+01
            220.0000   6.1992E+01   9.3394E+00
            235.0000   6.8681E+01   7.8723E+00
            269.0000   7.5223E+01   6.5816E+00
              0.       0.           0.
PLANE =    9
TOTAL ULLAGE WIDTH  =     7.3946E+01
TOTAL POOL WIDTH  =     7.4151E+01
             45.0000   1.0585E+01   1.7608E+01
             12.0000   2.9155E+01   1.4708E+01
            348.0000   4.4623E+01   1.1323E+01
            315.0000   6.3361E+01   9.1642E+00
            270.0000   7.3946E+01   7.4914E+00
            128.0000   7.5750E+00   1.7907E+01
            140.0000   1.2977E+01   1.6616E+01
            155.0000   2.1168E+01   1.5265E+01
            160.0000   2.4166E+01   1.4152E+01
            165.0000   2.7261E+01   1.3546E+01
            180.0000   3.6889E+01   1.2280E+01
            195.0000   4.6517E+01   1.0365E+01
            200.0000   4.9612E+01   9.0998E+00
            205.0000   5.2610E+01   8.4938E+00
            220.0000   6.1174E+01   8.6078E+00
            235.0000   6.7735E+01   8.3676E+00
            269.0000   7.4151E+01   7.0769E+00
              0.       0.           0.
PLANE =   11
TOTAL ULLAGE WIDTH  =     7.3778E+01
TOTAL POOL WIDTH  =     7.3778E+01
             45.0000   1.0585E+01   1.4000E+01
             12.0000   2.9155E+01   1.4000E+01
            348.0000   4.4623E+01   1.4000E+01
            315.0000   6.3193E+01   1.2750E+01
            270.0000   7.3778E+01   1.1500E+01
            128.0000   7.5750E+00   1.4000E+01
```

```
                 140.0000    1.2977E+01     1.4000E+01
                 155.0000    2.1168E+01     1.4000E+01
                 160.0000    2.4166E+01     1.4000E+01
                 165.0000    2.7261E+01     1.4000E+01
                 180.0000    3.6889E+01     1.4000E+01
                 195.0000    4.6517E+01     1.4000E+01
                 200.0000    4.9612E+01     1.4000E+01
                 205.0000    5.2610E+01     1.4000E+01
                 220.0000    6.0801E+01     1.2750E+01
                 235.0000    6.7361E+01     1.1500E+01
                 269.0000    7.3778E+01     1.1500E+01
                   0.        0.             0.
     PLANE =  2D
     TOTAL ULLAGE WIDTH  =      7.3924E+01
     TOTAL POOL WIDTH  =      7.3924E+01
                  45.0000    1.0658E+01     1.7660E+01
                  12.0000    2.9228E+01     1.7660E+01
                 348.0000    4.4696E+01     1.7660E+01
                 315.0000    6.3267E+01     1.7660E+01
                 270.0000    7.3924E+01     1.7660E+01
                 128.0000    7.6481E+00     1.7660E+01
                 140.0000    1.3050E+01     1.7660E+01
                 155.0000    2.1241E+01     1.7660E+01
                 160.0000    2.4239E+01     1.7660E+01
                 165.0000    2.7334E+01     1.7660E+01
                 180.0000    3.6962E+01     1.7660E+01
                 195.0000    4.6590E+01     1.7660E+01
                 200.0000    4.9685E+01     1.7660E+01
                 205.0000    5.2684E+01     1.7660E+01
                 220.0000    6.0874E+01     1.7660E+01
                 235.0000    6.7435E+01     1.7660E+01
                 269.0000    7.3924E+01     1.7660E+01
                  -7.5000
```

APPENDIX C

DATA MANAGEMENT METHODS

DATA MANAGEMENT METHODS

INTRODUCTION

Proceeding from raw pressure data to the final 3-D and 2-D hydrodynamic vertical load functions is implemented in four basic steps:

(1) Management of data records and retrieval of PSE data from archival storage.
(2) Correction of the pressure data to account for systematic transducer error and static head.
(3) Calculation of the HVLF and associated standard deviation using the corrected pressure data.
(4) Postprocessing of computational results to obtain required output.

Because the hydrodynamic vertical load function (HVLF) calculation requires the systematic manipulation of up to 66 individual data files for each of 24 texts, computer-aided methods of processing the PSE data on a production basis were developed to automate the calculation procedure as much as possible.

PSE data is processed by four independent computer routines (controllees) which were developed specifically for the HVLF calculation. These routines are as follows:

PSEPREP--performs general record management for the PSE data bases, including extraction of all applicable pressure data files from archival storage.
PRESLOC--calculates pool geometry and static head based on the elevation of the pool surface.
INTERPP--corrects the PSE pressure data for systematic and random error and, where applicable, for static head.
TORIS --calculates the HVLF and error based on the corrected pressure data.

Postprocessing of the HVLF results is executed using SOCKITTOME,[7] a general graphics postprocessor currently available and in use by Lawrence Livermore Laboratory's L-Division (computational physics).

The basic logic flow of the HVLF calculation is shown schematically in Fig. C-1. At present, execution of the three controllees required to perform all data processing through preparation of the corrected PSE data is interfaced with PSEHVLF, an ORDER[16] control routine. A similar control routine, PSEPLOT, was developed earlier to generate time plots of the complete PSE data base and proved to be very successful in an application where a large number of data files had to be processed in a systematic manner.[17] Each subsidiary controllee within the control routine has a specific function, similar to a subroutine in an integrated routine, yet can be executed independently of the others if necessary. This multiple-controllee approach also provides considerable flexibility with regard to the execution of various public utility routines used to interface the execution of the HVLF controllees.

Output from the PSEHVLF controller are files containing the spatial data (DXDZ) and the corrected pressure histories (INTORI). Using these files as input, the fourth HVLF controllee, TORIS, is executed "stand-alone" to produce the extensive files for postprocessing.

RECORD MANAGEMENT AND DATA RETRIEVAL

Data retrieval from archival storage is performed by the controllee PSEPREP, a general record management routine developed specifically for the PSE data base. PSEPREP accepts as input a list of transducers or a defined transducer subset, then uses PSE library conventions (see Ref. 17 for details) to generate the names and archival directory locations of the particular files containing PSE data from a specified test. This is achieved through extensive internal indexing that correlates each transducer designator (commonly referred to as the "P-number") with the physical location and LOFAU (Low Frequency Acquisition Unit) connection of the corresponding transducer. Using this information combined with the PSE test number, the names of the engineering files storing data from the specified transducers are generated according to the conventions of the PSE data base. Library files containing the individual transducer data files are copied from archival storage to disk, then are unpacked to obtain the data files for transducers available during

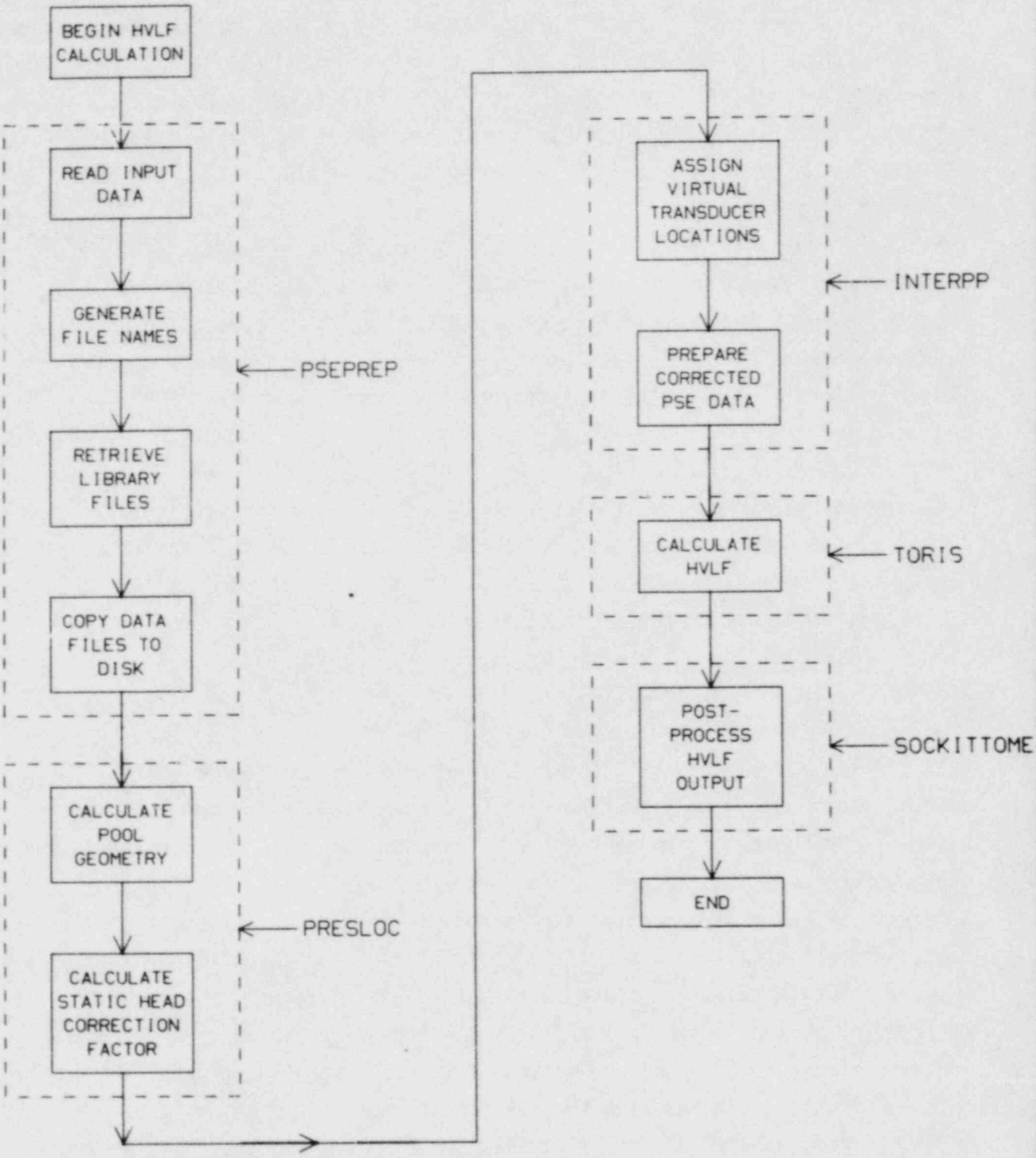

FIG. C-1. Basic logic flow for the PSE HVLF calculations.

the specified test.[1] After execution is complete, an output file OUTPREP is left on disk listing the available transducers together with the corresponding physical locations and data file names. This output file also contains a specified time window which has no function for the file management operations, but is subsequently used in actual analysis of the transducer data.

PREPARATION OF TORIS INPUT

Preparation of input for the TORIS code is the function of two routines, PRESLOC and INTERPP. PRESLOC calculates the pool geometry based on the elevation of the pool surface relative to the shell horizontal centerline for both the 7.5° and 45° test sections (see Appendix A). The wetted (pool) and unwetted (ullage) distances across the shell in each instrumentation plane and along the circumference of the torus at each instrumentation angle are written to a disk file (DXDZ) that is later used as input to TORIS. PRESLOC also calculates the static head correction to be applied to data from pool transducers located at angles between 128 and 235 degrees. The static head correction factors are written to a disk file INHCOR that is subsequently used by INTERPP as part of the data correction process.

INTERPP serves three functions: (1) to correct PSE data to reflect systematic errors and static head; (2) to calculate the standard deviation of the data; and (3) to assign virtual locations for existing data for use in the HVLF calculations. For each PSE test analyzed, INTERPP accepts input data from three disk files:

OUTPREP--time window, list of available transducers with corresponding physical locations and data file names;
INHCOR--static head correction data;
MATRIX--transducer assignment map.

Systematic end-to-end (ETE) error data and standard deviation data obtained during in-situ calibration of each pressure transducer[4] are independent of the particular PSE test considered and therefore have been data-loaded into the INTERPP code to reduce program execution time requirements. The basic logic flow for INTERPP is shown schematically in Fig. C-2. INTERPP begins execution by buffer-loading the analytic time window, the transducer list

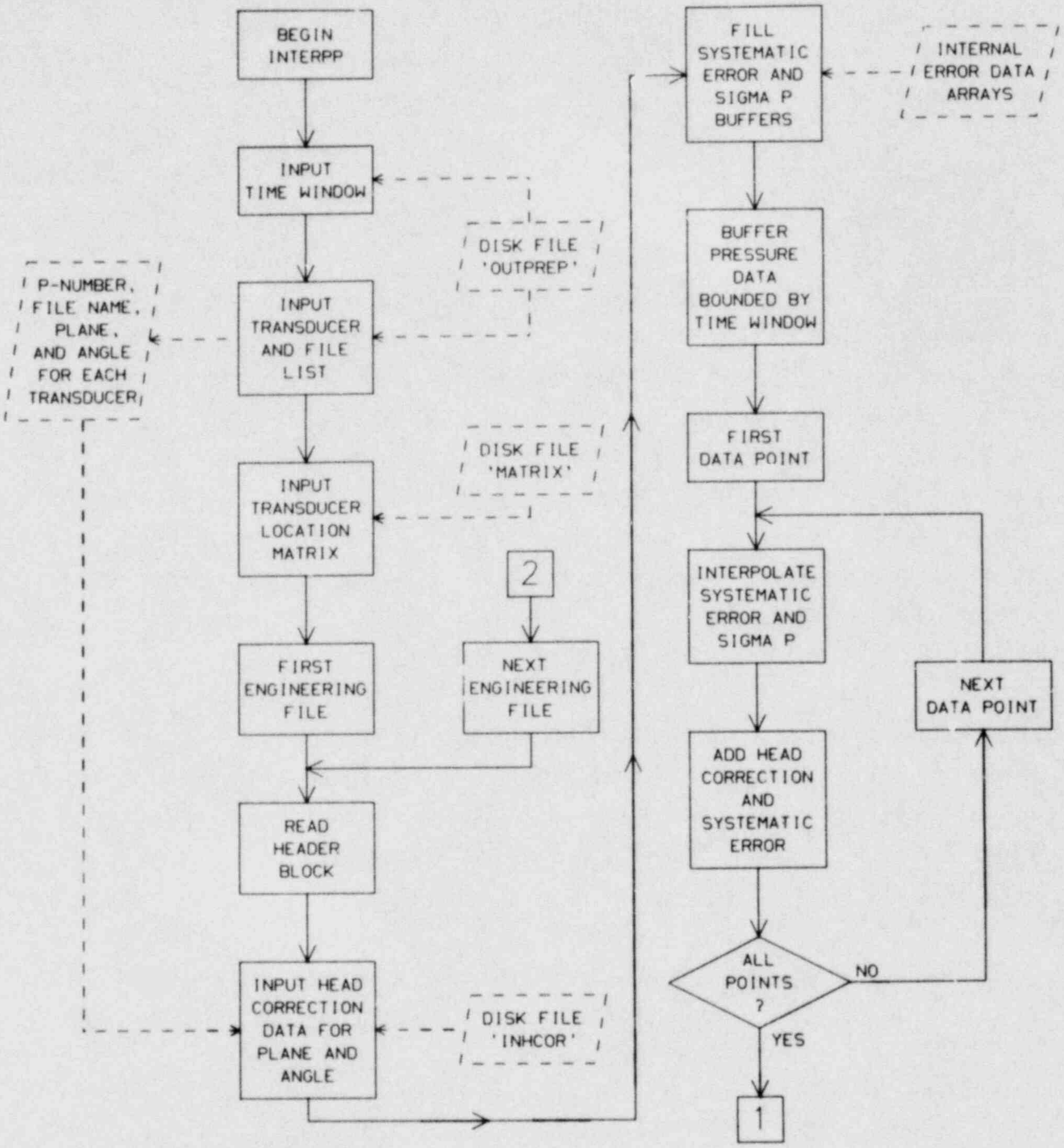

FIG. C-2. Basic logic flow for INTERPP.

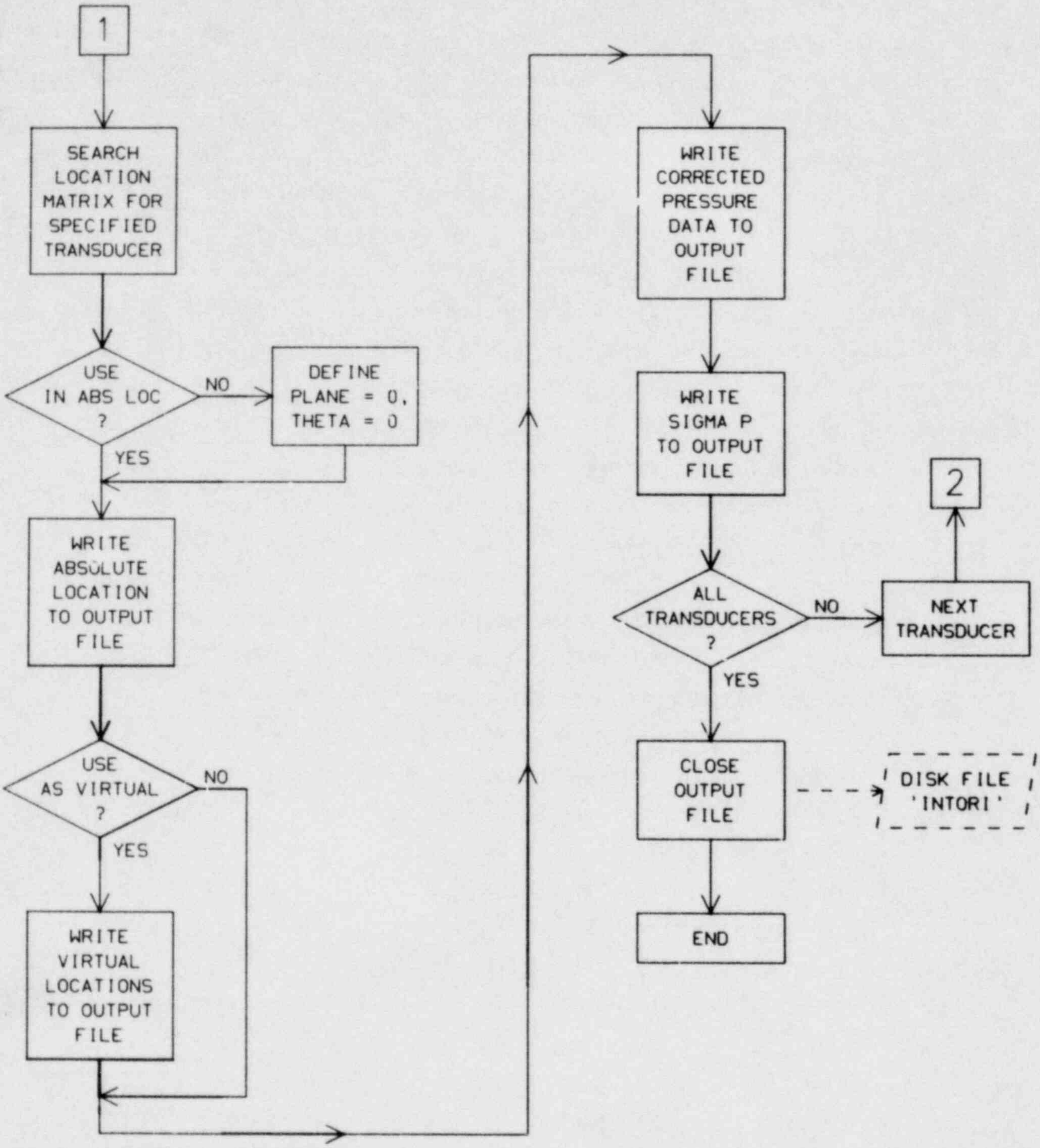

FIG. C-2. (Continued) Basic logic flow for INTERPP.

with file names and the transducer assignment map. The physical files INTORI and OINTORI are then created. INTORI becomes the primary input file for TORIS, containing the corrected pressure data for the specified time window, while OINTORI is simply a regurgitation of the corresponding uncorrected data which is retained as a check on code execution. After the initial setup phase is complete, INTERPP loops through the list of available transducers as follows:

(1) An engineering file is opened. The header information about the subject transducer is read and copied to each output file.
(2) Head correction data for the angular location of the transducer is read from INHCOR. No correction is applied if the angle of the transducer is less than 128 degrees or greater than 235 degrees.
(3) ETE error data and standard deviation data for the transducer is loaded into two temporary error buffers.
(4) The uncorrected pressure data bounded by the specified time window is read from the engineering file and loaded into an appropriate buffer.
(5) For each pressure point, the systematic error and the standard deviation are determined through interpolation of the appropriate error buffer. If the pressure is outside the bounds of the available data, the nearest endpoint values of error or standard deviation are used. The systematic error and static head correction (if any) are then applied to the pressure point and the result stored in a new temporary buffer. The corresponding value of standard deviation is similarly stored.
(6) The location matrix is then searched for the specified transducer. The absolute location of the transducer, followed by any virtual location assignments, are written to INTORI. The list of absolute and virtual locations is then terminated by an end-of-record sentinel.

If the specified transducer is not included at its absolute location (according to the data in OUTPREP), it is assigned to an imaginary plane ("plane zero") at 0 degrees. This instrumentation plane is transparent to the TORIS code and simple allows the option of assigning data from the specified transducer to virtual locations without necessarily using the transducer data at its absolute location. In either case, an absolute location is always written to INTORI as follows:

- The buffers containing the corrected pressures and the corresponding standard deviations are emptied to INTORI.
- The buffer containing the uncorrected pressures is emptied to OINTORI.

All temporary buffers are then cleared and the process repeated until all of the transducers have been processed, at which time the output files are closed and execution of INTERPP is terminated.

APPENDIX D

HVLF CHARACTERIZATION DATA

Test 1.3.1

- Section D.1 contains results of trapezoidal interpolation
- Section D.2 contains results of parabolic interpolation

D.1. HVLF CHARACTERIZATION DATA

(Trapezoidal Interpolation)

Test 1.3.1

```
1          NRC AIR TEST NO. 1.3.1                                          TRAPEZOIDAL

                             FORCE SUMMARY  (MEAN    STANDARD DEVIATION)

          45 DEGREE SECTOR - 3D

                             T1                   T2                   T3                   T4

          TIME,SECONDS    3.1126E+00          3.1269E+00          3.1470E+00          3.2472E+00

          POOL           -40093.  101.4   -34562.  100.9   -38634.   96.4   -32451.   42.0

          ULLAGE          23698.   69.6    24200.   80.1    25595.  101.7    40235.  356.5

          NET            -16396.  123.0   -10361.  128.8   -13039.  140.1     7785.  359.0



         7.5 DEGREE SECTOR - 2D

                             T1                   T2                   T3                   T4

          TIME,SECONDS    3.1069E+00          3.1212E+00          3.1327E+00          3.2329E+00

          POOL            -6608.   12.9    -5567.   12.8    -6283.   12.9    -5386.   12.5

          ULLAGE           3935.   11.4     4041.   11.5     4121.   11.6     6508.   12.6

          NET             -2673.   17.2    -1525.   17.2    -2162.   17.3     1122.   17.8



          NET FORCE RATIOS

          3D/2D            1.022  0.010     1.132  0.019     1.005  0.013     1.156  0.056
```

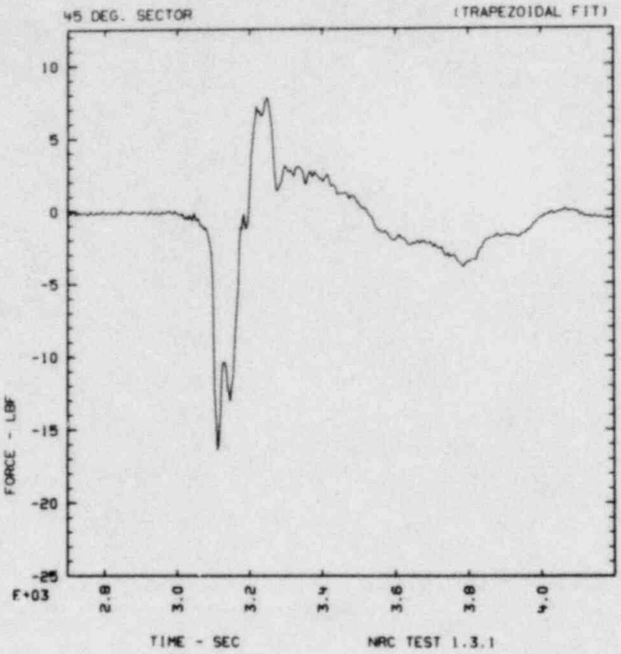
45 DEG. SECTOR
(TRAPEZOIDAL FIT)
10
5
0
-5
-10
-15
-20
-25
FORCE - LBF
E+03
2.8
3.0
3.2
3.4
3.6
3.8
4.0
TIME - SEC
NRC TEST 1.3.1

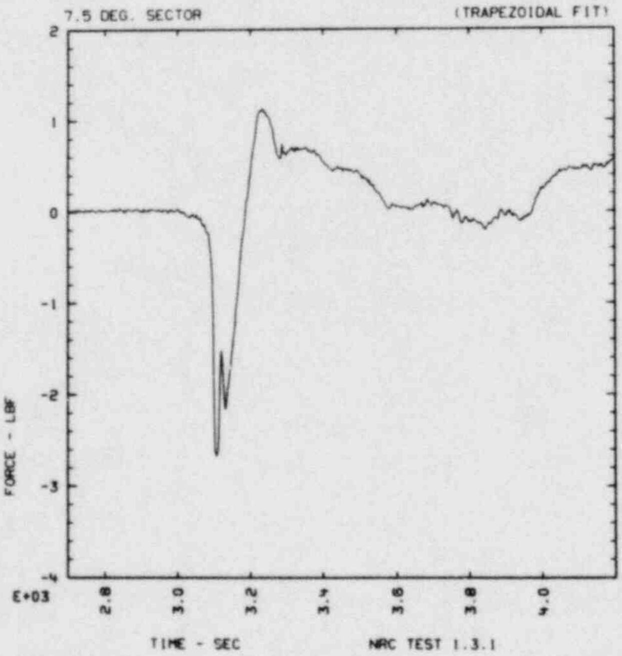
7.5 DEG. SECTOR
(TRAPEZOIDAL FIT)
2
1
0
-1
-2
-3
-4
FORCE - LBF
E+03
2.8
3.0
3.2
3.4
3.6
3.8
4.0
TIME - SEC
NRC TEST 1.3.1

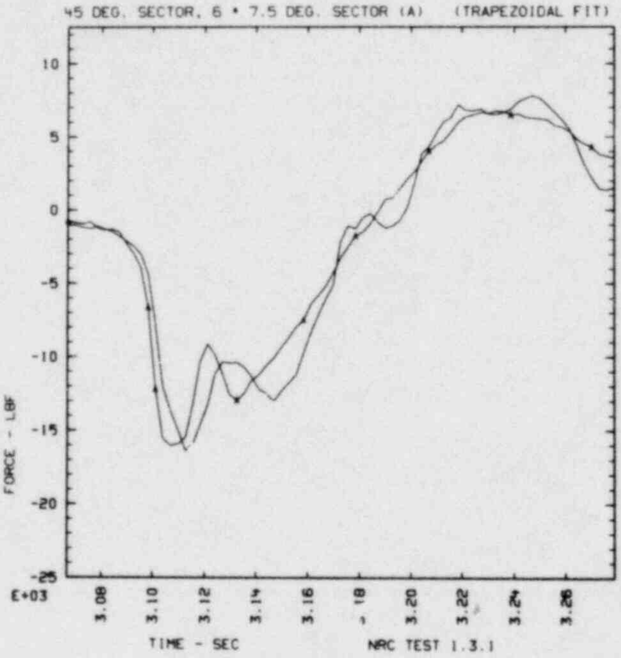
45 DEG. SECTOR, 6 * 7.5 DEG. SECTOR (A) (TRAPEZOIDAL FIT)
FORCE - LBF
10
5
0
-5
-10
-15
-20
-25
E+03
3.08
3.10
3.12
3.14
3.16
3.18
3.20
3.22
3.24
3.26
TIME - SEC
NRC TEST 1.3.1

NRC TEST NO. 131 TRAPEZOID FIT - FUL IN POOL AT T1 -
FILE(S):T1.P131

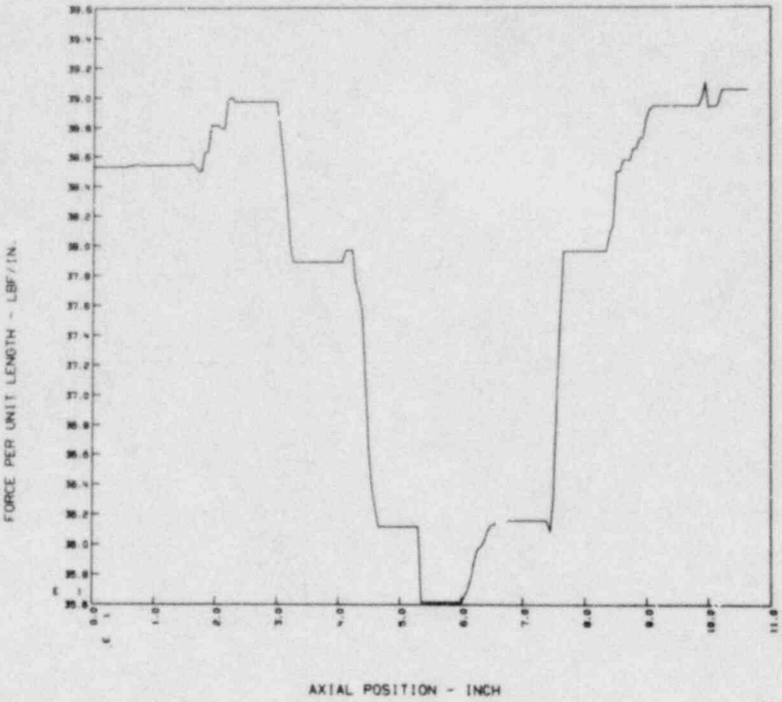

NRC TEST NO. 131 TRAPEZOID FIT - FUL IN ULLAGE AT T1 -
FILE(S):T1.U131

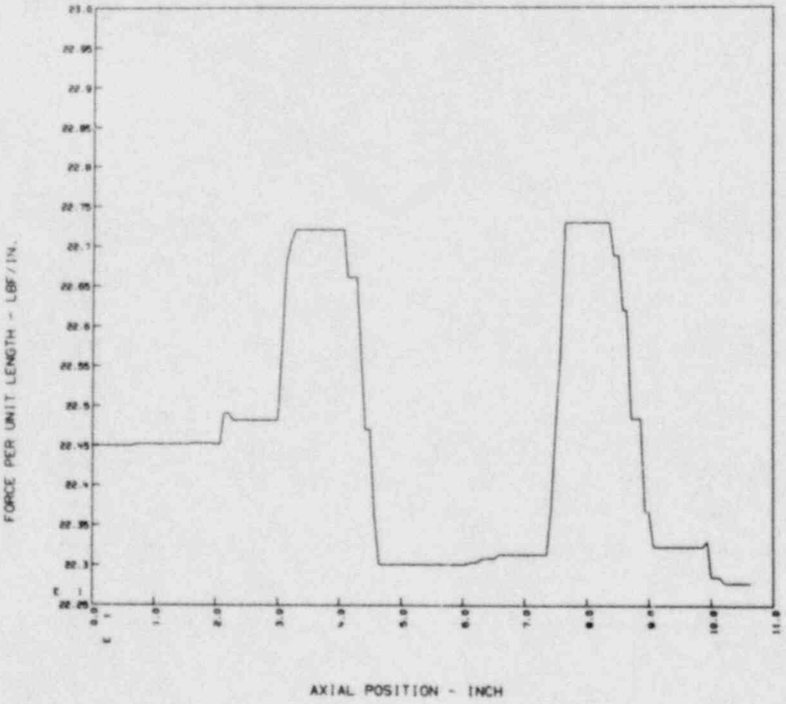

NRC TEST NO. 131 TRAPEZOID FIT - NET 3D FUL AT T1 -
FILE(S):T1.N131

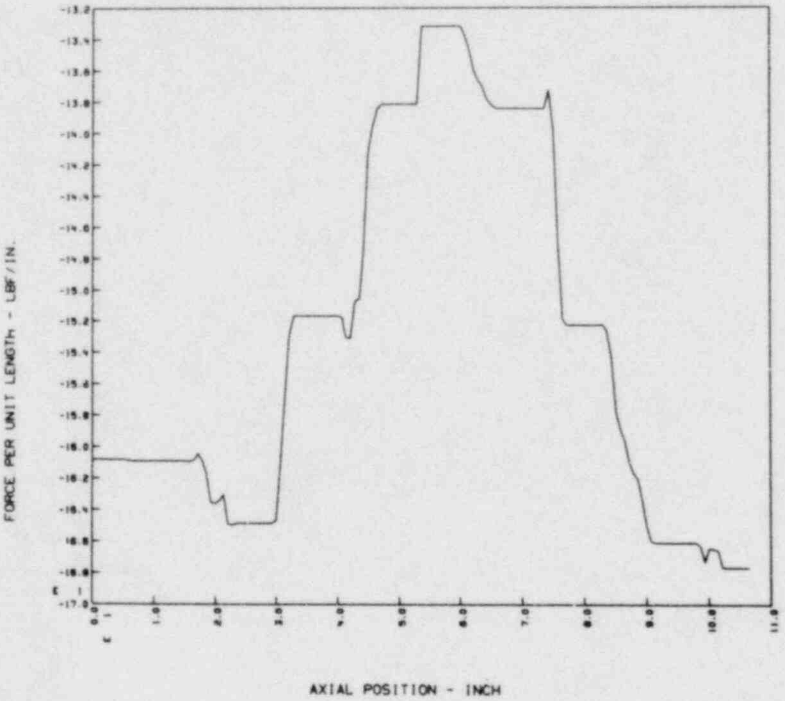

NRC TEST NO. 131 TRAPEZOID FIT - FUL IN POOL AT T2 -
FILE(S):T2.P131

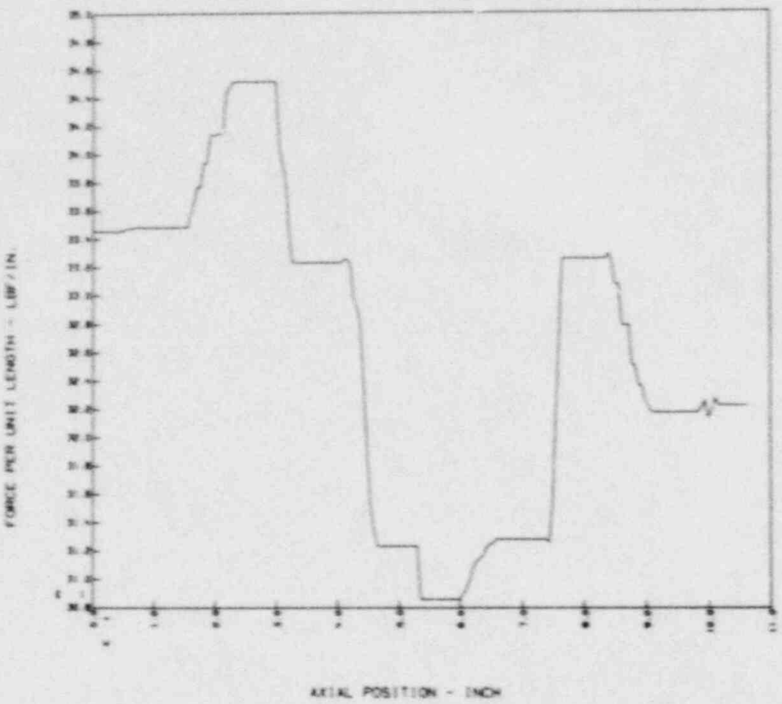

NRC TEST NO. 131 TRAPEZOID FIT - FUL IN ULLAGE AT T2 -
FILE(S):T2.U131

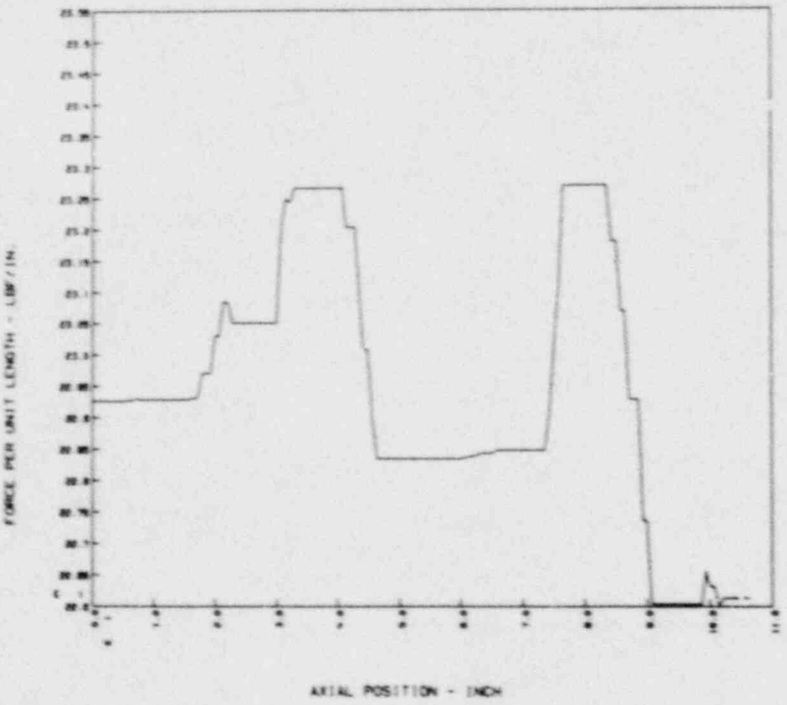

NRC TEST NO. 131 TRAPEZOID FIT - NET 3D FUL AT T2 -
FILE(S):T2.N131

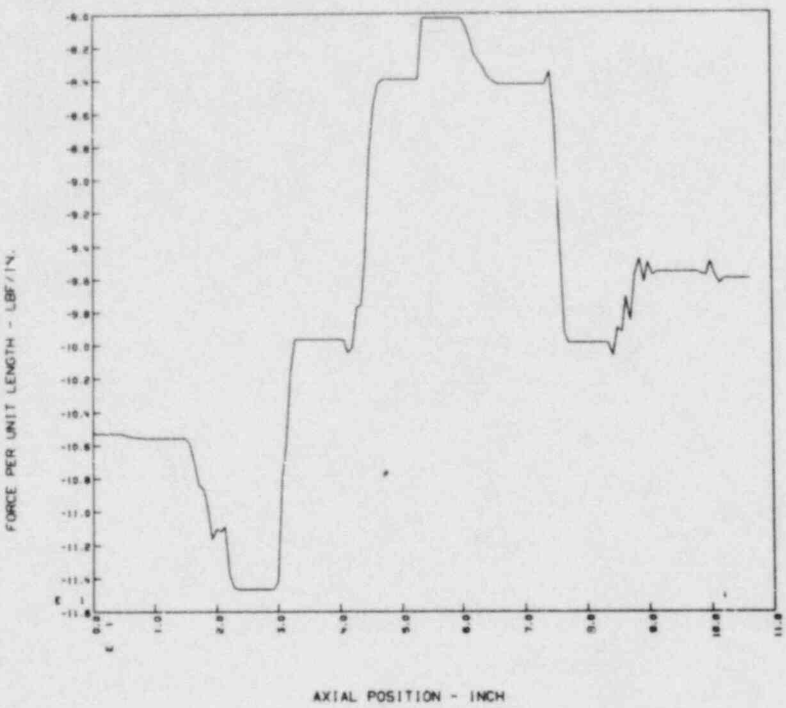

NRC TEST NO. 131 TRAPEZOID FIT - FUL IN POOL AT T3 -
FILE(S):T3.P131

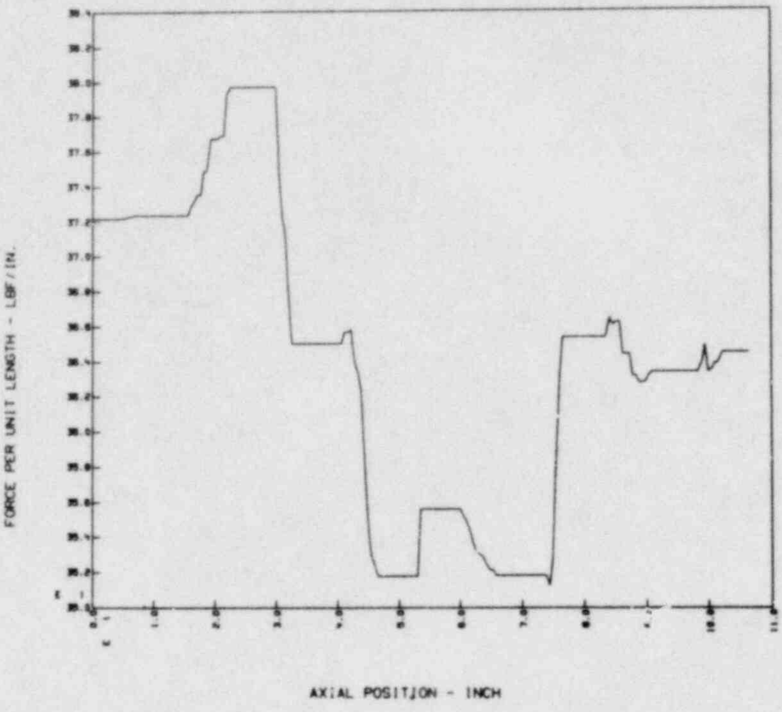

NRC TEST NO. 131 TRAPEZOID FIT - FUL IN ULLAGE AT T3 -
FILE(S):T3.U131

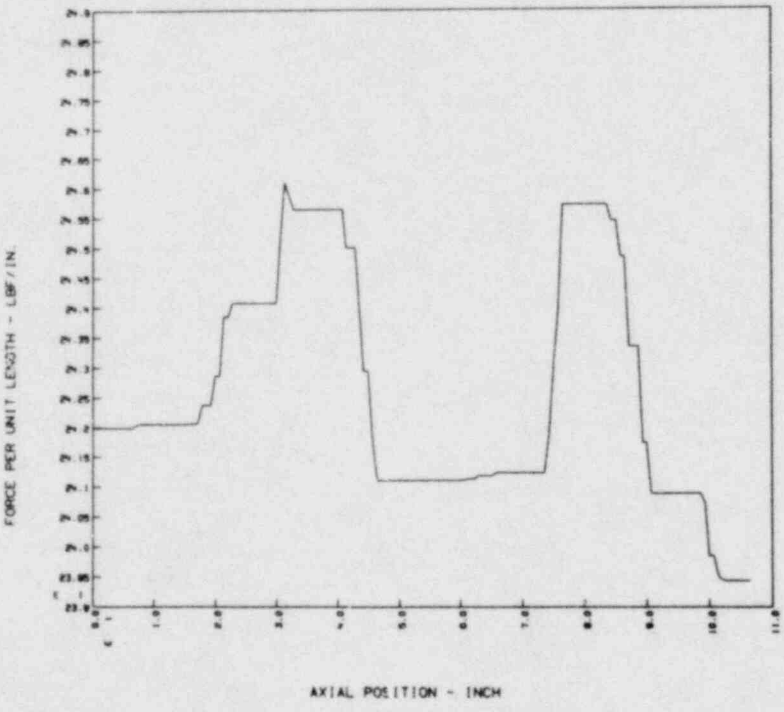

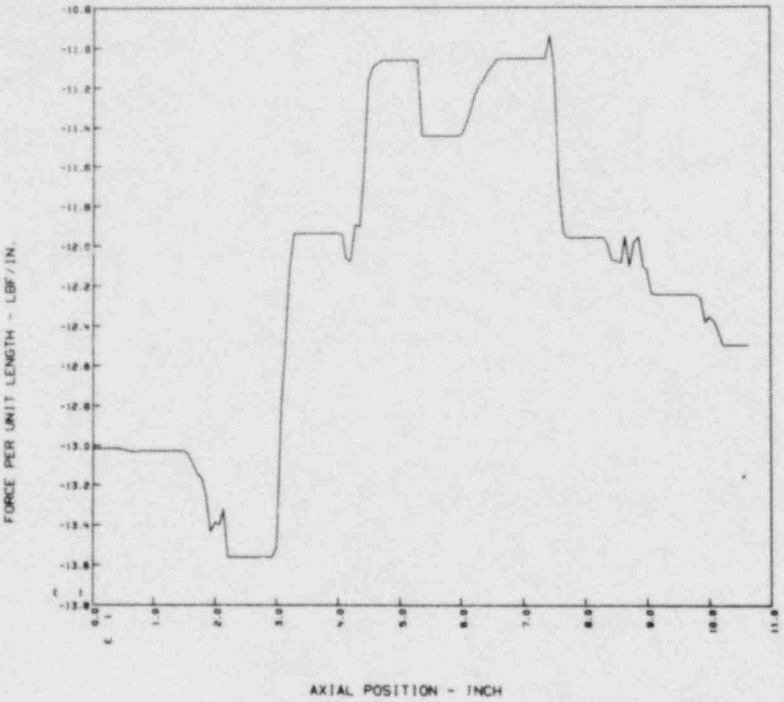

NRC TEST NO. 131 TRAPEZOID FIT - NET 3D FUL AT T3 -
FILE(S):T3.N131

NRC TEST NO. 131 TRAPEZOID FIT - FUL IN POOL AT T4 -
FILE:S1:T4.P131

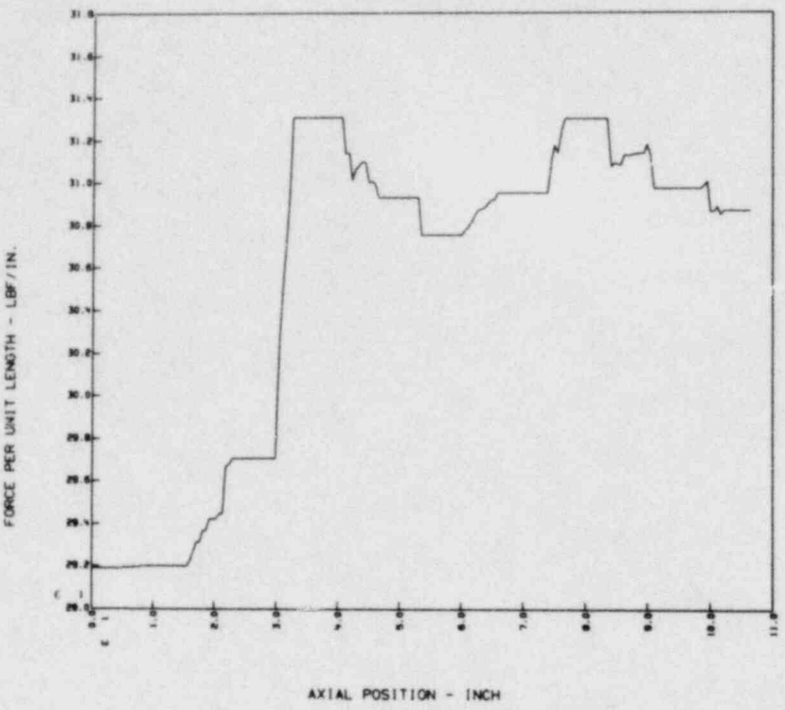

NRC TEST NO. 131 TRAPEZOID FIT - FUL IN ULLAGE AT T4 -
FILE:S1:T4.U131

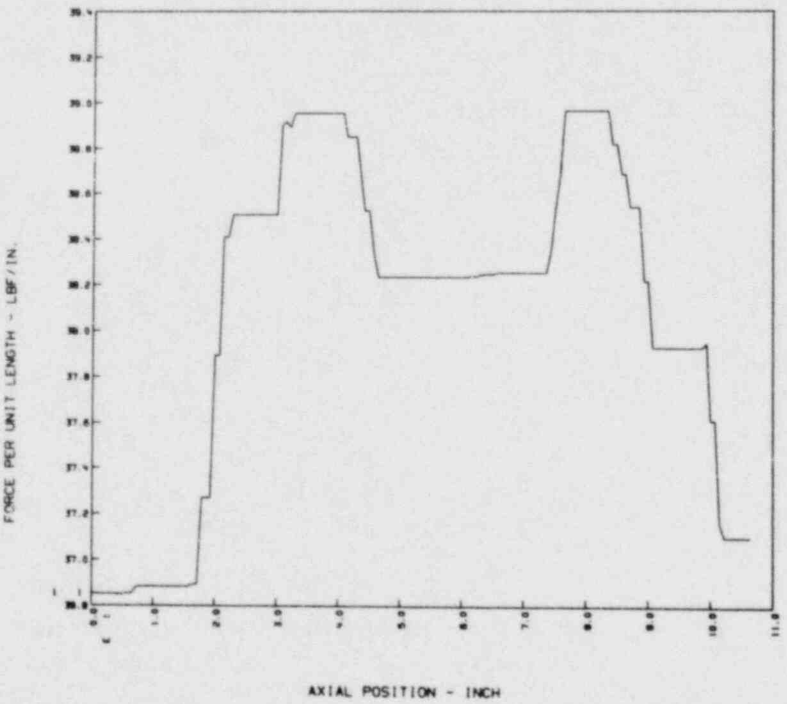

NRC TEST NO. 131 TRAPEZOID FIT - NET 3D FUL AT '4 -
FILE(S):T4.N131

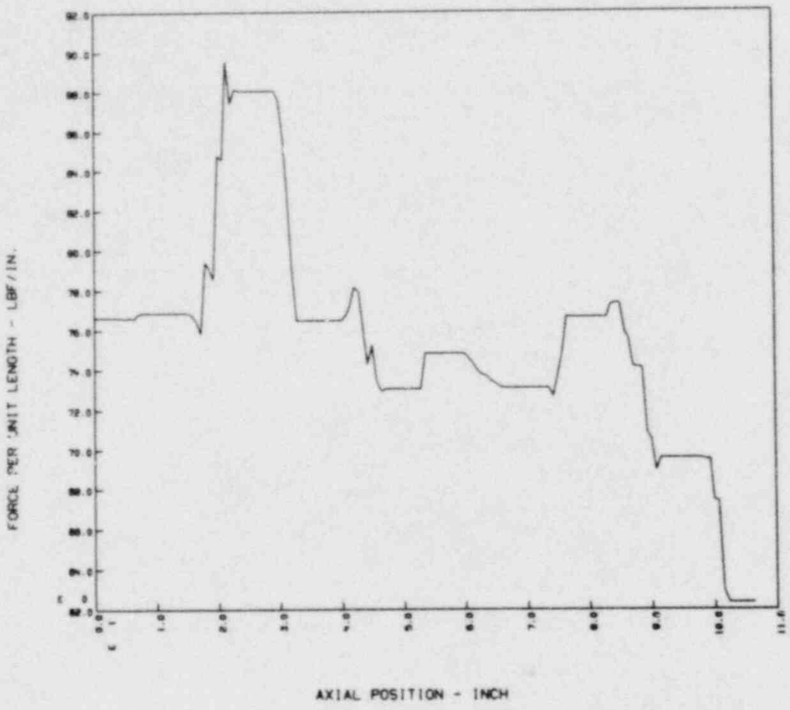

TEST131 TRAPEZOID FIT PRESSURE PROFILE PLANE4 T1, AT MAX DOWNLOAD
FILE(S):POOL.MRK (A)-ULLAGE.MRK

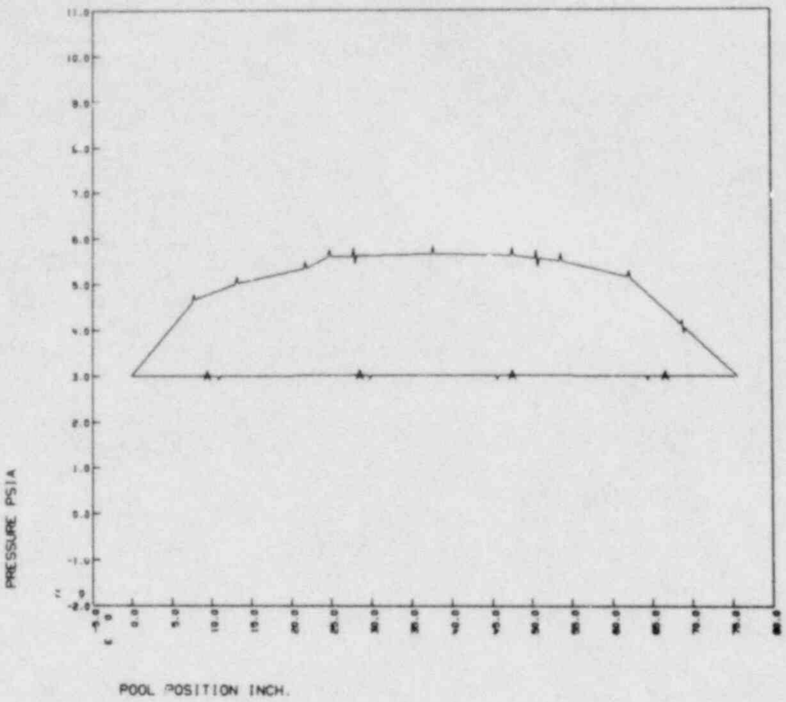

TEST131 TRAPEZOID FIT PRESSURE PROFILE PLANE6 T1, AT MAX DOWNLOAD
FILE(S):POOL.MRK (A)-ULLAGE.MRK

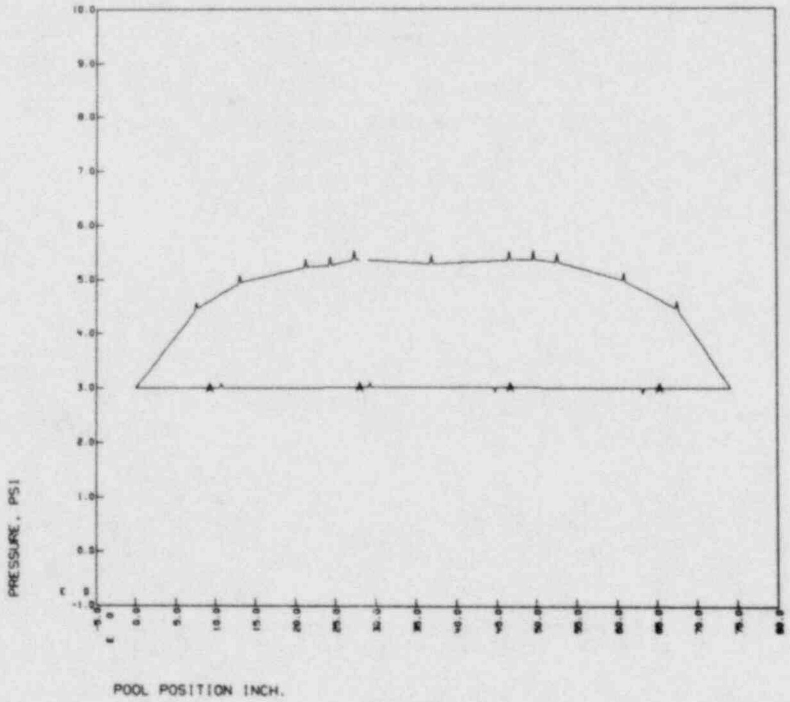

TEST131 TRAPEZOID FIT PRESSURE PROFILE PLANE9 T1, AT MAX DOWNLOAD
FILE(S):POOL.MRK   (A)-ULLAGE.MRK

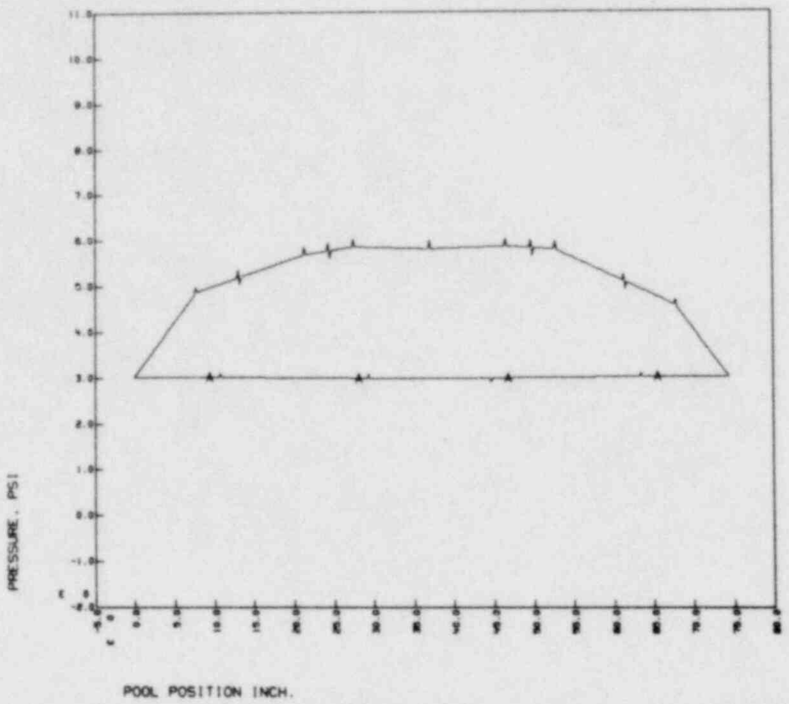

TEST131 TRAPEZOID FIT PRESSURE PROFILE PLANE11 T1, AT MAX DOWNLOAD
FILE(S):POOL.MRK   (A)-ULLAGE.MRK

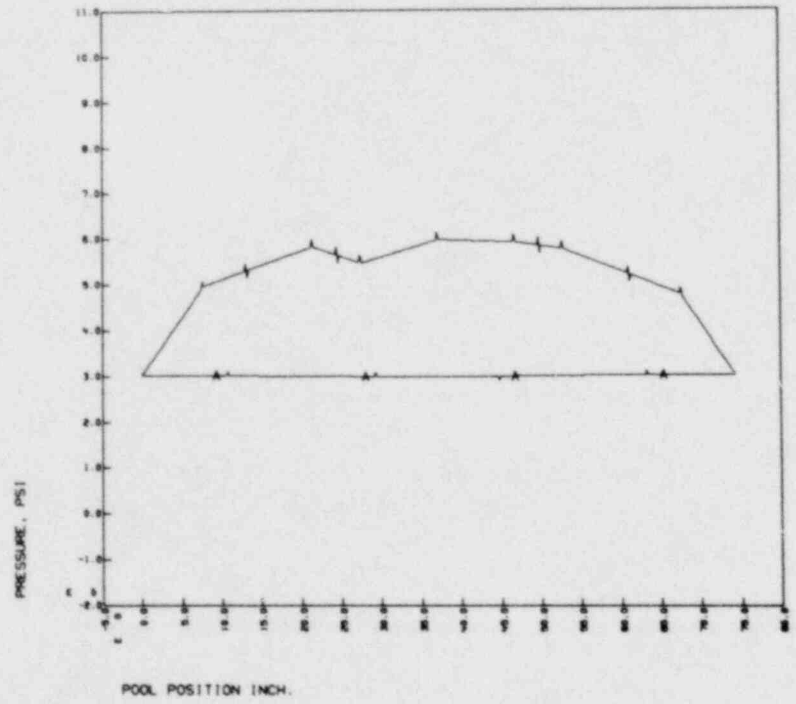

TEST(3) TRAPEZOID FIT PRESSURE PROFILE PLANE2D T1, AT MAX DOWNLOAD
FILE(S):POOL.MRK (A)-ULLAGE.MRK

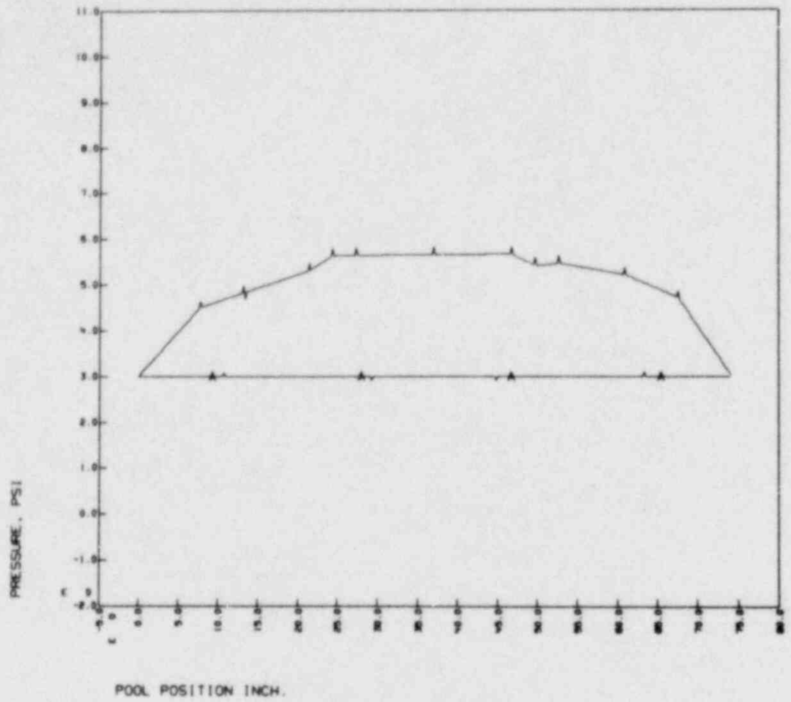

TEST131 TRAPEZOID FIT PRESSURE PROFILE PLANE4 T2
FILE(S):POOL.MRK (A)-ULLAGE.MRK

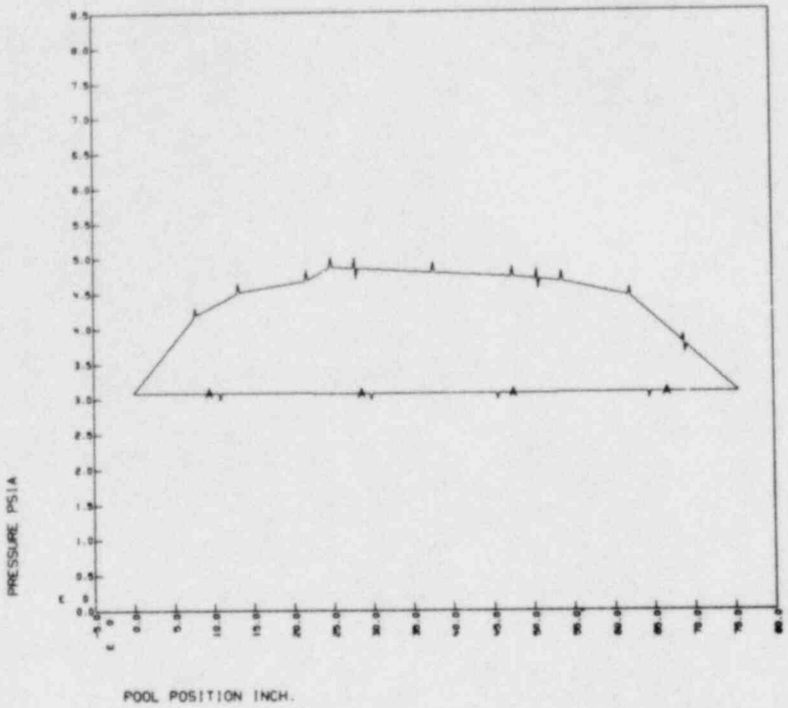

TEST131 TRAPEZOID FIT PRESSURE PROFILE PLANE6 T2
FILE(S):POOL.MRK (A)-ULLAGE.MRK

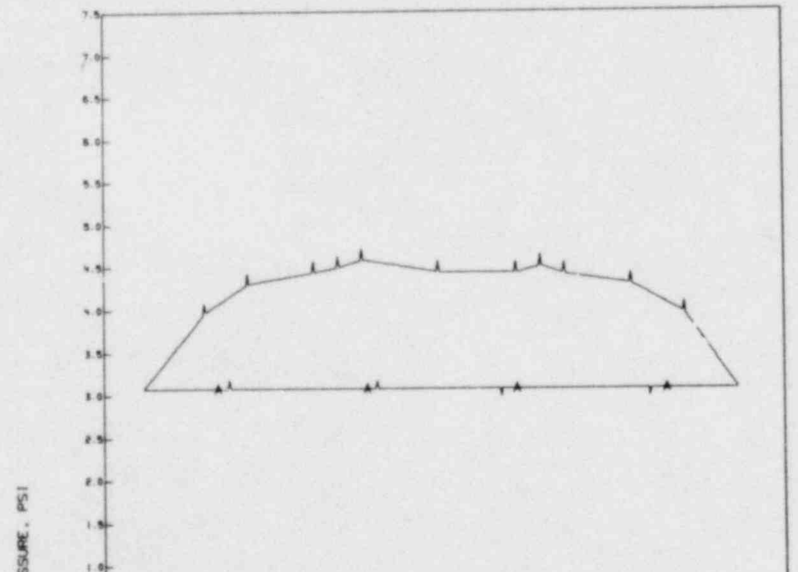

TEST131 TRAPEZOID FIT PRESSURE PROFILE PLANE9 T2
FILE(S):POOL.MRK (A)-ULLAGE.MRK

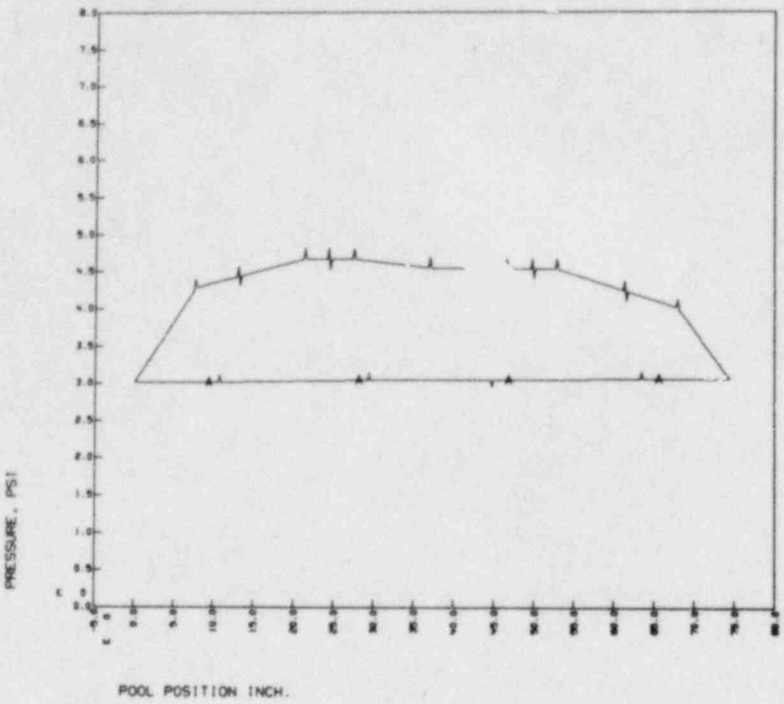

TEST131 TRAPEZOID FIT PRESSURE PROFILE PLANE11 T2
FILE(S):POOL.MRK (A)-ULLAGE.MRK

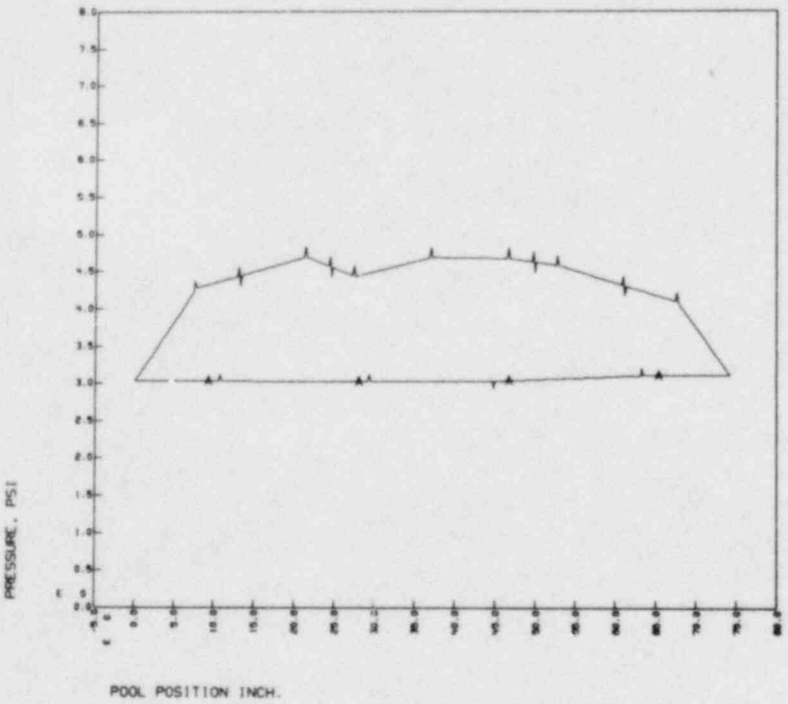

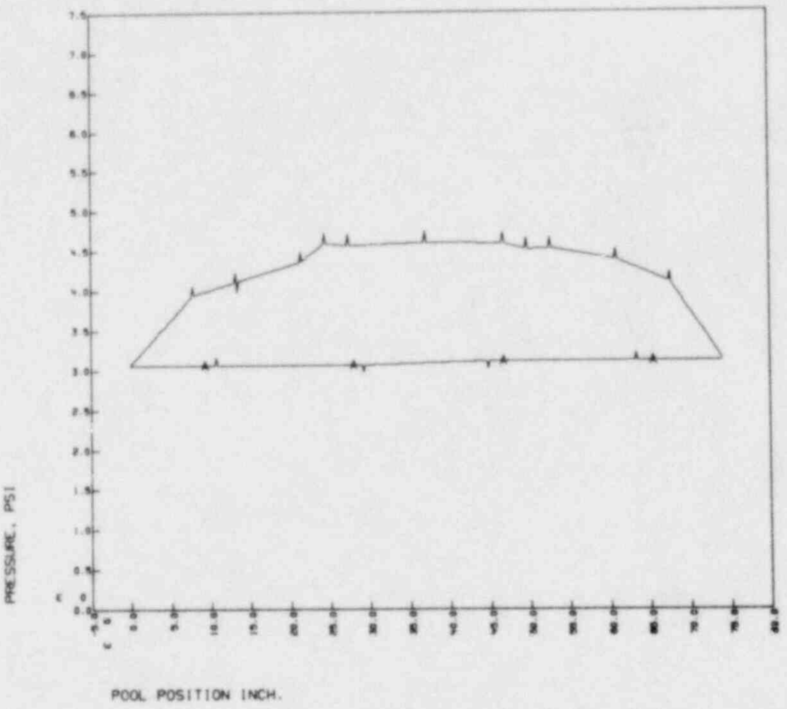

TEST131 TRAPEZOID FIT PRESSURE PROFILE PLANE2D T2

FILE(S):POOL.MRK (A)-ULLAGE.MRK

TEST131 TRAPEZOID FIT PRESSURE PROFILE PLANE4 T3
FILE(S):POOL.MRK (A)-ULLAGE.MRK

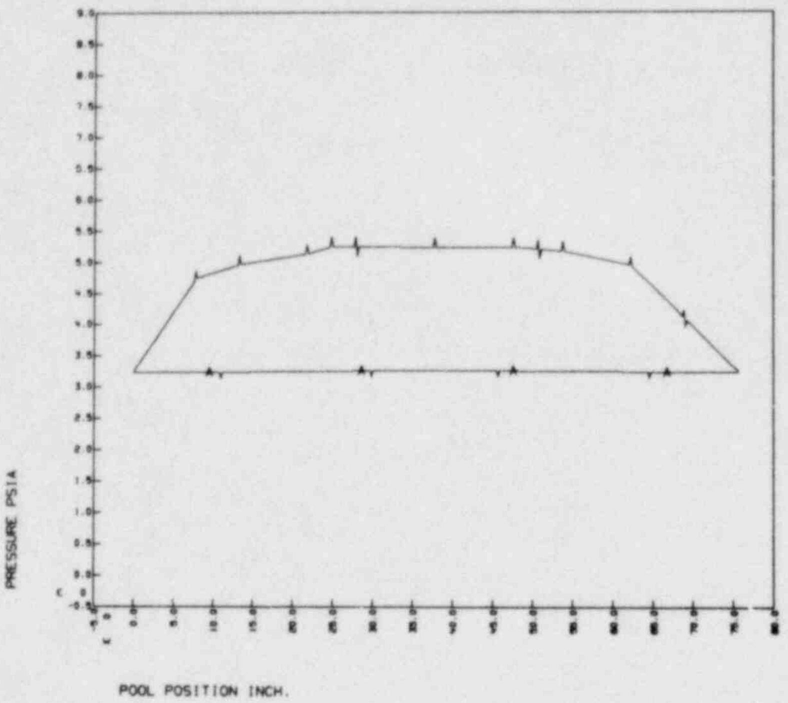

TEST131 TRAPEZOID FIT PRESSURE PROFILE PLANE6 T3
FILE(S):POOL.MRK (A)-ULLAGE.MRK

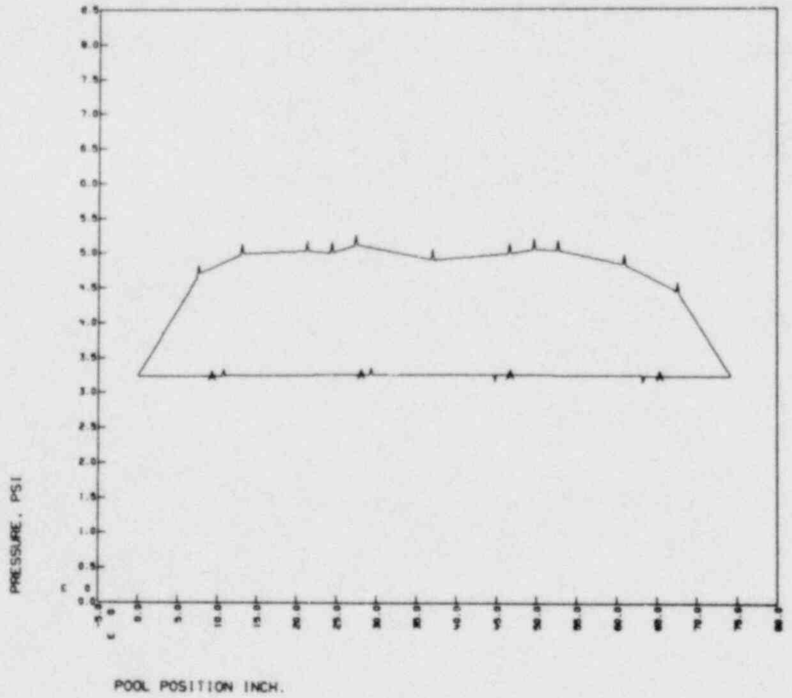

TEST131 TRAPEZOID FIT PRESSURE PROFILE PLANE9 T3
FILE(S):POOL.MRK (A)-ULLAGE.MRK

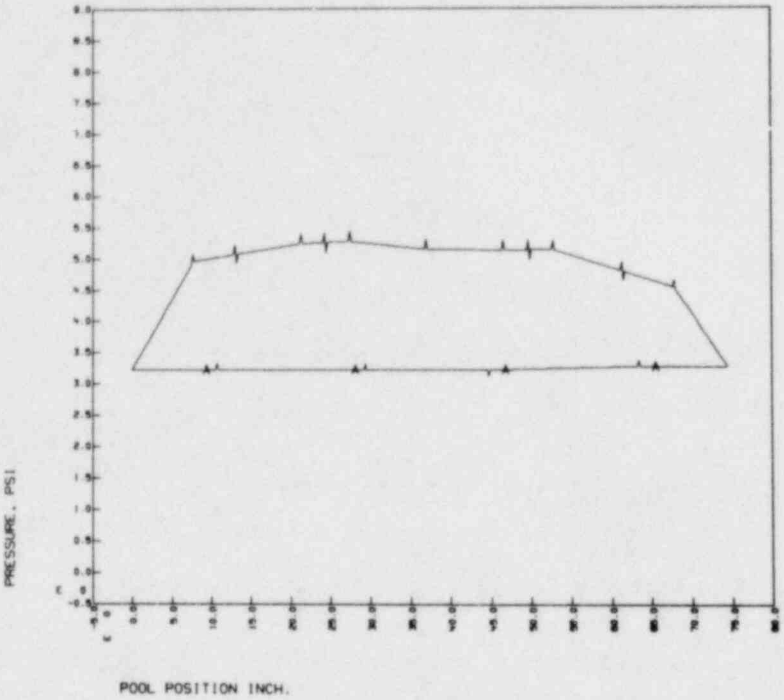

TEST131 TRAPEZOID FIT PRESSURE PROFILE PLANE11 T3
FILE(S):POOL.MRK (A)-ULLAGE.MRK

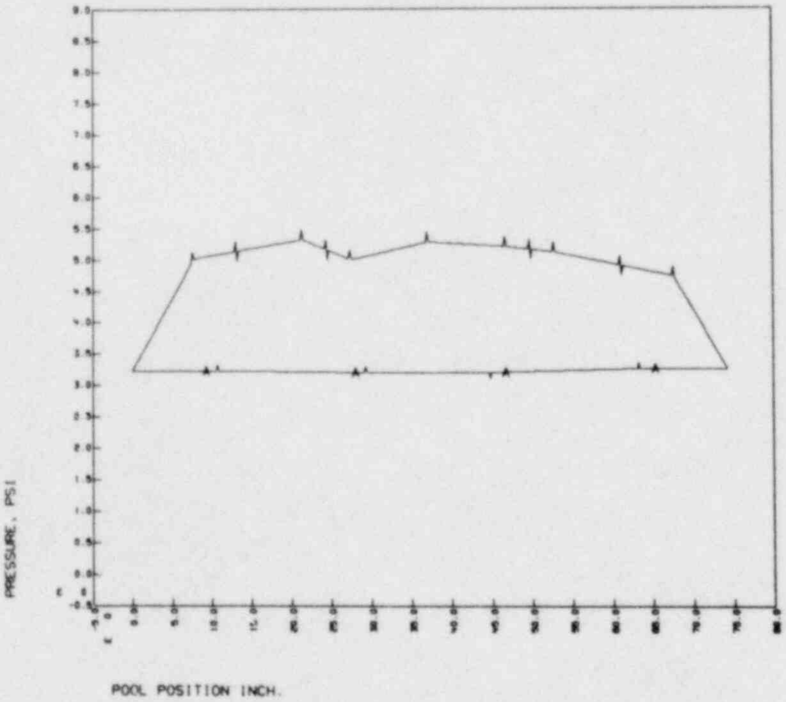

TEST131 TRAPEZOID FIT PRESSURE PROFILE PLANE2D T3
FILE(S):POOL.MRK (A)-ULLAGE.MRK

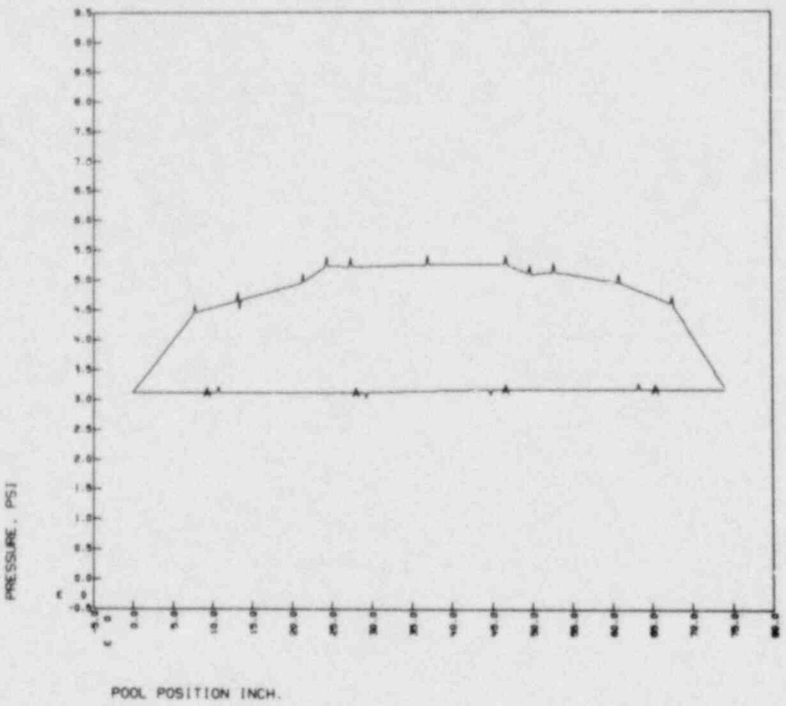

TEST131 TRAPEZOID FIT PRESSURE PROFILE PLANE4 T4, AT MAX UPLOAD
FILE(S):POOL.MRK (A)-ULLAGE.MRK

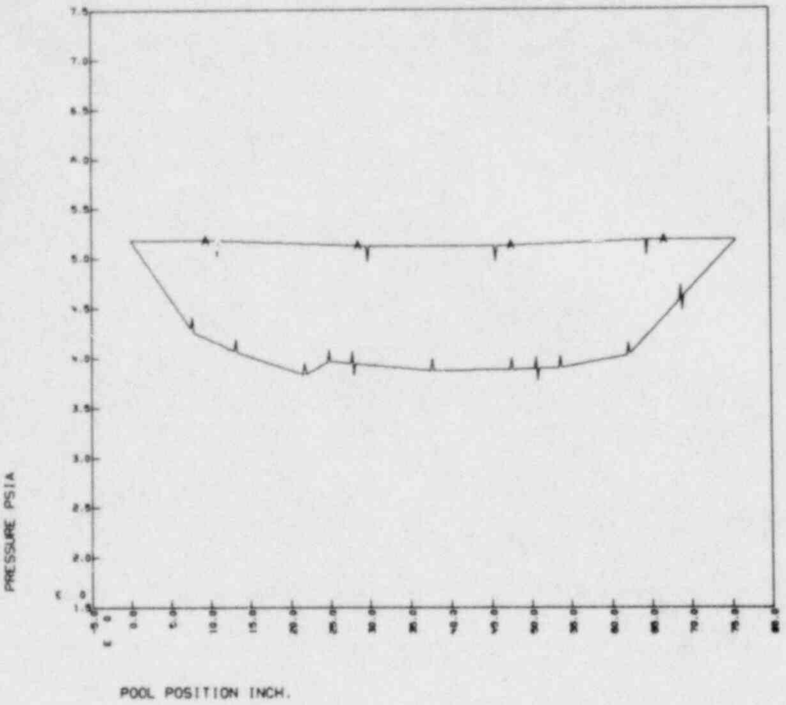

TEST131 TRAPEZOID FIT PRESSURE PROFILE PLANE6 T4, AT MAX UPLOAD
FILE(S):POOL.MRK (A)-ULLAGE.MRK

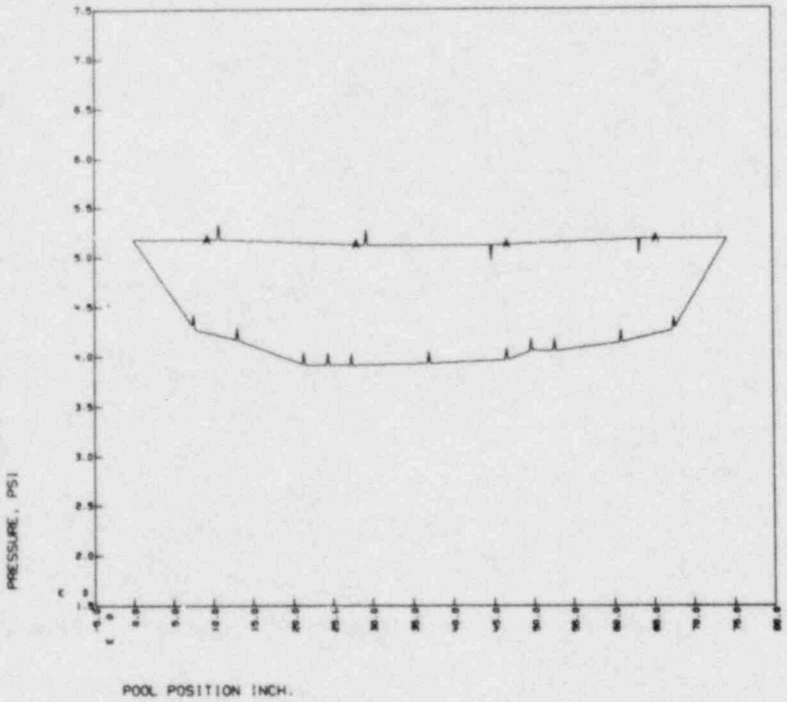

TEST:31 TRAPEZOID FIT PRESSURE PROFILE PLANE9 T4, AT MAX UPLOAD
FILE(S):POOL.MRK (A)-ULLAGE.MRK

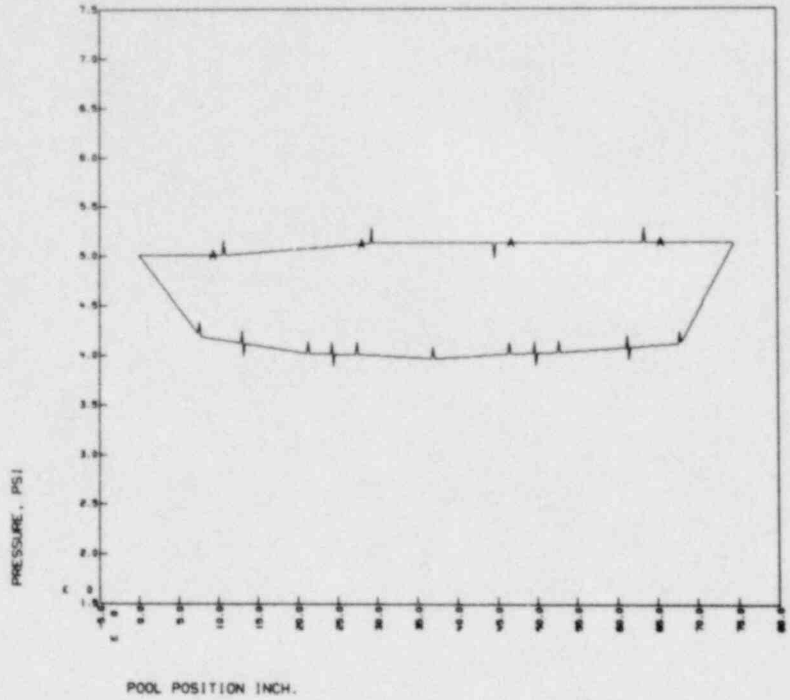

TEST:31 TRAPEZOID FIT PRESSURE PROFILE PLANE11 T4, AT MAX UPLOAD
FILE(S):POOL.MRK (A)-ULLAGE.MRK

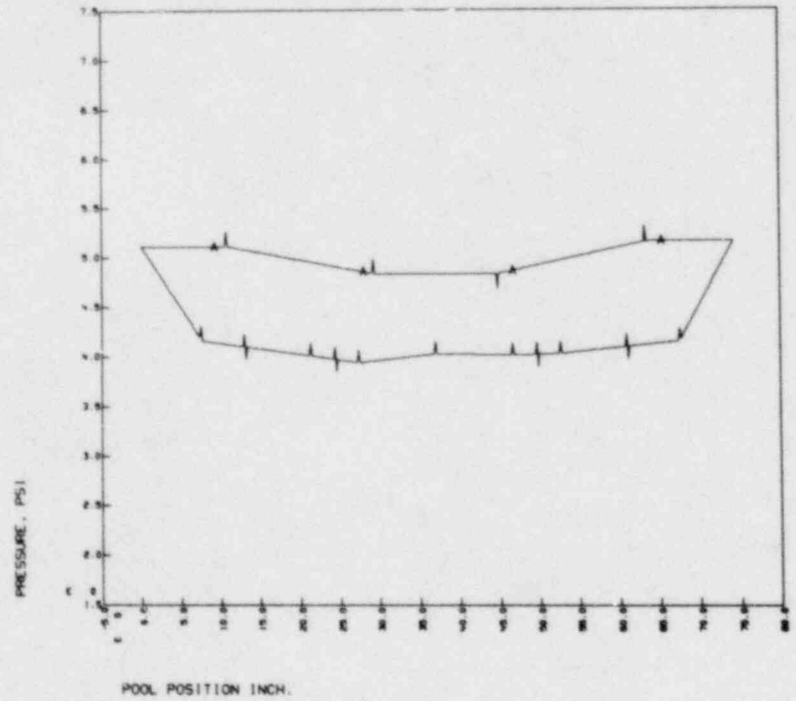

TEST(3) TRAPEZOID FIT PRESSURE PROFILE PLANE2D T4, AT MAX UPLOAD
FILE(S):POOL.MRK (A)-ULLAGE.MRK

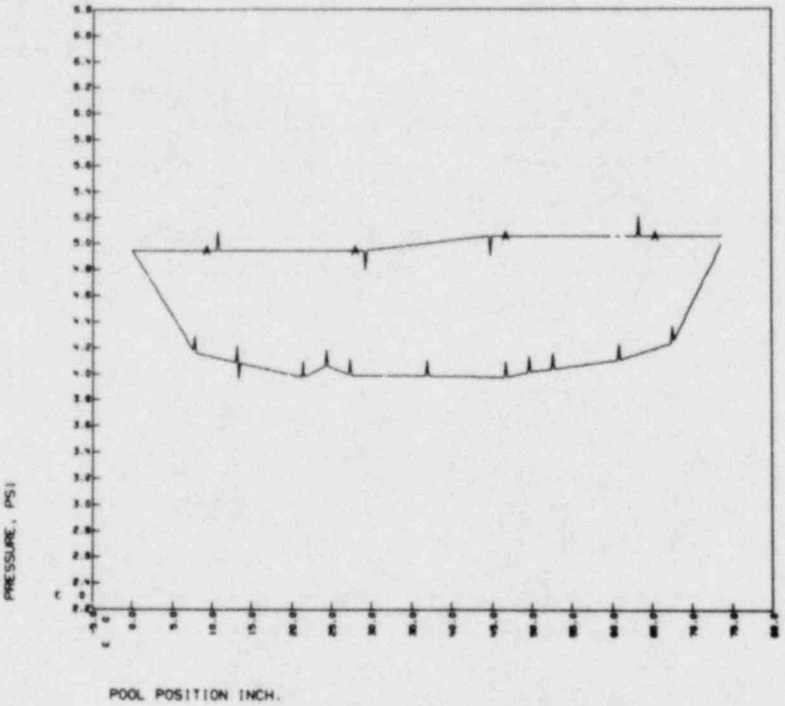

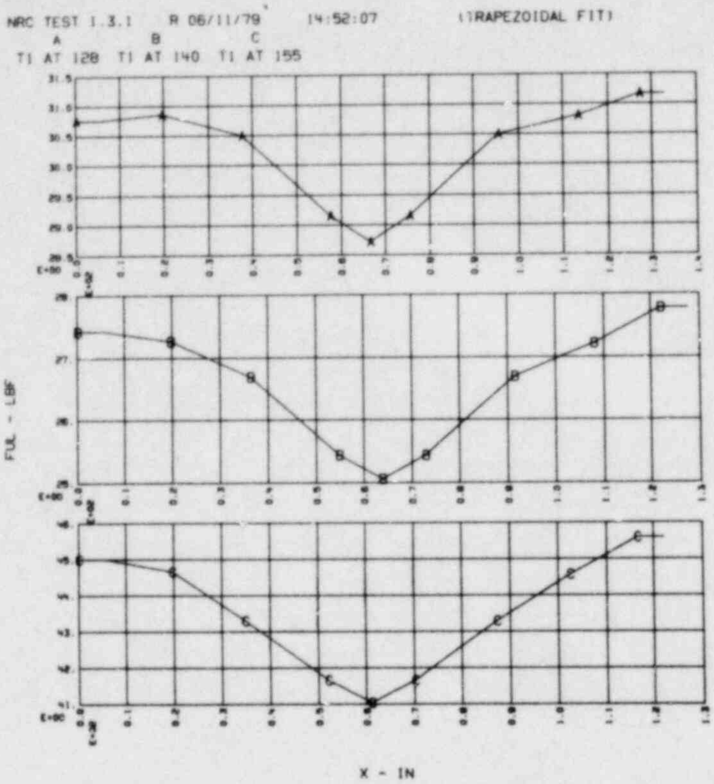
NRC TEST 1.3.1 R 06/11/79 14:52:07 (TRAPEZOIDAL FIT)
A B C
T1 AT 128 T1 AT 140 T1 AT 155
31.5
31.0
30.5
30.0
29.5
29.0
28.5
28
27.
26.
25.
46.
45.
44.
43.
42.
41.
E+00
E-02
0.0
0.1
0.2
0.3
0.4
0.5
0.6
0.7
0.8
0.9
1.0
1.1
1.2
1.3
FUL - LBF
X - IN

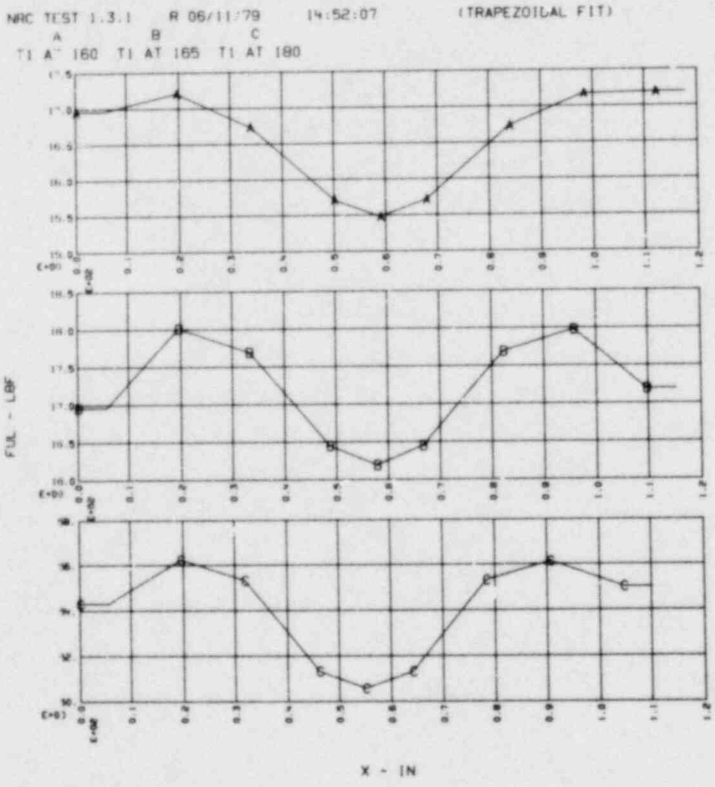
NRC TEST 1.3.1 R 06/11/79 14:52:07 (TRAPEZOIDAL FIT)
A B C
T1 AT 160 T1 AT 165 T1 AT 180
17.5
17.0
16.5
16.0
15.5
15.0
18.5
18.0
17.5
17.0
16.5
16.0
58.
56.
54.
52.
50.
E+00
E-02
0.0
0.1
0.2
0.3
0.4
0.5
0.6
0.7
0.8
0.9
1.0
1.1
1.2
FUL - LBF
X - IN

NRC TEST 1.3.1 R 06/11/79 14:52:07
A B C
TI AT 195 TI AT 200 TI AT 205

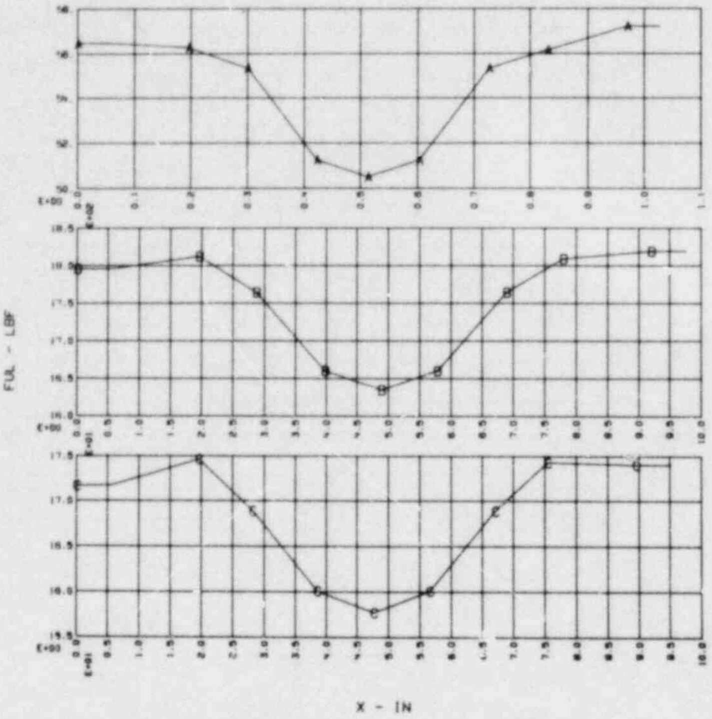

NRC TEST 1.3.1 R 06/11/79 14:52:07 (TRAPEZOIDAL FIT)
A B C
TI AT 220 TI AT 235 TI AT 269

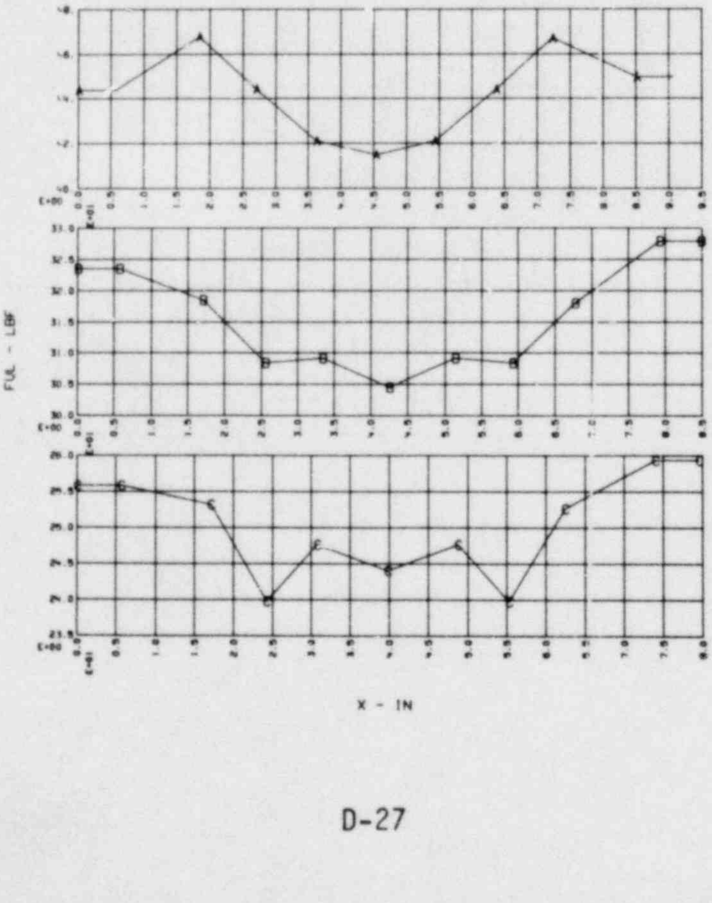

NRC TEST 1.3.1   R 06/11/79   14:52:07   (TRAPEZOIDAL FIT)
A B C
TI AT 345 TI AT 278 TI AT 348

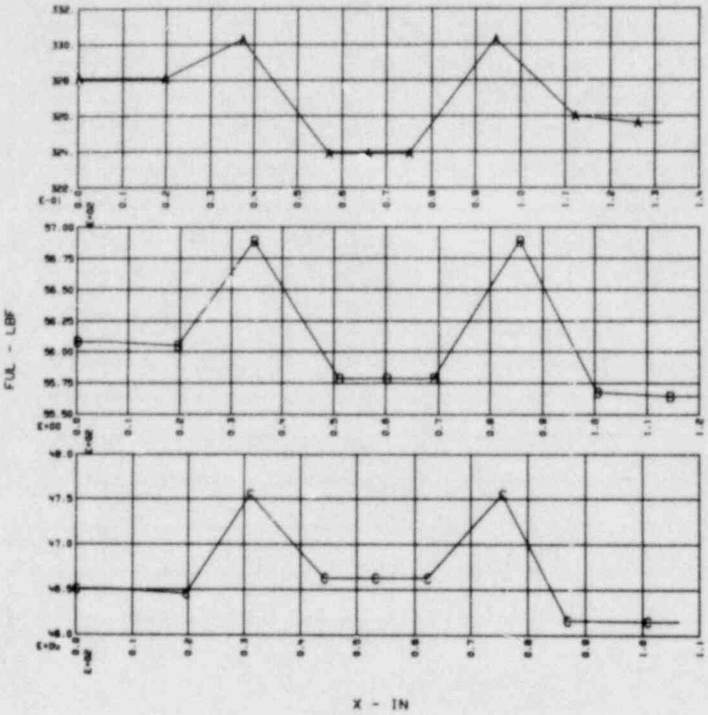

NRC TEST 1.3.1   R 06/11/79   14:52:08   (TRAPEZOIDAI FIT)
A B
TI AT 315 TI AT 270

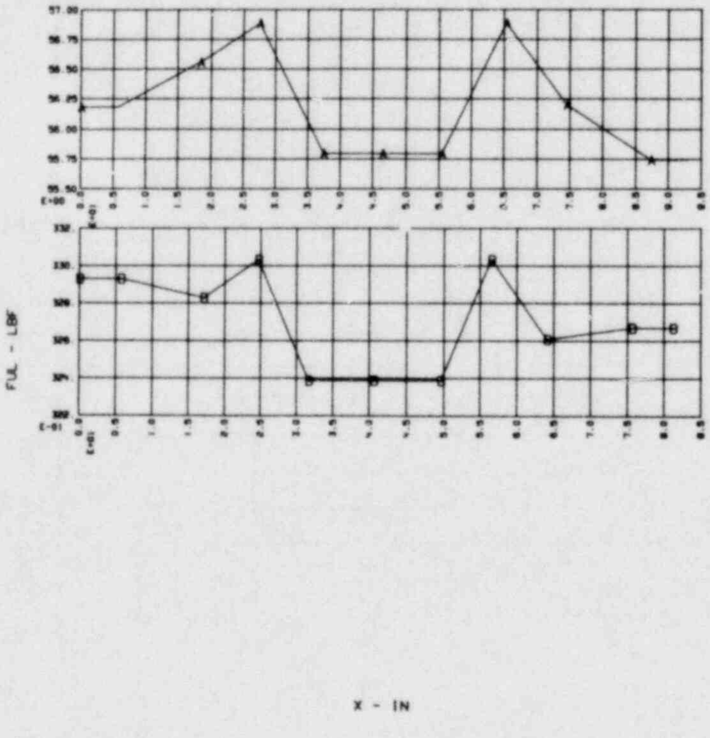

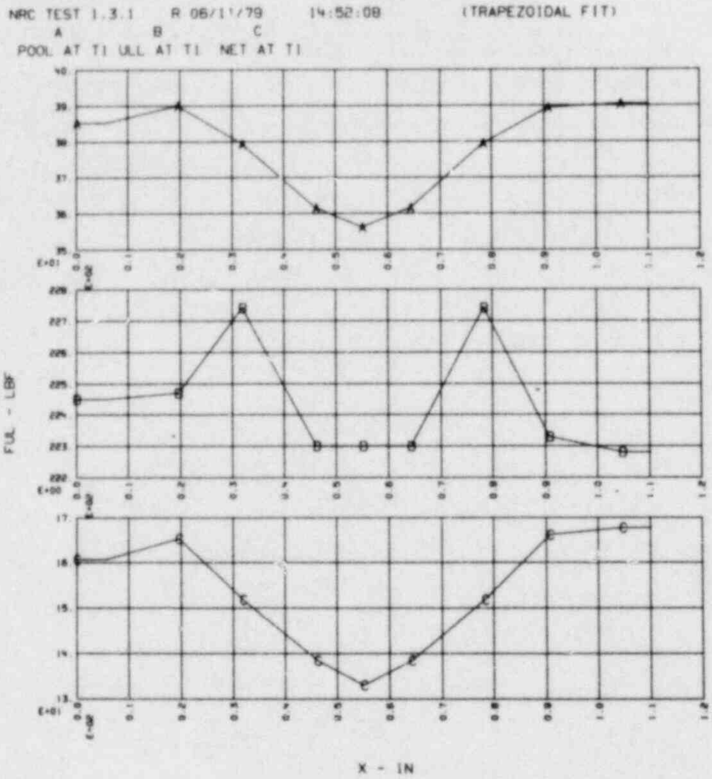
NRC TEST 1.3.1 R 06/11/79 14:52:08 (TRAPEZOIDAL FIT)
A B C
POOL AT TI ULL AT TI NET AT TI
40.
39.
38.
37.
36.
35.
E+01
228.
227.
226.
225.
224.
223.
222.
E+00
17.
16.
15.
14.
13.
E+01
0.0
0.1
0.2
0.3
0.4
0.5
0.6
0.7
0.8
0.9
1.0
1.1
1.2
FUL - LBF
X - IN

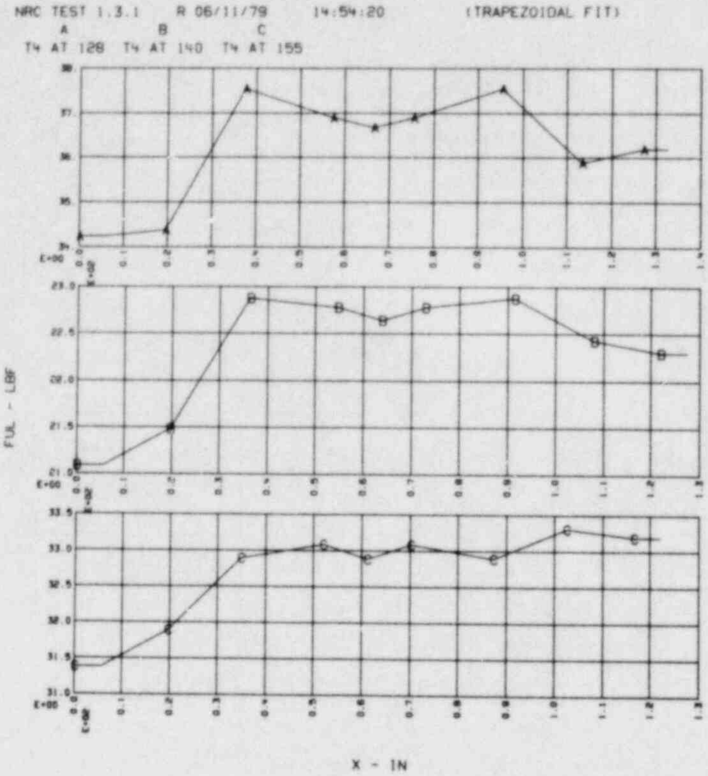
NRC TEST 1.3.1 R 06/11/79 14:54:20 (TRAPEZOIDAL FIT)
A B C
T4 AT 128 T4 AT 140 T4 AT 155
38.
37.
36.
35.
34.
E+00
E-02
23.0
22.5
22.0
21.5
21.0
33.5
33.0
32.5
32.0
31.5
31.0
0 0.1 0.2 0.3 0.4 0.5 0.6 0.7 0.8 0.9 1.0 1.1 1.2 1.3
FUL - LBF
X - IN

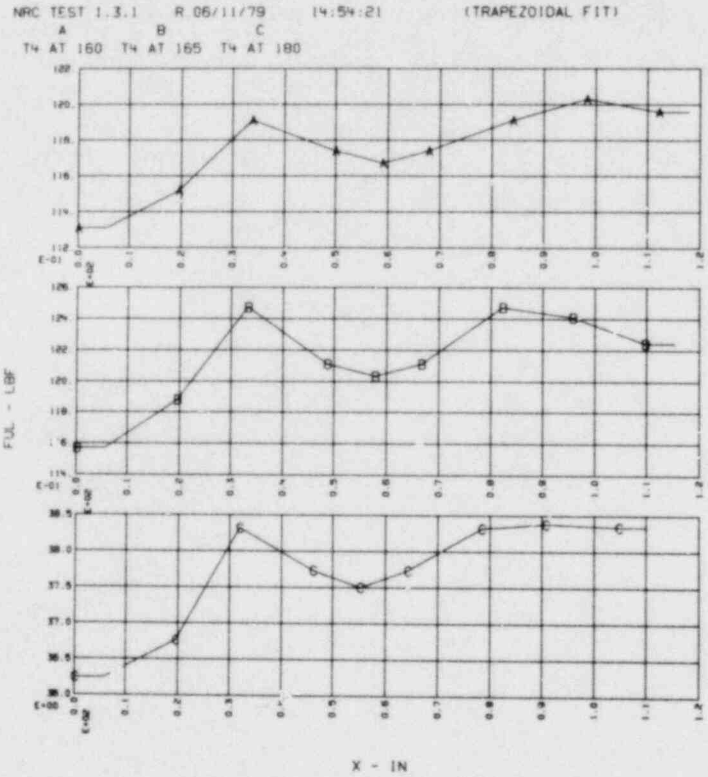
NRC TEST 1.3.1 R 06/11/79 14:54:21 (TRAPEZOIDAL FIT)
A B C
T4 AT 160 T4 AT 165 T4 AT 180
122
120.
118
116
114
112
E-01
E-02
126
124
122
120.
118
116
114
38.5
38.0
37.5
37.0
36.5
36.0
E+00
0 0.1 0.2 0.3 0.4 0.5 0.6 0.7 0.8 0.9 1.0 1.1 1.2
FUL - LBF
X - IN

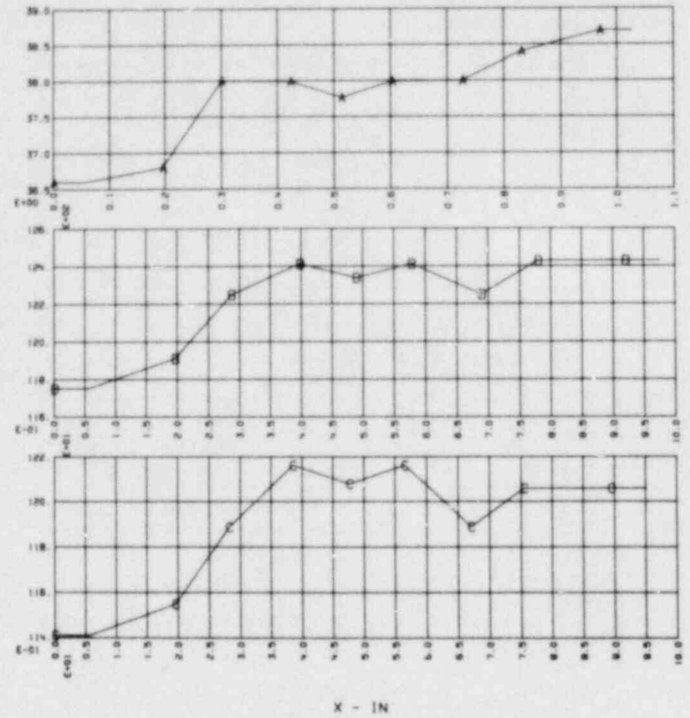

NRC TEST 1.3.1 R 06/11/79 14:54:21 (TRAPEZOIDAL FIT)
A B C
T4 AT 195 T4 AT 200 T4 AT 205

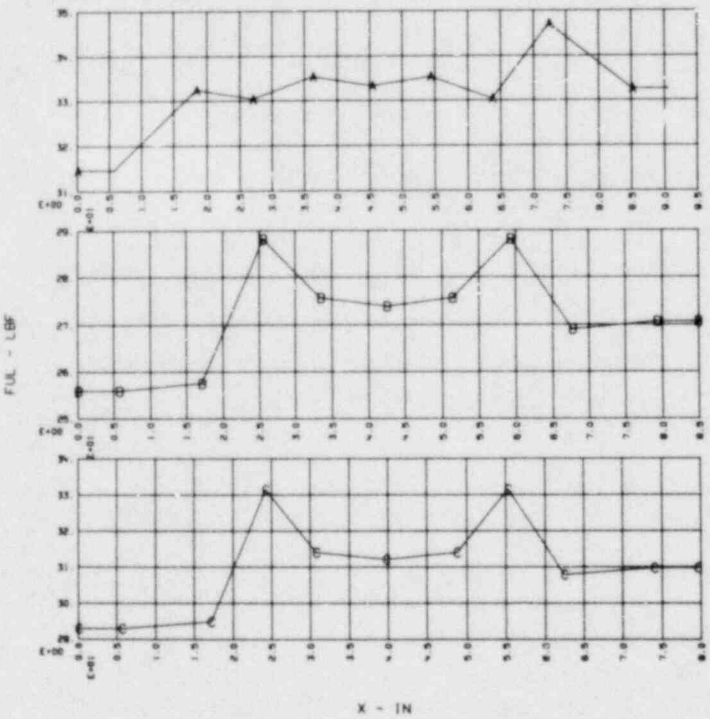

NRC TEST 1.3.1 R 06/11/79 14:54:21 (TRAPEZOIDAL FIT)
A B C
T4 AT 220 T4 AT 235 T4 AT 269

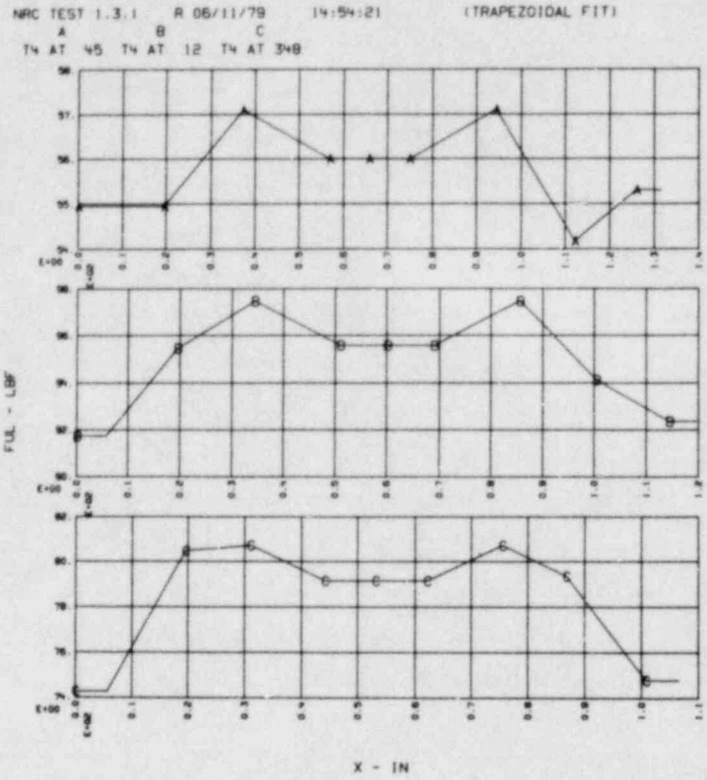
NRC TEST 1.3.1 R 06/11/79 14:54:21 (TRAPEZOIDAL FIT)
A
B
C
T4 AT 45
T4 AT 12
T4 AT 348
FUL - LBF
X - IN
E+00
E-02

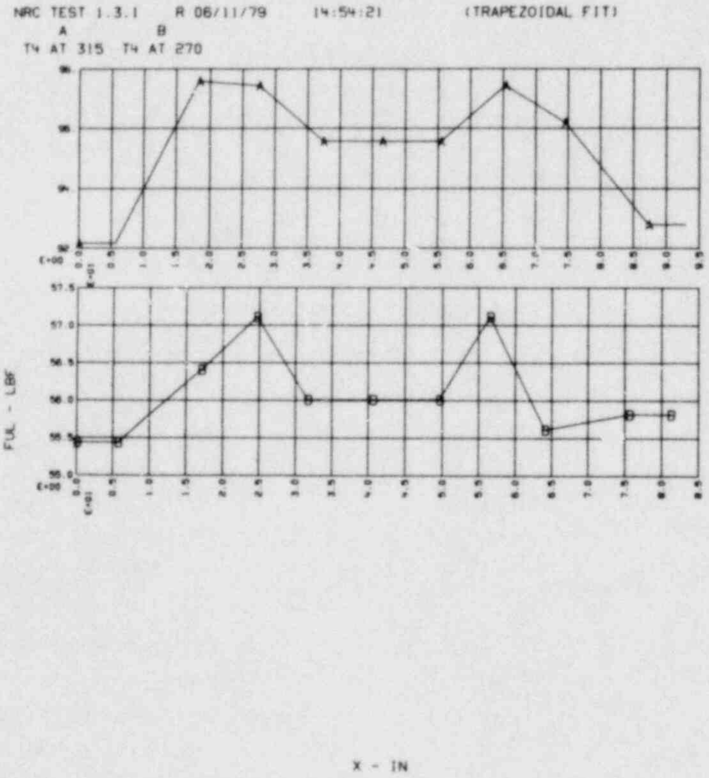
NRC TEST 1.3.1 R 06/11/79 14:54:21 (TRAPEZOIDAL FIT)
A
B
T4 AT 315
T4 AT 270
FUL - LBF
X - IN
E+00
E-01
57.5
57.0
56.5
56.0
55.5
55.0

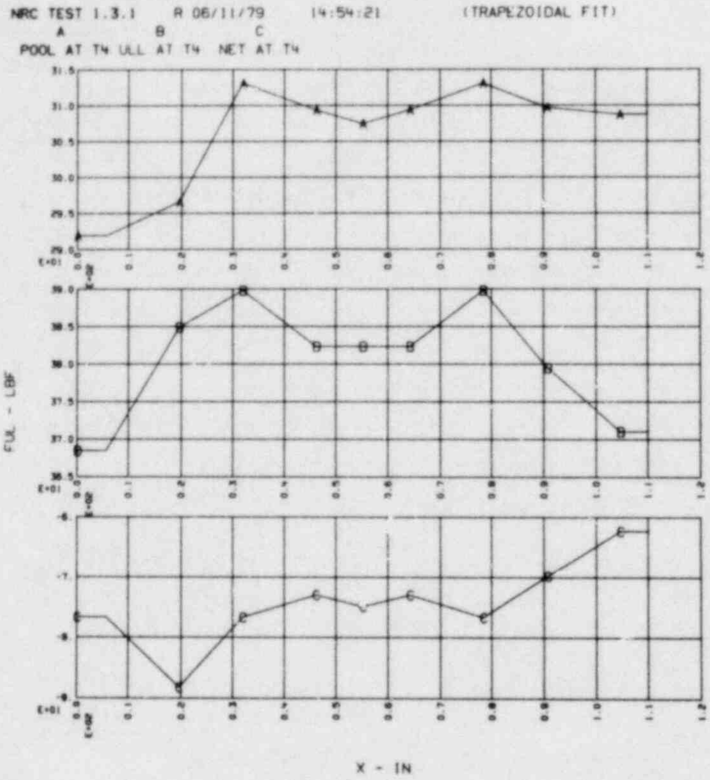
NRC TEST 1.3.1 R 06/11/79 14:54:21 (TRAPEZOIDAL FIT)
A B C
POOL AT T4 ULL AT T4 NET AT T4
31.5
31.0
30.5
30.0
29.5
29.0
39.0
38.5
38.0
37.5
37.0
36.5
-6.
-7.
-8.
-9.
E+01
E-02
0.0
0.1
0.2
0.3
0.4
0.5
0.6
0.7
0.8
0.9
1.0
1.1
1.2
FUL - LBF
X - IN

D.2 HVLF CHARACTERIZATION DATA

(Parabolic Interpolation)
Test 1.3.1

```
1        NRC AIR TEST NO. 1.3.1                                              SECOND ORDER
                     FORCE SUMMARY  (MEAN    STANDARD DEVIATION)

         45 DEGREE SECTOR - 3D
                            T1                  T2                  T3                  T4
         TIME,SECONDS   3.1126E+00          3.1269E+00          3.1470E+00          3.2472E+00

         POOL          -40773.   111.4    -35048.   109.6    -39261.   103.0    -32387.    19.3

         ULLAGE         23892.    69.7     24401.    81.9     25808.   106.9     40617.   401.8

         NET           -16882.   131.5    -10647.   136.8    -13454.   148.4      8230.   402.2


        7.5 DEGREE SECTOR - 2D
                            T1                  T2                  T3                  T4
         TIME,SECONDS   3.1069E+00          3.1212E+00          3.1327E+00          3.2358E+00

         POOL           -6663.    15.0     -5592.    14.8     -6329.    15.0     -5397.    14.5

         ULLAGE          3935.    11.4      4041.    11.5      4121.    11.6      6562.    12.7

         NET            -2728.    18.8     -1551.    18.8     -2208.    19.0      1164.    19.3


         NET FORCE RATIOS

         3D/2D            1.031  0.011      1.144  0.020      1.016  0.014      1.178  0.061
```

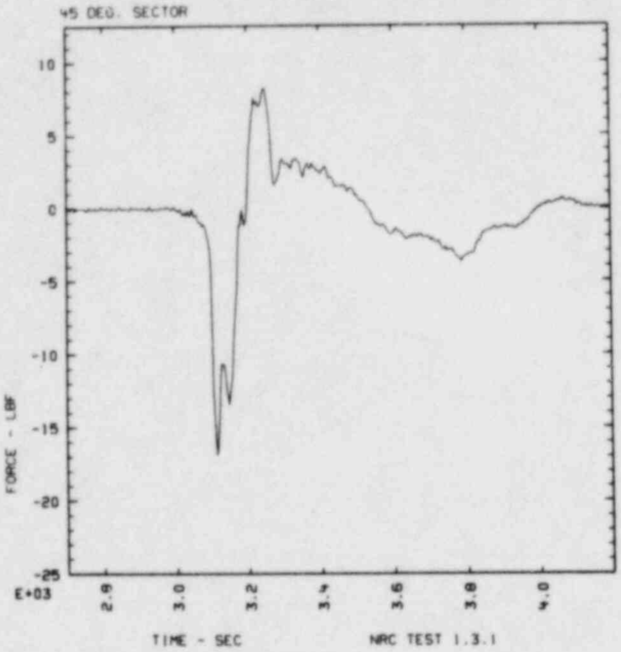
45 DEG. SECTOR
FORCE - LBF
10
5
0
-5
-10
-15
-20
-25
E+03
2.8
3.0
3.2
3.4
3.6
3.8
4.0
TIME - SEC
NRC TEST 1.3.1

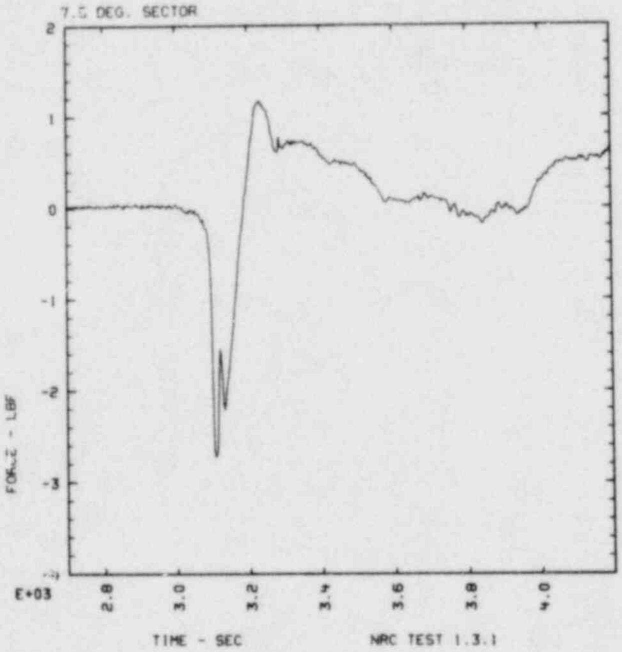
7.5 DEG. SECTOR
FORCE - LBF
2
1
0
-1
-2
-3
-4
E+03
2.8
3.0
3.2
3.4
3.6
3.8
4.0
TIME - SEC
NRC TEST 1.3.1

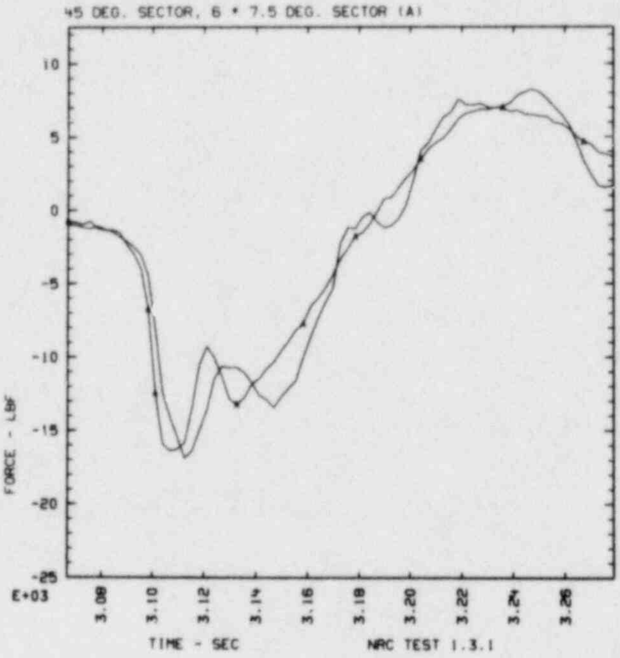
45 DEG. SECTOR, 6 * 7.5 DEG. SECTOR (A)
10
5
0
-5
-10
-15
-20
-25
FORCE - LBF
E+03
3.08
3.10
3.12
3.14
3.16
3.18
3.20
3.22
3.24
3.26
TIME - SEC
NRC TEST 1.3.1

NRC TEST NO. 131 SEC. ORDER FIT - FUL IN POOL AT T1 -
FILE(S):T1.P131

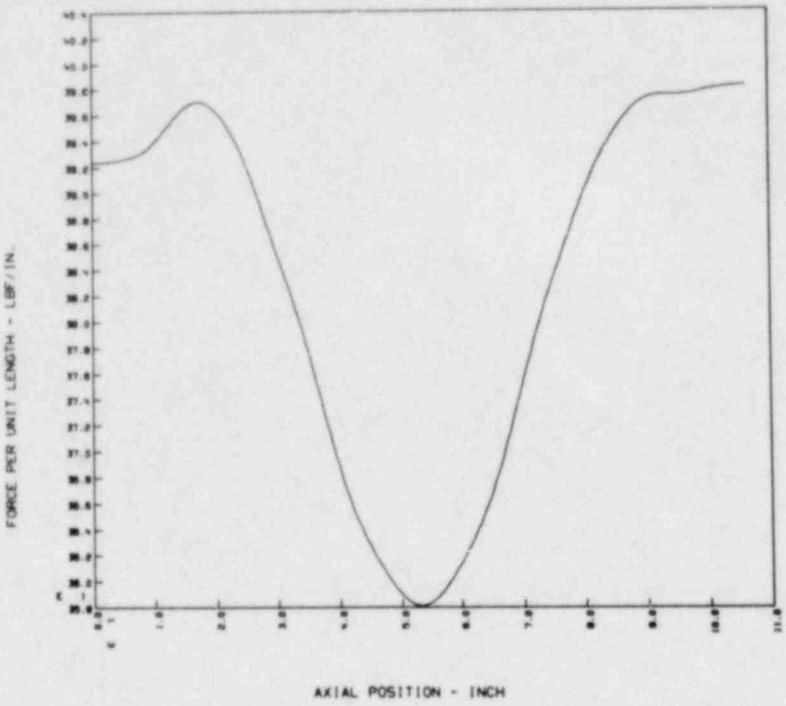

NRC TEST NO. 131 SEC. ORDER FIT - FUL IN ULLAGE AT T1 -
FILE(S):T1.U131

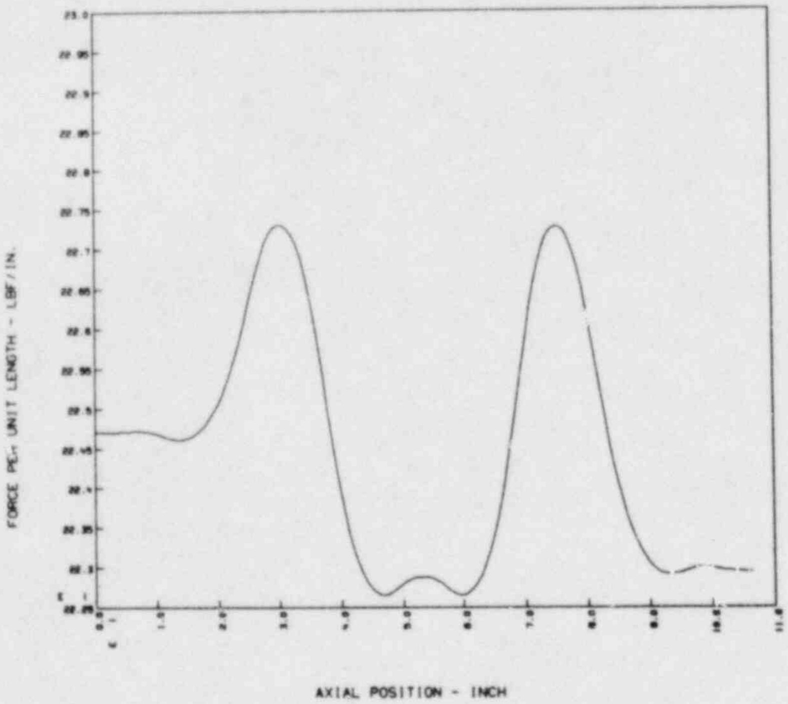

NRC TEST NO. 131 SEC. ORDER FIT - NET 3D FUL AT T1 -
FILE(S):T1.N131

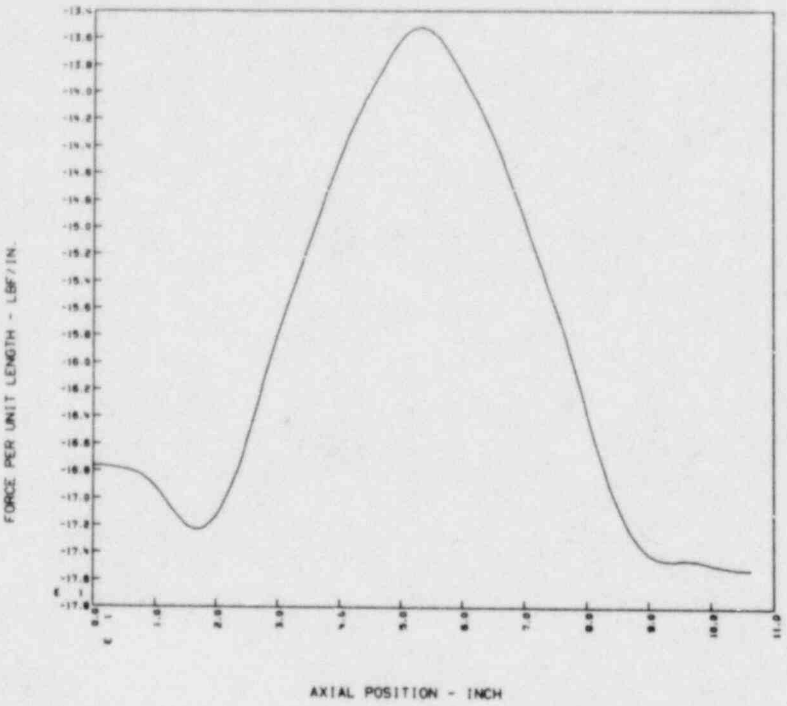

NRC TEST NO. 131 SEC. ORDER FIT - FUL IN POOL AT T2 -
FILE(S):T2.P131

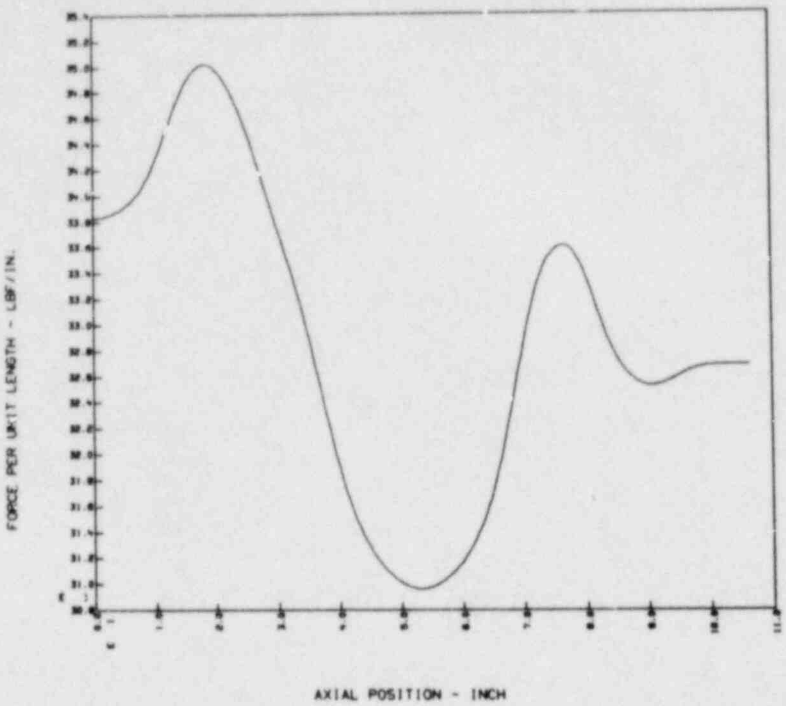

NRC TEST NO. 131 SEC. ORDER FIT - FUL IN ULLAGE AT T2 -
FILE(S):T2.U131

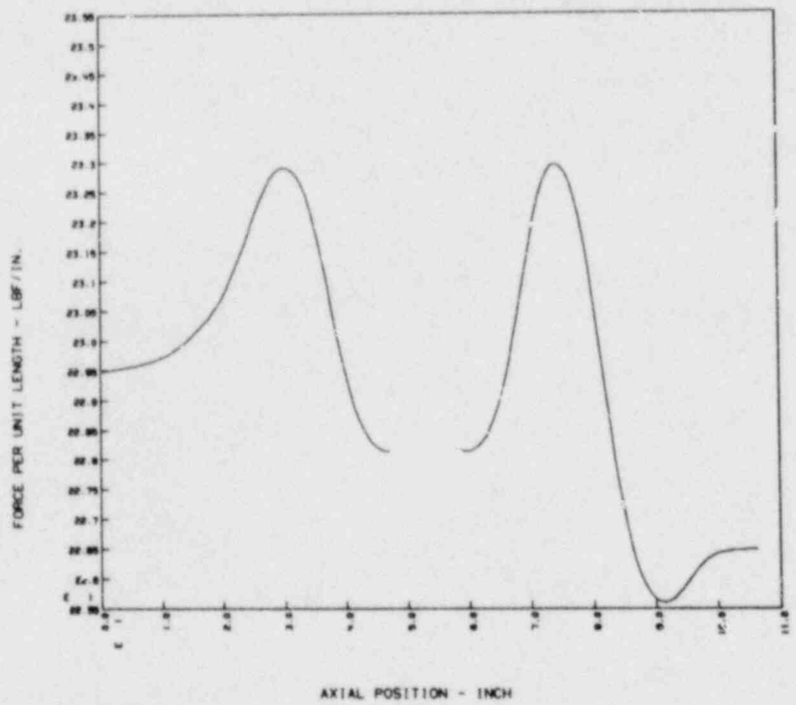

NRC TEST NO. 131 SEC. ORDER FIT - NET 3D FUL AT T2 -
FILE(S):T2.N131

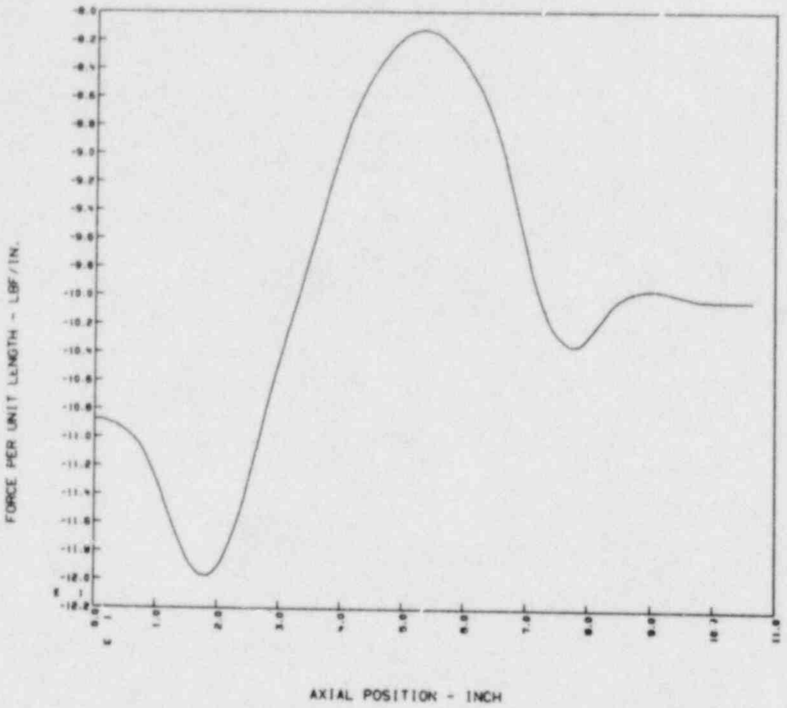

NRC TEST NO. 131 SEC. ORDER FIT - FUL IN POOL AT T3 -
FILE(S):T3.P131

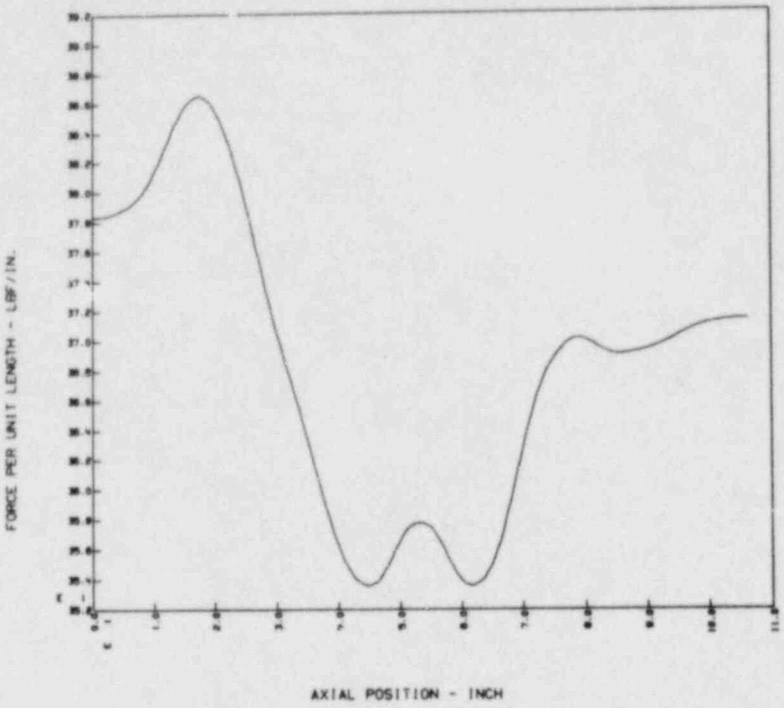

NRC TEST NO. 131 SEC. ORDER FIT - FUL IN ULLAGE AT T3 -
FILE(S):T3.U131

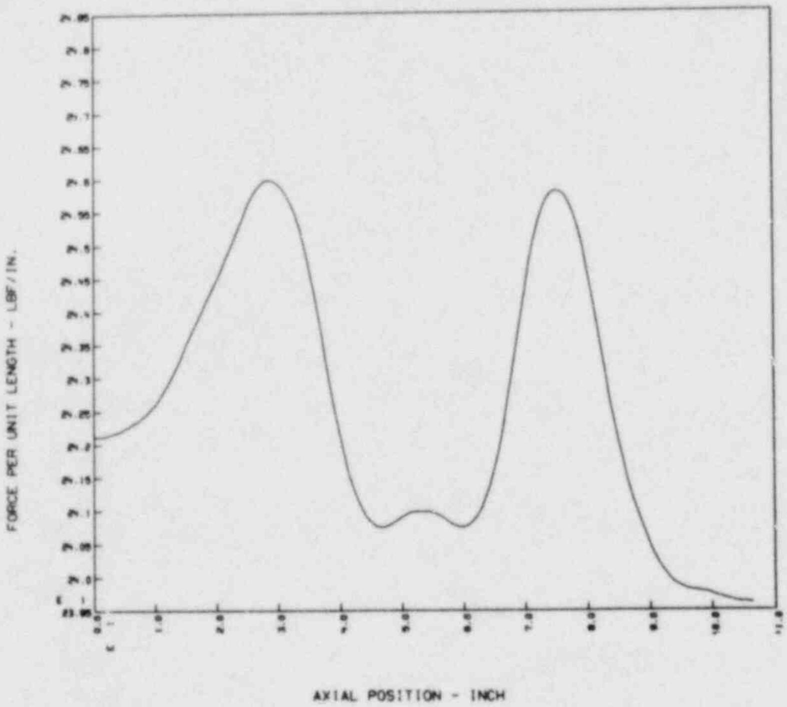

NRC TEST NO. 131 SEC. ORDER FIT - NET 3D FUL AT T3 -
FILE(S):T3.N131

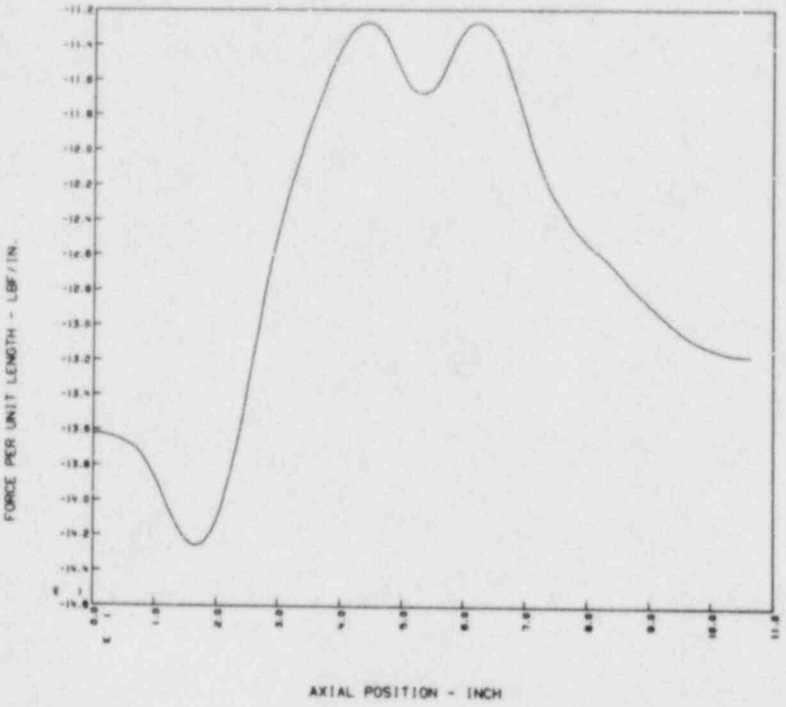

NRC TEST NO. 131 SEC. ORDER FIT - FUL IN POOL AT T4 -
FILE(S):T4.P131

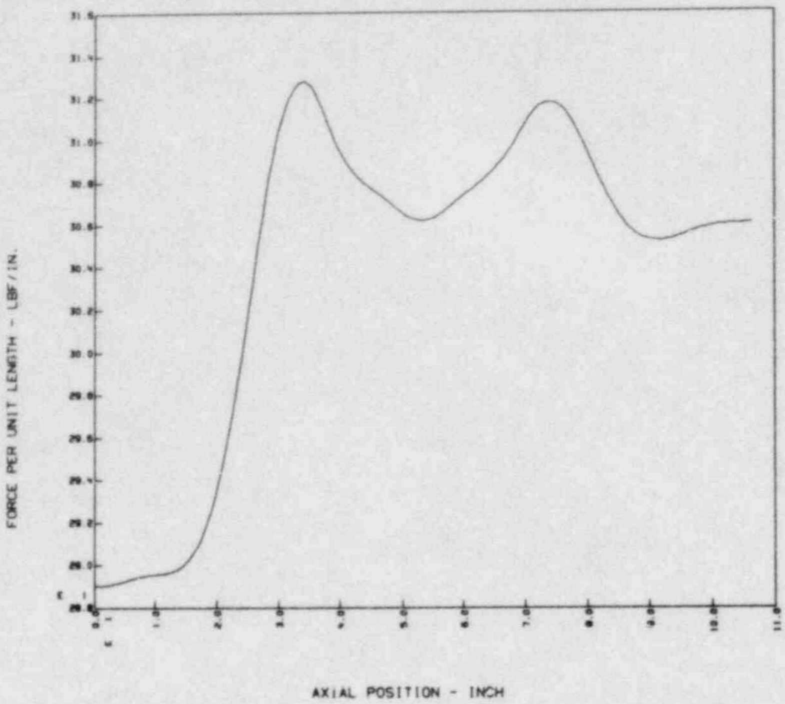

NRC TEST NO. 131 SEC. ORDER FIT - FUL IN ULLAGE AT T4 -
FILE(S):T4.U131

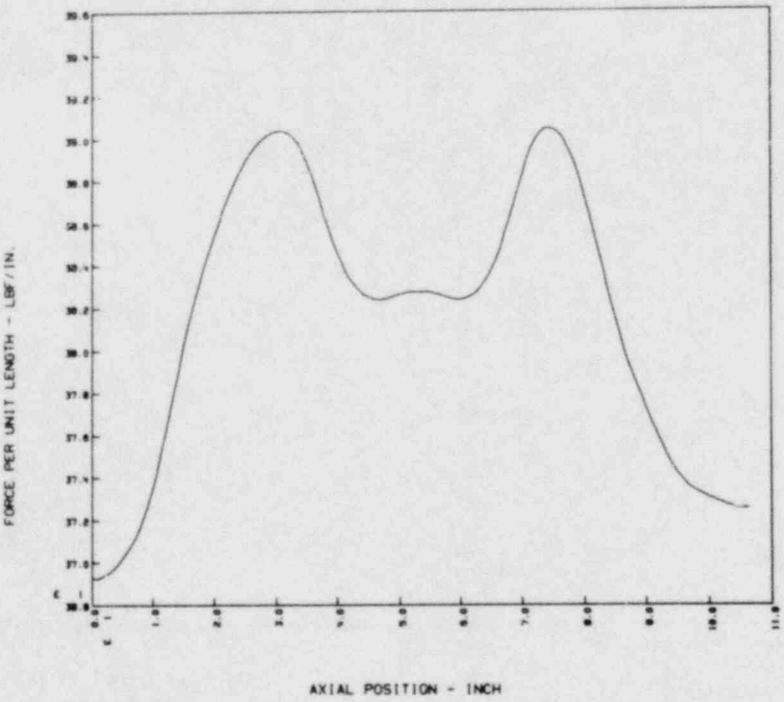

NRC TEST NO. 131 SEC. ORDER FIT - NET 3D FUL AT T4 -
FILE(S):T4.N131

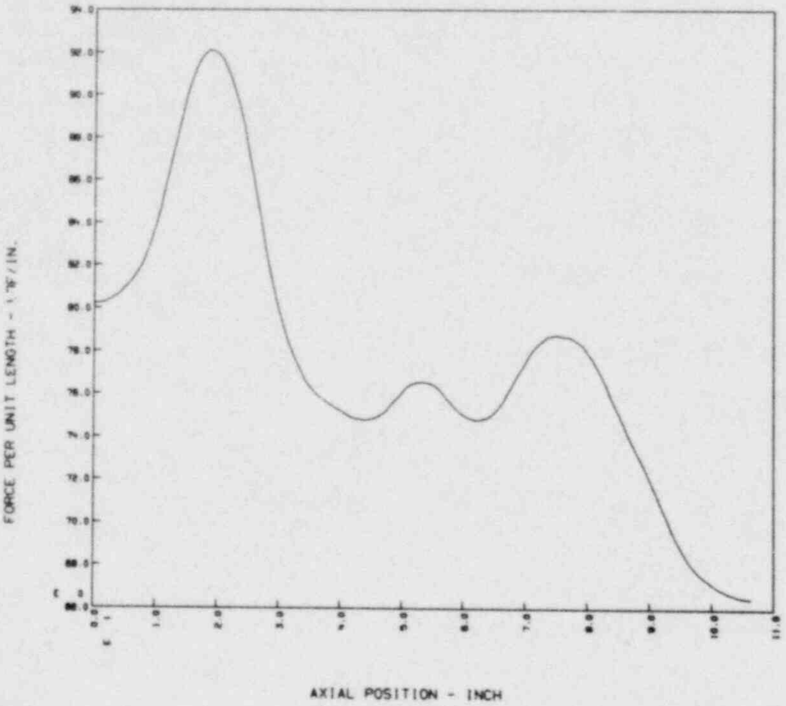

TEST131 SEC. ORDER FIT PRESSURE PROFILE PLANE4 T1, AT MAX DOWNLOAD
FILE(S):POOL.MRK (A)-ULLAGE.MRK

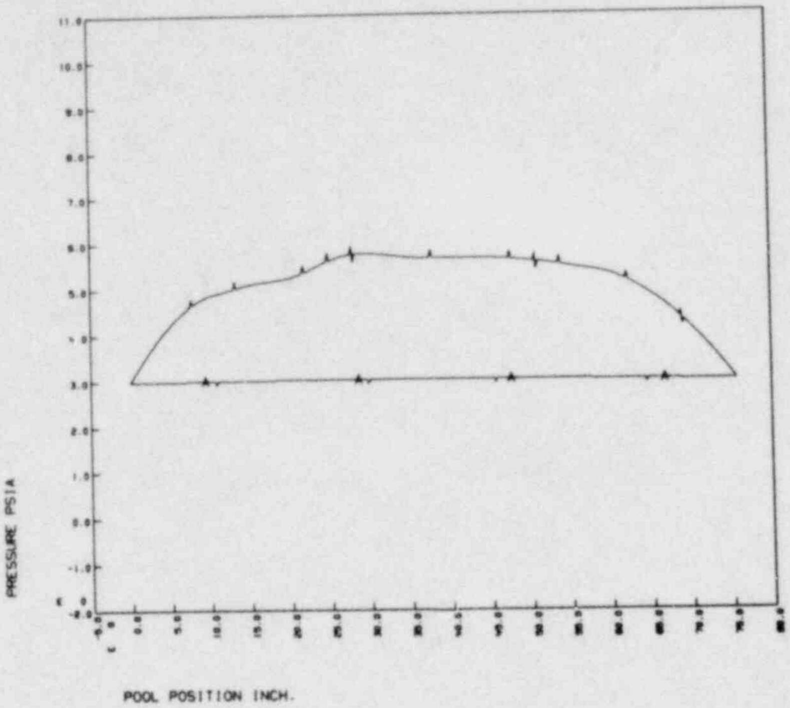

TEST131 SEC. ORDER FIT PRESSURE PROFILE PLANE6 T1, AT MAX DOWNLOAD
FILE(S):POOL.MRK (A)-ULLAGE.MRK

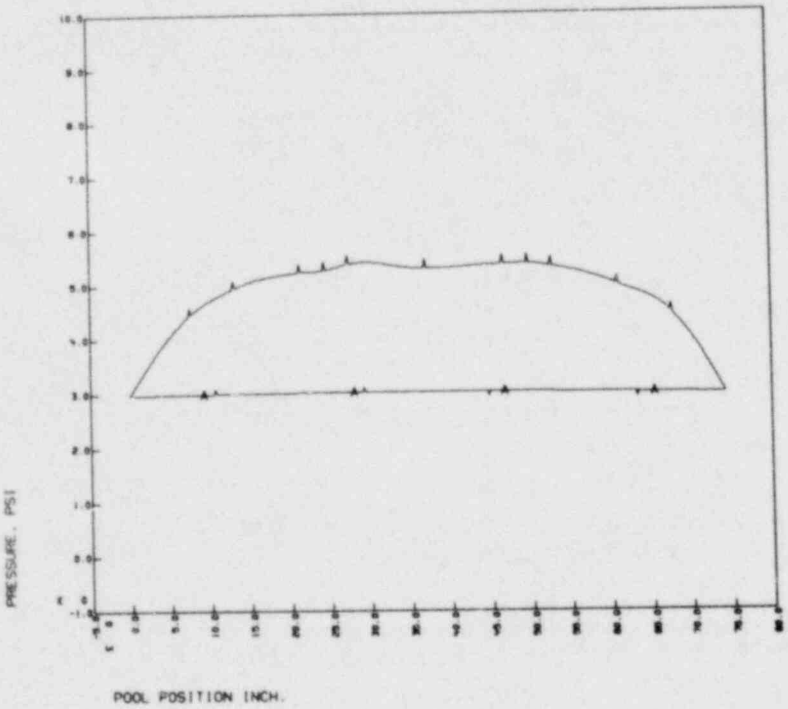

TEST131 SEC. ORDER FIT PRESSURE PROFILE PLANE9 T1, AT MAX DOWNLOAD
FILE(S):POOL.MRK (A)-ULLAGE.MRK

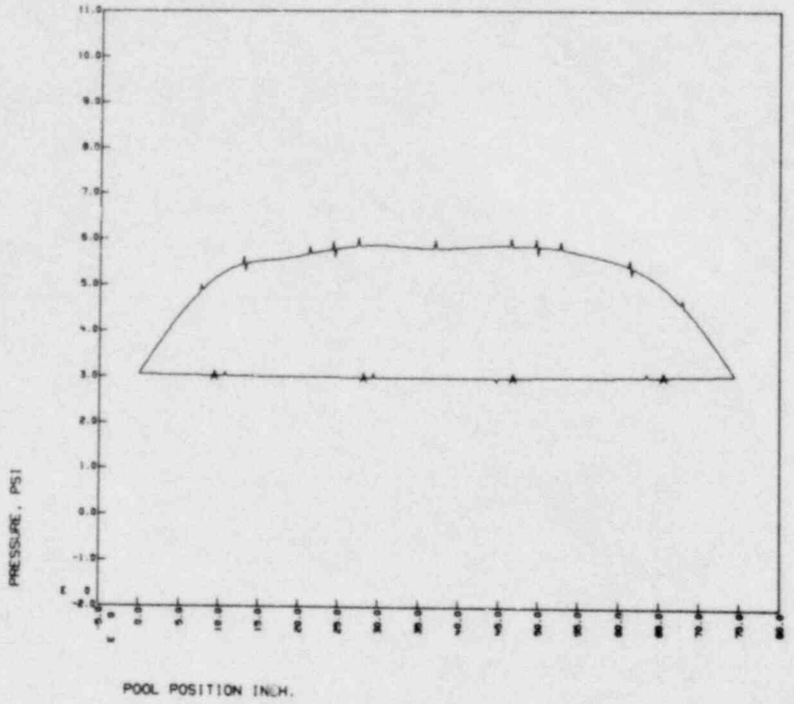

TEST131 SEC. ORDER FIT PRESSURE PROFILE PLANE11 T1, AT MAX DOWNLOAD
FILE(S):POOL.MRK (A)-ULLAGE.MRK

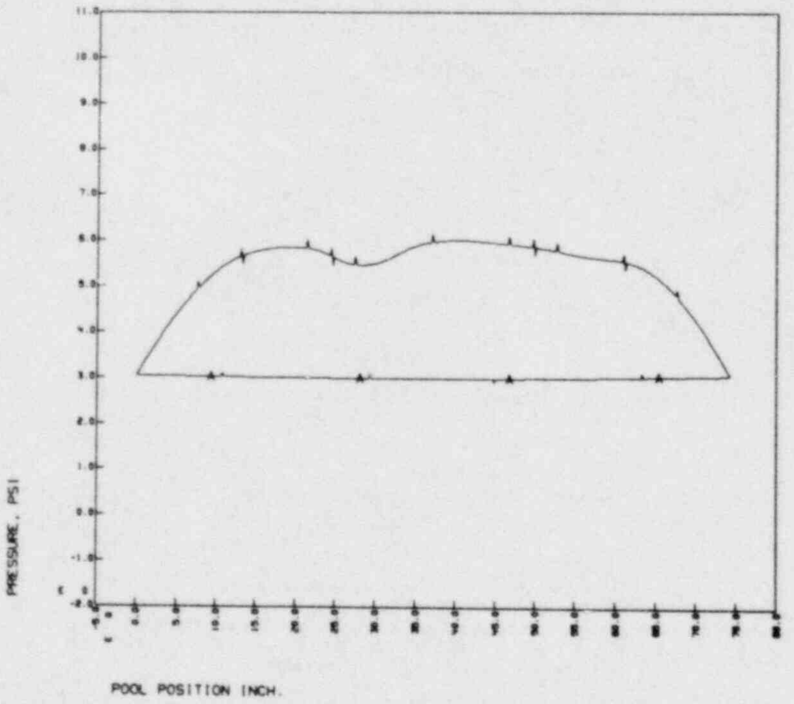

TEST131 SEC. ORDER FIT PRESSURE PROFILE PLANE2D T1, A: MAX DOWNLOAD
FILE(S):POOL.MRK (A)-ULLAGE.MRK

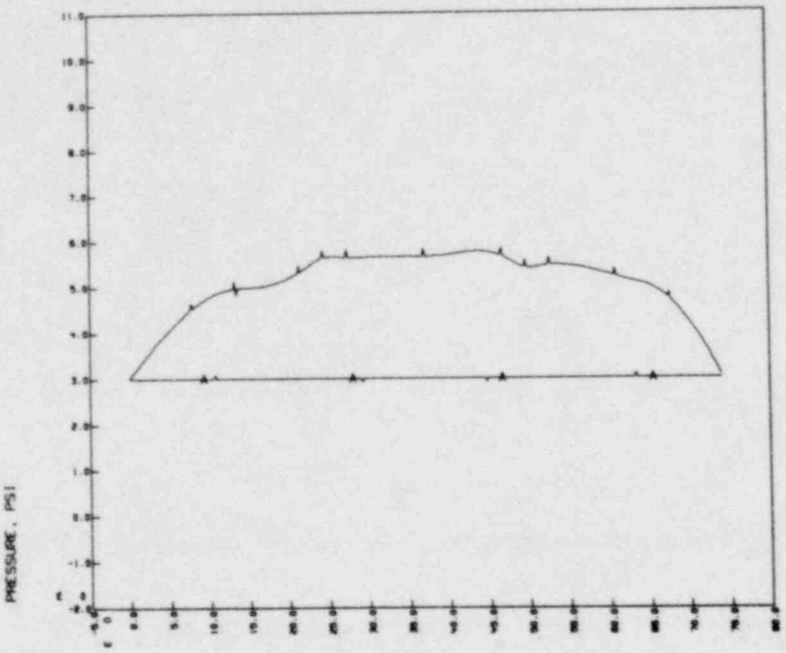

POOL POSITION INCH.

TEST131 SEC. ORDER FIT PRESSURE PROFILE PLANE4 T2
FILE(S):POOL.MRK (A)-ULLAGE.MRK

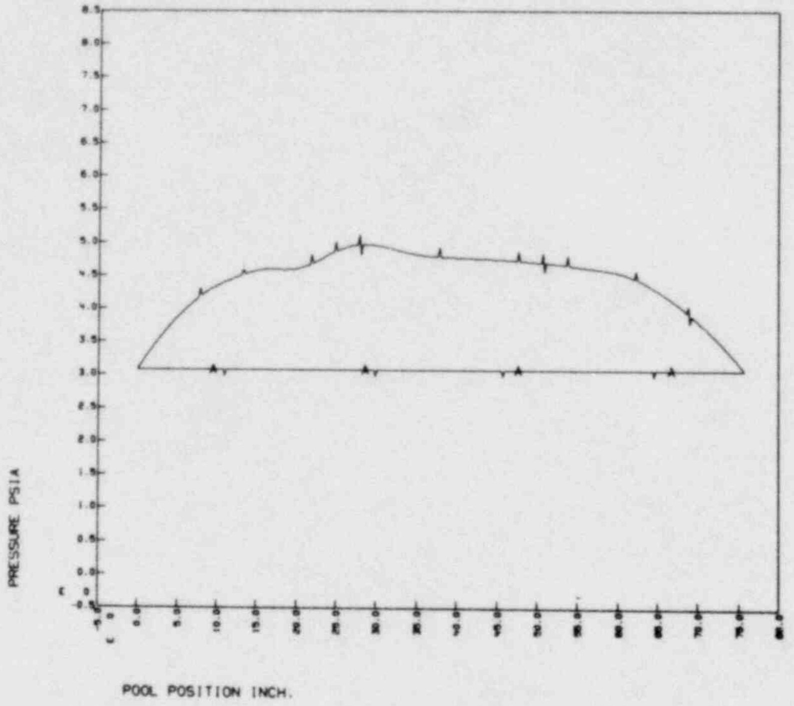

TEST131 SEC. ORDER FIT PRESSURE PROFILE PLANE6 T2
FILE(S):POOL.MRK (A)-ULLAGE.MRK

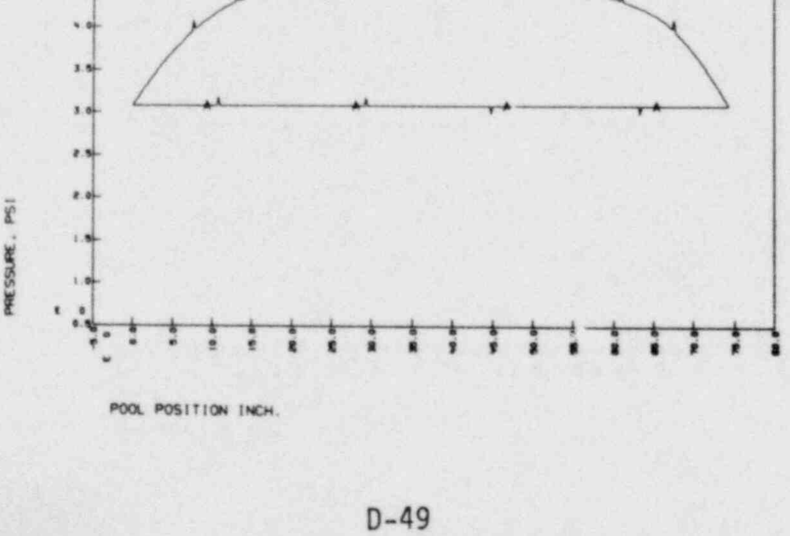

TEST131 SEC. ORDER FIT PRESSURE PROFILE PLANE9 T2
FILE(S):POOL.MRK   (A)-ULLAGE.MRK

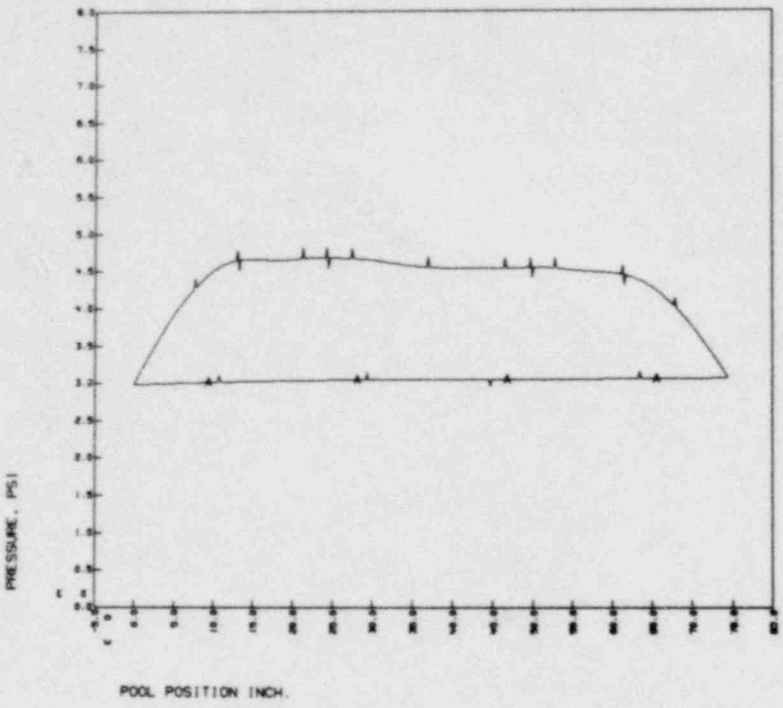

TEST131 SEC. ORDER FIT PRESSURE PROFILE PLANE11 T2
FILE(S):POOL.MRK   (A)-ULLAGE.MRK

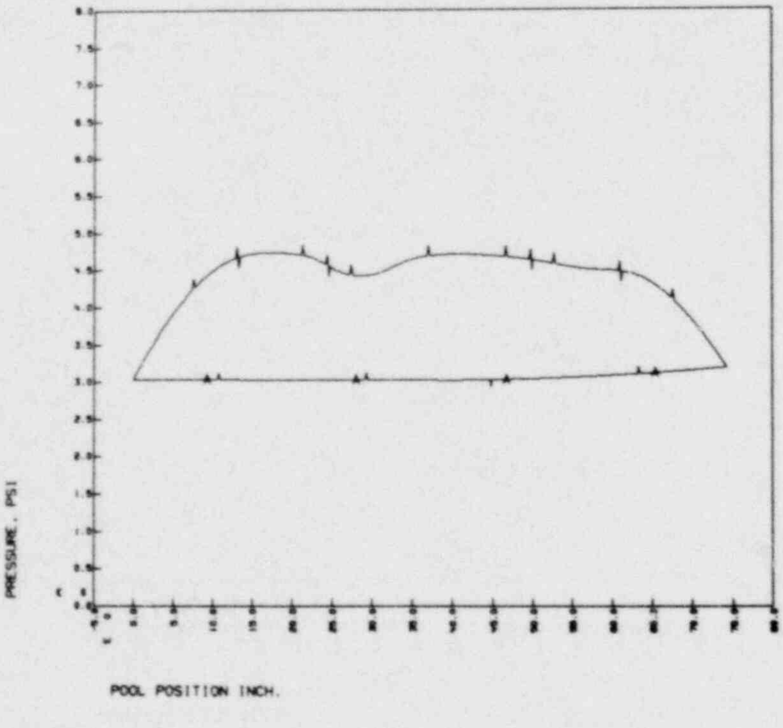

TEST131 SEC. ORDER FIT PRESSURF PROFILE PLANE2D T2
FILE(S):POOL.MRK (A)-ULLAGE.MRK

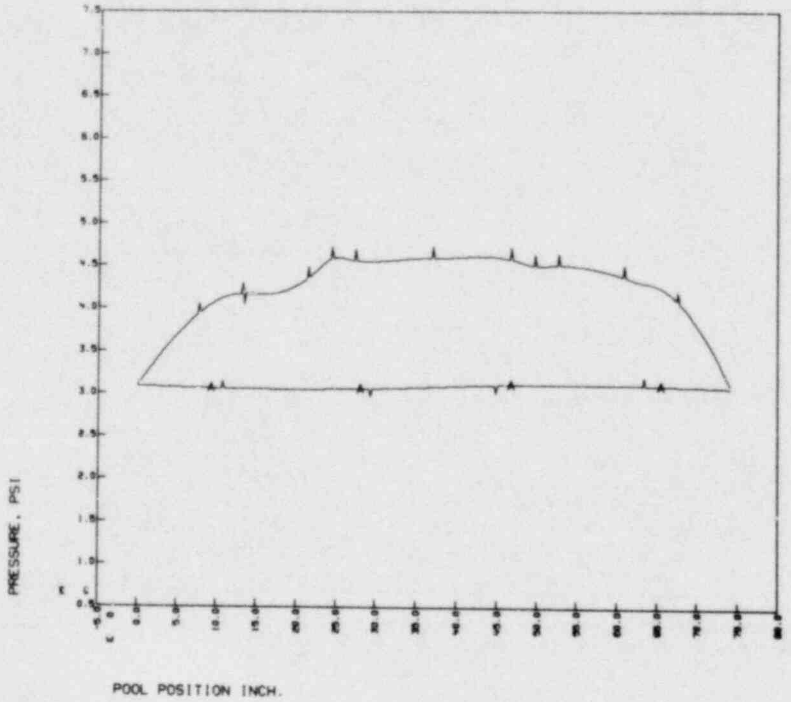

TEST131 SEC. ORDER FIT PRESSURE PROFILE PLANE4 T3
FILE(S):POOL.MRK (A)-ULLAGE.MRK

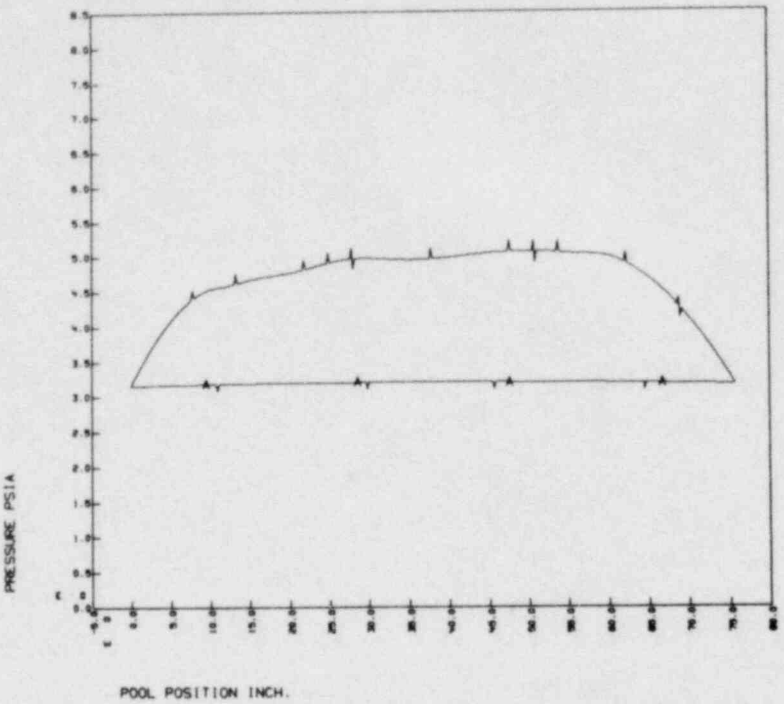

TEST131 SEC. ORDER FIT PRESSURE PROFILE PLANE6 T3
FILE(S):POOL.MRK (A)-ULLAGE.MRK

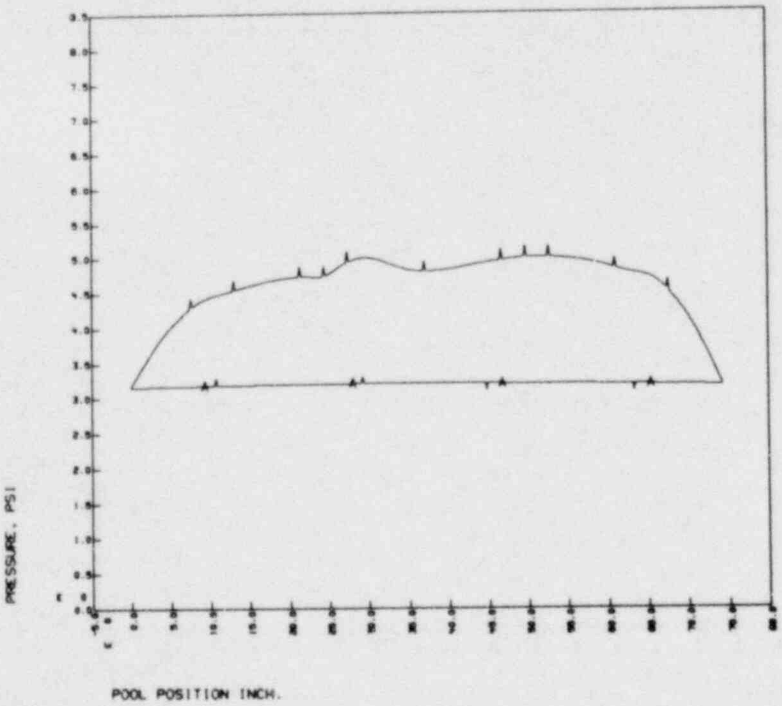

TEST131 SEC. ORDER FIT PRESSURE PROFILE PLANE9 T3
FILE(S):POOL.MRK   (A)-ULLAGE.MRK

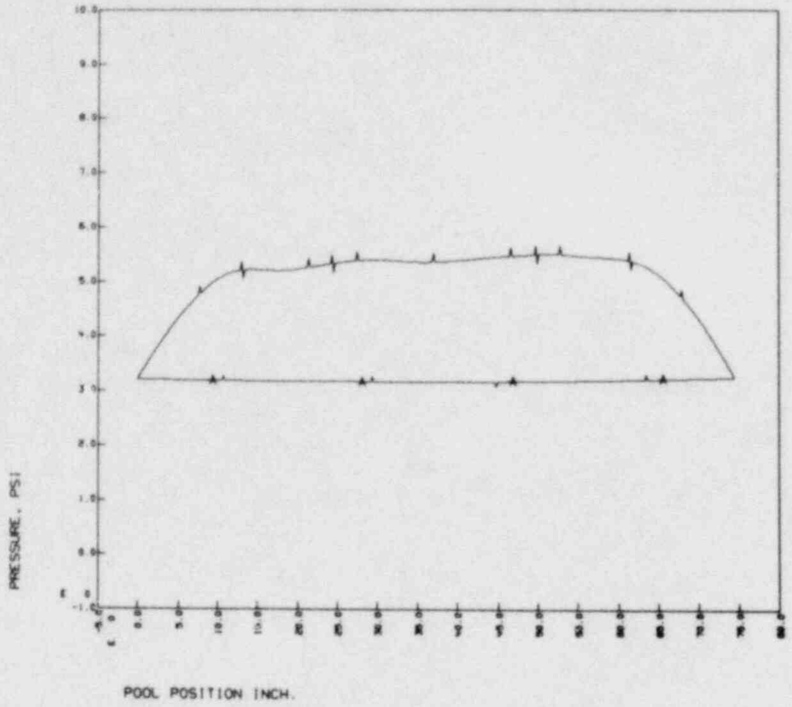

TEST131 SEC. ORDER FIT PRESSURE PROFILE PLANE11 T3
FILE(S):POOL.MRK   (A)-ULLAGE.MRK

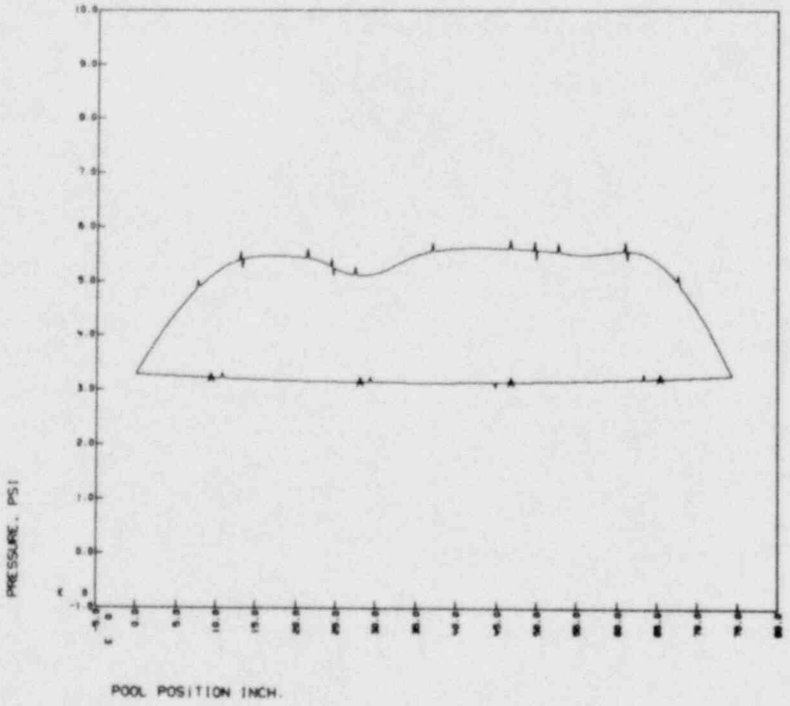

TEST131 SEC. ORDER FIT PRESSURE PROFILE PLANE2D T3
FILE(S):POOL.MRK (A)-ULLAGE.MRK

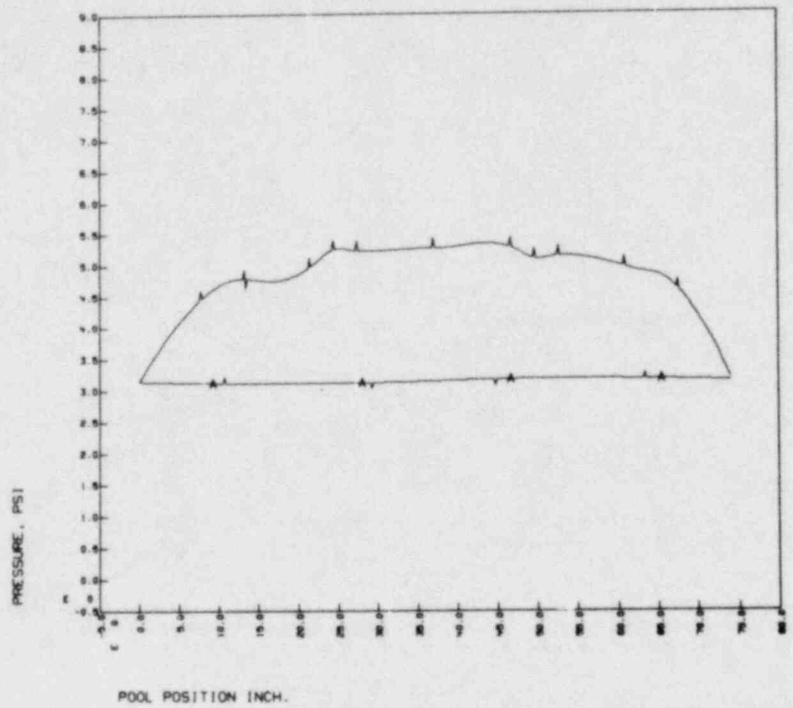

TEST131 SEC. ORDER FIT PRESSURE PROFILE PLANE4 T4, AT MAX UPLOAD
FILE(S):POOL.MRK (A)-ULLAGE.MRK

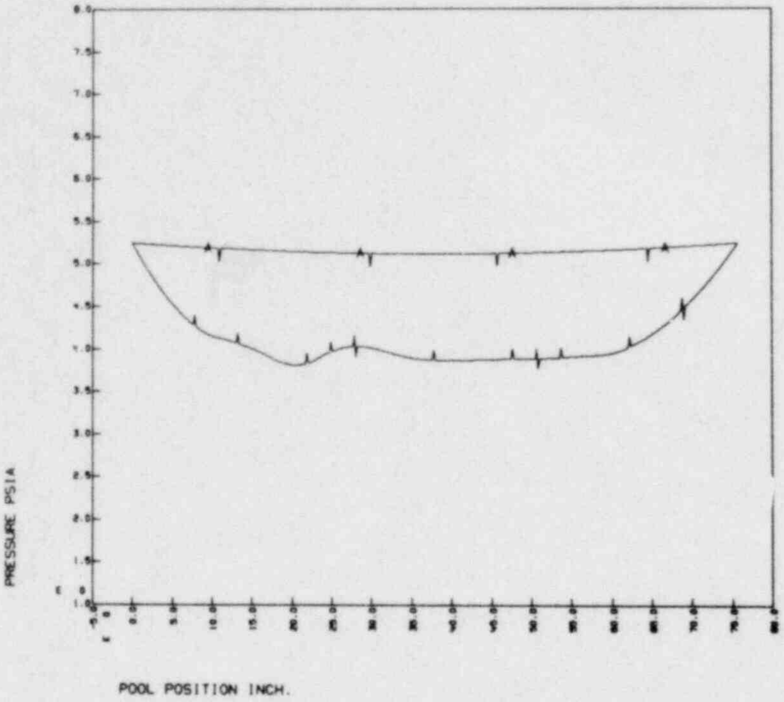

TEST131 SEC. ORDER FIT PRESSURE PROFILE PLANE6 T4, AT MAX UPLOAD
FILE(S):POOL.MRK (A)-ULLAGE.MRK

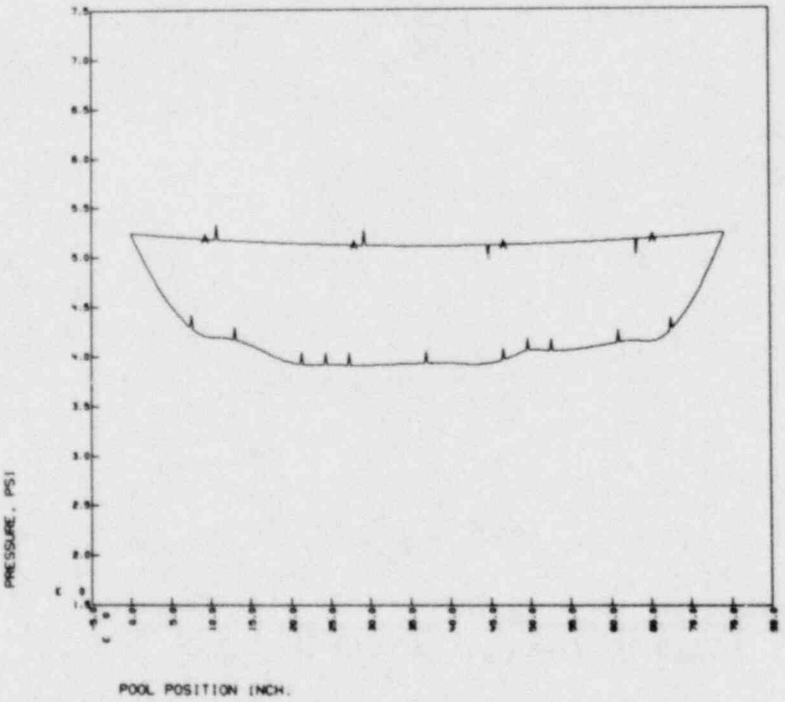

TEST131 SEC. ORDER FIT PRESSURE PROFILE PLANE9 T4, AT MAX UPLOAD
FILE(S):POOL.MRK   (A)-ULLAGE.MRK

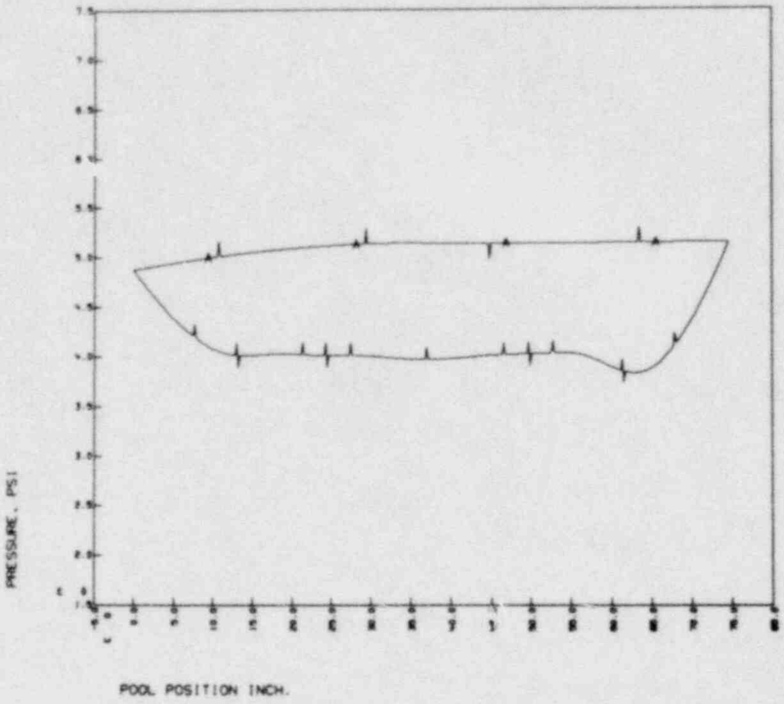

TEST131 SEC. ORDER FIT PRESSURE PROFILE PLANE11 T4, AT MAX UPLOAD
FILE(S):POOL.MRK   (A)-ULLAGE.MRK

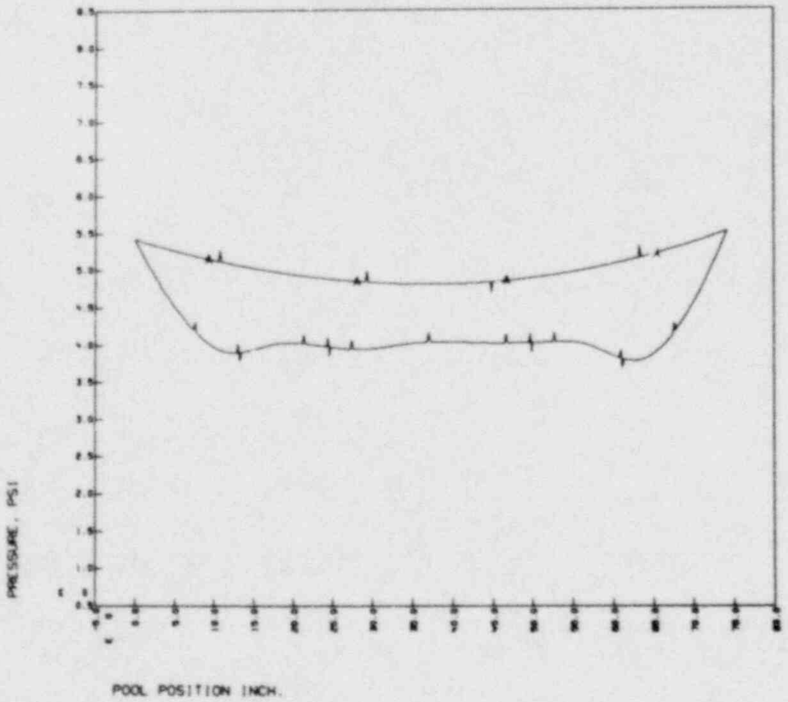

TEST131 SEC. ORDER FIT PRESSURE PROFILE PLANE2D T4, AT MAX UPLOAD
FILE(S):POOL.MRK (A)-ULLAGE.MRK

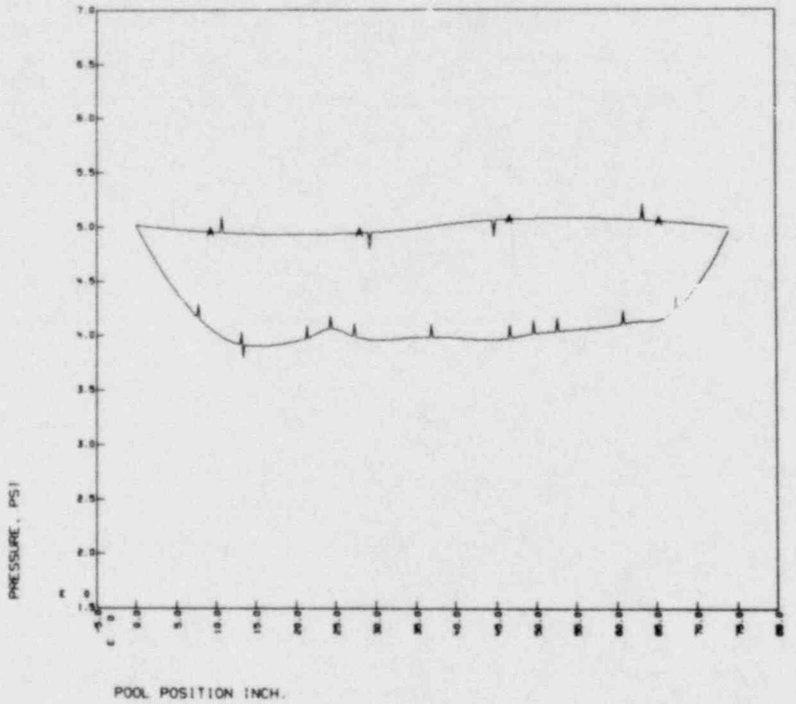

NRC TEST 1.3.1 R 03/01/79 15:56:25
A B C
T1 AT 128 T1 AT 140 T1 AT 155

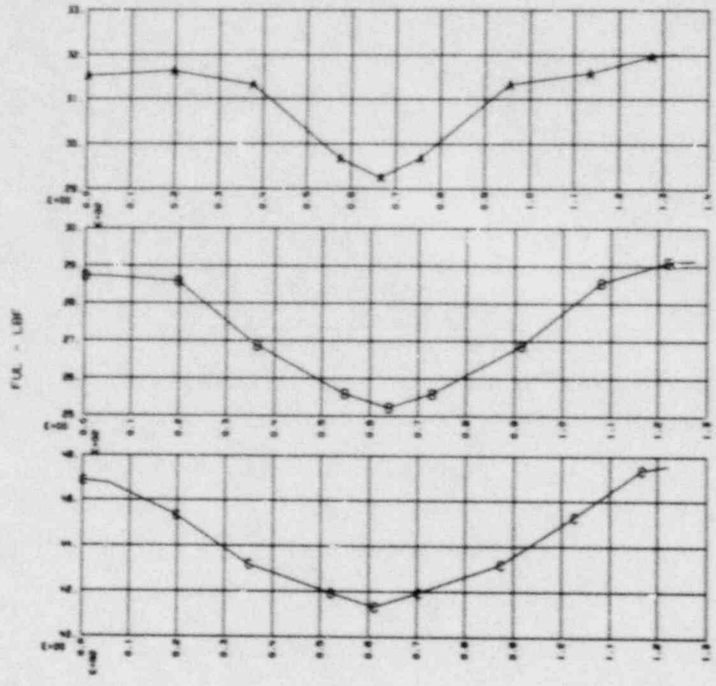

NRC TEST 1.3.1 R 03/01/79 15:56:26
A B C
T1 AT 160 T1 AT 165 T1 AT 180

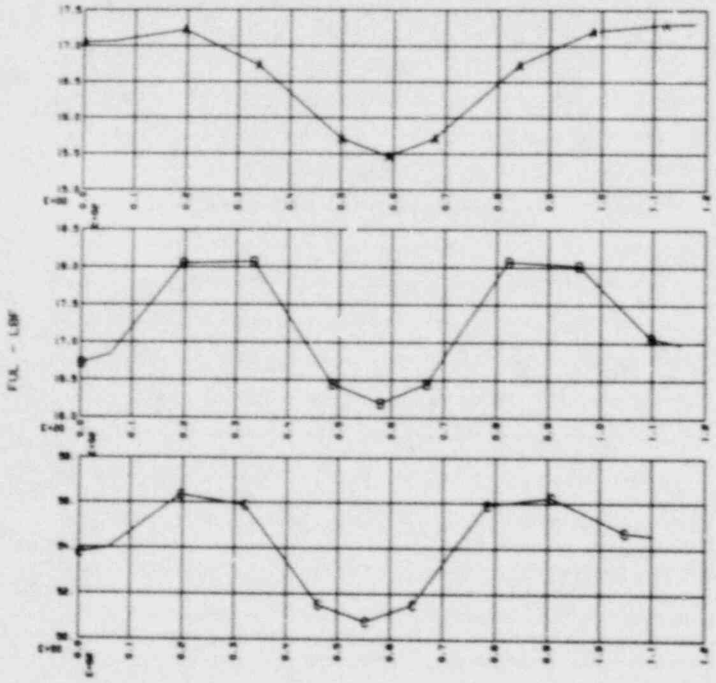

NRC TEST 1.3.1 R 03/01/79 15:56:26
A B C
TI AT 195 TI AT 200 TI AT 205

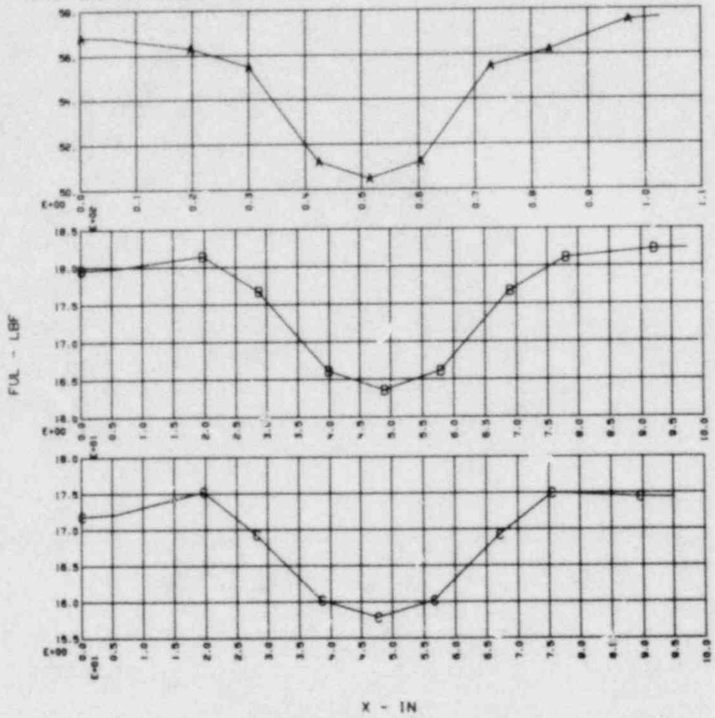

NRC TEST 1.3.1 R 03/01/79 15:56:26
A B C
TI AT 220 TI AT 235 TI AT 269

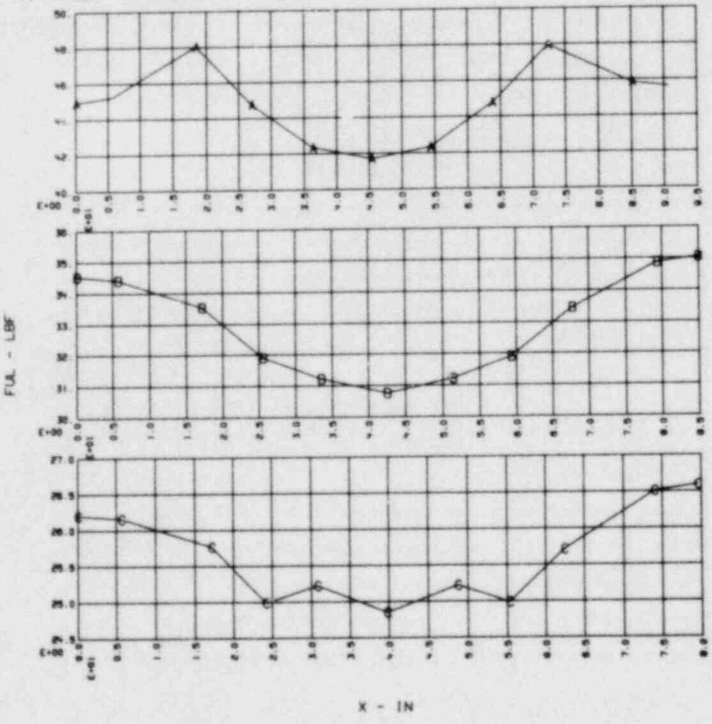

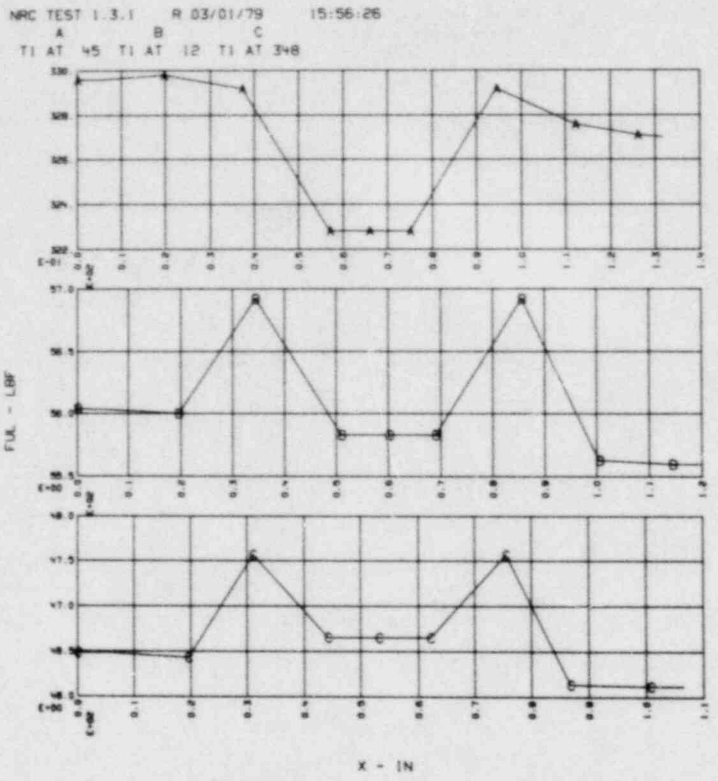
NRC TEST 1.3.1 R 03/01/79 15:56:26
A B C
TI AT 45 TI AT 12 TI AT 348
330
328
326
324
322
57.0
56.5
56.0
55.5
48.0
47.5
47.0
46.5
46.0
FUL - LBF
X - IN

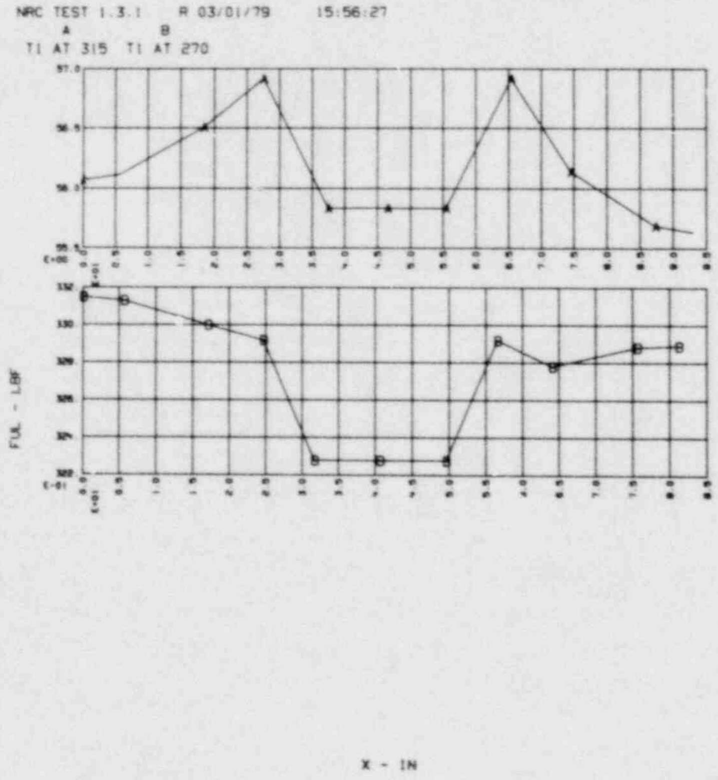
NRC TEST 1.3.1 R 03/01/79 15:56:27
A B
TI AT 315 TI AT 270
57.0
56.5
56.0
55.5
332
330
328
326
324
322
FUL - LBF
X - IN

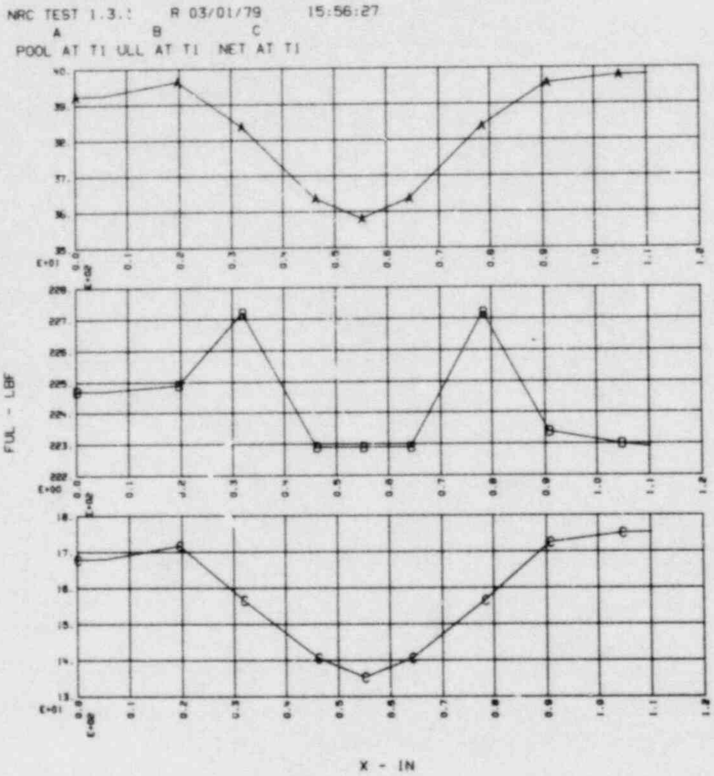
NRC TEST 1.3.1 R 03/01/79 15:56:27
A B C
POOL AT T1 ULL AT T1 NET AT T1
40.
39.
38.
37.
36.
35.
E+01
222.
223.
224.
225.
226.
227.
228.
E+00
13.
14.
15.
16.
17.
18.
E+01
0.0
0.1
0.2
0.3
0.4
0.5
0.6
0.7
0.8
0.9
1.0
1.1
1.2
E-02
FUL - LBF
X - IN

NRC TEST 1.3.1 R 03/01/79 15:56:30
A B C
T4 AT 128 T4 AT 140 T4 AT 155

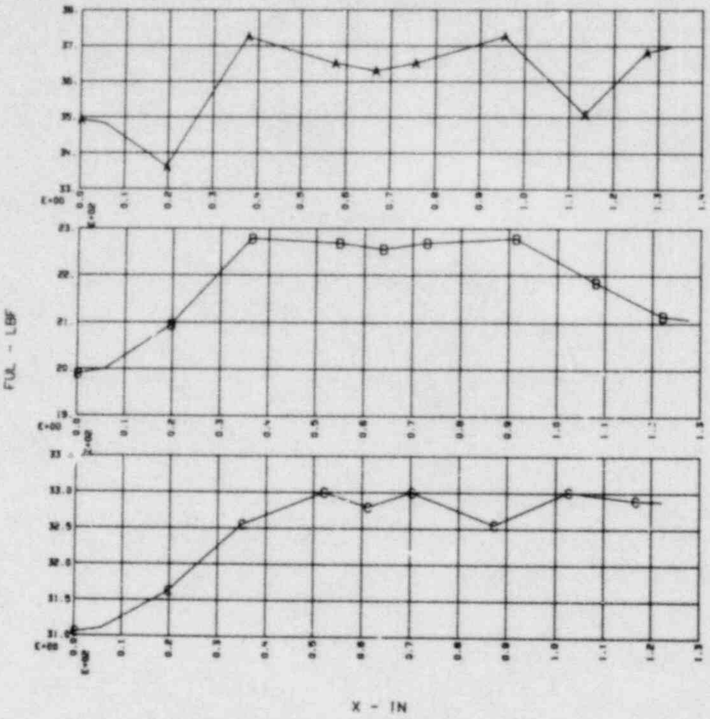

NRC TEST 1.3.1 R 03/01/79 15:56:30
A B C
T4 AT 160 T4 AT 165 T4 AT 180

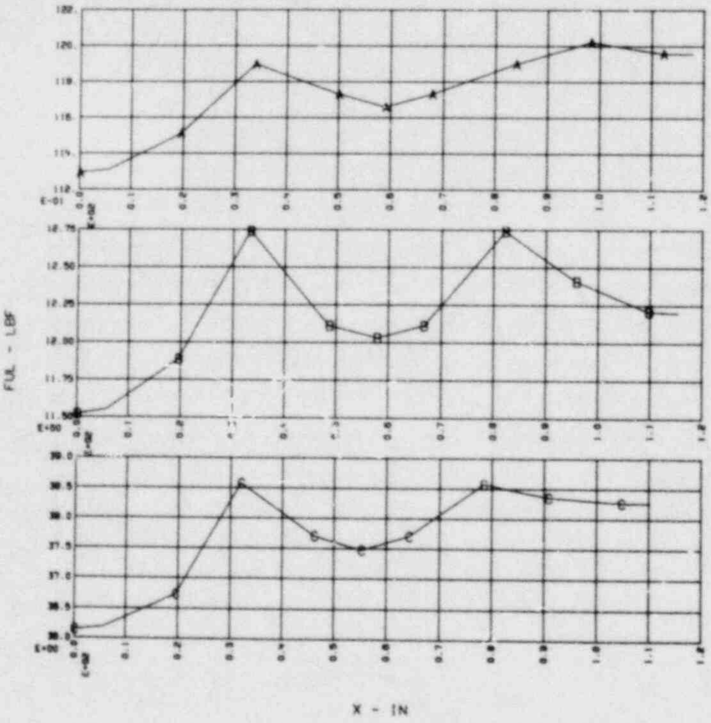

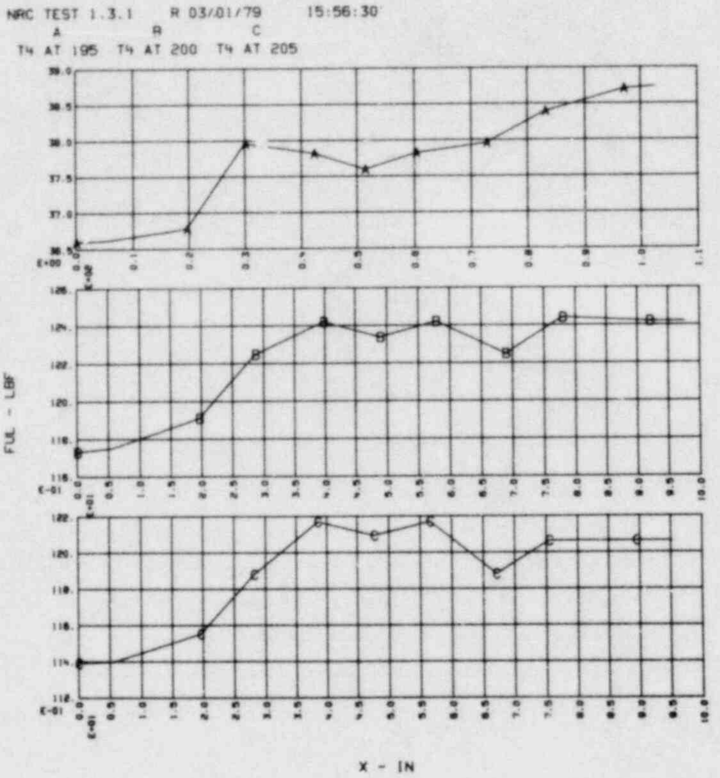
NRC TEST 1.3.1 R 03/01/79 15:56:30
A B C
T4 AT 195 T4 AT 200 T4 AT 205
FUL - LBF
X - IN

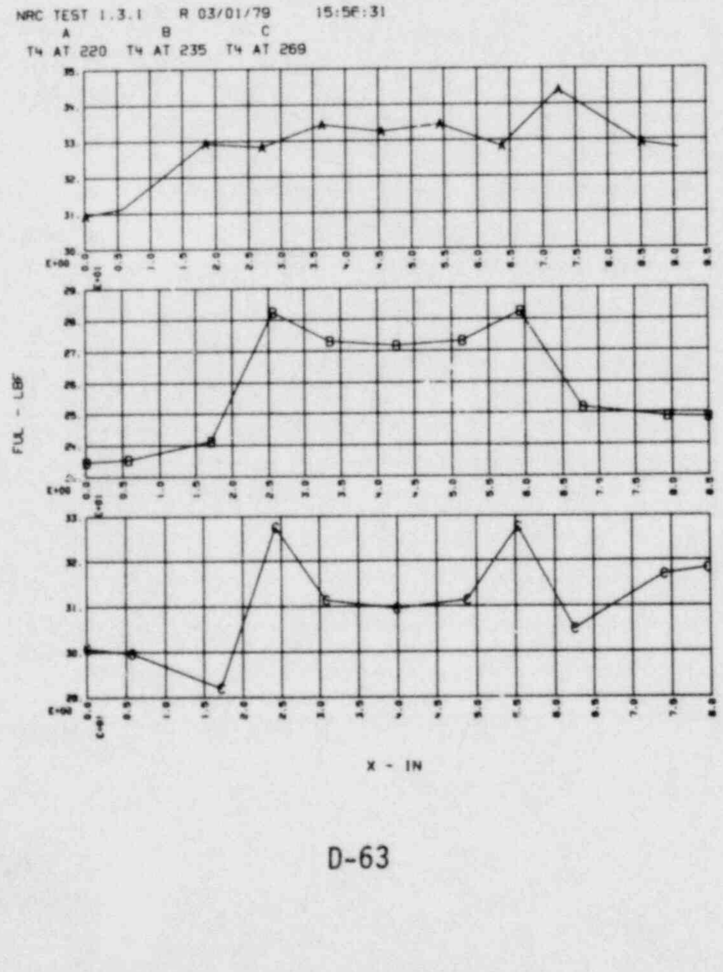
NRC TEST 1.3.1 R 03/01/79 15:56:31
A B C
T4 AT 220 T4 AT 235 T4 AT 269
FUL - LBF
X - IN

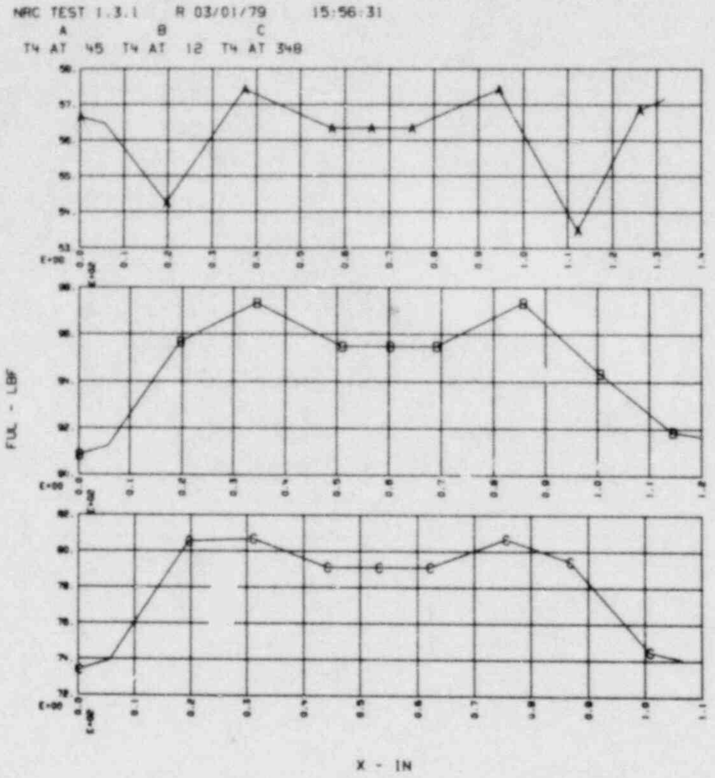

NRC TEST 1.3.1 R 03/01/79 15:56:31
A B C
T4 AT 45 T4 AT 12 T4 AT 348

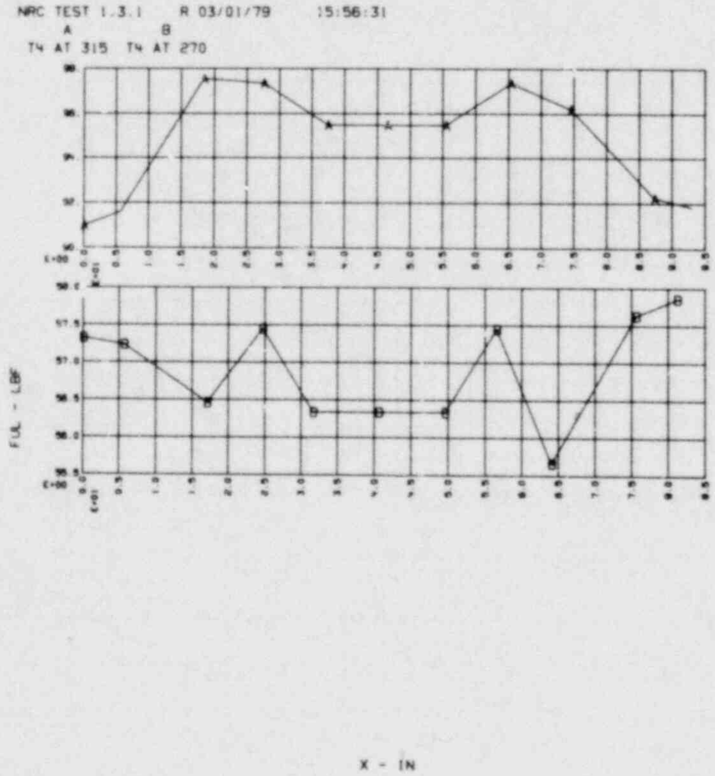

NRC TEST 1.3.1 R 03/01/79 15:56:31
A B
T4 AT 315 T4 AT 270

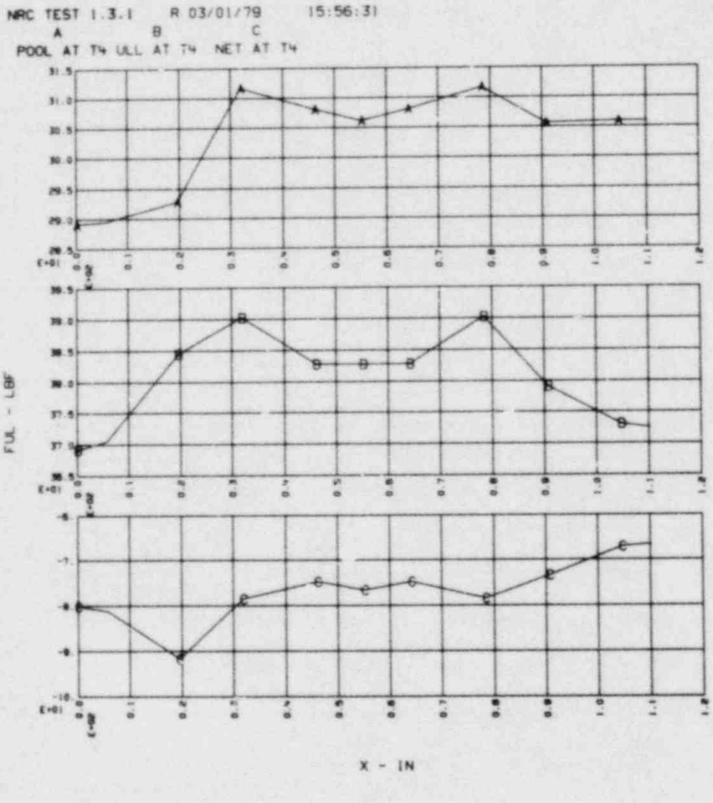
NRC TEST 1.3.1 R 03/01/79 15:56:31
A B C
POOL AT T4 ULL AT T4 NET AT T4
31.5
31.0
30.5
30.0
29.5
29.0
28.5
39.5
39.0
38.5
38.0
37.5
37.0
36.5
-6.
-7.
-8.
-9.
-10.
E+01
0.0
0.1
0.2
0.3
0.4
0.5
0.6
0.7
0.8
0.9
1.0
1.1
1.2
FUL - LBF
X - IN

APPENDIX E

EXTENDED ANALYSIS MICROFICHE

TABLE E-1. Summary of microfiche descriptions.

Appendix section	Microfiche group	Description of contents	Included air tests	Number of microfiche
E.1	1	HVLF characterization data (parabolic fit)	1.1 - 3.5[a]	7
	2	HVLF force summary tables (trapezoidal fit)	1.1 - 3.5[a]	1
E.2	3	HVLF impulse plots for: 45°; $\overline{t}_o \leq t \leq t_{pos}^{45^{\circ}}$ 7.5°; $\overline{t}_o \leq t \leq t_{pos}^{7.5^{\circ}}$ 7.5°; $\overline{t}_o \leq t \leq t_{pos}^{45^{\circ}}$	1.1 - 3.5[a]	1
E.3	4	Computed load cell and RVL force time-history plots for structural inertial effects load cases .+, .-, .2, and .3	1.3.1	1
	5	Frequency analysis plots for measured and computed (case .0) force time-histories	1.3.1	
E.4	6	Vent pipe enthalpy flux time-history plots	1.1 - 3.5[a]	1
	7	Vent pipe mass flow and temperature time-history plots	1.1 - 3.5[a]	1
	8	Summary sheets for inferred enthalpy flux at downcomers	1.1 - 3.5[a]	1

[a] Except for air test 1.2.

NRC FORM 335
(7-77)

U.S. NUCLEAR REGULATORY COMMISSION

BIBLIOGRAPHIC DATA SHEET

1. REPORT NUMBER *(Assigned by DDC)*
NUREG/CR-0761
UCRL-52707

4. TITLE AND SUBTITLE *(Add Volume No., if appropriate)*
Extended Analysis of Data from the 1/5-Scale Mark I Boiling Water Reactor Pressure Suppression Experiment

2. *(Leave blank)*
N/A

3. RECIPIENT'S ACCESSION NO.
N/A

7. AUTHOR(S)
E. W. McCauley, G.S. Holman, E. W. Carr, W. Lai, & J.E.Mellor

5. DATE REPORT COMPLETED

MONTH	YEAR
September	1980

9. PERFORMING ORGANIZATION NAME AND MAILING ADDRESS *(Include Zip Code)*

P.O. Box 808
Livermore, CA 94550

DATE REPORT ISSUED

MONTH	YEAR
July	1980

6. *(Leave blank)*

8. *(Leave blank)*

12. SPONSORING ORGANIZATION NAME AND MAILING ADDRESS *(Include Zip Code)*
U.S. Nuclear Regulatory Commission
Analysis Development Branch
Division of Reactor Safety Research
Washington, D. C. 20555

10. PROJECT/TASK/WORK UNIT NO.

11. CONTRACT NO.
FIN A0118-9

13. TYPE OF REPORT
Technical Report

PERIOD COVERED *(Inclusive dates)*
N/A

15. SUPPLEMENTARY NOTES
N/A

14. *(Leave blank)*

16. ABSTRACT *(200 words or less)*

An extensive analysis of data from the 1/5-scale Mark I BWR Pressure Suppression Experiment (PSE) air transient tests has been completed. Primary focus was placed on computing a best estimate of the hydrodynamic vertical load function (HVLF) and determining the associated peak forces and their standard error. These results were then applied to develop the sensitivity of the HVLF to various major parameters (for example, drywell pressurization rate), to evaluate the impulse of the HVLF, and to analytically model the response vertical load function (RVLF). In addition, a complete evaluation of the enthalpy flux distribution in the vent system was provided for each test. Finally, pool swell dynamics were quantified for a subset of the test series and correlated to the observed ringheader strut loads.

17. KEY WORDS AND DOCUMENT ANALYSIS
N/A

17a. DESCRIPTORS

17b. IDENTIFIERS/OPEN-ENDED TERMS
N/A

18. AVAILABILITY STATEMENT
Unlimited

19. SECURITY CLASS *(This report)*
UNCLASSIFIED

20. SECURITY CLASS *(This page)*
UNCLASSIFIED

21. NO. OF PAGES

22. PRICE
S

NRC FORM 335 (7-77)

☆ U.S. GOVERNMENT PRINTING OFFICE: 1980 O— 325-791